"On ne découvre pas de terre nouvelle sans consentir à perdre de vue, d'abord et longtemps, tout rivage"

André Gide

***In* Les faux-monnayeurs**

**"To discover new lands,
one must first lose sight of the coast for a long time"**

(personal, free translation)

Genetic and developmental studies of neuronal migration defects in the mouse

Maria Cristina Martins da Costa

A thesis submitted for the degree of Doctor of Philosophy in the University of London

December 1999

Institute of Child Health
University College London
30 Guilford Street
London WC1N 1EH

Abstract

The *dreher* mutation is inherited as an autosomal recessive trait. Homozygotes are deaf, have an abnormal inner ear, display circling behaviour and have white belly spots. They also have misplaced neurons (heterotopia) in the central nervous system, involving both the cerebral hemispheres and the cerebellum.

The main goals of this thesis were to accurately map the *dreher* gene, in order to develop a reliable way of genotyping each mouse, to assess candidate genes in the *dreher* region, and to elucidate the mechanisms underlying neuronal migration defects in dr^J homozygous mutant mice.

Using microsatellite DNA markers to genotype the progeny from known heterozygotes, recombinant animals have been identified on the basis of PCR polymorphism analysis. This has enabled the repositioning of the *dreher* gene to a 5.22 cM interval on distal mouse Chromosome 1, proximally to its previously assigned location. Two genes mapping to the critical region, *astrotactin* and *Pou2f1*, were evaluated as candidates for *dreher.* Expression analysis and limited gene sequencing failed to disclose consistent differences in either gene between dr^J/dr^J and wild type embryos.

Studies of the survival of dr^J/dr^J mice in the prenatal period, and at various post-natal ages, indicate that there is increased mortality among homozygous mutants postnatally, probably as a result of starvation caused by the circling behaviour.

In order to evaluate the possible mechanisms underlying the presence of heterotopic neurons in layer I of the neocortex, birthdating studies have been performed by labelling with bromodeoxyuridine. This analysis shows that the misplaced neurons are generated predominantly or exclusively during the late stages of neocortical histogenesis in dr^J/dr^J fetuses. A histopathological and immunohistochemical analysis of dr^J/dr^J brains indicates that the glial limiting membrane overlying the areas of heterotopic neurons is disrupted. This abnormality is suggested to play a central role in the pathogenesis of misplaced neurons in dr^J/dr^J brains, by defective radial glial-guided neuronal migration.

Acknowledgements

I would like to thank Professor Andrew Copp, for his continuing support and kindness throughout the production of this thesis. My thanks also go to Professor Jorge Soares, who has followed my career over more than 15 years and agreed to be my co-supervisor, and to Dr. Brian Harding, for letting me study his collection of neuropathological cases with developmental defects.

I am indebted to everyone I worked in the Neural Development Unit, particularly to Debbie Henderson, with whom I learned so many things on Molecular and Developmental Biology.

Several other people made my work a lot easier on different occasions, and I am, therefore, very grateful to them. They are: the Pathology technicians at the Histopathology Department of the GOS Hospital for Children, and at the Morphological Pathology Department of the Portuguese Institute of Oncology, who shared with me their "tricks of the trade"; Dr Moura Nunes, who always listened patiently and gave useful advice on various aspects of this work; and all of those who helped me in the final sprint, in particular Isabel Palmeirim and Pedro Fernandes (at the Gulbenkian Institute of Science) and Jenny Murdoch, at the Institute of Child Health.

My special thanks to Charles Duyckaerts, at the Laboratory of Neuropathology, Salpêtrière Hospital, Paris, who guided me through his morphometry programme and made me understand that a fresh look at an old problem is often the quickest way to solve it.

I am also very grateful to all the friends who helped me during difficult moments, in particular Pilar Díaz, Olívia Leitão and Maria José Marinho.

Most of all, I am deeply indebted towards my family: to my parents, who gave me the opportunity and means to learn, to my sister Guida for her unconditional support, and, last but not least to Nuno, my husband, for understanding that I had to go and discover new lands.

This work was sponsored by the Gulbenkian PhD. Programme in Biology and Medicine, the Praxis XXI programme and by the British Council.

Abbreviations

APS	Ammonium persulphate
ATP	Adenosine 5'-triphosphate
BAC	Bacterial artificial chromosome
BCIP	5-bromo-4-chloro-3-indolyl-phosphate
bp	Base pair
BSA	Bovine serum albumen
cDNA	Complementary deoxyribonucleic acid
cM	Centimorgan
CNS	Central nervous system
CP	Cortical plate
CR	Cajal-Retzius cell(s)
CSPG	Chondroitin sulphate proteoglycan
DAB	Diaminobenzidine
ddH_2O	Deionised distilled water
ddNTP	Dideoxynucleoside triphosphate; dideoxynucleotide
DEPC	Diethyl pyrocarbonate
DIC	Differential interference contrast (Nomarski)
DMEM	Dulbecco's Modified Eagle's Medium
DMSO	Dimethyl sulfoxide
DNA	Deoxyribonucleic acid
dNTP	Deoxynucleoside triphosphate; deoxynucleotide
DTT	Dithiothreitol
E	Embryonic day
ECM	Extracellular matrix
EDTA	Ethylenediaminetetraacetic acid
EST	Expressed sequence tag
FISH	Fluorescence *in situ* hybridisation
HGMP	Human Genome Mapping Project
HPRT	Hypoxathine-guanine phosphoribosyltransferase
IMS	Industrial methylated spirit
IPTG	Isopropyl-1-thio-β-D-galactoside
IZ	Intermediate zone
kb	Kilobase

LB	L-broth
LMP	Low melting point
MMLV	Moloney murine leukemia virus
mRNA	Messenger ribonucleic acid
MZ	Marginal zone
NBT	4-nitro blue tetrazolium chloride
NMD	Neuronal migration defects
NTMT	Sodium chloride/Tris/magnesium chloride/Tween buffer
PBS	Phosphate-buffered saline
PBT	Phosphate-buffered saline with 0.1% Tween-20
PCR	Polymerase chain reaction
PFA	Paraformaldehyde
PNS	Peripheral nervous system
RNA	Ribonucleic acid
RNAse	Ribonuclease
rpm	Rotations per minute
RT	Reverse transcription
SDS	Sodium dodecyl sulphate
SP	Subplate
SSC	Sodium chloride/sodium citrate buffer
SVZ	Subventricular zone
TAE	Tris/acetate buffer
TBE	Tris/borate buffer
TdT	Terminal deoxynucleotidyl transferase
TE	Tris/EDTA buffer
TEMED	*N,N,N',N'*-tetramethylethylenediamine
TESPA	3-aminopropyltriethoxysilane
Tris	Tris(hydroxymethyl)aminomethane
UTR	Untranslated region
UV	Ultraviolet
VZ	Ventricular zone
Xgal	5-bromo-4-chloro-3-indolyl-β-D-galactoside

Table of contents

List of Tables

List of Figures

Chapter 1

General Introduction

1.1. Normal development of the forebrain

The mature, adult brain of mammals forms by the growth, folding, subdivision and differentiation of the primitive neural tube. The anteriormost portion of the neural tube will give rise to the prosencephalon or forebrain, which will subdivide into the diencephalon and the paired telencephalic vesicles. The latter will become the mature cerebral hemispheres (Figure 1.1). The cerebral cortex is the peripheral grey matter ribbon of the cerebral hemispheres.

Many genes, such as *Sonic Hedgehog*, *BF1*, and those belonging to the *Emx*, *Otx*, *Dlx*, and *Nkx* families, are known to be involved in the induction, growth and patterning of the prosencephalon (reviewed in Rubenstein and Beachy, 1998). Mutations in early-expressed genes of these types produce major malformations of the forebrain. This is illustrated, for instance, by mutations in the human *Sonic Hedgehog* gene, which cause holoprosencephaly (a major disorder of brain patterning in which there is incomplete or absent division of the forebrain into left and right cerebral hemispheres) (Roessler *et al.*, 1996).

1.2. Formation of the cerebral cortex

The cerebral cortex is a highly complex structure that originates from the undifferentiated pseudostratified epithelium of the anterior neural tube. The neocortex (also called isocortex) is the phylogenetically most recent part

Figure 1.1

Development of the mammalian brain

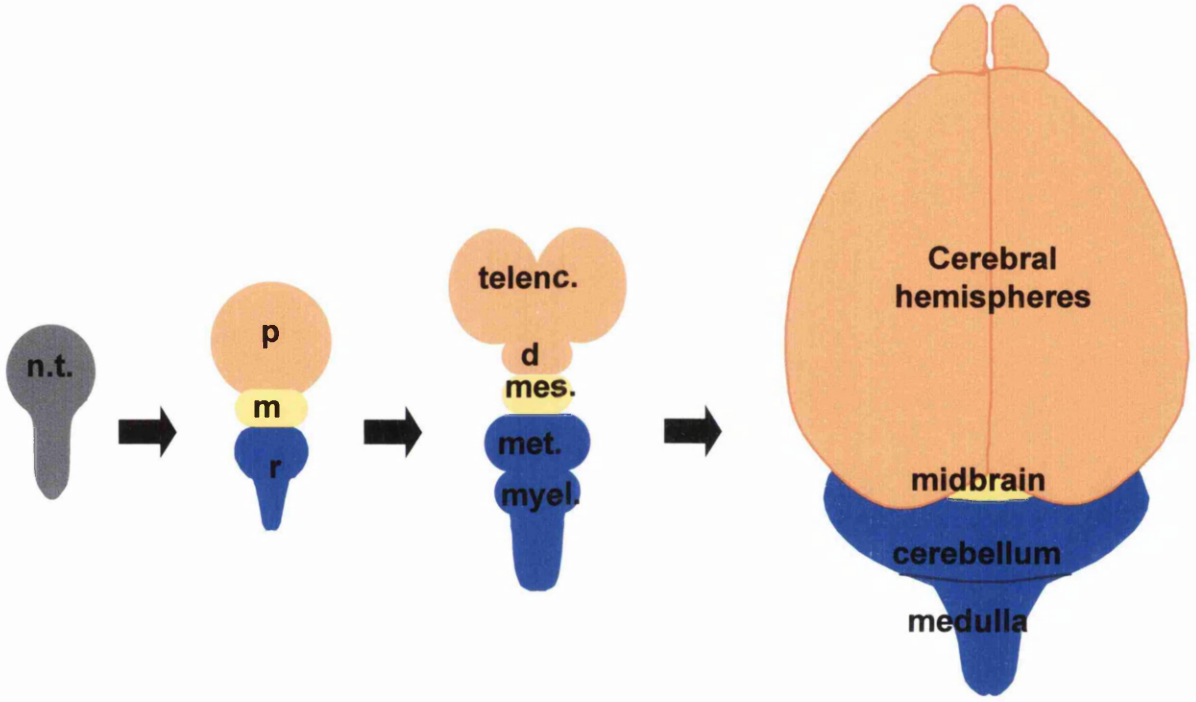

The adult mammalian brain is formed by the progressive growth, partitioning and differentiation of the primitive neural tube (n.t.). Initially, the anterior part of the neural tube balloons into three primary vesicles: the prosencephalon (p) or forebrain, the mesencephalon (m) or midbrain and the rhombencephalon (r) or hindbrain. The anteriormost portion, the prosencephalon, will give rise to the diencephalon (d) and to the paired telencephalic vesicles (telenc.), which will later become the cerebral hemispheres. The mesencephalic vesicle does not divide further and becomes the midbrain. The rhombencephalon will be subdivided into the metencephalon (met), which will give rise to the cerebellum, the pons (a part of the brainstem), and to the myelencephalon (myel.), which will become the future medulla.

(Northcutt and Kas, 1995). It is situated between the medial hippocampal formations and the lateral olfactory cortices (Northcutt and Kas, 1995). The neocortex has six layers, each of which has its own neuronal cell types, synaptic connections and functions (Caviness, 1975) (see also Figure 6.4A).

To understand the organisation of the adult mammalian cerebral cortex, it is crucial to know about the events occurring during the prenatal development of the telencephalic vesicles, i.e. the process of corticogenesis.

The pseudostratified epithelium of the neural tube gives rise to all cell types belonging to the central nervous system, i.e. all the different types of neurons and glial cells (The Boulder Committee, 1970; Friede, 1989a). In the case of the neuronal lineage, neuronal precursor cells proliferate within the ventricular zone, become postmitotic, migrate and settle into layers, where they grow, differentiate by elaborating specialised cytoplasmic processes (axons and dendrites) and establish synaptic connections (Sidman and Rakic, 1973; Caviness, 1989).

1.2.1. Proliferation, commitment to the neuronal lineage and asymmetric divisions

Proliferation of precursor cells in the ventricular zone of the forebrain is the first step of corticogenesis. The transcription factor BF1 probably plays a role in controlling the timing of the switch from a proliferation mode to a differentiation mode. BF-1 null mutant mice have a severe reduction in the size of the telencephalon, secondary to a depletion of progenitor cells, which seem to differentiate into neurons prematurely (Xuan *et al.,* 1995). Growth factors have

been reported to stimulate proliferation (e.g. bFGF) of progenitor cells or their differentiation into neurons (e.g. NT3, BDNF) (reviewed in Temple and Qian, 1995).

The population of proliferating cells is maintained during neurogenesis in the cerebral cortex of the mouse (which takes place between embryonic days 11 and 17) by symmetrical mitotic divisions of precursor cells, in which both daughter cells re-enter the cell cycle (Caviness *et al.,* 1995; Chenn and McConnell, 1995). It is believed that asymmetric divisions give rise to an apical post-mitotic, migrating neuroblast and a basal progenitor cell that may continue to cycle (Caviness *et al.,* 1995; Chenn and McConnell, 1995).

Notch proteins act as receptors in signalling pathways for cell fate specification during development. This role was first identified for Notch in *Drosophila*, where interactions between Notch and its ligand Delta control various developmental pathways, such as neurogenesis and myogenesis (reviewed in Greenwald, 1994; Blaschuk and ffrench-Constant, 1998). This is thought to occur through a process of lateral inhibition of cellular differentiation (Muskavitch, 1994). Recent studies suggest that Notch proteins may play a role in regulating cell fate in the higher vertebrate nervous system as well (Pompa *et al.,* 1997). Among other roles, Notch proteins may be involved in the above-mentioned asymmetrical divisions of precursor cells in the mammalian neural tube, since it has been shown that Notch1 protein is present in the basal pole of proliferating ventricular zone cells and is inherited asymmetrically by the basal daughter during mitosis (Chenn and McConnell, 1995; McConnell, 1995).

1.2.2. Early events in the formation of the cerebral cortex: Origin, function and fate of the early-maturing neurons of the marginal zone and subplate

The first pioneer cells that migrate away from the ventricular zone of the telencephalon accumulate in the primitive plexiform layer (PPL) or preplate (Marin-Padilla, 1978). Subsequently, younger cells proliferating in the ventricular zone exit the cell cycle and migrate to form the densely cellular cortical plate, that splits the preplate into a marginal zone (MZ), and a deeper layer called the subplate (SP) (Figure 1.2). Birthdating experiments on rats indicate that marginal zone cells are produced shortly before subplate cells (Bayer and Altman, 1990). In the mouse, they are generated on gestational days E11 and E12 (Wood *et al.,* 1992; Price *et al.,* 1997). Subplate neurons are among the first to mature, and they play the crucial role of establishing pioneer synaptic contacts with thalamic neurons while the cortical plate is developing (reviewed in Allendoerfer and Shatz, 1994). Cajal-Retzius (CR) cells are the main neuronal type of the marginal zone and they are therefore among the first to mature in the developing telencephalon (reviewed in Supèr *et al.,* 1998). It is believed that CR cells play a fundamental role in the formation of the normally stratified cerebral cortex: they produce Reelin, a secreted protein which, when defective (as is the case in the *reeler* mutant mouse) causes major abnormalities of corticogenesis (Caviness, 1982; D'Arcangelo *et al.,* 1995; Hoffarth *et al.,* 1995; Ogawa *et al.,* 1995). Birthdating studies (see Chapter 7) indicate that in the mouse, as in other mammals, most preplate-derived neurons are fated to die, by apoptosis, during late gestation and in the early post-natal period (Wood *et al.,* 1992; Price *et al.,* 1997). Shortly before birth, most early-

Figure 1.2

Neuronal migration in the cerebral cortex: early events

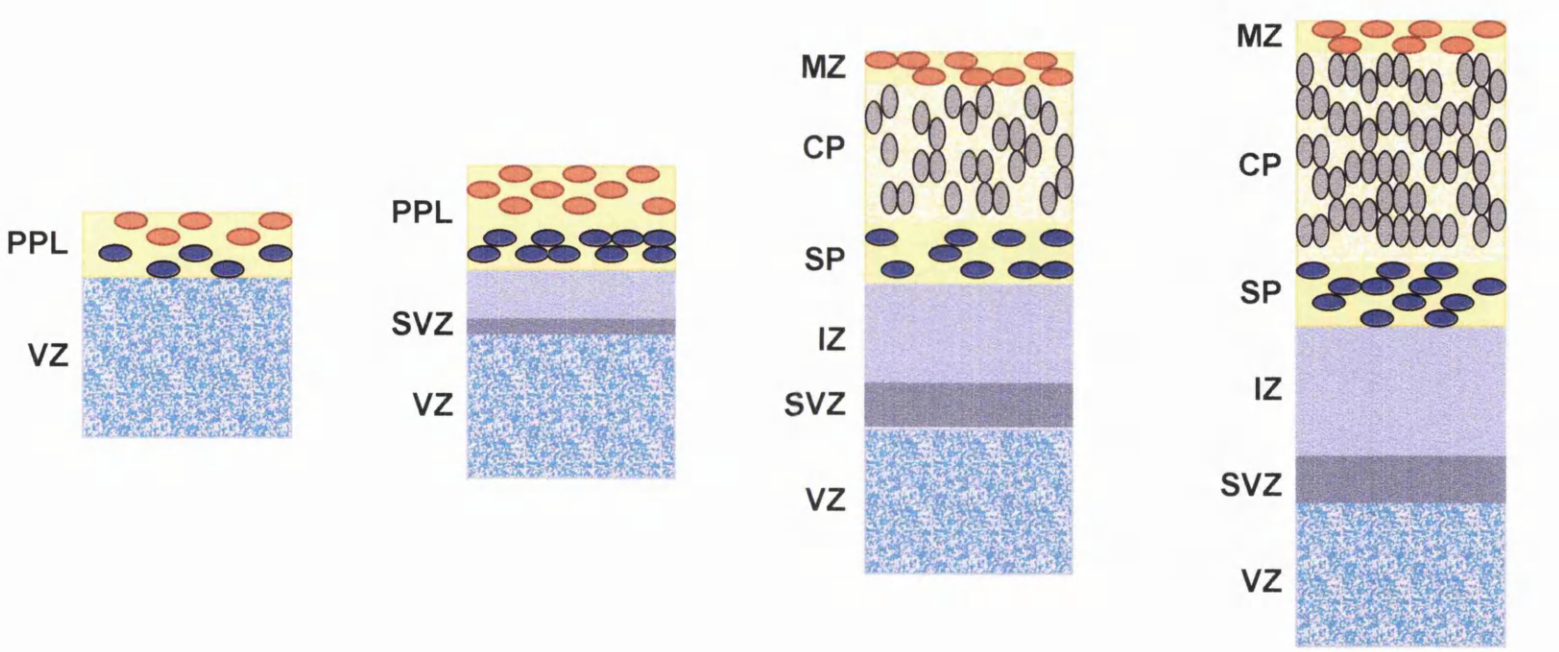

Neuronal precursors proliferate in the ventricular zone (VZ). The first neurons to mature in the developing cerebral cortex accumulate in the primitive plexiform layer (PPL) or preplate. This layer is subsequently split in two by the incoming neurons of the cortical plate (CP). Layers II to VI will form by the migration and settling of neurons into the cortical plate. Most preplate-derived neurons die by apoptosis during embryonic development or in the early post-natal period.The marginal zone (MZ) gives rise to layer I in the adult animal. Surviving subplate (SP) neurons remain as deep layer VI and interstitial neurons of the white matter. IZ: intermediate zone. SVZ: subventricular zone. Adapted from *Bayer and Altman, 1990.*

generated neurons lie below the cortical plate, and a minority of them (including CR cells) occupies the marginal zone and the deep part of the cortical plate. By postnatal day 21 (P21), very few of these early-generated neurons remain, and they are localised in deep cortical layers, suggesting that most have died postnatally (Price *et al.,* 1997).

Apoptotic cell death during development of the cerebral cortex is a well-recognised event, especially among preplate-derived neurons (Wood *et al.,* 1992; Price *et al.,* 1997; Blaschke *et al.,* 1999). Interestingly, recent studies using a very sensitive technique to assess apoptosis, ISEL+ (a modification of the technique of *in situ* end labelling of double-stranded DNA fragments produced during apoptosis) indicate that the magnitude of programmed cell death during development of the cerebral cortex of the mouse is much higher than was previously believed. According to these studies, apoptosis is most abundant in proliferative regions and affects up to half of the cells produced at the peak of the neurogenesis period (Blaschke *et al.,* 1999).

1.2.3. Formation of layers II-VI of the cerebral cortex

1.2.3.1. Glial-guided neuronal migration

Postmitotic cells committed to the neuronal lineage and destined for layers II to VI of the cerebral isocortex migrate away from the ventricular zone and are guided to their final positions by radial glial cells (Sidman and Rakic, 1973) (Figure 1.3). These specialised bipolar glial cells have processes spanning the thickness of the developing cerebral cortex, from the ventricular to the superficial pial surface. The radial glial cells are attached to the latter by cytoplasmic expansions known as endfeet. At the external surface of the brain,

Figure 1.3

Glial-guided neuronal migration

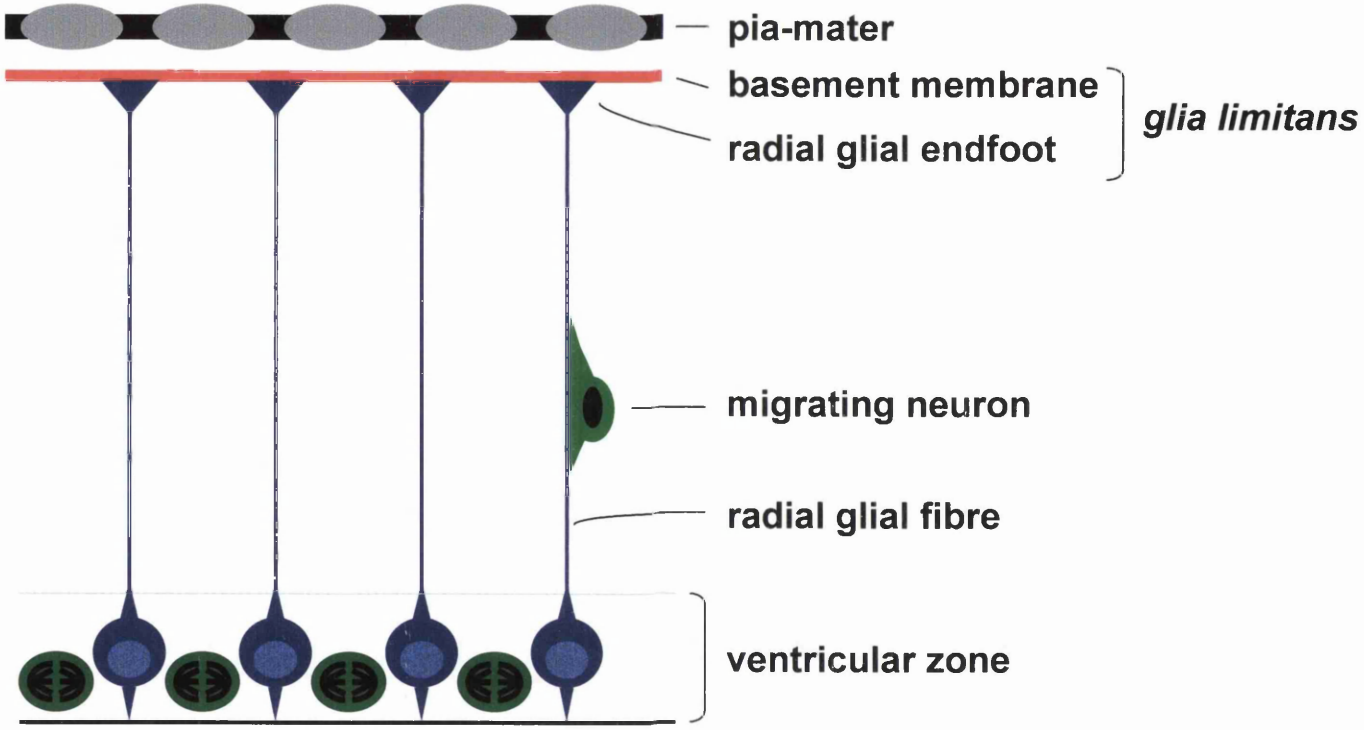

Precursor cells become committed to a neuronal fate, exit the cell cycle and migrate to their final positions. In doing so, they are guided by a scaffold of radial glial cells. The processes of these cells span the full thickness of the neural tube. The basement membrane underlying the inner sheath of the leptomeninges (the pia-mater) together with the endfeet of radial glia constitutes the *glia limitans*.

these cellular expansions, together with the basement membrane underlying the *pia-mater* (the inner layer of the meninges), form the *glia limitans*, also known as the external glial limiting membrane (Figure 1.3).

Radial glial cells play a crucial role in guiding migrating neurons from the ventricular zone to their final positions in the cerebral cortex (Sidman and Rakic, 1973; Caviness, 1982; Rakic, 1988; Edwards *et al.,* 1990; Rakic, 1990). Bipolar radial glial cells are present from E10 in the forebrain of the mouse, (Edwards *et al.,* 1990). Their processes attain maximal density by day E14-16, then most of the radial glia lose their pial and ventricular attachments and undergo branching, eventually differentiating into multipolar astrocytes (Misson *et al.,* 1991) (see Figure 1.4). Silver impregnation using the Golgi method on human and monkey brains indicate that a few glial cells remain persistently connected to the pial surface at the *glia limitans*, whereas others probably become ependymal cells lining the ventricular surface of the cerebral hemispheres (Schmechel and Rakic, 1979; Marin-Padilla, 1995). In the rat, it has been demonstrated that the peak of glial cell proliferation coincides with the end of glial-guided neuronal migration in the cerebral neocortex (Das, 1979).

1.2.3.2. Neuron-glia interactions during glial-guided neuronal migration

The normal binding and migration of neurons along radial glial fibres depends on the integrity of several receptor systems. One of the molecules that seems to be crucial for this process of glial-guided neuronal migration is Astrotactin, a neuronal membrane protein expressed at the surface of migrating neurons. Blocking Astrotactin function results in major perturbation of the rate of glial-guided neuronal migration (see Chapter 4). More recently, the role of the glial

Figure 1.4

Fate of radial glial cells in the cerebral cortex

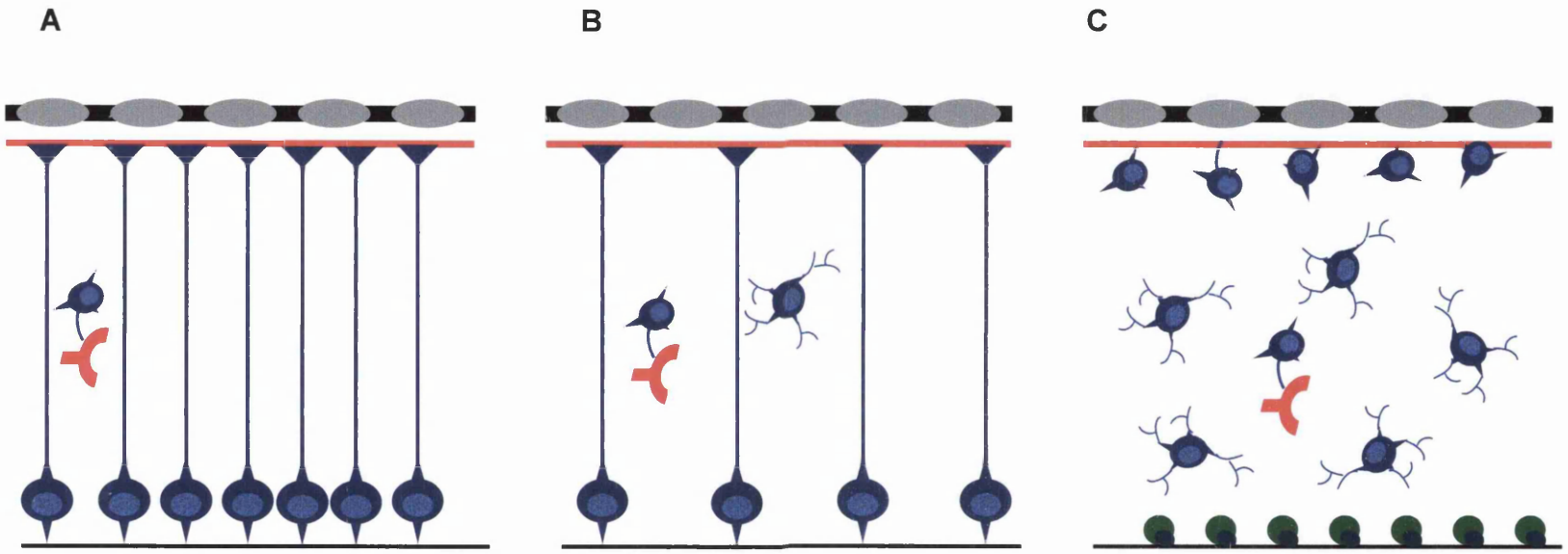

Bipolar radial glial cells are present at E10 in the forebrain, before the onset of neuronal migration. Their cell bodies are situated in the ventricular zone and their processes extend from the ventricular surface to, in most cases, the pial membrane (endfeet) (A). Some glial cells attach themselves to the walls of blood vessels. By E17, radial glial cells start to divide. They progressively lose their attachment to the pial and ventricular surfaces (B). Some will remain adherent to the ventricular surface and differentiate into ependymal cells, but most undergo branching and eventually become multipolar astrocytes of the adult brain (C). Partially adapted from *Misson, et al., 1991*.

growth factor (GGF)-erbB2 receptor system in neuronal-glial interactions in the developing cerebral cortex has been elucidated. GGF is a member of the Neuregulin gene family, which exerts its cellular effect through ErbB2, a receptor tyrosine kinase encoded by a gene of the epidermal growth factor family (Carraway and Burden, 1995). Like astrotactin, GGF is expressed by migrating neurons of the cerebral cortex, whereas ErbB2 is expressed by radial glia (Anton *et al.,* 1997). GGF promotes neuronal migration and radial glial fibre elongation, an effect that is at least partially mediated by BLBP (brain lipid binding protein), a molecule necessary for maintaining radial glial differentiation during brain development (Feng and Heintz, 1995; Anton *et al.,* 1997).

1.2.3.3. Neuronal migration in layers II-VI follows an inside-out gradient

The process of normal cortical histogenesis has been studied (Angevine and Sidman, 1961; Caviness, 1982) by the use of *in utero* labelling of cells undergoing their last mitotic cycle (i.e. before beginning their migration) with tritiated thymidine (see Chapter 7, section 7.1.3 and Figure 1.5). E11-born neurons migrate to the subplate layer and, to a lesser extent, to the marginal zone, as seen by examination of the brain at E15. Most cells labelled on day 11 become polymorphic cells of layer VI in the adult animal. E13 injections label neurons destined for the cortical plate at E15. They generate mainly pyramidal cells, but also some granule and polymorphic cells (of layers IV to VI) in the adult animal. Injections of tritiated thymidine at E15 label cortical plate cells, predominantly granule cells and medium pyramidal cells destined to become layers III and IV in the adult animal. Cells destined for superficial layers II and III in the adult are labelled with E17 injections, and become small and medium pyramidal neurons. Thus, cohorts of newly-born neurons migrate through

Figure 1.5

Neuronal migration in the murine cerebral cortex: Birthdating studies

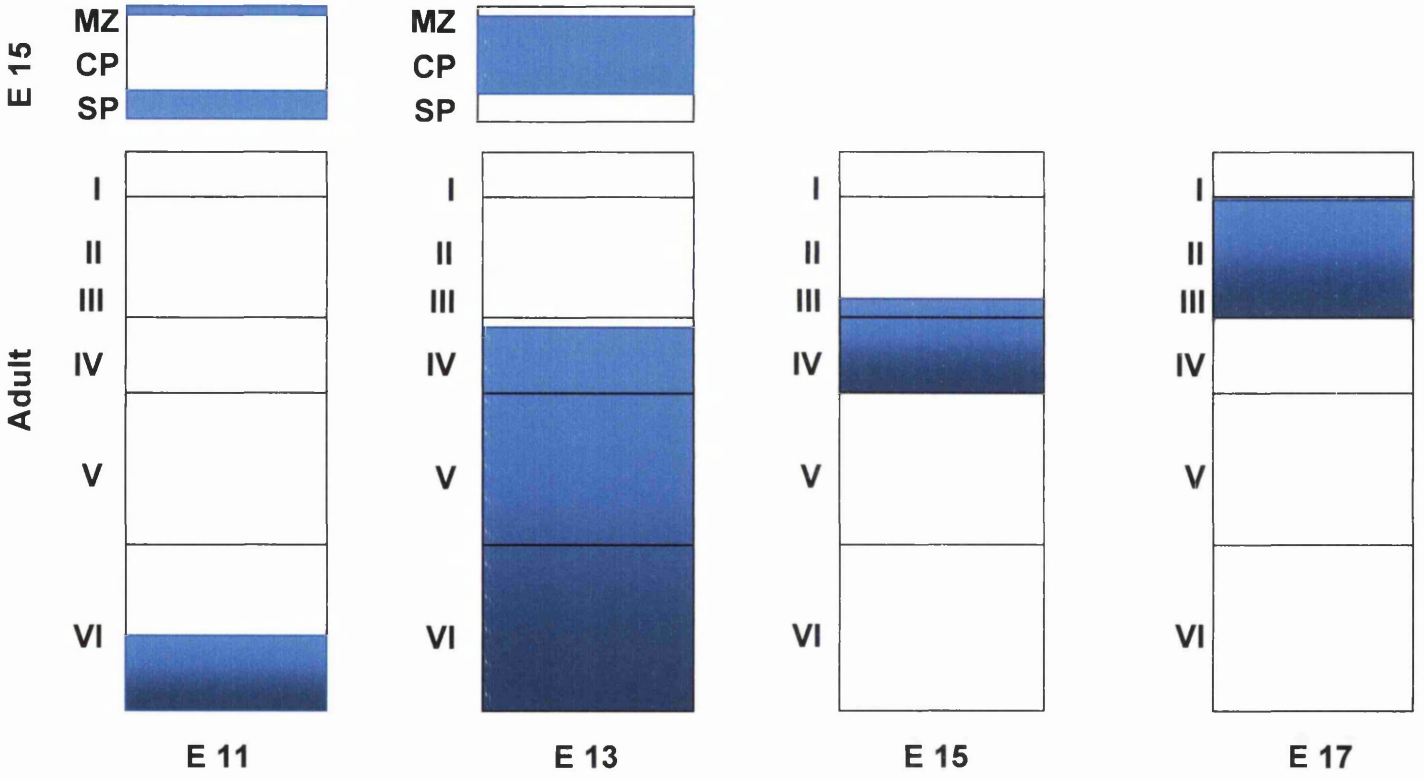

Injection of an S-phase marker during the period of neurogenesis will label neurons destined to populate different cortical layers, according to the day of injection. Early injections (E11) label neurons belonging to preplate-derived neurons of the marginal zone and subplate, as confirmed by analysis at E15.Most of these neurons are found in deep layer VI in the adult animal. Injections at E13 label cortical plate (CP) neurons, which later populate deep layers of the mature cortex. Injections at later stages of cortical development (e.g. E17) label neurons in more superficial layers IV to II. Adapted from Caviness, 1982.

previously formed layers to occupy their final positions, creating an inside-out gradient of neurogenesis in the developing cerebral neocortex. Neurons that form later occupy more superficial layers, whereas earlier-migrating neurons will settle into deeper positions (see Figure 1.5). The immature, trilaminated appearance of the murine cerebral cortex persists until the first post-natal week, when layers II to VI become distinct (Rice and Van der Loos, 1977) by the addition of increasing numbers of settled neurons.

Besides the inside-out pattern of neurogenesis mentioned above, there is also a spatial gradient of neurogenesis over each of the cerebral hemispheres: more rostrally and laterally situated regions of the neocortical ventricular zone cease proliferation and initiate migration before the more caudo-medial ones. This has been shown for both the pre-plate derived neurons and for those of layers II to VI (Caviness, 1982; Price *et al.,* 1997).

1.2.3.4. Laminar determination of neurons in the developing cerebral cortex occurs before their last mitotic cycle in the ventricular zone

Transplantation experiments in ferrets have suggested that the fate of cortical neurons is determined during their last mitotic cycle (McConnell and Kaznowski, 1991). In these experiments, presumptive neuronal precursor cells are transplanted into older developing host brains. Neurons that had already exited the cell cycle at the time of transplantation were found to have migrated to the layer that they would have populated in their cortex of origin (i.e. according to their day of birth). If, however, they were grafted during the S phase, i.e. before becoming postmitotic, they were found to adopt the same laminar fate as the neurons belonging to the host layer into which they had been transplanted (McConnell and Kaznowski, 1991). This suggests that prospective neurons are

sensitive to environmental cues for their final positioning in the cerebral cortex, during their cell cycle, but that laminar fate is determined following the final S-phase.

1.2.4. Role of extracellular matrix molecules in brain development

Migrating neurons have to go through a progressively expanding and increasingly complex cortical plate to reach their final destinations.
The extracellular matrix that surrounds them comprises molecules such as fibronectin, chondroitin sulphate proteoglycans (CSPGs), tenascin and laminins. These molecules have been shown to play an important role in the development of the mammalian central nervous system (Reichardt and Tomaselli, 1991). The distribution patterns of several components of the extracellular matrix are known to undergo changes which parallel sequential stages in the development of the cerebral cortex (Sheppard *et al.,* 1991). For example, the spatial distribution of CSPGs is intimately associated with that of preplate-derived cells of the marginal zone and subplate; immunoreactivity for CSPGs disappears in parallel with cortical plate differentiation in the mouse (Sheppard *et al.,* 1991). Reelin is an extracellular matrix-like protein secreted by CR cells of the marginal zone. This molecule is essential for normal lamination of the developing cerebral cortex (D'Arcangelo *et al.,* 1995; Sheppard and Pearlman, 1997), presumably by controlling cell adhesion (Hoffarth *et al.,* 1995).

1.3. Tangential migration of precursor cells and postmitotic neurons during development of the cerebral cortex: glia-independent neuronal migration

Although the predominant mode of neuronal migration in the cerebral neocortex appears to be dependent on radial glial fibres, there is now considerable evidence to implicate other glial-independent pathways of neuronal migration in the mammalian forebrain (Figure 1.6). Both precursor cells and postmitotic neurons have been shown to employ tangential modes of migration (Tan and Breen, 1993; Rakic, 1995; Reid *et al.,* 1995; Soriano *et al.,* 1995; Tan *et al.,* 1995; O'Rourke *et al.,* 1997). Progenitor cells may move within the ventricular zone prior to their last mitotic cycle (Fishell *et al.,* 1993). Retroviral lineage studies carried out in the rat have shown that progenitor cells are capable of moving through the ventricular zone and, at regularly spaced intervals, generating either single cell type clones or clones of both neuronal and glial cells (Reid *et al.,* 1995). The spatial dispersion of clones of cells is not necessarily incompatible with radial migration, since it remains possible that the progeny cells of these tangentially moving progenitor cells migrate radially with the help of radial glial cells (Rakic, 1995). This notion of combined radial and tangential migration has been supported by studies using transgenic mice (Tan and Breen, 1993; Soriano *et al.,* 1995; Tan *et al.,* 1995). In one of these studies (using transgenic mice carrying an X-inactivated marker), radially-oriented bands of cells (presumed to consist of clonally-related, radially-migrating cells) were seen in the cerebral cortex, along with areas with no identifiable borders (probably generated by tangential, horizontal migration of progenitor cells) (Tan and Breen, 1993). Neuronal precursor cells from the subventricular zone (SVZ)

Figure 1.6

Modes of neuronal migration in the mammalian forebrain

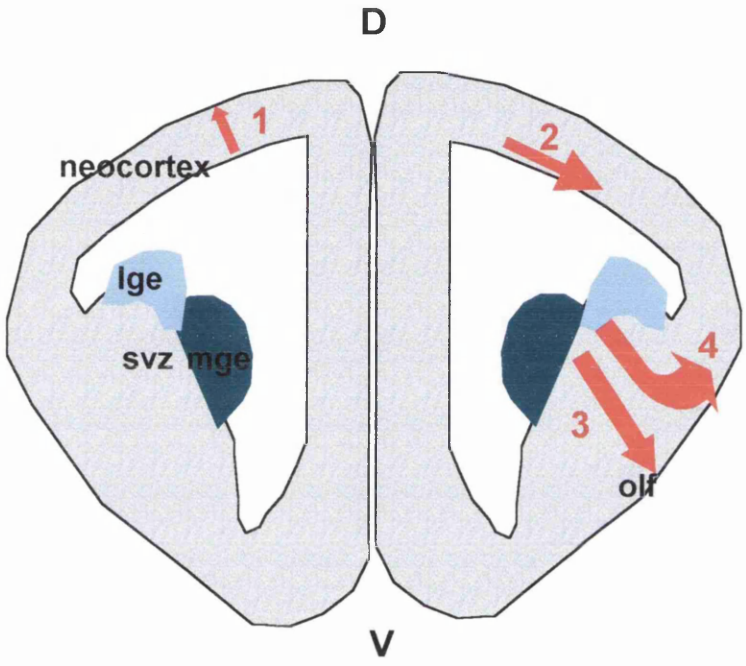

1- Radial glial-guided neuronal migration.
2- Tangential migration in proliferative zones.
3 - Chain migration, from the subventricular zone into the olfactory lobe and the future layer I.
4 -Tangential migration within the marginal zone.
D-dorsal. V-ventral. lge-lateral ganglionic eminence.
mge- medial ganglionic eminence. svz-subventricular zone
olf-olfactory lobe.

of the rat are capable of migrating rostrally from the walls of the lateral ventricle into the olfactory bulb, without the assistance of radial glia or axonal processes. This tangential migration is known as "chain migration", because migrating cells form elongated chains of tightly packed cells which slide against each other (Wichterle *et al.,* 1997). Postmitotic neurons have also been shown to migrate tangentially: in the ferret, this type of migration has been demonstrated within the subventricular and ventricular zones (O'Rourke *et al.,* 1997). Moreover, after migrating radially from the lateral ganglionic eminence (in the ventro-lateral walls of the telencephalic vesicles) to the cortical surface, rodent neurons possess the ability to move tangentially within the marginal zone (De Carlos *et al.,* 1996).

1.4. The spectrum of neuronal migration defects

"Neuronal migration defects" (NMD) is a broad term that encompasses developmental malformations of the brain caused by abnormalities which affect neuronal migration primarily or secondarily (e.g. due to an imbalance between proliferation and programmed cell death-see Chapter 7). Neuronal migration defects have increasingly recognised as a cause of various types of epilepsy in humans, particularly in children (Sarnat, 1992). They have also been associated with dyslexia (Galaburda, 1993), as well as other, non-genetically determined conditions. Only a small fraction of all known human NMD is genetic in origin, the majority being secondary to acquired lesions of the brain (e.g. infectious, hypoxic-ischemic, toxic or metabolic) (Sarnat, 1992).

In humans, most of the already known gene mutations causing NMD produce a severe phenotype, which usually includes epilepsy and mental retardation. These conditions include the X-linked and non X-linked (Chr.17) lissencephalies, the condition known as subcortical band (or laminar) heterotopia (SCBH)/Lissencephaly spectrum, bilateral periventricular neuronal heterotopia (BPNH). The lissencephalies comprise several syndromes having in common a brain lacking sulci, usually with a thick and disorganised cortical ribbon (Friede, 1989b). In subcortical band (or laminar) heterotopia (SCBH), a band of heterotopic neurons is situated beneath the cortex and parallel to it. Between the two lies a layer of white matter. The mutated gene, *doublecortin*, has been cloned. In bilateral periventricular neuronal heterotopia, nodules of differentiated heterotopic neurons protrude into the lateral ventricles. Genes involved in patterning of the forebrain, such as *PAX6,* have also been shown to be associated with neuronal migration defects (Table 1.1).

More subtle neuronal migration disorders include minor defects collectively known as microdysgenesis. The genetic origin of the latter is unclear, yet they may also be the source of significant disability (due to resulting epilepsy) or learning difficulties (e.g. dyslexia). Figure 1.7 illustrates the various types of human cerebral microdysgenesis, based on the review of Meencke and Veith (1992) .

Microdysgenesis includes subpial aggregates of neurons (1), a diffuse (2) or focal (3) increase of neuronal density in layer I, (4) and (5) irregularity of the upper border of layer II, (6) cell-free spaces, (7) and (8) minor abnormalities in

Table 1.1

Genetic mutations in human neuronal migration defects (NMD)

Syndrome	Gene	Chr.	Type of mutation	Gene	Pathology	Phenotype	Ref.
FCMD	*?*	9	Insertion in 3'utr	Fukutin	Lissencephaly Leptomeningeal heterotopia Polymicrogyria possible	Muscular dystrophy Mental retardation, epilepsy.	1
Miller-Dieker lissencephaly	*LIS1+ contiguous gene(s)*	17	Deletions of Lis1 and contiguous genes	Pafah1b1	Lissencephaly (more severe in posterior regions), polymicrogyria, glio-neuronal heterotopias, agenesis of the corpus callosum, cerebellar hypoplasia	Epilepsy Mental retardation Characteristic facial malformation	2
ILS	*LIS1*	17	Small deletions of *Lis1*	Pafah1b1	Lissencephaly	Epilepsy Mental retardation	3
X-linked lissencephaly/ subcortical band heterotopia	*doublecortin*	X	Protein truncation mutations, single aa substitution	Doublecortin	Females: Subcortical band heterotopia. Males: lissencephaly (more severe in anterior regions)	In males, phenotype is similar to that of Chr. 17 lissencephalies (epilepsy, mental retardation). Phenotype is milder in affected females.	4
BPNH	*?*	X	Inverted duplication Xq28	?	Periventricular nodules of heterotopic neurons	Females: Epilepsy, normal or near normal intelligence. Males: mental retardation, epilepsy, other malformations, high prenatal lethality	5
Aniridia,	*PAX6*	11	Point mutations, splicing errors, deletions, insertions	Pax6	Abnormal stratification, polymicrogyria, absent c.callosum, reduced numbers of neurons. Single cavity. In cerebellum, dysplasia	Aniridia, anophthalmia, congenital cataracts, other cranio-facial malformations.	6

References (Ref.) - 1: Takada *et al.,* 1987; Kobayashi *et al.,* 1998; Nakano *et al.,* 1996; Sarnat, 1992. 2: Chong *et al.,* 1997; Adachi *et al.,* 1997; Dobyns *et al.,* 1999; Hattori *et al.,* 1994; Friede, 1989. 3: Chong *et al.,* 1997; Dobyns *et al.,* 1999; Adachi *et al.,* 1997. 4: Gleeson *et al.,* 1998; Dobyns *et al.,* 1996; Ross *et al.,* 1997; Gleeson *et al.,* 1999; Des Portes *et al.,* 1998. 5: Dobyns *et al.,* 1997; Dobyns *et al.,* 1996. 6: Glaser *et al.,* 1994; Jordan *et al.,* 1992. FCMD-Fukuyama congenital muscular dystrophy. Pafah1b1: Platelet activating factor acetylhydrolase, isoform ib, beta 1 subunit. aa: aminoacids. Chr: chromosome. ILS-isolated lissencephaly sequence. BPNH-bilateral periventricular nodular heterotopia.

Figure 1.7

Types of microdysgenesis

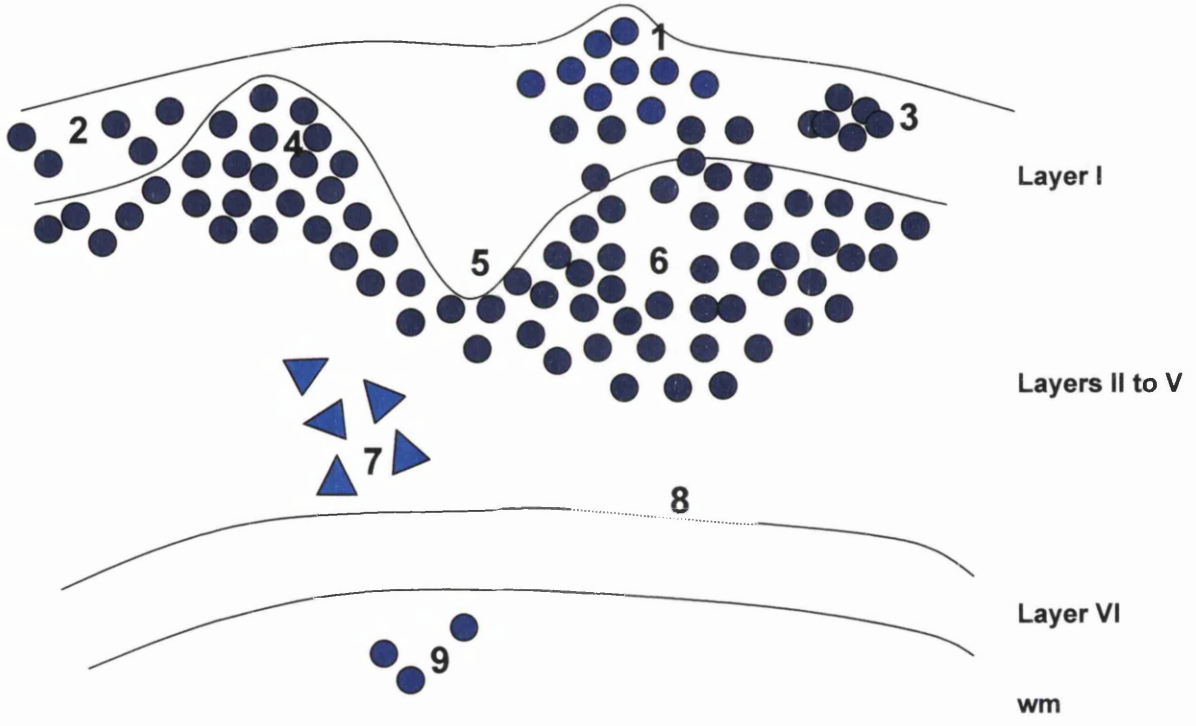

Focal protrusions of neurons (1), a diffuse (2) or nodular (3) increase in layer I neuronal density, digitations of layer II into layer I, hollows (5), neuron-free spaces (6), disturbances of cytoarchitecture in the layers below (7), including blurring of the border between adjacent layers (8) and heterotopic neurons (9) in the subcortical white matter (wm). Based on Meencke and Veith, 1992.

cytoarchitecture of deeper layers, and (9) heterotopic neurons in the white matter. These pathological features are strikingly characteristic of the findings in the brains homozygous for the *dreher* (*dr*^{J}) mutation in the present study.

1.5. Genetic animal models of neuronal migration defects

The analysis of genetic animal models has enabled dissection of the cellular and molecular mechanisms involved in normal brain formation, particularly in the process of corticogenesis.

Mouse mutations causing neuronal migration defects include apoptosis-related molecules such as CPP-32, molecules that are crucial for migration itself (Reelin, Mdab1 and Cdk5 and its receptor p35), as well as those which seem to be important for neuron-glial interactions (e.g. ErbB2, a receptor for Neuregulin) and those necessary for the integrity of the pial-glial barrier (e.g. the defective protein of the MARCKS mutant mouse) (Table 1.2). See also Table 6.8. The nature of the predisposition in New-Zealand Black mice is unknown. These mice are considered models for the cortical abnormalities found in human dyslexic patients (see Chapter 6).

Table 1.2

Murine models of neuronal migration defects

Mutant/ K.O.	Gene	Chr.	Type of mutation	Gene product	Phenotype	Pathology	Ref
reeler	*Reln (reelin)*	5	spontaneous	Reelin	Unstable gait, trmors	Aberrant axonal trajectories in the cortex Inverted cortex MZ absent	1
cdk5- deficient	*Cdk5 (cyclin-dependent kinase*	5	K.O.	*cdk5*	Late embryonic or perinatal lethality	Abnormal cortical lamination	2
p35-deficient	*Cdk5r (cdk5 regulatory subunit)*	11	K.O.	p35	Adult lethality (>=3w.), possibly because of seizures. Viable, fertile	Similar to reeler(inverted order of cortical layers(BrdU). No lamination of neocortex. Abn. orientation of pyr cell soma and dendrites Aberrant fibre fascicles running through neocortex. Layer I present	3
yot (yotari)	*Mdab1 (mouse disabled 1)*	NR	K.O.	NR	Unstable gait, tremors	Similar to reeler	4
scr (scrambler)	*Mdab1 (mouse disabled 1)*	4	spontaneous	NR	Scrambler;Viable> 1 year. Body tremor Small size. Unstable gait	Similar to reeler Scattering of pyramidal and granule cells	5
Sey (Small eye)	*Pax6 (Paired box 6)*	2	spontaneous	Pax-6	Aplasia of eyes, nasal cavities, olfactory bulbs and perinatal lethality in homozygotes.	Forebrain patterning defects. In developing cerebral cortex: No MZ. CP extends to pial border. Reduced number of cells in CP. Increased numbers of proliferative cells. Intracortical and leptomeningeal heterotopias	6

Table 1.2 (cont.)

Mutant/ K.O.	Gene	Chr.	Type of mutation	Gene product	Phenotype	Pathology	Ref.
Pafah1b1	*Pafah1b1*	11	K.O.	Pafah1b1	Embryonic lethality among homozygotes	Deficient laminar organisation, with blurring of the boundaries between layers. MZ is present. Frontal regions are the most severely affected.	7
CPP32-deficient	*Casp3*	8	K.O.	Caspase 3	Smaller at birth. Die at 1-3w PN. Embryonic lethality likely (E12 ratios normal)	Decreased apoptosis in developing cortex Ectopic cell masses (neurons and astrocytes) beneath the cerebral cortex. No distinct lamination of overlying cortex. Protrusions of brain tissue through skull.	8
MARCKS-deficient	*Macs*	10	K.O.	MARCKS	Perinatal lethality.	Decreased CSPGs in marginal zone Disruption of the *glia limitans*. MZ and leptomeningeal heterotopias.	9
NZB	Unknown	Unknown	Unknown	Unknown	Learning disabilities	Discrete areas of layer I heterotopias (usually in somatosensory cortex). Neuron-free spaces and disruption of radial glial fibres in the layers below.	10
dr^{J} (dreher^{J})	Unknown	1	spontaneous	Unknown	Circling Deafness White belly spots	Diffuse and nodular collections of neurons in layer I. Neuron –free spaces in layers II to VI	11

Pafah1b1: Platelet activating factor acetylhydrolase, isoform 1b, beta 1 subunit. CPP32: Caspase 3. MARCKS: myristoylated alanine rich protein kinase C substrate. NZB: New Zealand Black mouse. MZ: marginal zone; CP: cortical plate. Chr.: chromosome.
References (Ref.)- 1: D'Arcangelo *et al.*, 1995; Goffinet, 1979; 2: Gilmore *et al.*, 1998; Ohshima *et al.*, 1996; 3: Chae *et al.*, 1997; 4: Sheldon *et al.*, 1997; 5: Sweet *et al.*, 1996; Sheldon *et al.*, 1997; 6: Stoykova *et al.*, 1996; Schmahl *et al.*, 1993; 7: Hirotsune *et al.*, 1998; 8: Kuida *et al.*, 1996; 9: Blackshear *et al.*, 1997; 10: Sherman *et al.*, 1985; Sherman *et al.*, 1992; Sherman *et al.*, 1990; 11: Sekiguchi *et al.*, 1987; Sekiguchi *et al.*, 1994.

1.6. *dreher*^{J} as a mouse model for neuronal migration defects

The *dr*^{J} mutant mouse has neocortical abnormalities that partially resemble those of New Zealand Black mice. The reported cerebral neocortical defects include diffusely distributed or clustered misplaced (i.e. heterotopic) cells in layer I, as well as neuron-free spaces in the layers below. Hence, *dreher* may provide a model for understanding the origin of microdysgenesis. The main aim of this work was to attempt at understanding the mechanisms of generation of heterotopic layer I cells in this mouse model.

1.7.Plan of the thesis

A brief outline of the contents of this thesis is given below:

This Chapter provided a brief overview of the main steps of formation of the normal cerebral cortex in mammals, and of some genetic aspects of neuronal migration disorders. Chapter 2 comprises descriptions of the methods which are common to all the studies in this thesis. Chapter 3 includes refinement of the mapping of *dreher*, which was essential for identifying the genotype of each animal in subsequent experiments. General aspects of the phenotype and descriptions of the brain abnormalities of *dr*^{J} homozygous mutants are dealt with in Chapters 5 and 6, respectively. The issue of how heterotopias are produced in the cerebral cortex of *dr*^{J}/*dr*^{J} mice is addressed in Chapter 7, through the use of *in vivo* DNA-labelling studies. In Chapter 8, remaining questions and possible future investigations on this mouse mutant are discussed.

Chapter 2

General methods

2.1. Introduction

Breeding of *dr*^{J} mice, generation of experimental litters and genotyping of each animal were essential steps underlying all studies contained in this thesis. Most of the materials and methods involved in those procedures are described in the present Chapter. Details concerning DNA markers used for genotyping can be found in Chapter 3. Other methods specific to an experiment or set of experiments are described within the corresponding chapter.

2.2. Animal breeding and maintenance

Heterozygous *dr*^{J} mice of the B6C3Fe-a/a-*dr*^{J} strain (which originated as a C3H/He x C57BL/6 F_1 hybrid) were purchased from the Jackson Laboratory, Bar Harbor, U.S.A. Mice were kept in the animal house of the Institute of Child Health, with free access to food and water. They were maintained on a 16-hour light, 8-hour dark cycle with the dark period centred on 1 a.m.

The *dr*^{J} colony used in these studies originated from a single pair of heterozygous mice (see section 3.3.1. for further details). Female offspring of the original breeding pair were mated to their father and heterozygous mice (*dr*^{J}/+) of subsequent generations were interbred, avoiding brother-sister matings whenever possible. Occasionally, breeding pairs were set between a heterozygous mouse (*dr*^{J}/+) and a wild-type one (+/+).

2.3. Generation of experimental litters

Experimental litters were usually generated by crossing *dr*^{J}/+ males to females of the same genotype. When timed pregnancies were necessary for experiments, animals were placed together overnight. Pregnancy was ascertained by the presence of a vaginal plug on the following morning between 9 and 9:30 a.m. Twelve o'clock noon of the day the copulation plug was found was considered to be embryonic day 0.5 (E 0.5).

2.4. DNA extraction and PCR amplification for genotyping

Genotyping was done in each case by PCR amplification of polymorphic DNA sequences in the vicinity of the *dreher* locus. The primers used for amplification of polymorphic DNA sequences were microsatellite markers flanking *dreher* proximally (*D1Mit452*) and distally (*D1Mit15*). Details of microsatellite markers can be found in Chapter 3 ("Mapping studies of the *dreher* gene").

2.4.1 Collection of tissue for DNA extraction

Whenever embryos were necessary for experiments, pregnant females were killed by cervical dislocation and the embryos were dissected from the uterus in Dulbecco's Modified Eagle's Medium (DMEM, Gibco BRL) containing 10% fetal calf serum, and washed in phosphate buffered saline (PBS). For embryos of 11.5 days or less, the yolk sac was rinsed in PBS (to avoid contamination with maternal blood) and used as the source of DNA. Fetuses and postnatal mice

underwent a tail biopsy, involving the whole tail (fetuses) or just the tailtip (all mice in the postnatal period). As a general rule, and for breeding purposes, mice were tail-tipped at weaning age, i.e., at 3 weeks of postnatal life. Each mouse was ear-marked on that occasion, ensuring its correct identification at a later date. Younger mice (less than 3 weeks of age) were genotyped for specific purposes, e.g. for birthdating studies (see Chapter 7). The procedure followed was similar to that described below for mice of weaning age.

2.4.2. Crude DNA extraction for amplification by the polymerase chain reaction

Three different methods were used. Initially, potassium acetate precipitation and phenol-chloroform extraction were tried. Subsequently, a faster and simpler method was optimised that yielded DNA of sufficient quality for genotyping. The latter was adopted for its simplicity and speed.

2.4.2.1. Preparation of DNA using potassium acetate precipitation

A fragment of tissue (e.g. a tailtip, 1-2 mm long) was incubated for at least 3 hours (usually overnight) at 52-55ºC with 100 µl of 10 mg/ml fungal proteinase K (Promega) and 900 µl of proteinase K buffer (0.1 M ethylenediaminetetraacetic acid [EDTA] pH 8.0, 0.2 M Tris(hydroxymethyl)aminomethane [Tris]-HCl pH 8.5, 1% sodium dodecyl sulphate [SDS]). Five hundred microliters of the digest thus obtained was used for DNA extraction. The remainder of the digest was stored at –20ºC. Protein was precipitated from the supernatant by adding 0.2 volume 5 M potassium acetate and incubating on ice for 30 minutes. Next, the protein precipitate was removed by centrifugation at 13,000 rotations per minute (rpm) at 4°C for 10

minutes. DNA was precipitated from the supernatant by the addition of 2 volumes of ice-cold 99% ethanol followed by incubation at -20°C for 30 minutes. The DNA was pelleted by centrifugation at 13,000 rpm for 10 minutes at 4°C, washed in 70% ethanol and re-suspended in 50 μl distilled water.

2.4.2.2. Phenol-chloroform extraction

DNA was obtained by phenol extraction. Briefly, a fragment of tailtip was incubated with 100 μl of 10 mg/ml proteinase K and 900 μl of proteinase K buffer. Protein digestion was carried out for a minimum of 4 hours at 52-55°C. Five hundred microliters of the digest were used for DNA extraction. An equal volume of equilibrated phenol was added to the digest, homogenised and spun for 3 minutes at 12,000 rpm at room temperature, to remove any remaining protein. The aqueous phase was transferred into a new microfuge tube. The phenol extraction was repeated once. Chloroform was then added and the tube was homogenised with a vortex and spun for 15 seconds at 12,000 rpm (room temperature), to remove the phenol. The upper, aqueous (DNA-containing) phase was transferred into a new microfuge tube. DNA was precipitated with an equal volume of isopropanol at - 20°C for at least 2 hours. Tubes were spun at 13,000 rpm for 20 minutes at 4°C. At each step the samples were mixed gently to avoid shearing the DNA. The supernatant was discarded and the pellet was washed with 500μl of 70% ethanol, by mixing and spinning for 5 minutes at 13,000 rpm at 4°C. The supernatant was again discarded and the pellet was air-dried, then re-suspended in 20-50 μl of distilled water.

2.4.2.3. Quick method of DNA extraction

This quick preparation of DNA was already in use for embryonic DNA in our laboratory. Minor adjustments were required in the volume of the various solutions to account for larger samples of tissue. In the case of tail tip fragments from weaners or younger mice, a fragment of tail tip (about 1 to 2 mm long) was incubated for a minimum of 4 hours with 50 µl of 10 mg/ml fungal proteinase K (Promega) and 450 µl of PBS in a microfuge tube at 52-55°C. When yolk sacs were used, 20 µl of 10 mg/ml fungal proteinase K and 180 µl of PBS were added and digestion was allowed to proceed for an hour. When digestion was completed, tubes were vortexed, heated at 100°C for 5 minutes and spun for 1 minute at 13,000 rpm (at room temperature). The supernatant was collected into a new tube and used for PCR reactions.

2.5. Amplification of DNA by the polymerase chain reaction (PCR)

2.5.1. Rationale of the polymerase chain reaction

The polymerase chain reaction (PCR) is a rapid and efficient technique used to produce large numbers of copies of a particular DNA sequence without resorting to cloning. PCR employs two oligonucleotide primers, one designed to a sequence on the (+) DNA strand and the other to the reverse sequence on the (-) strand, a mixture of deoxynucleotides and a thermo-stable DNA polymerase to amplify specific DNA sequences. Repeated cycles of denaturation, annealing and extension are used to generate multiple copies of the DNA that lies between the two primers.

2.5.2. Designing and synthesising primers for PCR

PCR primers for microsatellite analysis were either synthesised on an Applied Biosystems 381A DNA Synthesizer by Dr Paul Rutland (Institute of Child Health, London) or were obtained from Genosys (Cambridge, UK).

Primers were designed to be 18-22 nucleotides in length with a G/C content of 50-60%. The primer sequences were chosen to avoid palindromic regions (which could result in hairpin formation), as well as complementarity between the 3' ends of the primer pair (which could lead to the formation of primer-dimers). Runs of Gs or Cs at the 3' ends of primers were also avoided, as this could lead to mispriming in G/C-rich regions.

2.5.3. Basic PCR protocol

PCR reactions were performed in 0.5 ml thin-walled microfuge tubes, usually in a total volume of 25 microliters. A single mix for all the reactions to be used was first prepared containing, for each reaction, 1x NH_4 reaction buffer (16 mM ammonium sulphate, 67 mM Tris-HCl and 0.01% Tween 20 per reaction-Bioline), 0.8-1.5 mM $MgCl_2$ (depending on primer pair), 0.1 to 0.2 mM each deoxynucleoside triphosphate (dNTP, Promega), 0.5 to 1 mM forward and reverse primers and 1 Unit of *Taq* or Biopro polymerase (Bioline). Two microliters of DNA template were used for each PCR reaction, whatever the method of DNA extraction. Each batch of reactions included a negative control tube, in which no DNA was added. Each sample was overlaid with 2 drops of mineral oil to prevent evaporation, then loaded into the thermocycler (Hybaid Omnigene). The cycling reactions involved an initial denaturing step of 95°C for

5 minutes, followed by 30 to 35 amplification cycles (depending on method of DNA extraction) consisting of three phases: 92ºC for 1 minute (denaturation), 55-62°C, depending on primer pair, for 1 minute (primer annealing) and 72°C for 1 minute (primer extension). A final step of 72ºC for 10 minutes ensured that the PCR products were full length.

2.5.4. Optimising PCR reactions

The precise reaction conditions varied, depending on the primers used, and the optimal conditions for each primer pair were determined experimentally. Primer pairs were tested initially with 1.5 mM magnesium in the reaction mix, and with an annealing temperature suggested by their GC content, or starting with 55ºC. If the specificity of the reaction needed to be increased, the magnesium concentration was decreased to 1.0 mM and the annealing temperature was increased in steps of 2°C (up to 62°C), until the bands were clear but no (or few) non-specific bands were amplified. If the initial attempt yielded no bands, the reaction specificity was decreased by increasing the magnesium concentration (in 0.5 mM increments up to 4.0 mM) and by lowering the annealing temperature of the cycling reaction in steps of 2°C (down to 49°C). In the case of one of the primer pairs (*D1Mit452*), the above-mentioned techniques yielded only very faint bands. To solve this problem, cycling reactions with *D1Mit452* included an initial step of DNA denaturation, without *Taq* polymerase in the reaction, after which the polymerase was added and the reactions were allowed to proceed as usual. This modification of the PCR protocol produced a significant improvement in the brightness of bands as seen on 4% agarose gels.

2.5.5. Separation and visualisation of PCR products

PCR amplification products were separated by horizontal gel electrophoresis in Horizon gel tanks (Gibco BRL), using ethidium bromide-stained agarose gels in TAE buffer (10 x TAE = 0.4 M Tris-acetate pH 7.0, 10 mM EDTA). The agarose concentration varied according to the size of the DNA products and the degree of resolution required. In general, PCR products for genotyping were small (100-300 bp) and high resolution was required to distinguish alleles with a size difference of only 6-20 bp. Therefore, 4% gels were used (a ratio of low melting point (LMP) agarose to normal agarose of 3:1 in 1x TAE running buffer). Gels with agarose concentrations of 1% were used to analyse DNA fragments of larger sizes where low resolution was needed, or when bands obtained by PCR amplification were of very different sizes (e.g. size difference of 92 bp in the case of *D1Mit200* - see Chapter 3). Gels made with 1% low melting point (LMP) agarose were used for the purpose of DNA purification. Depending on the number of samples to be analysed, gels were prepared as either midi-gels (11 x 14 cm) or mini-gels (5.7 x 8.3 cm). Product sizes were determined by running DNA markers alongside the DNA sample. The DNA marker used most commonly was the 1 kb ladder (Gibco BRL), but a 123 ladder, another marker from the same manufacturer, was also used. Typically, 3 µl of loading buffer (prepared by mixing 10% glycerol in ddH_2O with an amount of Orange G powder sufficient to colour the solution deep orange) was added to 10-15 µl of PCR product. Ethidium bromide (20 mg/ml) which intercalates into DNA and fluoresces in long-wave UV light, was added to both running buffer and agarose solution at a concentration of 0.5 µg/ml, to allow for visualisation of size-fractionated DNA bands by U.V. transillumination. Electrophoresis was allowed to proceed for 1 to 3 hours at 70-90 V.

Gels were visualised and photographed using a Polaroid camera (BioRad) or a Mitsubishi Video Copy system connected to a long-wave UV transilluminator (see Figure 3.3. for an example). Details of the *dreher* and the wild-type allele band sizes for each microsatellite marker can be found in Chapter 3.

Chapter 3

Mapping studies of the *dreher* gene

3.1. Introduction

This chapter describes the construction of a genetic map, using molecular markers, around the *dreher* locus on mouse Chromosome 1. The reasons for this mapping exercise were severalfold. First, accurate genotyping of each dr^J mouse was a pre-requisite for both breeding and experimental purposes throughout the studies of this thesis. Genotype at the *dreher* locus cannot be ascertained reliably by phenotypic characteristics alone: wild type and heterozygous mice are externally normal, and thus indistinguishable from one another. Test-breeding with a known heterozygote, in order to determine whether homozygous offspring are produced, is a possible method for distinguishing heterozygotes from wild type mice, but is a lengthy, costly procedure and does not permit genotyping of embryos or young animals. Therefore, it was necessary to identify closely linked polymorphic genetic markers that could be used to determine genotype independently of phenotype. This procedure also enabled confirmation of the reported full penetrance of the circling phenotype in the homozygous mutant mice. Another reason for constructing a detailed map around the *dreher* locus was to provide a starting point for future identification of the gene that is mutated in dr^J mice, either by positional cloning or by assessment of candidate genes in the region.

3.1.1 Previous mapping studies

At the time the present studies were performed, previously published mapping data on *dreher* alleles had relied solely on three-point crosses against visible and biochemical markers (Washburn and Eicher, 1986; Lyon, 1961). The first mapping study performed on *dreher* mice was that of Lyon (1961), who

conducted linkage tests with recessive and dominant markers, by crossing homozygous mutant *dreher* mice with animals from different linkage stocks. *Dreher* was included in linkage group XIII, the gene order being: *dr (dreher)* 22.3 ± 4.1% - *Dh* (*Dominant hemimelia)* 1.9 ± 1.3% - *In* (*leaden).*

More recently, an autosomal recessive mutation, sst^{2J}, was described (Washburn and Eicher, 1986) that proved to be allelic with sst^{J} (*shaker-short tail J*) and *dreher.* In order to map sst^{2J}, AKR/J-sst^{2J}/+ mice were crossed with C57BL/6 and the heterozygous F_1 offspring were intercrossed. The genotype for various polymorphic isoenzymic loci was determined in a total of 68 meiotic events within the F_2 mutant progeny. The position of the sst^{2J} gene, according to these results, was: *Pep-1 (dipeptidase-1)* - 19.1+/- 4.8 – sst^{2J} - 13.2 +/- 4.1 - *Akp-1 (alkaline phosphatase-1)*, on mouse Chromosome 1. The authors suggested that the mutation should be renamed *dreher-2J* (dr^{2J}).

No further mapping data on *dreher* or its alleles had been published since that study. According to the Mouse Genome Database (MGD), at http://mgd.hgmp.mrc.ac.uk, and the Mouse Chromosome Committee Report, the assigned position for the *dreher* locus at the start of the present studies was 88.5 cM from top of mouse Chromosome 1 (Figure 3.1). Figure 3.2 depicts the relative position of two *dreher* alleles in relation to other genes in previous mapping studies, in comparison with the localisation of *dreher* in a more recent (1997) map of mouse Chromosome 1.

The large distances between *dreher* and the visible and biochemical markers used in the previous mapping studies (and therefore the large number of

Figure 3.1

Mouse chromosome 1 consensus map in the region of *dreher* at the start of these studies

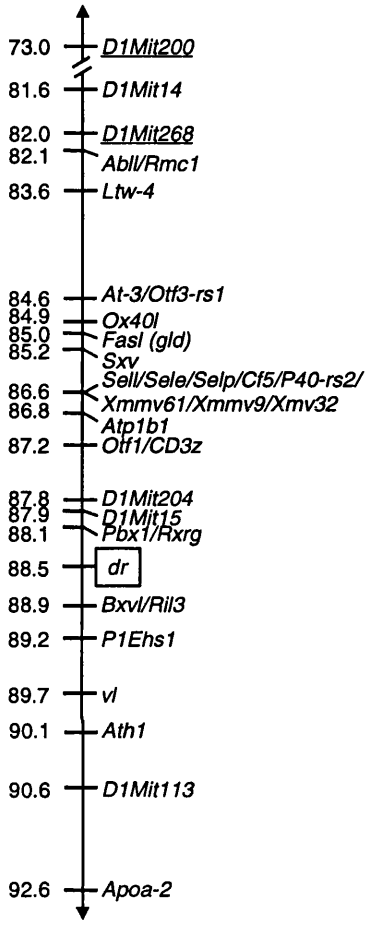

Distances are in centimorgans (cM). Adapted from Seldin (1994). Note that *D1Mit200* and *D1Mit268* (two of the microsatellite markers used for the mapping study) were not included at that time in the consensus map. *D1Mit200* has since been included at 73.0 cM and *D1Mit268* at 82.0 cM (underlined).

Figure 3.2

Comparative chart illustrating previous mapping data on two *dreher* alleles

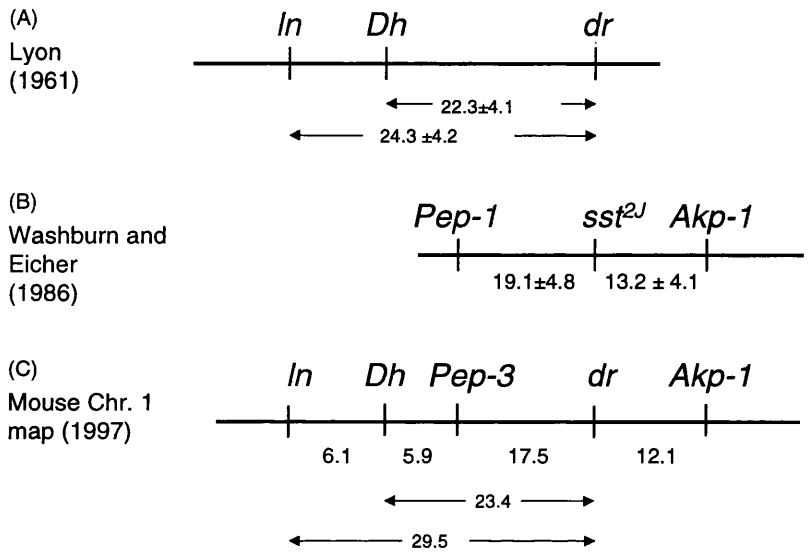

(A) Mapping data on *dreher (dr)*; **(B)** mapping of its allele *dreher-2J* (*dr*^{2J}), formerly known as *shaker short tail-2J* (*sst*^{2J}); **(C)** the position of *dreher* in the MGD consensus map of mouse Chromosome 1 (1997). Gene names are as follows: *In, leaden; Dh, dominant hemimelia*; *Pep-1, dipeptidase-1; Pep-3, peptidase-3; Akp-1, alkaline phosphatase-1. Pep1* (previously known as *dipeptidase 2*) maps to mouse Chromosome 18 in the 1997 consensus map. Although no information could be obtained on renaming of *Pep-1*, a gene from the same isoenzyme family (*Pep3*) was found approximately at the expected position for *Pep-1* on distal mouse Chromosome 1. *Pep3* (assigned in 1993) was previously known as dipeptidase 1 (*Dip-1*).

animals that are expected to be recombinant within each interval) renders these markers unsuitable for the systematic genotyping of mice. The advent of closely spaced microsatellite DNA markers, on the other hand, offered the possibility of identifying tightly-linked markers for *dreher*.

3.1.2. Rationale for using polymorphic microsatellite DNA markers in the mapping of *dreher*

Microsatellite DNA markers (also called simple repetitive elements, simple sequence repeats or simple sequence length polymorphisms) are short di-, tri- or tetranucleotide DNA repeats that are distributed throughout mammalian genomes and have been found to be highly polymorphic. They provide a rapid and reliable system for genetic analysis (Dietrich *et al.,* 1994; Love *et al.,* 1990). It has been estimated that 98.8% of the mouse genome lies within 2.2 cM of a microsatellite marker, therefore enabling any gene to be mapped to high resolution (Dietrich *et al.,* 1994). Microsatellites can be analysed by PCR using primers flanking the repetitive sequence, and in a majority of cases, the size difference between alleles enables resolution through agarose gel electrophoresis (Dietrich *et al.,* 1992; Cornall *et al.,* 1991; Dietrich *et al.,* 1994). The likelihood that any particular microsatellite marker thus generated is polymorphic between different inbred laboratory strains is around 50% (Dietrich *et al.,* 1992; Dietrich *et al.,* 1994). Detailed lists and genetic maps of microsatellites spanning a part or the whole of the mouse genome have been generated (Hearne *et al.,* 1991; Dietrich *et al.,* 1992; Cornall *et al.,* 1991; Dietrich *et al.,* 1994) and integrated with other mouse genetic maps (Seldin, 1997; Copeland *et al.,* 1993).

At the time my studies were conducted, the *dreher* locus could be found in a current consensus map, in the close vicinity of several microsatellite markers (Figure 3.1) (Seldin, 1997). However, the *dreher* gene had not been mapped directly against any of these microsatellites. In order to determine the genotype of each mouse at the *dreher* locus, several polymorphic microsatellite markers situated near *dreher* were first used to create a map of that region. Subsequently, the two closest flanking markers (situated on each side of *dreher*) were selected and used systematically for genotyping purposes.

3.2. Materials and Methods

3.2.1. Animals

General maintenance of animals was as described in Chapter 2. For mapping purposes, heterozygous (*dr^{J}/+*) animals were mated with wild-type (*+/+*) or *dr^{J}/+* mice from the same genetic background, which originated as a C3H/He x C57BL/6 F_1 hybrid.

3.2.2. Microsatellite DNA markers

Six DNA microsatellite markers situated in the region of *dreher*, *D1Mit200*, *D1Mit14*, *D1Mit268*, *D1Mit452*, *D1Mit15* and *D1Mit113*, were selected after searching both the MGD and the Whitehead Institute for Medical Research databases (obtained via internet at http://mgd.hgmp.mrc.ac.uk and at genome_database@genome.wi.mit.edu). These markers were all reported to detect polymorphisms between the two strains from which the *dr^{J}* genetic background was derived (C3H/He and C57BL/6) and therefore were likely to be informative in the present mapping studies. PCR oligonucleotide primer sequences (Table 3.1) were obtained for each microsatellite via Internet, either through an e-mail server (at mapbase@genome.wi.mit.edu) from the Whitehead Institute for Medical Research, M.I.T. (Massachusetts Institute of Technology), or from the Mouse Genome Database (MGD), Jackson Laboratory. Primers were synthesised by and obtained from Genosys, U.K. Each mouse used in the mapping study was tested with all 6 markers. Another two microsatellites, *D1Mit506* and *D1Mit204*, (reported to map to the *D1Mit452-D1Mit15* interval) were used on a subset of animals only.

Table 3.1

Microsatellite details

Marker		PCR primer sequence	PCR product size (bp)	
Name	Position (cM)		C3H/He allele	C57BL/6 allele
D1Mit200	77.9	(F) GCCATGTTCATGTACATAGGTAGG (R) ATGGATGGATGGTTTTCCTG	205	297
D1Mit14	82.4	(F) GCCAGACAGGGCTACATTGT (R) AGACTGAACTCTGGCCTCCA	180	202
D1Mit268	82.9	(F) CATCTTGATGCAGAGGCATG (R) AAACTGGGTTTGCAGACACC	131	123
D1Mit452	84.6	(F) ACACATCTATATCACTGCCCCC (R) ATCTCATTCCTGAGCCTTATGTG	98	92
D1Mit506	84.6	(F) CAGGCTCAGCATCAAATGAA (R) TTCCTCTTTACCTAAAGCACGC	120	123
D1Mit 204	85.8	(F) TCCCCCTCCAGGTAAAATGAA (R) TAAGAAATAAGGGAATTCTG	125	119
D1Mit15	86.9	(F) TCCACAGAACTGTCCCTCAA (R) ATACACTCACACCACCCCGT	160	183
D1Mit113	90.3	(F)CCTCAAAATCAGGATTAAAAGGG (R) ACATGGGGTGGACTTGTGAT	206	224

Microsatellite loci positions are given in centimorgans (cM) from top of mouse Chromosome 1. Data on relative marker positions, oligonucleotide sequences and interstrain polymorphisms were obtained at mapbase@genome.wi.mit.edu (1995). Forward (F) and reverse (R) oligonucleotide sequences are shown. Expected size of amplification products is given in base pairs (bp) for the C3H/He (*dr*-linked) and C57BL/6 (*+*-linked) alleles. *D1Mit506* was used in all cases of meiotic recombination between *D1Mit268* and *D1Mit15*. *D1Mit204* was not informative. The other 6 markers were used to genotype all mice included in the study.*D1Mit506* and *D1Mit204*, (reported to map to the *D1Mit452-D1Mit15* interval) were used on a subset of animals only.

3.2.3. DNA extraction and PCR reactions

Genomic DNA was prepared from tail tip biopsies performed at three weeks post-natally, as described in Chapter 2. Two microliters of this template were used for each PCR reaction, which included NH_4 buffer (16 mM ammonium sulphate, 67 mM Tris-HCl and 0.01% Tween 20 per reaction), 0.8 to 1.5 mM $MgCl_2$, depending on primer pair, 0.1 to 0.2 mM each dNTP, 0.5 to 1 mM each primer and 1 Unit of Taq polymerase (Bioline). The number of amplification cycles was 30 for DNA extracted through the potassium acetate and phenol-chloroform methods, and 35 for DNA prepared by the "quick method" for PCR (see Chapter 2). PCR amplification products were electrophoresed through 4% ethidium bromide-stained agarose gels (except for those amplified with *D1Mit200*, which were run on 1% agarose gels), and analysed by U.V. transillumination. A typical gel is shown in Figure 3.3.

Figure 3.3

Typical PCR profile after amplification with D1Mit15 primers and electrophoresis through a 4% agarose gel

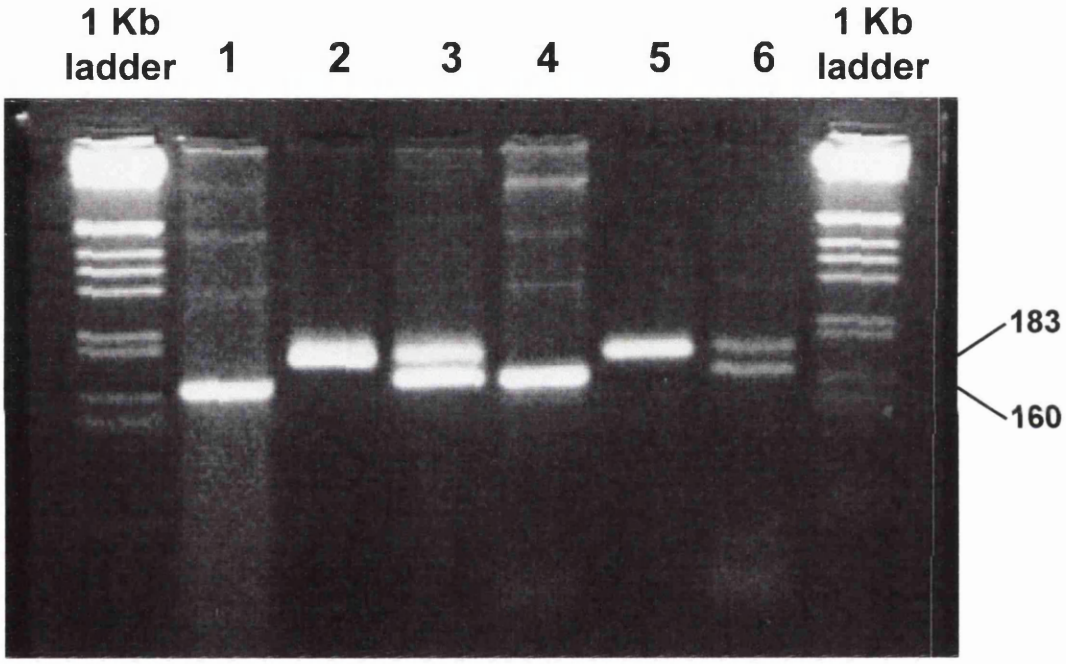

Expected band sizes are 183 bp for the C57BL/6-type allele (+) and 160 bp for the C3H/He-type allele (dr^J). Molecular marker used is a 1 Kb ladder (Gibco). The gel was run for 1.5 hours at 90 V. Lane 1: dr^J/dr^J. Lane 2: +/+. Lane 3: dr^J/+. Lane 4: dr^J/dr^J. Lane 5: +/+. Lane 6: positive control (dr^J/+). Although not shown here, a negative control (no DNA in the PCR reaction) was included in every PCR run.

3.3. Results

3.3.1. Confirming polymorphisms of microsatellite markers

Four heterozygous *dr*^{J} mice (two males and two females) were obtained from the Jackson Laboratories (Bar Harbor, Maine, U.S.A.), in order to found a breeding colony, and were tested with the six microsatellite markers (*D1Mit200*, *D1Mit14*, *D1Mit268*, *D1Mit452*, *D1Mit15* and *D1Mit113*). One male and one female proved to be heterozygous for alleles at every one of these loci and these mice were used as founder mice. The other two animals had recombinant genotypes, with homozygosity at one or more loci, presumably as a result of previous recombinant events in the vicinity of the *dreher* locus since the origin of the mutation in a C3H/He x C57BL/6 F_1 hybrid mouse. These recombinant animals were not used for subsequent breeding.

Although the six markers used initially to genotype all 188 mice in the mapping study proved to be informative in our cross, *D1Mit204* was found not to show the reported polymorphism between the C3H/He and C57BL/6 strains (according to the Whitehead Institute/MIT Center for Genome Research, at mapbase@genome.wi.mit.edu), and so its use was discontinued. *D1Mit506* (a marker co-localising with D1Mit452) was tested in all cases of meiotic recombination between *D1Mit268* and *D1Mit15*. The expected interstrain polymorphism with *D1Mit506* was confirmed, but this marker was found to co-segregate with *D1Mit452* in every case, and so its use did not provide additional mapping information. Unfortunately, at the time of the study, no other polymorphic microsatellite markers that could be analysed by agarose gel

electrophoresis were available in the *D1Mit452-D1Mit15* interval in order to provide a fast and more precise positioning of the *dreher* gene.

3.3.2. Full penetrance of the circling phenotype

Discounting those mice with meiotic recombinations between the flanking markers and *dreher*, all other circling mice proved to be *D1Mit452*$^{drJ/drJ}$/*D1Mit15*$^{drJ/drJ}$, and their genotype at the *dreher* locus was therefore considered to be dr^J/dr^J. Conversely, all animals showing a *D1Mit452*$^{drJ/drJ}$/*D1Mit15*$^{drJ/drJ}$ genotype displayed circling behaviour. This means that, in our colony, the circling phenotype is a fully penetrant trait, and that dr^J is a truly recessive mutation. Therefore, where meiotic recombination occurred between one of the flanking markers and *dreher,* and where one of the flanking markers genotyped as dr^J/dr^J (*D1Mit452* $^{drJ/drJ}$ or *D1Mit15* $^{drJ/drJ}$), the genotype at the *dreher* locus was inferred from the presence or absence of the circling phenotype (Table 3.2, lines 6-9).

3.3.3. Distinguishing between wild-type and heterozygous dr^J mice in cases of meiotic recombination between the two flanking markers

Mice with a normal external phenotype and recombinant genotypes (i.e. different PCR product patterns for *D1Mit452* and *D1Mit15*) included in our mapping study were test-bred with a known heterozygote, in order to determine their genotype at the *dreher* locus (Table 3.2, lines 4 and 5). Mating was stopped when one or more circling animals were found in the progeny (thus, confirming heterozygosity) or when there were only normal animals in the

Table 3.2

Genotype at microsatellite loci and inferred genotype at the *dreher* locus

	External phenotype	Observed genotype, *D1Mit452* locus	Observed genotype, *D1Mit15* locus	Inferred genotype, *dreher* locus
1	normal	*D1Mit452*$^{+/+}$	*D1Mit15*$^{+/+}$	+/+ (non-recombinant)
2	normal	*D1Mit452*$^{drJ/+}$	*D1Mit15*$^{drJ/+}$	dr^J/+ (non-recombinant)
3	circling	*D1Mit452*$^{drJ/drJ}$	*D1Mit15*$^{drJ/drJ}$	dr^J/dr^J (non-recombinant)
4	normal	*D1Mit452*$^{+/+}$	*D1Mit15*$^{drJ/+}$	Assessed by test-breeding[(a)]
5	normal	*D1Mit452*$^{drJ/+}$	*D1Mit15*$^{+/+}$	Assessed by test-breeding[(a)]
6	normal	*D1Mit452*$^{drJ/drJ}$	*D1Mit15*$^{drJ/+}$	dr^J/+[(b)]
7	normal	*D1Mit452*$^{drJ/+}$	*D1Mit15*$^{drJ/drJ}$	dr^J/+[(b)]
8	circling	*D1Mit452*$^{drJ/+}$	*D1Mit15*$^{drJ/drJ}$	dr^J/dr^J [(b)]
9	circling	*D1Mit452*$^{drJ/drJ}$	*D1Mit15*$^{drJ/+}$	dr^J/dr^J [(b)]

[(a)] Breeding with a known heterozygote and analysing the progeny for the presence of circling mice. [(b)] The genotype at the *dreher* locus was inferred, based on the full penetrance of the circling phenotype. See text (sections 3.3.2 to 3.3.4) for further discussion.

progeny after at least 30 offspring from consecutive litters had been examined (thus, confirming wild type genotype at the *dreher* locus).

3.3.4. Using recombinant genotypes to determine the position of *dreher*

Table 3.3 depicts a few examples of how the position of the *dreher* gene was inferred from the study of animals with recombinant genotypes in the mapping study:

Case number 15 is a circling animal that, in view of the fully penetrant nature of the mutation, must have a dr^J/dr^J genotype at the *dreher* locus. Yet, on PCR genotyping, it proved to be $dr^J/+$ at the *D1Mit200* locus ($D1Mit200^{drJ/+}$). This means that meiotic recombination had occurred between *D1Mit200* and *D1Mit14,* and that the *dreher* gene must lie distally to the breakpoint in this case. In case number 19 (see alsoTable 3.2, line 7), the animal has a normal phenotype, which means that its genotype at the *dreher* locus is either heterozygous or wild type. The *dreher* locus is therefore located proximally to the meiotic recombination breakpoint between *D1Mit452* and *D1Mit15.* In case number 38 (see also Table 3.2, line 6), the animal is phenotypically normal, showing that the *dreher* locus must lie distal to a recombination breakpoint between *D1Mit452* and *D1Mit15.*

3.3.5. Haplotype distribution and new positioning of *dreher*

A total of 345 meiotic events were scored: 314 from $dr^J/+$ x $dr^J/+$ matings and 31 from $dr^J/+$ *x* +/+ matings (Table 3.4). At least one recombination was found in each interval between pairs of adjacent markers. Eighteen recombinations were

Table 3.3

Some examples of recombinants used to infer the position of *dreher*

	Case 15 (circling)	Case 19 (normal)	Case 38 (normal)
D1Mit200	$dr^J/+$	$dr^J/+$	dr^J/dr^J
D1Mit14	dr^J/dr^J	$dr^J/+$	dr^J/dr^J
D1Mit268	dr^J/dr^J	$dr^J/+$	dr^J/dr^J
D1Mit452	dr^J/dr^J	$dr^J/+$	dr^J/dr^J
dreher *(inferred genotype)*	dr^J/dr^J	$dr^J/+$	$dr^J/+$
D1Mit15	dr^J/dr^J	dr^J/dr^J	$dr^J/+$
D1Mit113	dr^J/dr^J	dr^J/dr^J	$dr^J/+$

Genotypes at the various microsatellite loci used in the mapping study. All three animals (case numbers 15, 19, 38) were obtained from crosses between animals that showed heterozygosity at the six loci. The *dreher* interval was inferred from data obtained from these and other recombinants to lie between *D1Mit452* and *D1Mit15.* The external phenotype is shown in brackets. *+* (wild type-linked allele); *dr* (*dreher*-linked allele). Black bars indicate recombination breakpoints.

Table 3.4

Number of mice used for the mapping study according to the type of mating and number of meiotic events scored.

	Number of mice			
	Single meiotic event scored	**2 meiotic events scored**	**3 meiotic events scored**	**1 meiotic event scored**
From *dr^J*/+ x *dr^J*/+ matings	0	155	1[(a)]	1[(b)]
From *dr^J*/+ x +/+ matings	31	0	0	0
Total	188			

(a) A third meiotic event was added in one case, where one of the chromosomes underwent 1 recombination and the other recombined in 2 different intervals between pairs of markers. (b) In another case, also that of a double recombinant, the type of recombination could only be ascertained in one instance. The PCR genotype was the same for both flanking markers (*D1Mit452*$^{+/+}$ and *D1Mit15*$^{+/+}$). Although the mouse in question came from a mating between heterozygous parents, only a single recombination event was counted in this case.

found in the region flanking the *dr*^{J} locus, 10 of them between *D1Mit452* and *dr*^{J} and 8 between *dr*^{J} and *D1Mit15*. This positions *dr*^{J} in a 5.22 cM interval between these 2 flanking markers. Both *D1Mit452* and *D1Mit15* were subsequently used for systematic genotyping of *dr*^{J} mice in our colony.

Based on our results, we propose that the position of *dr*^{J} on mouse Chromosome 1 is: *D1Mit452* – 2.90 ± 0.92 - *dr*^{J} - 2.32 ± 0.82 - *D1Mit 15*. Figure 3.4A shows the complete data set for haplotype distribution, obtained with 188 offspring from fully heterozygous parents. Each column corresponds to one haplotype. Figure 3.4 B is a map of the region of mouse Chromosome 1 around the *dr*^{J} locus, compiled from the data shown in Figure 3.4 A.

Figure 3.4

(A) Haplotype distribution of 188 offspring
(B) Linkage map of the region around the *dr*^{J} locus, obtained from pedigree analysis in (A)

A

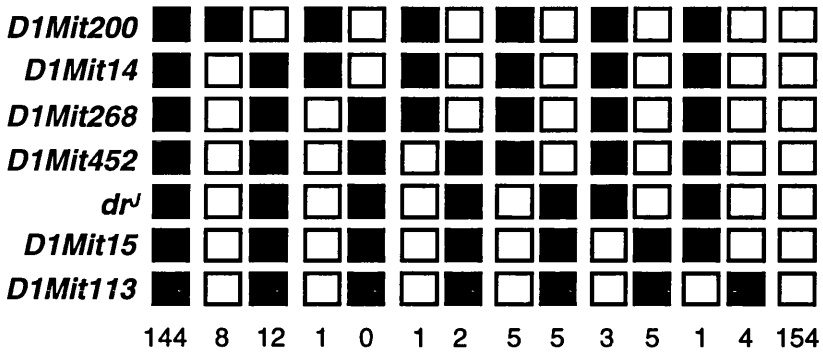

B

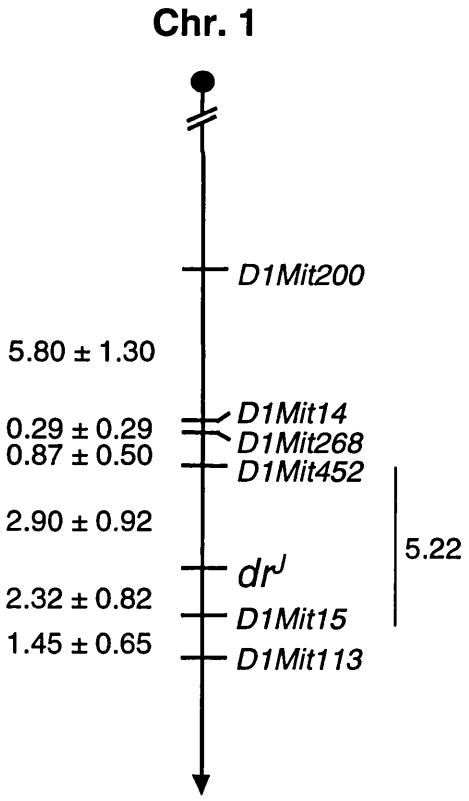

(A) Haplotype distribution of 188 offspring. Three-hundred and forty-five meiotic events were scored. The numbers at the bottom of each column correspond to the number of animals with each haplotype. Filled boxes represent the C3H/He (*dr*-linked) allele and empty boxes the C57BL/6 (*+*-linked) allele. In one case, a double cross-over occurred in a single chromosome, and is shown as two single meiotic events. The other chromosome also underwent meiotic recombination (3 meiotic events in total). In another case in which both parent chromosomes recombined, the recombination breakpoint could only be determined in one of them (counted as a single meiotic event).
(B) Centromere is to the top. Distances are in centimorgans (cM).

3.4. Discussion

In this haplotype analysis of mice generated in an intercross mapping study the position of the *dreher* locus was determined in relationship to closely linked DNA microsatellite markers. The results locate *dreher* to a more proximal position than originally reported, distal to *D1Mit452* and proximal to *D1Mit15* (compare Figure 3.1 to Figure 3.4 B). The estimated distance between these two markers from the present study (5.22 cM) is, however, considerably larger than previous published estimates for this interval.

For instance, the Whitehead Institute for Medical Research database quotes 2.1 cM as the distance between *D1Mit452* and *D1Mit15*. This discrepancy is even higher when the present data are compared with the established distance for the same interval provided by the Mouse Genome Database (1.3 cM). Possible explanations for these discrepancies include differences in genetic background, the number of animals included in each mapping analysis (and, therefore, the accuracy of the study), and the existence of a putative, strain-dependent recombinational hotspot in this region. However, the rates of recombination in the *D1Mit452-D1Mit15* and *D1Mit15-D1Mit113* intervals seem to be reversed in the present study, relative to those obtained through MGD (Table 3.5). This suggests another explanation for the recombination data in the present study. A chromosomal inversion in an ancestor of the dr^J mice, used for the present study, could encompass both *dreher* and *D1Mit15*, bringing the latter marker closer to

Table 3.5

Comparative chart showing distances between microsatellite DNA markers around the *dreher* locus according to different sources

	Present study	MGD	MIT Database
D1Mit200 - D1Mit14	5.80	8.6	6.6
D1Mit14 - D1Mit268	0.29	1.8	0
D1Mit268 - D1Mit452	0.87	3.2	2.2
D1Mit452 - D1Mit15	5.22	1.3	2.1
D1Mit15 - D1Mit113	1.45	4.4	5.5

Distances are in centimorgans (cM). MIT data concerns only distances between different microsatellites, i.e. does not include any gene loci. The shaded area represents the interval where *dreher* is situated according to the present study. Notice that the magnitude of the values for the *D1Mit452-D1Mit15* and *D1Mit15-D1Mit113* intervals seem to be reversed in the present study, when compared with those provided by the MGD and the MIT. See text for further discussion.

D1Mit113 and far away from *D1Mit452.* This inversion could affect the likelihood of meiotic recombination in the *D1Mit452- D1Mit15* interval, although it would be expected to reduce the recombination rate, not increase it, as observed. Such a case of suppression of recombination related to chromosomal inversion has been reported for the mouse *t* complex (Herrmann *et al.,* 1986; Shin *et al.,* 1983).

The present results also confirm the full penetrance of the circling phenotype: all mice with a non-recombinant dr^{J}/dr^{J} genotype at markers flanking the *dreher* locus proved to have a mutant phenotype. All non-recombinant animals with a mutant phenotype had a dr^{J}/dr^{J} genotype at the *dreher* locus, and none of the mice that were proven heterozygotes at the *dreher* locus had a mutant phenotype. These findings support those of Falconer and Sierts-Roth (1951) concerning the fully recessive nature of the *dr* mutation, and suggest that both *dr* and dr^{J} are loss-of-function mutations.

By performing linkage studies, flanking markers on either side of the *dreher* gene have been determined that allow accurate genotyping of each animal independent of the mutant phenotype. It thus becomes possible to select heterozygous animals for breeding as well as to perform experiments on any animal, even before their phenotype becomes apparent during development. This method has been used throughout the present thesis in investigations of the pathogenesis of the developmental defects in dr^{J} mutant mice.

Repositioning *dreher* to a considerably shorter interval than had previously been achieved provides a basis from which to evaluate candidate genes for the dr^{J}

mutation. The region around the *dreher* locus contains several known genetic loci (see Figure 3.1 and Table 3.6), including genes coding for cell-surface molecules such as selectins (*Sele, Sell* and *Selp)* and the zeta chain of T cell receptor Cd3 complex (*CD3z*). *P40-rs2* was first described as a putative laminin receptor because of sequence homologies with other laminin receptors (Douville and Carbonetto, 1992), but this view has been challenged (Yang *et al.,* 1998). Other genes situated in the *dreher* interval are POU domain, class 2, transcription factor 1 (*Pou2f1,* also known as *Otf1*) and ATPase (Na^+,K^+) beta 1 (*Atp1b1*). *Pou2f1* is expressed in the mouse brain (Schoeler *et al.,* 1989; Dominov and Miller, 1996) and *Atp1b1* is known to be expressed in the CNS of the rat (Peng *et al.,* 1997; Cameron *et al.,* 1994).

The existence of a large region of homology between mouse and human chromosomes in the area around *dreher* makes it possible to evaluate additional candidate genes, whenever human genes situated in that interval are positioned. For instance, *astrotactin* was mapped to cytogenetic band 1H2 of the mouse, a region of mouse Chromosome 1 overlapping the *dreher* interval, after its human homologue had been positioned in the syntenic region of human chromosome 1, at in 1q25.2 (Fink *et al.,* 1997). *Astrotactin* is known to play a crucial role in glial-guided neuronal migration in the developing brain (Stitt and Hatten, 1990; Fishell and Hatten, 1991), and is thus a possible candidates for the *dreher* mutation. *Tenascin-R* is another human gene situated at 1q24 in the region of largely conserved synteny with that surrounding the *dreher* locus (Arrigo, 1997; Carnemolla *et al.,* 1996), and therefore, could also be a potential candidate for the *dreher* gene. Human *tenascin-R* codes for an extracellular matrix molecule

Table 3.6

Known genes in the *dreher* region and their expression in the central nervous system

Gene symbol	Gene name	Position on Chr. 1 (cM)	Function	Expression in CNS
Cf5	Coagulation factor V	86.6	Prothrombin activator (coagulation cascade)	Not reported
P40-rs2	P40-related sequence 2	86.6	Putative laminin receptor	Not reported
Sele	Selectin, endothelial cell	86.6	Receptor, cell-surface antigen Adhesion molecule	Not reported
Sell	Selectin, lymphocyte	86.6	Receptor, cell-surface antigen Adhesion molecule	Not reported
Selp	Selectin, platelet	86.6	Receptor, cell-surface antigen Adhesion molecule	Not reported
Xmmv9	xenotropic-MCF leukemia virus 9	86.6	Endogenous virus (present in C57BL/6)	Not reported
Xmv32	xenotropic murine leukemia virus 32	86.6	Endogenous virus (present in C57BL/6)?	Not reported
Atp1b1	ATPase, Na^+,K^+ transporting, beta 1 polypeptide	86.8	Sodium-potassium pump enzyme subunit	Not reported in mouse; present in rat brain
Pou2f1	POU domain, class 2, transcription factor 1	87.2	Transcription factor	Yes
CD3z	T cell receptor CD3 complex, zeta chain subunit	87.2	Receptor, cell surface antigen	Not reported
astn	astrotactin	*	Neuronal, cell-surface molecule	Yes

Position is given in centimorgans (cM) from top of mouse Chromosome (Chr.) 1 (source: MGD), except for *astrotactin* (*mapped by F.I.S.H. to band 1H2) (Fink *et al.*, 1997).

expressed exclusively in the central nervous system (Wintergerst *et al.,* 1993; Pesheva *et al.,* 1997; Pesheva *et al.,* 1989). Surprisingly, the mouse homologue of *tenascin-R*, known as *restrictin* (symbol *Tnr*), has recently been mapped to Chromosome 4 band E2 by fluorescent *in situ* hybridisation (Arrigo, 1997), suggesting a possible break of synteny in that region, and ruling *restrictin* out as a candidate. Both *Pou2f1* and *astrotactin* were considered of particular interest at the time of these mapping studies, and their evaluation as candidate genes for the dr^{J} mutation forms the subject of the next chapter.

3.5. Final comments

Since the collection and analysis of the data presented in this chapter, an independent mapping study of the *dreher* was published (1999) by Bergstrom, and colleagues (1999). Initially, crosses segregating for two different alleles (dr^{6J} and dr^{7J}), of which there had been no previous published reports, were used to map *dreher* to a 7.1 cM interval between *D1Mit506* and *D1Mit15* with SSLP (simple sequence length polymorphism) markers. Subsequently, the *dreher* region was further narrowed using a different intersubspecific cross segregating for the dr^{6J} allele, localising the *dreher* gene to a 0.13 cM region with flanking markers *D1Mit110* proximally and *D1Mit370* distally. Although this study mapped *dreher* to a cM position apparently well distal to the location identified in this thesis, the *dreher* critical region was confirmed as lying between *D1Mit452* (which co-localises with *D1Mit506*) and *D1Mit15*, consistent with my own data. Hence, Bergstrom and colleagues (1999) find *D1Mit15* to lie considerably more distally than other studies.

In the same article, the authors were successful in excluding several genes situated in the *dreher* region as candidates for the mutation (Bergstrom *et al.*, 1999). *Astrotactin* was ruled out on the basis of the absence of STSs (sequence tagged sites) designed from the *astrotactin* gene sequence within a BAC (bacterial artificial chromosome) contig spanning the *dreher* interval. *Pou2f1* was also excluded as a candidate gene: polymorphic DNA markers designed from this gene were mapped against a panel of recombinant DNA samples from a dr^{6J} cross, localising *Pou2f1* proximally to *dreher*.

In conclusion, the mapping data from the present study are in complete agreement with the more detailed mapping study of Bergstrom et al (1999).

Chapter 4

Assessment of candidate genes

4.1. Introduction

According to consensus maps of mouse Chromosome 1 (Seldin, 1997), many genes have been assigned positions in the *dreher* interval, although many of them have not been mapped against microsatellite DNA markers in that region. As mentioned in the previous Chapter, two genes (*Pou2f1* and *astrotactin*) were selected as candidates for the dr^J mutation on the basis of previous mapping studies and because they were known to be expressed in the developing brain (see below). Other genes in the region were not studied, mainly because of time constraints, but also because their known expression pattern made it less likely that they would be implicated in the dr^J mutation.

The present chapter contains preliminary data on sequence analysis of *Pou2f1*, as well as studies of the *in situ* expression of *Pou2f1* and a*strotactin* in dr^J embryos. At the time these studies were conducted, it was expected that these data would provide a starting point in the search for the mutated gene in dr^J. Expression analysis, for instance, would be expected to disclose whether the temporal and spatial expression of either of these genes was compatible with the profile expected for the gene mutated in *dreher* mice. More specifically, a likely candidate for *dreher* should be expressed at or before the time-point when the first morphological changes have been observed in *dreher* embryos: data presented in this thesis (Chapter 5) indicate that dr^J/dr^J mutants can be recognised as early as E11.5 on the basis of their external phenotype. According to an early publication on the embryogenesis of ear defects in *dr* homozygous mutants, the first identifiable abnormalities are seen in the otic vesicles at E11 (Fischer, 1958).

Therefore, expression of a likely candidate gene should start no later than E11. Secondly, the spatial pattern of expression of a candidate gene for *dreher* should include the cortical plate and developing cerebellum, as well as the otic vesicles, since all these structures exhibit abnormal development in *dreher.* Expression in the hindbrain adjacent to the otic vesicles is an alternative possibility, if *dreher* represents adefectiveinduction of otic vesicle development (see also Section 5.4.1).

The evaluation of *astrotactin* and *Pou2f1* as candidates for the *dreher* mutation has, to some extent, been superseded by the fact that finer mapping of *dreher* has recently been published (Bergstrom *et al.,* 1999), ruling out both *astrotactin* and *Pou2f1* as candidates. Nevertheless, the data presented in this Chapter includes previously unreported information on the expression of the *astrotactin* gene outside the CNS. It also helps to clarify the expression pattern of *Pou2f1* in the mouse, on which conflicting evidence has been published.

4.1.1. *Pou2f1* as a candidate for the dr^J mutation

4.1.1.1. *Pou2f1* has been mapped to the *dreher* region

The murine POU domain, class 2 transcription factor 1 gene (*Pou2f1*) has been mapped to 87.2cM from top of mouse Chromosome 1 (Hsieh *et al.,* 1990; Hoopes *et al.,* 1992; Hunter *et al.,* 1993; Seldin, 1997), within the *dreher* interval, between *D1Mit452* and *D1Mit15.*

4.1.1.2. *Pou2f1* codes for a transcription factor with a POU domain

Pou2f1 (previously known as octamer transcription factor 1, *Oct-1* and *Otf-1*) belongs to the POU-domain regulatory gene family, named after the initials of some of its members (Pit-1, Oct-1 and Oct-2,mammalian proteins, and Unc-86, a *C. elegans* regulatory protein). POU genes are known to play important roles in development and cellular differentiation (Schoeler, 1991; Verrijzer and van der Vliet, 1993).

Classification of POU-domain proteins is based on sequence similarities: Pou2f1 (Oct-1) and Oct-2 belong to POU protein class II. The POU domain consists of two conserved subdomains, a POU-homeodomain and an even more conserved POU-specific domain, connected by a shorter and variable linker region. The POU-domain (160 amino acids long) is required for binding to the DNA motif 5'-ATGCAAAT-3' (hence the previous designation *Oct-1*, from octamer-binding) (Verrijzer *et al.,* 1990; Schoeler, 1991; Verrijzer and van der Vliet, 1993). Alternative mRNA splicing generates three different isoforms (a, b and c) of *Pou2f1*, with differential tissue levels of expression (Suzuki *et al.,* 1993; Seldin, 1994). Murine *Pou2f1* has been cloned (Sturm *et al.,* 1988), and the cDNA sequences corresponding to two of the splice forms have been published (Jaffe *et al.,* 1995).

4.1.1.3. Conflicting evidence exists as to the pattern of expression of *Pou2f1* and little is known about its functions

The functions of *Pou2f1* are unclear. This gene probably plays an important role in early development, since disruption of its expression is believed to be responsible for a high perinatal mortality (Koyasu *et al.,* 1994; Ohno *et al.,*

1994). Pou2f1 is involved in the activation of ubiquitous genes such as those encoding small nuclear RNA and histone H2B promoter genes (reviewed in (Verrijzer and van der Vliet, 1993)). Recent studies on the mouse (Pogulis *et al.,* 1995) have suggested that Pou2f1 is the same protein as collagen intron-binding factor I binding factor I (CIBF-I). The latter is required for full activation of the mouse pro alpha 2 (I) Col gene. This raises the possibility that *Pou2f1* may also regulate the expression of the type I Col gene.

Conflicting evidence has been reported on the pattern of distribution of *Pou2f1* expression in rodents. The expression of *Pou2f1* has been considered ubiquitous by several authors (Sturm *et al.,* 1988; Schoeler *et al.,* 1989; Suzuki *et al.,* 1993; Dominov and Miller, 1996), both in embryonic and adult mice, on the basis of Northern blotting and ribonuclease protection assays (Suzuki *et al.,* 1993; Dominov and Miller, 1996), electrophoretic mobility shift assays (Schoeler *et al.,* 1989) and mouse cell line culture studies (Sturm *et al.,* 1988).

However, more recent publications based on *Xenopus* (Veenstra *et al.,* 1995) and rat (He *et al.,* 1989) embryos seem to indicate that expression becomes progressively more restricted during embryogenesis and postnatal development, namely in neural tissues, suggesting that *Pou2f1* (like other POU-domain genes) may play a role in and cellular determination and differentiation during central nervous system development.

In *Xenopus*, by the gastrula stage, expression is seen in ectoderm- and mesoderm-derived tissues, and later disappears from most mesoderm-derived structures except for the somites. In the ectodermal cell lineage, there is a

progressive spatial restriction of expression to head structures (otic vesicles, several cranial nerve ganglia, neurepithelium). In neural tube derivatives, expression is especially high at the midbrain-hindbrain boundary, but is also seen in the diencephalon and in restricted areas of the telencephalon and rhombencephalon). Outside the head, neural crest derivatives such as the branchial arches still display high levels of expression. *Pou2f1* expression in *Xenopus* embryos was unrelated to cell density or proliferation (Veenstra *et al.,* 1995).

In both mouse and rat, *Pou2f1* is expressed in the central nervous system (CNS) (He *et al.,* 1989; Schoeler *et al.,* 1989; Suzuki *et al.,* 1993; Jaffe *et al.,* 1995). The gene is also expressed in the otic vesicles of the rat (Ryan *et al.,* 1991). This pattern of expression made it a potentially good candidate for the dr^{J} mutation.

Murine *Pou2f1* is also expressed at high levels in precursors of myelin-producing cells (Schwann cells) in association with peripheral nerves. Expression is down-regulated in parallel with progressive differentiation of Schwann cells, suggesting that *Pou2f1* may play a role in development of the peripheral nervous system (Blanchard *et al.,* 1996).

4.1.2. *Astrotactin* as a candidate for the *dr*^{J} mutation

4.1.2.1. *Astrotactin* maps to the *dreher* region

Astrotactin has been mapped by fluorescence *in situ* hybridisation to band 1H2 on the long arm of mouse Chromosome 1 (Fink *et al.,* 1997), in a region likely to encompass the *dreher* interval. The chromosomal location for human *Astrotactin* (ASTN) has been found by the same technique to be in the syntenic region of human Chromosome I, at 1q25.2 (Fink *et al.,* 1997).

4.1.2.2. The predicted protein structure of *astrotactin* suggests it has properties of an adhesion molecule

The murine *astrotactin* gene (*astn*) has recently been cloned (Zheng *et al.,* 1996). The predicted amino-acid structure of the Astrotactin (ASTN) protein includes regions of homology with known cell-adhesion molecules, such as those of the epidermal growth factor and fibronectin type III families (Zheng *et al.,* 1996). This is not surprising for a molecule that is believed to play a crucial role in neuronal migration (see below).

4.1.2.3. *Astrotactin* is expressed by migrating neurons in the CNS of the mouse and plays an important role in glial-guided neuronal migration

In situ hybridisation studies have shown that *astrotactin* is expressed in the central nervous system (CNS) of the mouse by neurons undergoing glial-guided migration and association into layers, namely in the external granular layer of the cerebellum, the dentate gyrus, the cerebral neocortex and the olfactory bulbs (Stitt *et al.,* 1991; Zheng *et al.,* 1996). In the cerebellum, its expression is low in the late embryonic period, increases to high levels in the early post-natal period, and falls to low levels in adulthood (Stitt *et al.,* 1991). The timing of

onset of expression of *astrotactin* during CNS development is nevertheless unclear from previously published reports.

In vitro studies suggest that Astrotactin acts to promote neurone binding to astroglia and to be able to induce or maintain glial cell differentiation. (Stitt and Hatten, 1990; Fishell and Hatten, 1991; Zheng *et al.,* 1996). The addition of anti-Astrotactin antibodies to early post-natal mouse cerebellar microcultures is capable of severely reducing the rate of neuronal migration along radial glial fibres by preventing the binding of neurons to glia (Edmondson *et al.,* 1988; Fishell and Hatten, 1991).

The spatial distribution pattern of the early post-natal expression of Astrotactin in the cerebral hemispheres, hippocampal formation, olfactory bulbs and cerebellum of the mouse (Stitt *et al.*, 1991; Zheng *et al.*, 1996) closely correlates with the areas where the neuronal migration defects are seen in dr^{J}/dr^{J} mice. *Astrotactin* thus seemed a likely candidate for the *dreher* gene.

4.2. Methods

4.2.1. Overview of methods used

4.2.1.1. Evaluation of *Pou2f1* as a candidate gene

The evaluation of *Pou2f1* included comparing the sequences of a well conserved region of this gene in normal and homozygous mutant dr^J mice, as well as the study of its mRNA expression by wholemount *in situ* hybridisation of dr^J embryos.

The first step included sequencing the POU-specific domain (the most conserved sequence of *Pou2f1*) in dr^J/dr^J and control mice. A database search (GenBank) yielded one cDNA sequence (see Figure 4.1), based on which PCR primers were designed. Oligonucleotide sequences were as follows:

Forward primer: CAG ACA CTT CCA CAG AGC CA
Reverse primer: CTA CGA TTC AAG CCC TCA GC

The PCR product had a predicted size of 359 bp.

This study was done relatively early in the course of working on this thesis. For that reason, and because breeding of dr^J mice had just started, there were no animals in the colony with a proven +/+ genotype at the *dreher* locus. For this reason, dr^J/dr^J mice (identified on the basis of their circling phenotype) were compared with control mice from a normal laboratory strain (CD1).
The first step involved RNA extraction from brain tissue and RT-PCR in order to obtain cDNA. Next, cDNA was amplified with the *Pou2f1* primers, using a high-

Figure 4.1

cDNA sequence of murine *Pou2f1*

1 CCTATGGTGT AACTGAAGTT GTAGTTTGCT TCTCTTGTTA ATTCACTTTC CACTCTTCCC
61 ACCCTTGTTC TCTTAAGAAC ATAGTACAGA TTTGTTAGAA ATAGTAGTTT TTCCCCCAAA
121 CGCTACCTGT TCCTTCTTGC TTTGGACTGT CTGCACCTCT TGAAGATTTT ACAGCCATGC
181 TGGACTGCAG TGACTGTGTT CTAGACTCAA GAATGAATAA TCCATCAGAA ACCAATAAAT
241 CATCTATGGA GAGTGAAGAT GCCAGCACAG GCACACAAAC CAATGGTCTG GACTTTCAGA
301 AACAGCCCGT GCCCGTTGGA GGAGCGATCT CCACAGCCCT GGCGCAGGCC TTCCTCGGAC
361 ATCTTCACCA GTCTAAATCC AGTGAAGAGT CGGGAGATTC GCAGCAGTCG AGCCAGCCTT
421 CTTCCCAGCC GCCTTCAGTG CAGTCAGCCA TTCCCCAGAC CCAGCTAATG CTGGCTGGGG
481 GACAGATAAC TGGGCTCACG TTGACCCCAG CCCAGCAACA GTTACTGCTA CAGCAGGCGC
541 AGGCCCAGGC ACAGCTCCTG GCCGCTGCAG TGCAGCAACA CTCCGCCAGC CAACAGCACA
601 GTGCTGCTGG GGCCACCATC TCAGCCTCCG CCGCCACACC CATGACGCAG ATCCCCCTGT
661 CTCAGCCCAT ACAGATTGCA CAGGATCTTC AACAATTGCA ACAGCTTCAG CAGCAAAATC
721 TCAACTTGCA ACAGTTTGTG TTGGTGCACC CAACCACCAA CCTGCAACCA GCACAGTTTA
781 TCATCTCACA GACCCCCCAG GGCCAGCAGG GTCTCCTGCA AGCGCAAAAT CTTTTAACGC
841 AACTACCTCA GCAAAGCCAA GCCAACCTCC TACAGCCACA GCCAAGCATC ACCCTCACGT
901 CCCAGCCTAC CACCCCAACT CGCACAATAG CAGCAGCCTC AGTTCAGACACTTCCACAGA
961 GCCA→GTCAAC ACCAAAGCGA ATTGACACTC CCAG CTTGGA GGAGCCCAGT GACCTTGAGG
1021 AGCTTGAGCA GTTTGCCAAG ACTTTCAAAC AAAGACGAAT CAAACTTGGA TTCACTCAGG
1081 GTGATGTTGG GCTCGCTATG GGGAAATTAT ATGGAAATGA CTTCAGCCAA ACCACCATCT
1141 CTCGCTTTGA AGCCTTGAAC CTCAGCTTTA AGAACATGTG CAAGTTAAAG CCCCTTTTAG
1201 AGAAGTGGCT AAATGAT GCA GAGAACCTCT CATCTGATTC→TACAGCATCT AGCCCAAGTG
1261 CTTTGAATTC TCCAGGATTG GGG←GCTGAGG GCTTGAATCG TAGG AGGAAA AAACGCACCA
1321 GCATCGAGAC CAACATCCGT GTGGCCTTAG AGAAGAGTTT CATGGAGAAT CAAAAGCCTA
1381 CCTCGGAAGA CATCACCTTG ATTGCTGAAC AGCTCAATAT GGAAAAGGAG GTGATTCGTG
1441 TTTGGTTTTG TAACCGCCGC CAGAAGGAGA AAAGAATCAA CCCGCCCAGC AGTGGTGGGA
1501 CCAGCAGCTC ACCTATCAAA GCAATTTTCC CCAGCCCAGC CTCATTGGTG GCAACCACTC
1561 CAAGCCTTGT GACAAGCAGT ACGGCAACTA CCCTCACAGT CAACCCTGTC CTCCCTTTAA
1621 CCAGTGCTGC TGTGACTAAT CTCTCTCTTA CAGGCACTAC AGACTCGACG TCCAACAACA
1681 ACACGGCCAC GGTGATTTCC ACAGCACCCC CTGCTTCCTC AGCAGTCACA TCCCCTTCCT
1741 TGAGTCCCTC TCCCTCTGCC TCGGCCTCCA CCTCAGAGGC CTCCAGTGCC AGTGAGAC←CA
1801 ACACGACACA GACCACCTCC ACGCCTCTTC CCTCCCCTCT CGGAGCCAGC CAGGTGATGG
1861 TGACCACGCC CGGCTTACAG ACAGCAGCCG CCGCTCTCCA AGGAGCGGCA CAGTTGCCAG
1921 CAAACGCCAG TCTTGCTGCT ATGGCTGCTG CTGCGGGACT CAGCCCAGGC CTCATGGCAC
1981 CCTCACAGTT TGCTGCTGGG TAAGGAGCTT TCCCATTCCG TTTGCATCCA GAACAGAACT
2041 AGGATCTCAT TCCTGCAGCT CCCGGGGAAA ATTTGTTATC GCTGTCTTAG GTGGAAAGTA
2101 TATCTGAGAT GGGTTTGCAC TTAAGTTTCT AAGTAGCCAC ATTGTCATTT CCACATGATG
2161 ACACAGAACT GAGTCACTGA GTAACTCAGT GAGAGAACCA GG

The cDNA sequence was obtained through Internet, at the GenBank database, with accession number X56230.

POU-specific domain. POU homeodomain. Forward (→) and reverse (←) primers used for cloning the POU-specific domain Forward (→) and reverse (←) primers used for the preparation of a riboprobe for wholemount *in situ* hybridisation.

fidelity Taq polymerase. Purified cDNA was ligated with pGEM-T vector, transformed into competent bacterial cells and plated. Colonies containing the insert were selected and grown in an appropriate medium. Plasmid DNA was extracted, linearised and purified. cDNA was sequenced using the manual conventional ^{35}S method.

4.2.1.2. Wholemount *in situ* expression studies

As a part of the assessment of *Pou2f1* as a candidate gene for *dreher*, the embryonic expression of this gene was studied using the wholemount *in situ* hybridisation technique with digoxygenin-labelled probes. Initially the cDNA clone already used to sequence the POU-specific domain was also used as a template for the production of a mRNA probe. This was used for wholemount *in situ* hybridisation with control embryos. Later, another digoxygenin-labelled probe was designed from a region distally (i.e. 3') to the POU-specific domain (See Figure 4.1), in a region of low homology with *Oct2* (the latter is the gene with the highest homology with *Pou2f1*).

The primers used to amplify the cDNA sequence before transcription were:

Forward primer: GCA GAG AAC CTC TCA TCT GA TTC
Reverse primer: AGG TGG TCT GTG TCG TGT TG

The expected PCR product size was 601 bp.

RNA from CD1 embryos (at E13) was extracted and cDNA was produced by RT-PCR, then cloned into a pGEM-T vector. The plasmid was partially

sequenced to ensure the desired clone was in use. The making of the RNA probe was carried out as below (Section 4.2.3.4). This riboprobe was tested on *dr*^{J} embryos at E9.5, E10.5 and E11.5. Homozygous mutant embryos were compared to heterozygotes and wild-type age-matched embryos.

4.2.1.3. Evaluation of *astrotactin* as a candidate gene

The evaluation of *astrotactin* as a candidate gene was restricted to *in situ* hybridisation studies of gene expression in whole embryos. The riboprobe used for this analysis was prepared from a cDNA clone obtained by searching the Genbank dbEST database at the UK HGMP resource centre with the murine *astrotactin* cDNA sequence. The cDNA clone selected was requested via internet from the I.M.A.G.E. Consortium at mgd.hgmp.mrc.ac.uk. A sequence comparison with *astrotactin* showed a 100% identity of the full sequence within the 3' untranslated region of that gene (see Figure 4.2). Plasmids containing the cDNA clone (in a pT3T73D vector) were linearised, plasmid DNA was purified and the sequence of the DNA insert was confirmed by automated sequencing with fluorescent primers. Subsequently, a digoxygenin-labelled RNA probe was prepared and used for wholemount *in situ* hybridisation on *dr*^{J} embryos at E9.5, E10.5 and E11.5. Homozygous mutant *dr*^{J} embryos were compared with heterozygotes and wild-type embryos of the same gestational age.

Figure 4.2

Murine *Astrotactin* cDNA sequence

1 GCACTGCCCT TCCTGCGCGA GAACGACCTG AGCATCATGC ACAGTCCCTC GGCCTCCGAA
61 CCCAAGCTTC TCTTCTCCGT GCGCAATGAC TTCCCGGGAG AAATGGTCGT GGTGGACGAC
121 TAGAGAACAC GGAGCTACCC TATTTGTGCT GGAGATCTCA GGGAATACAG AAGACATCCC
181 CCTGGTGCGC TGGAGGCAGC AATGGCTGGA GAATGGCACT TTACTCTTTC ATATTCACCA
241 CCAAGATGGT GCTCCAAGTC TCCCTGGACA AGACCCAACT GAAGAACCCC AACATGAATC
301 AGCAGAGGAA GAGCTGAGGA TCCTGCACAT CTCAGTCATG GGTGGCATGA TCGCTCTGTT
361 GCTATCCATC TTGTGCCTGG TGATGATCCT GTACACTCGC AGGCGCTGGT GCAAACGTCG
421 CGGTTCCCCA GCCCCAGAAG AGTGCCAGTG CAGAGGCAGC AAATGAGATT CACTACATCC
481 CATCTGTGCT GATTGGAGGC CATGGGCGGG AAACGTTGCG CAATGCCCGT GTGCAGGGCC
541 ACAACTCCAG TGGCACTCTG AGCATTCGGG AGACACCCAT CCTGGATGGC TATGAGTATG
601 ACATCACAGA CCTGCGTCAC CACCTGCAAA GGGAGTGTAT GAATGGAGGG GAGGACTTTG
661 CCAGTCAGGT CACACGCACT TTGGACTCCT ACAGGGATGC AATGAGAAGT CTGGGATGGA
721 TCTAACACCA GGGAGTGACA ATGCCAAGCT TTCCCTGATG AACAAGTATA AAGACAATAT
781 CATAGCCACA AGCCCCGTGG ATTCTAACCA CCAGCAAGCC ACTCTGCTCT CCCACACCTC
841 CAGCAGCCAG AGAAAGAGGA TCAACAATAA AGCCAGAGCT GGTTCTGCCT TCTTGAACCC
901 TGAAGGGGAC TCCAGCACAG AGGCCGAAAA TGACCCACAG CTGACCTTCT ACACAGACCC
961 CTCTCGGAGC CTGGCGCAGT CGAGTGGGCT CTCCCCGAAG TCCTGTGAAT AAGACCACCT
1021 TGACCCTGAT CAGTGTCACC AGCTGCGTGA TTGGCCTCGT GTGCTCTTCT CATGTCAGCT
1081 GCCCTCTTGT TGTCAAGATC ACCCTACACG TCCCTGAGCA CTTGATCGCT GATGGGAGCC
1141 GCTTCATCCT GCTGGAGGGG AGCCAGCTGG ATCGCAGTGA CCTGGCTGAA CCCTGCCCAA
1201 GTGGTTCTCT TCTCTCAGCA GAACTCCAGC GGGCCCTGGG CCATGGACCT CTGTGCCCGG
1261 CGGCTCCTGA CCCTTGTGAA CACCAATGTG ACCCCGAAAC TGGTAGGCGG GAGCACCGGG
1321 CAGACGGGGG AATGCCTGTG CTATGAAGGC TACATGAAGG ATCCTGTCCA CAAGCACCTT
1381 TGCATTCGGA ATGAATGGGG GACCAACCAG GGGCCTTGGC CTTACACGAT ATTTCAGCGA
1441 GGCTTTGACC TGGTTTTGGG AGAGCAACCC TCTGATAAGA TATTCAGATT CACCTATACC
1501 CTCGGGGAAG GCATGTGGTT ACCCCTCAGT AAGAGCTTTG TGATCCCACC AGCTGAACTA
1561 GCCATCAATC CATCAGCAAA GTGTAAGACG GATATGACTG TGATGGAAGA TGCTGTAGAG
1621 GTCAGAGAGG AGCTGATGAC ATCATCATCC TTTGACAGCC TGGAGGTCCT ATTAGACTCC
1681 TTTGGGCCAG TGCGTGATTG CAGCAAAGAT AACGGAGGCT GCAGTAAGAA TTTTCGCTGC
1741 ATTTCAGATC GCAAGTTGGA CTCTACTGGT TGTGTGTGTC CTTCAGGACT CAGCCCTATG
1801 AAGGACAGCT CAGGCTGCTA TGATCGCCAT ATCGGAGTGG ACTGCTCAGA TGGTTTCAAC
1861 GGCGGCTGCG AACAGCTGTG TCTCCAGCAG ATGGCGCCGT TCCCAGAGGA CCCCACCTTG
11921 TACAACATCC TTATGTTCTG CGGGTGTATC GAAGACTACA AGCTTGGTGT GGATGGACGC
1981 TCTTGCCAAC TTGTCACTGA GACCTGCCCA GAGGGAGGTG ACTGTGGGGA AAGCAGAGAG
2041 GTTCCCATGA ACCAGACTCT CTTTGGAGAA ATGTTCTTTG GCTACAACAA CCAGTCCAAG
2101 GAAGTAGCCA CTGGACAGGT GCTAAAAGGA ACATTCAGAC AGAACAACTT TGCTCGTGGT
2161 TTAGACCAGC AACTGCCGGA TGGTCTTGTG GTTGCCTCTG TCCCACTGGA GAATCAGTGC
2221 CTAGAGGAAA TCTCAGAGCC CACCCCAGAC CCTGACTTCT TGACTGGGAT GGTGAACTTC
2281 AGTGAAGTGT CTGGATACCC GGTGCTGCAG CACTGGAAGG TTCGGTCTGT GATGTACCAC
2341 ATCAAACTCA ACCAAGCAGC CATCTCGCAG GCCTTCAGCA ATGCTCTTCA CTCCTTGGAT
2401 GGGGCTACAT CTCGTGCAGA TTTTGTGGCT TTGTTGGATC AGTTTGGAAA CCATTACATC
2461 CAGGAAGCTG TCTACGGCTT TGAGGAATCC TGTTCTATAT GGTACCCAAA CAAGCAAGTC
2521 CAGCGGAGAC TCTGGCTGGA ATATGAAGAC ATCAGTAAAG GCAACTCTCC ATCTGATGAG
2581 TCGGAGGAGC GGGAAAGGGA TCCCAAGGTG CTGACATTCC CAGAATACAT CGCTAGCCTG
2641 TCAGACTCTG GCACCAAGCG AATGGCAGCT GGAGTCCGGA TGGAGTGCCA GAGCAAGGGA
2701 CGGTGTCCTT CATCCTGTCC TTTATGTCAT GTGACATCCA GCCCTGAAAC CCCTGCTGAG
2761 CCAGTTCTAC TGGAAGTGAC CAGAGCATCC CCCATCTATG AACTGGTGAC CAATAACCAG
2821 ACCCAGAGGC TCTTACAGGA AGCCACCATG AGCTCTCTCT GGTGTTCAGG GACCGGAGAT
2881 GTCATTGAGG ACTGGTGCCG ATGCGACTCG ACTGCTTTTG GAGCAGATGG ACTTCCTACC
2941 TGTGCACCCC TCCCACAGCC TGTGCTGAGA CTTTCCACAG TACACGAGCC CAGCAGTAAC
3001 CTCGTGGTCC TGGAGTGGGA ACATTCAGAG CCGCCAATTG GGGTGCAGAT TGTAGACTAC
3061 CTGTACCGGC AAGAGAAAGT CACTGACCGG ATGGACCACT CCAAAGTAGA GACGGAAACA
3121 GTGCTGAGCT TTGTAGACGA CATCATCTCT GGAGCAAAGG CTCCATGTGC CATGCCGTCT
3181 CAGGTGCCAG ACAAACAGCT CACCACGATT TCTCTCATCA TCCGATGCCT GGAACCTGAC
3241 ACCATTTACA TGTTCACCCT CTGGGGAGTA GATAACACAG GGCGACGTTC CAGGCCAAGT
3301 GATGTGATTG TGAAGACCCC ATGTCCTGTG GTGGATGATG TCAAAGCCCA AGAAATAGCA
3361 GACAAGATCT ACAATCTCTT CAATGGCTAC ACCAGTGGAA AGGAGCAACA GACTGCCTAC
3421 AACACCCTTC TGGATCTGGG TTCTCCCACT TTGCACCGAG TCCTCTACCA CTATAACCAG
3481 CACTATGAGA GTTTTGGGGA ATTCTGGCGG TGTGAAGATG AGTTAGGACC CAGGAAAGCA
3541 GGCCTCATCC TTTCCCAGCT TGGAGATCTG AGCAGCTGGT GCAATGGACT CCTTCAGGAG
3601 CCCAAGATAA GCTTGAGGCG TGGTTCACTC AAGTACCTGG CTGGCCGCTA CAGTGAGATC
3661 AAACCCTATG GACTGGACTG GTCAGAGCTC AGTCGGGACC TCAGGAAGAC ATGTGAAGAA
3721 CAGACCCTGA GTGTCCCCTA CAATGACTAC GGGGACAGCA AAGACATCTA GCATCATGGG

(Astrotactin cDNA sequence-continued)

3781 ACCAGGAAAT AACTGCAGAA ATAAAGCAGG GGAGAAGAGG GCAACATCTG GGTTGGTTTG
3841 TGGATTCTTA GACATTTTTT AATGGAACAC CCAAAGCTCT ACAAGTCCCT TCTAAACCAG
3901 GAAGAGGGTA GACCTTTGCT CCCTGCAAGA TTTGTCCAGT GTGATATTCT CCACCTGCAT
3961 GACCAGTCAA CCCGCCAGCC AGTAGCTTCA TGCAGCACTG TTCGTTTTTG TTTTTGTTTT
4021 TGTTTTTGTT TTTGTTTTTT TCTTAGAAGA TTACCTTGAA ACTCACTTTG GTATCCATTG
4081 GTTTTGTTCA CTTTTTCGCC TTCAGTCAAC CCATCAGGAT TCTCAAGAGC ACTATCCTGC
4141 ATCCTACAGC AGGTCTAATG TGGAGGCTCT TCTGCCTAAT GGGTTCCCAA GTCTATGACA
4201 CCTGGGGACA GAAGTGAGGG CATAAAGCTT CTGCTGCCTC ATGCCCTTGC TCAGGCATTT
4261 CTTAGGAAGC ATCAGAATGT TGGGAGCAAG GCATGTACTG AAGAAGATAA TAAATGACCC
4321 ATGCCCTTTT CTCATGGGTT TTCCCCCAGA CTCTCTCCTG TTACTGTTTC CACACCTCAG
4381 AGGTAAACCT AAGCTCTGTT ACAGGACTGT TGGACATAAC AGAGATTTAG GTCTCTCTTC
4441 CCCCATTTTA AACCAGGACT CCAAGTTCTC GTTGATTTCT GTCCTTTCTT CTAAACAACC
4501 TGATCTTTGA GAGGCAGTGA GATAATACCT GTTAAATATG GCTCCAGAGA GGGCTACCTG
4561 CAAGATTATT TAGTAGCCTT CACTGTAGGA AATAAGTGGA GTTTATTTAA AAAAAAAAAC
4621 AGTTGTACAT GTCTAGAGTA TCATCAGAGT CCTAAGAGCC TTGATTCTGC TTGGTCCCAG
4681 GCCTTTTTCC CTGGACAGAA AGGACTTGGC TGTTGTTTGC TTTAGTCCAG GAATGAGATT
4741 ATTTCTTGTC AGTGTTTTAG TGAACTAAAG CTCTTATCAA TCTGAAAAGT ACTTCTGTCC
4801 GCACTGCCCT CACTAAATTT TCTTAATTAT ATTGTAAATT TTGACAGCCT ATTCTCTGAT
4861 GAAAATCATC AGTACTCTGT CATTGTCACT GCCTGCCCAC CCAACTCTGC CAGTTACTGA
4921 AGAGCAACAG AGCCTCTGGA GAGACCTGAA CATCTGATGA TTGCACATAA GGACTGAGGC
4981 TCCATTTGCA CACACTGCCC AAGGATGATG ATACGGTGAA CTAGCTACTA GGAAGCCTAG
5041 CCTGTTAGAA ACAACCTCAT GGGACCAGAA TGACTAACAA TGACCCAATG TACATTCAGC
5101 CAGCTTGCCT TGACTGGAAT TCTTCATGTG GAAACACAGC CTTCATGTGG AAGGCTCTAT
5161 AATTCAGCCA CTGAGCCTTA TTCATACTTT CCAATTAGGA ATAATGACAG ATGACATCTG
5221 AGGTGTGATG TGTGCTACTA TAATAACAGG AATCTCACAG GAATAATGAC AGATGACATC
5281 TGAGGTGTGA TGTGTGCTAC TATAAATAAC AGGAATCTCA CAGAACCCCT AAAGAAAGTT
5341 CTATTCCTAT TCACTATTCT TTTAGTAATG AGGAAAACAA GGAAGTGAGG TGACTTGCCA
5401 TTCCCCAGGT CCCTCATACA CTATATACCC TGAGCTGCAG TGCCTCTAGA ACACAGGAGT
5461 TTAACTACTC TGTGTTGCCT AAAGCATATG ACTGTTGAAG CTCTAAGCTC TACTGGGAAC
5521 ATGCCCAGAG AACTTCACCT TCCTAAGGGA CCGTGTACAA ATATACAATG AGTCAAAGTA
5581 CACCCATAGC CTTTGGAGTC AGGGCACCTT TGGTATGCTC AACACTGTGG CACACTAGCT
5641 TCCCACTGAT GAATAGGAAG GAAATTCAGT TGCAGGCTGG TCTTATTTCT CTCTTTGCTT
5701 CTTTGCAGAG AAATATTGGA AAACTTGCCT TGTACTTTTT GGCCTCAGAG ATACCATCAC
5761 TTTTAGAACA AAACACAGCA GAAAACTTAG CTGGCTTTCC TCTGGCCAGC ATAGGGATTT
5821 CAGTAAAAGT GCATCCGAAG GAAGCTTGTT CACTATTGCC AGAGAAGAGG ATGCTATGGG
5881 ACAGTGTGGC AGTGTGGACA GCATCCCTTT ACTGCCGTTC TTTTTCCACT CTTCTGTTCA
5941 ATCCTATGAA GAAAAGAGTG TCTTCTTTTG AACAGAATGA TAGTGAGACT GTGGATGCCT
6001 TCCAGCCCTG TTGGAGATAG GAACTTATGG GCTCAGGAGG GAGGACAGGA GTGATATAAT
6061 GATCACTACT GTTACCCACC CCATCTTTTA TTCCAGACAT ACTCTCCTCC TCTCTTTTAC
6121 CTTTATGCCC CATTTTCCAA AGATTTTTCA CCTCTCACAC ACATATCTCC TTTATCCTCC
6181 ATCTTTCCCC CCGCTTCCCA TCGACTGCCT TATTCTTTCA GTGTGCTCTT GTGTTTTCTC
6241 TTCAGATGTG TGTGTGTCTA TACACACACT CACTCCCAAG CACCACGTAC ATAGCTCCTA
6301 TTATTGGAGC AATGTACTTT TGAGTTAAAA ACTCCAACAT GAATGGATTG GGGGTCGTCT
6361 GGAGATGGTT CTACATGTTG CTGGAGGACT TTTACCCTCA GAGAGATCAT ATCACACCCT
6421 GCCAATGATT CTCAGTTTTT GCCTGGAGGA ACTGTCTAGA AAGGCTAATG TAATGAAGCC
6481 AGTATTAACC ACCTCATTTC TAAGCTGCCA AACAGGTCTT AAGGGAGCCA CTTCTGTCCA
6541 CCTAACCACC TCCAGCTCTG TGTCCAGCTG AGATCTCTAT TGTTTCCTCT TGAATGTCCA
6601 CGAACCACTG TAATAGCATC AGACCCTTAA ATGAGTGTGC AATTGTTTCT CTTGAAGTTT
6661 GGTCCATTCG TTATTTTTAA TTAACTGCAC TTCTTGATAT TCAAATGTTC TATTAAAAAT
6721 AATTGTGAAA AACACTCCAC TACTGTAGAA GAAAGAGGTG GTACAATGTG ACCAACTTCA
6781 ACTACAACAG TGTTGTTTAA GAGATTTATT GTACGATTAT GAAAAATGAA GTAATCGACT
6841 AAATAATAAA CAAAGCTGTC AGT

Accession number for the full *Astrotactin* cDNA sequence: U48797.

Region of overlap with the sequence of the *Astrotactin* cDNA clone used for the preparation of a probe for wholemount *in situ* hybridisation. The cDNA clone (accession number W10500) was obtained from the I.M.A.G.E. Consortium at H.G.M.P. See text for details.

4.2.2. DNA protocols

4.2.2.1. Purification of DNA from agarose gels

The purification of PCR products to be sequenced or cloned was performed by first separating them from non-specific products and unincorporated primers with electrophoresis through 1% LMP agarose gels. Subsequently, a slice of gel containing the DNA to be purified was cut and the DNA was extracted from the gel using the Wizard PCR Preps DNA Purification System (Promega) or an alternative phenol-chloroform protocol. In the case of the Wizard PCR Preps system, the gel slice containing the band of interest was melted at 70°C for 15 minutes then mixed with 1 ml Wizard PCR Preps DNA Purification Resin, a silica-based mixture that binds the DNA fragments. The mixture was pipetted into a 2 ml disposable syringe attached to a Wizard Minicolumn, then gently expelled from the syringe into the Minicolumn. The column retains the silica-DNA complex while allowing all other components (agarose, primers, dNTPs and salts) to pass through. The bound DNA was washed by passing 2 ml 80% isopropanol through the Minicolumn slowly and then dried by centrifuging at 12,000 rpm for 20 seconds at room temperature. Fifty microliters of de-ionised distilled water (ddH_2O) were added to the Minicolumn. One minute later, the purified DNA was eluted from the Minicolumn by centrifuging again for 20 seconds at 12,000 rpm.

In the alternative (phenol-chloroform) protocol, 500 μl ddH_2O were added to the gel slice-containing tube and the latter was heated to 65ºC for approximately 20 minutes, to allow the agarose to melt completely. An equal volume of equilibrated phenol was added to the digest, homogenised and spun for 3 minutes at 12000 rpm at room temperature, to remove any remaining protein.

The aqueous phase was transferred to a new microfuge tube and the phenol extraction was repeated once. Chloroform was then added and the tube was homogenised with a vortex and spun for 15 seconds at 12000 rpm (room temperature), to remove the phenol. The upper, aqueous (DNA-containing) phase was transferred into a new microfuge tube. DNA was precipitated with an equal volume of isopropanol and 50 μl 3M sodium acetate at -20° C for at least 2 hours. Tubes were spun at 13000 rpm for 15 minutes at 4°C. The supernatant was discarded and the pellet was washed with 100 μl of 70% ethanol, then spun for 5 minutes at 13000 rpm at 4°C. The supernatant was again discarded and the pellet was air-dried, then re-suspended in 20 μl of ddH_2O.

4.2.2.2. Restriction enzyme digestion of DNA

Restriction digests of DNA samples were carried out in accordance with the conditions suggested by the manufacturers for each enzyme (Promega, Gibco BRL or New England Biolabs). Each digestion included 4-6 μg DNA (usually plasmid DNA) and 10 units of the appropriate restriction enzyme, in a total volume of 20 μl. This mixture was incubated for one to two hours at the recommended temperature. The efficiency of the digestion was confirmed by the presence of bands of the expected sizes after electrophoresis of a small amount of digestion solution (approximately 3 μl) through a 1% agarose gel.

4.2.2.3. Cloning DNA fragments

4.2.2.3.1. Ligations

PCR products were cloned with the pGEM-T vector System (Promega). This vector has 5'-T overhangs at the insertion site, allowing for easy cloning of PCR products, since *Taq* (and BioPro) DNA polymerases add a single adenosine to

3'-DNA ends of amplified products, creating a 3' overhang. Prior to setting up the ligation reaction, PCR products were purified from unincorporated primers and nucleotides using the Wizard PCR Preps Purification System (Promega). Ligation reactions were set up in a total volume of 10 μl containing 50 ng vector and with the appropriate quantity of insert DNA to give a 3:1 molar ratio of insert: vector. Reactions also contained 1 Unit T4 DNA ligase and 1 x T4 DNA ligase buffer (Gibco BRL), and were incubated at 15°C for 5-14 hours. A positive control reaction (containing a control insert DNA instead of the PCR product) as well as a negative control reaction (containing no DNA) were run in parallel with the PCR product ligation reaction.

4.2.2.3.2. Transformation of plasmid DNA into competent bacterial cells

Supercompetent XL1 Blue or Ultracompetent XL2 Blue cells were used for transformations, according to the protocol of the supplier (Stratagene). Plasmid DNA was introduced into bacterial cells by heat shock. Supercompetent XL1 Blue or Ultracompetent XL2 Blue cells were thawed on ice, and 40 μl was used for each transformation. The efficiency of transformation was maximised by pre-incubating the cells with 0.7 μl β-mercaptoethanol for 10 minutes. The period of application of the heat shock and the temperature used differed according to the type of competent cells used: XL1 Blue cells required a heat shock at 42°C for 45 seconds, while for XL2 Blue the conditions were 42°C for 30 seconds. Reactions were stopped by putting tubes on ice for 2 minutes.

4.2.2.3.3. Growing colonies containing the insert of interest

The recombinant *E. coli* were selected on the basis of acquired resistance to ampicillin, since an ampicillin-resistance gene is present in the vector DNA. In

addition, pGEM-T has a multiple cloning site that lies within a functional β-galactosidase gene, which in the presence of isopropyl-1-thio-β-D-galactoside (IPTG) acts on 5-bromo-4-chloro-3-indolyl-β-D-galactoside (X-gal), a chromogenic substrate, to produce a blue product. If the vector contains no insert, the β-galactosidase gene is active and, therefore, in the presence X-gal and IPTG the colony turns blue. However, if DNA has been inserted into the multiple cloning site, the β-galactosidase gene is disrupted and the colony remains white after the addition of IPTG. This makes it possible to differentiate between colonies that contain a plasmid with an insert, and those that contain the vector with no insert. Transformation reactions, to which LB broth had been added, were plated onto LB-agar plates containing ampicillin, IPTG and X-Gal and incubated at 37º C overnight. White colonies were then grown in ampicillin-containing LB-broth, before plasmids were isolated following the protocol below.

4.2.2.3.4. Small-scale isolation of plasmid DNA

Small scale isolation of plasmid DNA (yielding 1-5 μg) was performed using the Wizard Minipreps DNA Purification System (Promega). Cultures were grown for 8-16 hours in L-broth with the appropriate selective antibiotic (ampicillin) and 3 ml was used for plasmid isolation. The cells were pelleted by centrifugation at 13,000 rpm for 2 minutes, then resuspended in 200 μl cell resuspension solution (50 mM Tris-HCl pH 7.5, 10 mM EDTA pH 8.0, 100 μg/ml ribonuclease [RNase] A). Next, cells were lysed and the DNA denatured by the addition of 200 μl cell lysis solution (0.2 M NaOH, 1% SDS), This was done by gently inverting the tube, to ensure all cells were lysed, but without causing shearing of the chromosomal DNA. Samples were neutralised by the addition of 200 μl neutralisation solution (1.32 M potassium acetate, pH 4.8), allowing the plasmid

DNA (but not the chromosomal DNA) to renature. The white precipitate of proteins and chromosomal DNA was removed by centrifugation at 13,000 rpm for 5 minutes, and the plasmid DNA was isolated using a Wizard Minipreps DNA Purification Minicolumn, as described in section 4.2.2.1. DNA was washed with 2 ml column wash buffer (83 mM NaCl, 8.3 mM Tris-HCl pH 7.5, 2.1 mM EDTA pH 8.0, 58% ethanol), and residual wash buffer was removed by centrifugation at 13,000 rpm for 2 minutes. The plasmid DNA was eluted from the minicolumn with 50 μl ddH_2O.

4.2.2.4. Qiagen purification protocol

Qiagen columns generate good quality DNA and were used for preparing plasmid DNA for automated sequencing. As described above, cultures were grown for 6-12 hours in L-broth with the appropriate antibiotic and 3 ml was used for plasmid isolation. The bacteria were pelleted by centrifugation at 13,000 rpm for 2 minutes, then resuspended in 0.3 ml resuspension buffer (100 μg/ml RNase A, 50 mM Tris-HCl pH 8.0, 10 mM EDTA pH 8.0). Cells were lysed and the DNA was denatured by the addition of 0.3 ml lysis buffer (200 mM NaOH, 1% SDS) followed by a 5 minute incubation at room temperature. The plasmid DNA was renatured and the chromosomal DNA and proteins were precipitated by adding 0.3 ml chilled neutralisation buffer (3.0 M potassium acetate, pH 5.5) and incubating on ice for 10 minutes. The bacterial DNA and proteins were pelleted by centrifugation for 15 minutes at 13,000 rpm at 4°C and the supernatant was applied to a Qiagen tip 20 after equilibration with 1 ml buffer QBT (750 mM NaCl, 50 mM MOPS, 15% ethanol, pH 7.0, 0.15% Triton X-100). The Qiagen tip contains Qiagen resin which binds DNA but does not, under the salt and pH conditions used, bind RNA, proteins or metabolites. The

bound DNA was washed four times with 1 ml buffer QC (1.0 M NaCl, 50 mM MOPS, 15% ethanol, pH 7.0), to elute any residual RNA and to disrupt any non-specific interactions. The DNA was eluted by adding 0.8 ml buffer QF (1.25 M NaCl, 50 mM Tris-HCl pH 8.5, 15% ethanol), then precipitated by adding 0.7 volumes isopropanol. The DNA was pelleted by centrifugation at 13,000 rpm for 15 minutes at 4°C, washed with 70% ethanol, then resuspended in TE.

4.2.2.5. Sequencing protocols

Sequencing of DNA was carried out by the conventional di-deoxy method, with the incorporation of ^{35}S, or with fluorescent ATP and automated sequencing. In both cases, the primer is annealed to a single-stranded DNA template and then extended in the presence of the four dNTPs and one dideoxynucleotide (ddNTP). Incorporation of a dideoxynucleotide prevents further DNA synthesis, and so a fraction of the extending products will terminate at each site where the ddNTP can be incorporated. Four separate reactions, each with a different ddNTP, give the complete sequence information. Acrylamide gel electrophoresis size fractionates the products, and inclusion of a labelled nucleotide (or primer) allows the products to be visualised (by fluorescence or autoradiography) and the sequence to be read.

4.2.2.5.1. Conventional manual sequencing with ^{35}S

This was carried out using the Sequenase 2.0 DNA Sequencing Kit (Amersham). The DNA template (3-5 μl) was first denatured by incubation with 0.1 volume 2 M NaOH/2 mM EDTA at 37ºC for 30 minutes. This mixture was then neutralised with the addition of 0.1 volume 3 M sodium acetate (pH 5.2). The DNA was then precipitated with 2 volumes ethanol on dry ice for 20

minutes, pelleted by centrifugation at 13000 rpm for 20 minutes, washed with 70% ethanol and dissolved in 7 μl of ddH_2O. Annealing reactions were performed by heating to 65ºC for 3 minutes the denatured DNA template to which 2 μl of reaction buffer and 1 ml of primer had been added. After allowing the mixture to cool to under 37ºC, over 15-30 minutes, labelling reactions were set on ice. For this, 1 μl of 0.1 M DTT (dithiothreitol) and 2 μl of labelling mix (diluted 1:5 with ddH_2O), 0.5 μl of [α-^{35}S]-dATP (10 μCi/μl, 1000 Ci/mmol; ICN) and 2 μl of Sequenase polymerase (diluted 1:8 in enzyme dilution buffer) were added to the mixture. This labelling mix was incubated for 5 minutes at room temperature, then aliquots (3.5μl) were transferred to new microfuge tubes containing 2.5 μl of either A.C, G or T termination mix (preheated to 37ºC). The reactions were carried out at the same temperature for about 5 minutes, then stopped by the addition of 4 μl bromophenol blue stop solution (95% formamide, 20 mM EDTA, 0.05% bromophenol blue, 0.05% xylene cyanol FF). Products were electrophoresed through 6% denaturing acrylamide gels.

4.2.2.5.2. Sequencing with fluorescently-labelled primers

This method was used to confirm the sequence of cloned cDNA fragments of murine *astrotactin* and *Pou2f1* genes, used for the preparation of RNA probes. Reactions were performed with the AutoRead sequencing kit (Pharmacia) with a fluorescently labelled Universal or Reverse primer (Pharmacia). Plasmid DNA was prepared using the Qiagen isolation procedure, yielding a highly pure DNA solution (section 4.2.2.4).

The template DNA (5-10 μg) was denatured by mixing 32 μl DNA with 8 μl of 2 M NaOH and incubating at room temperature for 10 minutes. DNA precipitation

was achieved by adding 7 μl of 3 M sodium acetate (pH 4.8), 4 μl ddH_2O and 120 μl ethanol and standing in dry ice for 15 minutes. Following centrifugation to pellet the DNA, it was washed with 70% ethanol then resuspended in 10 μl ddH_2O. The primer was annealed by mixing 10 μl denatured DNA, 2 μl fluorescent primer and 2 μl annealing buffer with incubation at 65°C for 5 minutes followed by incubation at 37°C for 10 minutes then at room temperature for 10 minutes. The annealed template-primer was mixed with 1 μl extension buffer, 3 μl DMSO and 2 μl T7 DNA polymerase (diluted 1:1 with enzyme dilution buffer), then 4.5 μl aliquots were mixed with 2.5 μl ddNTP mix preheated to 37°C. These termination reactions were incubated at 37°C for 5 minutes then stopped by adding 5 μl dextran blue stop solution (formamide containing 5 mg/ml Dextran Blue 2000). Samples were electrophoresed through 6% acrylamide gels using the automated laser fluorescence sequencer (section 2.12.3).

4.2.2.5.3. Acrylamide gel electrophoresis

Manual sequencing gels: Denaturing 6% acrylamide gels were used to analyse the products of ^{35}S sequencing reactions and were electrophoresed on a model S2 sequencing gel apparatus (Gibco BRL). The shorter of the two glass sequencing plates was wiped over with a silane-based solution (Sigmacote, Sigma) in order to ensure that the gel would remain adherent to the long plate when the plates were later separated. Gels were prepared with 0.35 mm spacers and a 48- or 64-well "sharkstooth" comb (Gibco BRL), using the Sequagel Sequencing System (National Diagnostics) to contain 6% or 8% acrylamide/bisacrylamide (19:1), 8.3 M urea and 1 x TBE buffer (10 x TBE = 0.88 M Tris, 0.89 M boric acid, 20 mM EDTA pH 8.0). Gels were polymerised by

the addition of ammonium persulphate (APS) to 0.06% and N,N,N',N'-tetramethylethylenediamine (TEMED) to 0.07% and allowed to stand for 30 minutes-14 hours before use.

Electrophoresis was carried out with 1 x TBE buffer, and the gel was heated before loading the samples by pre-running at 100 W for 20-30 minutes. Samples were denatured by heating at 75°C for 5 minutes, then loaded into the wells. Electrophoresis was performed at 75 W for 2-5 hours.

Each gel (still adhering to the longer glass plate) was fixed by immersion in 10% acetic acid/20% industrial methylated spirit (IMS) for 30 minutes. This step removes urea and sucrose. The acetic acid is then removed by immersion in tap water for 10 minutes. After blotting onto Whatmann 3MM paper, the gel was dried under vacuum for 1-2 hours at 80°C. Autoradiography was performed using blue sensitive X-ray film (Genetic Research Instrumentation) for 6 hours to 1 week, depending on the isotope used and the intensity of the signal.

Automated sequencing gels: Sequencing reactions containing a fluorescent label were electrophoresed on the automated laser fluorescence sequencer. Following thorough washing of the glass plates using a non-fluorescent detergent, the top 5 cm of both plates were treated with BindSilane (Pharmacia) to ensure that the gel forms a tight seal around the wells. Gels were assembled with 0.35 mm spacers. The gel itself contained 6% acrylamide, 7M urea and 1.2 x TBE and was prepared using Hydrolink Long Ranger modified acrylamide gel (Mallinckrodt Baker, UK) and automated laser fluorescence-grade urea (Pharmacia). The 40 ml gel mix was passed through a 0.45 μm filter, and

polymerised by the addition of 200 μl 10% APS and 20 μl TEMED. After pouring, a comb was inserted and clamped tightly into position, and the gel left to polymerise for at least 90 minutes.

Once placed into the sequencer, the position of the gel was adjusted to give the maximum laser brightness with the minimum interference from dust particles. The laser was set at 2-4 mW to give a background fluorescence of between 20 and 40% of the saturation level of the detectors. Gels were preheated to 50°C by water circulation for 10 minutes then the samples loaded in the order A, C, G, T, for each template. Electrophoresis was carried out with 0.6 x TBE buffer at 35 W overnight, with the detectors set to record a signal every 1.25 seconds over 600 minutes.

4.2.2.6. Sequence analysis

Sequence analysis was performed using software designed by the Genetics Computing Group (GCG, Wisconsin, USA), made available through the UK Human Genome Mapping Project (HGMP) Resource Centre at the internet address http://mgd.hgmp.mrc.ac.uk.

4.2.3. RNA protocols

4.2.3.1. General precautions taken while working with RNA

In order to avoid contamination of RNA preparations with RNAases, several precautions were taken. All glassware was baked overnight at 180°C before use. Sterile plastic-ware was assumed to be RNAse-free. All solutions for RNA work were made, where possible, from solid reagents. These solids were weighed out using sterile plastic-ware. As a general rule, solutions were treated with 0.05% diethyl pyrocarbonate (DEPC), a potent inhibitor of ribonuclease (RNAse), left overnight at room temperature, then autoclaved. Solutions containing Tris or EDTA, as well as non-autoclavable solutions such as SDS, were made up in DEPC-treated distilled de-ionised water, in bottles that had been DEPC-treated and autoclaved. Rubber gloves were worn at all times and the working area was kept as dust-free as possible.

4.2.3.2. RNA extraction

Total RNA was extracted from brain tissue using the TRI reagent (Gibco BRL). TRIzol promotes formation of RNA complexes with guanidine and water molecules and inhibits hydrophilic interactions of DNA and proteins. As a consequence, DNA and proteins are excluded from the aqueous phase, leaving the RNA, which can then be purified. Initially, the tissue to be used is homogenised in TRI reagent (in a ratio of tissue to TRI reagent that should not exceed 1:10). This was done by syringe pumping in and out through needles of decreasing gauge (21G, 23G, 25G), until a fine suspension was obtained. Next, the homogenised tissue was left at room temperature for 5 minutes to complete the dissociation of nucleoprotein complexes, then spun for 5 minutes at 13,000 rpm to pellet cellular debris. The supernatant was decanted into a new tube,

and one fifth volume of chloroform was added. The samples were vortexed for 15 seconds and incubated at room temperature for 5 minutes, then centrifuged at 12,000 rpm for 15 minutes at 4°C, in order to separate the upper aqueous phase contains the RNA from the protein-containing interface and the lower red, phenol-chloroform phase containing DNA and proteins. The aqueous phase was carefully pipetted out and transferred into a clean microfuge tube, mixed with an equal volume of isopropanol, then left to stand at room temperature for 10 minutes to precipitate the RNA. The samples were again centrifuged at 12,000 rpm at 4°C for 15 minutes, to pellet the RNA. The supernatant was discarded and the pellet was washed in 75% ethanol before re-spinning at 7500 rpm for 5 minutes. The pellet was air dried and re-suspended in 50-100 μl DEPC ddH_2O, depending on the size of the pellet. The RNA was stored at -70°C or -20°C until use.

4.2.3.3. Reverse transcription (RT) – PCR

RT-PCR was used generate cDNA fragments for sequence analysis. Total RNA was used as a template for first strand cDNA synthesis, by reverse transcription, and this single stranded cDNA was then used as a template for PCR. Reverse transcription was performed routinely from total RNA, using random hexanucleotides as the primers. Hexanucleotides were annealed to the RNA by mixing together approximately 300-500 ng total RNA (for example, half the total RNA extracted from a single E8.5 embryo) and 0.2 μg random hexanucleotides (Gibco BRL) in a volume of 9.5 μl. The mixture was denatured by heating to 70°C for 6-7 minutes, then annealed by incubating at 37°C for 10 minutes.

The reverse transcription reaction was performed in a 20 μl volume containing the 9.5 μl annealed RNA/hexanucleotide mixture, 1 x first strand RT reaction buffer, 0.25 mM each dNTP, 10 mM DTT, 0.5 μl RNase inhibitor (Pharmacia) and 1 μl (200 Units) Moloney murine leukemia virus (MMLV) reverse transcriptase (Gibco BRL). The RT mix was prepared as a single batch for each set of reactions, and then aliquoted. RT reactions were incubated at 37°C for 1 hour, then stopped by heating to 95°C for 5 minutes. The first strand cDNA product was then diluted to 40 μl and stored at -20°C.

RT-PCR was carried out as described for the conventional PCR reactions, using 1 μl first strand cDNA product and a high-fidelity Taq polymerase (Biopro, Bioline).

4.2.3.4. Wholemount *in situ* hybridisation

Wholemount *in situ* hybridisation of mouse embryos was carried out essentially as described previously (Wilkinson, 1992; Wilkinson, 1993). First, digoxygenin-labelled probes were synthesised to hybridise with target DNA. Embryos were collected and pre-treated with a pre-hybridisation mixture. Finally, hybridisation was performed, embryos were washed to remove unbound probe and the reaction was visualised by the addition of enzymes which produce a coloured reaction.

For the synthesis of single-stranded RNA probes, pGEM-T clones of the fragments of interest were used. The pGEM-T vector has two RNA polymerase initiation sites (for T7 and SP6 RNA polymerases) flanking the plasmid cloning site. This enables either sense-strand (control) or antisense

(probe) RNA to be synthesised from pGEM-T clones, depending on the orientation of the insert. Before transcription takes place, however, the plasmid has to be linearised by digestion with an appropriate restriction enzyme, in order that the RNA polymerase ceases RNA synthesis immediately after transcribing through the insert. If this is not done, plasmid sequences will be transcribed, resulting in a high level of background staining. Following purification, 2 μg of linearised plasmid DNA was transcribed in a 20 μl reaction containing also 1x transcription buffer, 10 mM DTT, 2 μl digoxygenin-RNA labelling mix (Boehringer Mannheim), 50 Units placental ribonuclease inhibitor, 10 Units (2μl) of either Sp6 or T7 RNA polymerase and 12 μl DEPC-ddH_2O. The transcription reaction was incubated at 37°C for 2 hours. Next, 1 μl of the transcription reaction was electrophoresed on a 1% agarose gel to check that the reaction had worked successfully and that a sufficient amount of RNA had been synthesised (if so, the RNA band should appear at least 10 fold more intense than the plasmid band). If the reaction was successful, the RNA was precipitated by the addition of 100 μl DEPC-TE, 10 μl 4M LiCl and 300 μl ethanol, mixing and incubating at -20°C for 30 minutes. The RNA probe was pelleted by centrifugation at 13,000 rpm for 10 minutes, washed in 70% ethanol and allowed to air-dry. The probe was re-dissolved in DEPC-TE at approximately 0.1 μg/μl and stored at -20°C. until needed.

Each embryo was dissected from its extra-embryonic membranes as described in section 2.4.1 and rinsed twice in cold DEPC-treated PBS, then fixed overnight at 5°C in 4% paraformaldehyde in DEPC-PBS. Embryos were washed twice in PBT (PBS including 0.1% Tween-20) at 4°C for 5 minutes each wash, then de-hydrated through a series of methanol solutions at 4ºC

(25%, 50%, 75% methanol in PBT and twice in 100% methanol) in order to prevent the formation of bubbles during treatment with hydrogen peroxide (see below). De-hydrated embryos were stored at –20°C until needed. Embryos were re-hydrated by taking them through 75%, 50%, 25% methanol solutions in PBT (DEPC-PBS with 0.1% Tween-20) for 10-15'at 4ºC and washing twice in PBT. They were incubated with 6% hydrogen peroxide (in DEPC-treated PBT) for 1 hour, to block endogenous peroxidases, then washed in PBT three times (5-10 minutes each wash). Next, bleached embryos were treated with 10 μg/ml proteinase K (in DEPC-treated PBT) for 4 minutes (E9.5 embryos), 5 minutes (E10.5) or 8 minutes (E11.5) at room temperature, to increase penetration of the probe. Proteinase K digestion was stopped by transferring embryos into a freshly prepared solution of 2 mg/ml glycine in PBT at room temperature for 10 minutes. Next, embryos were washed in PBT and re-fixed in freshly-prepared 0.2% glutaraldehyde in 4% PFA in DEPC-PBS for 20 minutes at room temperature and washed in DEPC-PBT. In order to avoid trapping of the labelled probe in the ventricular cavities of the brain, the roof of the IV ventricle was then pierced with a sterile needle under the stereomicroscope.

For the pre-hybridisation step, embryos were incubated for at least 1 hour at 70ºC in a pre-hybridisation solution, containing 50% formamide, 5 x SSC pH 4.5, 50 μg/ml heparin, 50 μg/ml yeast transfer RNA, and 1% SDS.

Next, embryos were hybridised overnight at 70°C in 1 ml fresh prehybridisation solution containing the digoxygenin-labelled RNA probe at 1 μg/ml. One tube was used per genotype group (e.g. *dr^{J}/+, +/+, dr^{J}/dr^{J}*) for the anti-sense probe

(containing embryos from the 3 age groups) and another one for the sense probe (which included at least one embryo from each age group).

Unless otherwise stated, all washes were for 5', carried out with gentle rocking, and at room temperature (RT). Following hybridisation, the embryos were transferred to 15 ml Falcon tubes to enable all the washing steps to be performed in a volume of around 10 ml. Washes aimed at removing any remains of probe that had not annealed to target RNA. Embryos were first washed twice in solution 1 (50% formamide, 5 x SSC pH 4.5, 1% SDS), then twice in solution 2 (50% formamide, 2 x SSC pH 4.5), for 1 hour each at 70°C. They were then washed in TBST [137 mM NaCl, 2.7 mM KCl, 25 mM Tris HCl pH 7.5, 1% Tween-20, 0.48 mg/ml Levamisole (Sigma)] three times for 5 minutes each at room temperature, then pre-treated with 10% sheep serum in TBST for 90 minutes at 4°C to prevent non-specific binding of the antibody. This was followed by incubation with an anti-digoxygenin antibody (Boehringer Mannheim) conjugated to alkaline phosphatase. The anti-digoxygenin antibody was diluted 1 in 1000 with TBST and 0.1% sheep serum, then pre-absorbed by incubating with embryo powder (homogenised E12.5 mouse embryos, washed with acetone), for 1 hour at 4°C. This was done to minimise non-specific binding of the polyclonal antibody. The antibody was then removed from the embryo powder by centrifugation, diluted with an equal volume TBST containing 1% sheep serum, then filtered through a 0.4 μm Millipore filter. Embryos were incubated overnight at 4°C with 2 ml pre-absorbed antibody solution, then washed at room temperature for 24 hours with 10 hourly changes of TBST. The TBST was replaced with NTMT (100 mM NaCl, 100 mM Tris HCl pH 9.5, 50 mM $MgCl_2$, 0.1% Tween-20).

Finally, embryos were transferred to glass vials and the colour reaction produced by incubation in the dark with 4.5 μl 4-nitro blue tetrazolium chloride (NBT) and 3.5 μl 5-bromo-4-chloro-3-indolyl-phosphate (BCIP) in 1 ml NTMT. After completion of the colour reaction the embryos were washed in PBT and photographed using a Zeiss SV11 stereomicroscope.

4.2.3.4.1. Vibratome sectioning of wholemount embryos

Embryos were equilibrated overnight in a gelatine-albumin mix (0.45g gelatine 300 Bloom, 27g chicken egg albumin grade II and 18g sucrose in 80 ml PBS) then orientated and set in a plastic mould with the addition of glutaraldehyde to 2.5%. The mix was allowed to set for at least 1 hour, then 50 μm thick sections were cut using a Series 1000 vibratome (Agar Scientific). Embedded embryos were sometimes stored in PBS at 4°C for several months before sectioning. Sections were mounted onto slides with 50% glycerol/PBT and examined using differential interference contrast (DIC; Nomarski) optics on an Axiophot microscope (Zeiss).

4.3. Results

4.3.1. Sequencing studies of *Pou2f1*

Sequencing of the POU-specific domain of *Pou2f1* in a homozygous mutant dr^J and a CD1 control mouse revealed no differences in either case from the published sequence of *Pou2f1* (Figure 4.1).

Reading the first 139 bases of the sequencing of the *Pou2f1* cDNA clone confirmed that the selected region of the gene had been cloned before preparation of the RNA probe for *in situ* hybridisation.

4.3.2. Analysis of the expression pattern of *Pou2f1* in wild type, heterozygous and homozygous mutant dr^J embryos by wholemount *in situ* hybridisation

The present analysis concerns embryos at E9.5, E10.5 and E11.5 that were hybridised with an anti-sense riboprobe designed from the region of *Pou2f1* that lies 3' to the POU-specific domain (depicted in Figure 4.1). The labelling pattern obtained with the probe for the POU-specific domain (used on control embryos only) was similar to that presented below. No staining of embryos was obtained with sense probes at any of the ages (E9.5 E10.5, or E11.5).

The expression patterns obtained with the antisense probe in heterozygous embryos were indistinguishable from their wild-type counterparts, and for this reason, heterozygote embryos are not shown in the figures.

With the antisense probe, at E9.5 (18 to 20 somite-stage), embryos from all three genotypes showed relatively strong staining in the branchial arches. A fainter signal was seen in the forelimb bud, ventral head region, otic vesicles and somites. (Figure 4.3A,B). Figure 4.4A depicts the expression of the *Pou2f1* riboprobe in transverse sections through the branchial arches of a dr^J/dr^J embryo at E9.5 .

At E10.5 (30-35 somite-stage), wild type, heterozygous and homozygous dr^J embryos all showed strong expression of the *Pou2f1* probe in the branchial arches, ventral region of the head, and both fore- and hindlimb buds (Figure 4.3C). Somites also expressed the riboprobe, although less intensely, with a stronger band of labelling at the level of the last forming somite, possibly corresponding to pre-somitic mesoderm (Figure 4.5A and B). A very low level of expression of the *Pou2f1* riboprobe could be detected in the midbrain-hindbrain boundary by this stage (Figure 4.3C).

In E11.5 embryos of all three genotypes, strong expression of the riboprobe seemed to have become almost restricted to the head region (Figure 4.3D,E). The intensity of expression was strongest at the midbrain-hindbrain boundary and in the ventral head region, although transcripts could also be detected more rostrally between the telencephalic vesicles. Coronal sections through the midbrain- hindbrain region show this region of strong expression of the *Pou2f1* riboprobe is restricted to the mesoderm-derived tissues around the neurepithelium of the differentiating neural tube, between the telencephalic vesicles and around the diencephalon and midbrain-hindbrain isthmus (Figure 4.6). No significant differences in the pattern or intensity of staining were seen

Figure 4.3

Wholemount *in situ* hybridisation with a *Pou2f1* riboprobe on wild type and dr^J/dr^J embryos at E9.5 (20-somite stage), late E10.5 (35-somite stage) and E11.5 (45-50 somite stage)

(A) E9.5. Left is wild type, right is dr^J/dr^J. **(B)** E9.5A dr^J/dr^J embryo showing high-level expression of the probe in the branchial arches (ba) and forelimb buds (flb). Faint staining is also seen in the presumptive diencephalic region (d) and in the somites (arrowhead). ov: otic vesicle. **(C)** E10.5 embryos. Left is wild type, right is dr^J/dr^J. Notice strong staining of branchial arches, limb buds, diencephalic region. Faint staining is starting to appear in the isthmus between the hindbrain and the midbrain (arrowheads). flb: forelimb bud. hlb: hind limb bud. ba:branchial arch. **(D)** and **(E)** E11.5 embryos. Left is wild type,right is dr^J/dr^J. Staining is mostly restricted to the head, although it is still seen in the limbbuds and in the somites (black arrowheads). The signal is particularly strong in the hindbrain-midbrain boundary (white arrowheads). Notice also the difference in shape of the dorsal-hindbrain transition between wild type and homozygous mutant. Scale bar represents: (A) 250 μm. (B) 150 μm. (C) 600 μm. (D) 720 μm. (E) 970 μm.

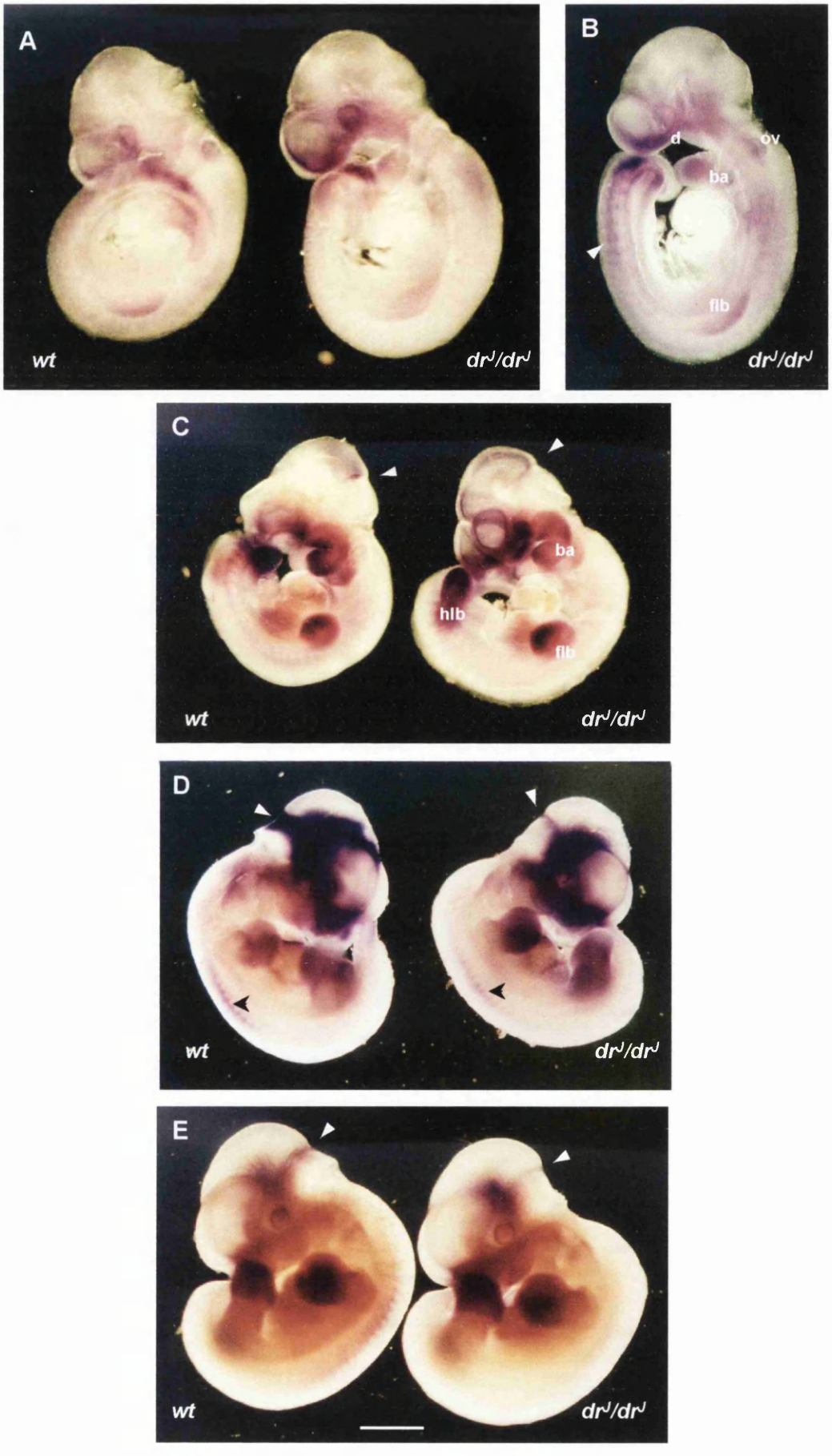
A
wt
dr^J/dr^J
B
d
ov
ba
flb
dr^J/dr^J
C
ba
hlb
flb
wt
dr^J/dr^J
D
wt
dr^J/dr^J
E
wt
dr^J/dr^J

Figure 4.4

Vibratome sections of *dr*^{J} embryos after wholemount *in situ* hybridisation with an antisense riboprobe for *Pou2f1*

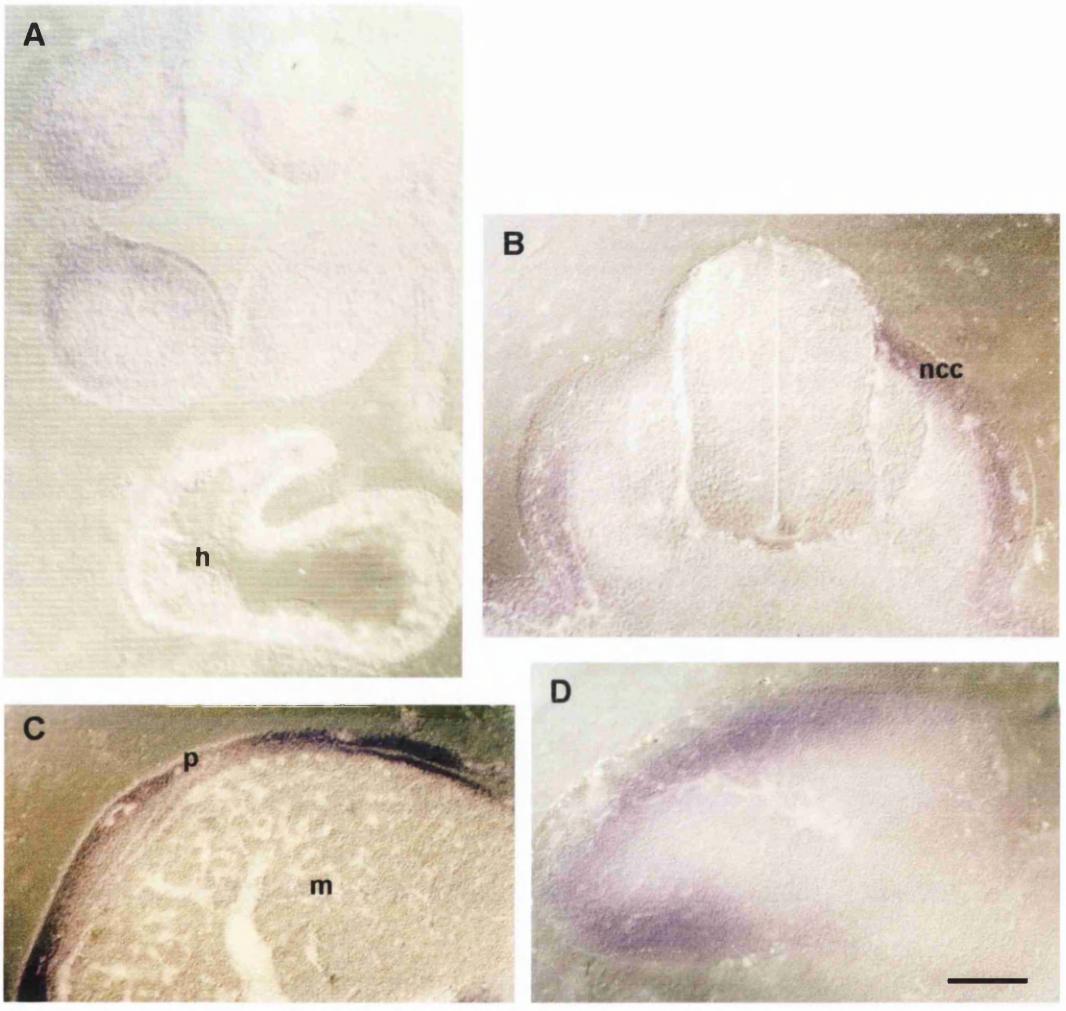

(A) Transverse section through the branchial arches and the heart of a *dr*^{J}/*dr*^{J} embryo at E9.5. Branchial arches express the labelled *Pou2f1* probe. **h**: heart. **(B)** Transverse section of a E11.5 wild type embryo to show migrating neural crest cells (**ncc**) and dermomyotome, both expressing *Pou2f1*. **(C)** The myocardium (**m**) is negative,whereas the pericardium (**p**) shows strong expression of the *Pou2f1* riboprobe. **(D)** Forelimb bud of a E11.5 wild type embryo. Transverse section of a E11.5 wild type embryo. The outer part of the limb buds expresses the labelled *Pou2f1* probe.
Scale bar represents: (A) 340 μm, (B) 590 μm, (C) 500 μm, (D) 500 μm.

Figure 4.5

Expression of *Pou2f1* in the somites of *dr*^{J} embryos by wholemount *in situ* hybridisation with an antisense riboprobe

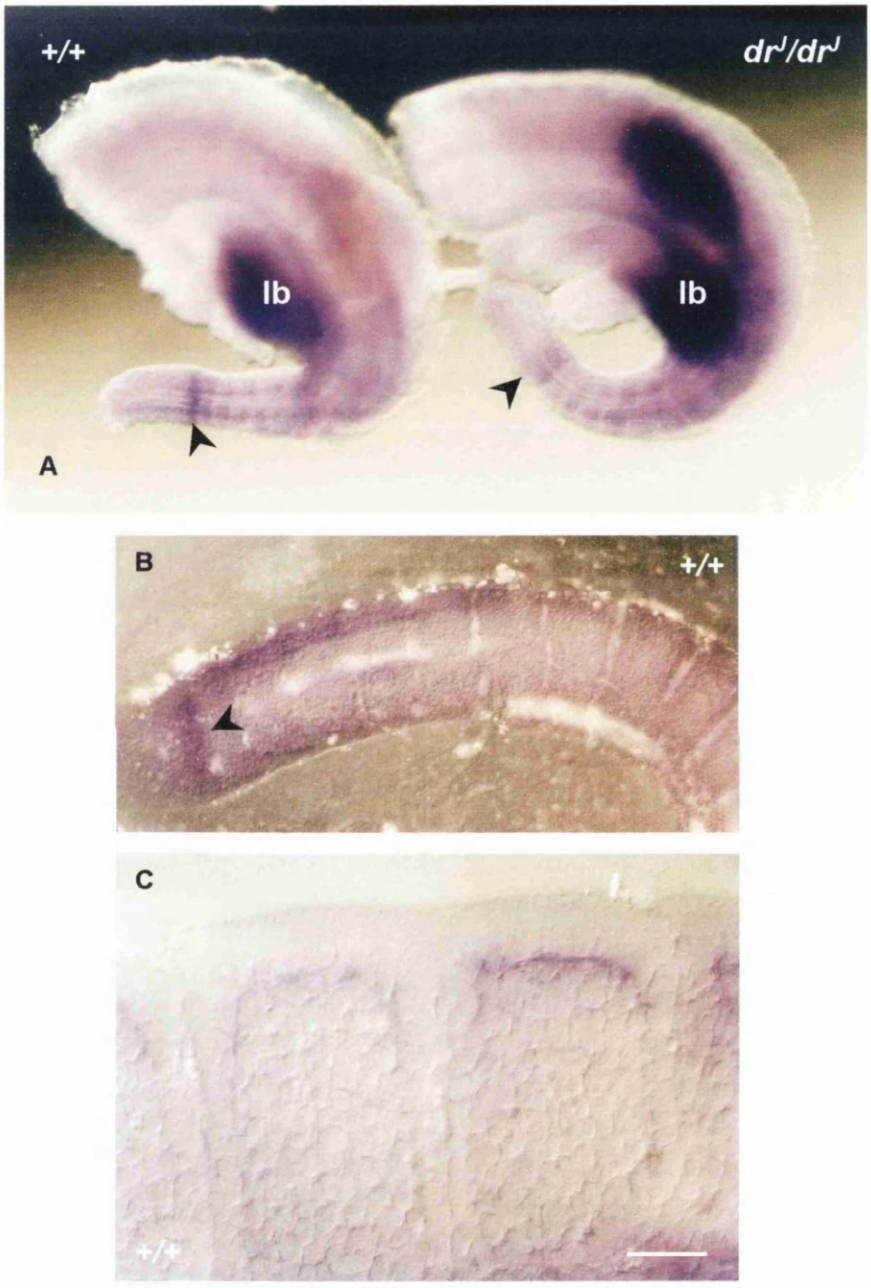

(A) Caudal part of embryos at E10.5. Left is wild type, right is *dr*^{J}/*dr*^{J}. There is faint expression in the somites and a stronger band of staining in the pre-somitic mesoderm, near the tailtip (arrowheads). **(B)** Vibratome section of a wild type embryo at E11.5. The arrowhead points to the band of *Pou2f1* mRNA expression in the pre-somitic mesoderm. **(C)** Vibratome section through the greater axis of the tail of a wild type embryo at E11.5, to show that expression is mostly confined to the outer somite, beneath the ectoderm. Scale bar represents: (A) 200 μm (B) 100 μm, (C) 60 μm.

Figure 4.6

Expression of *Pou2f1* at the hindbrain-midbrain boundary: Vibratome sections of *dr^{J}* embryos at E11.5, after wholemount *in situ* hybridisation with an antisense riboprobe.

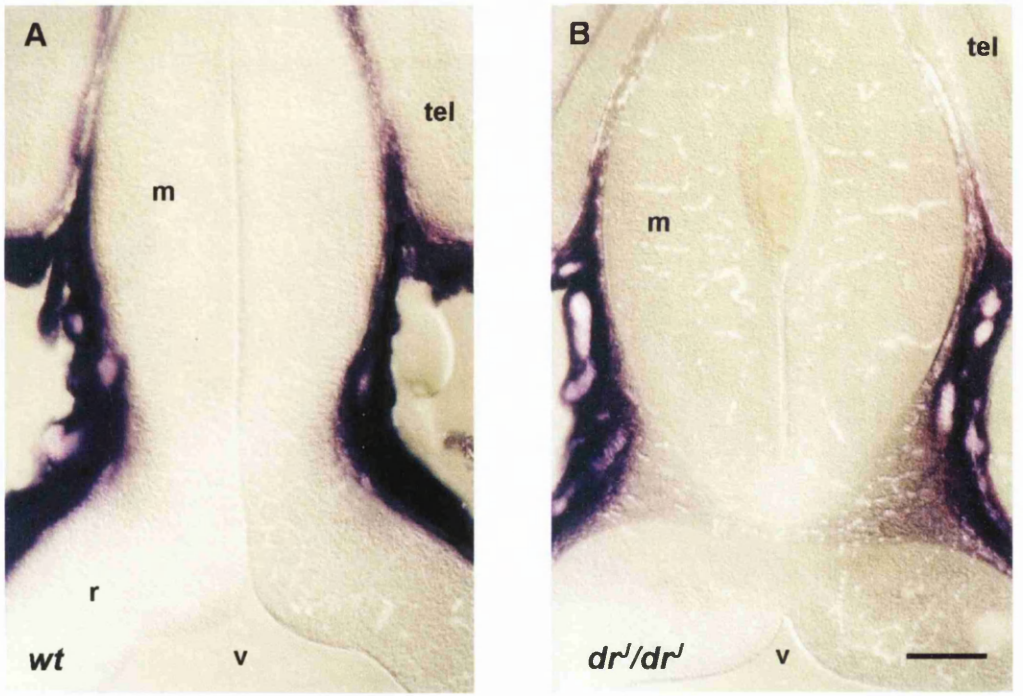

(A) Wild type and (B) homozygous mutant embryos at E11.5. Coronal sections showing intense staining in the mesoderm-derived tissues around the midbrain-hindbrain boundary. m: midbrain. tel: telencephalic vesicle. v: fourth ventricle. r: rhombencephalon. Scale bar represents: (A) 620 μm, (B) 600 μm.

between wild type and mutant embryos, except for a wider band of staining at the level of the midbrain-hinbrain boundary (where the cerebellar anlage is situated) in some of the wild type embryos, (compare wild type embryos on left of Figure 4.3D, E with dr^J/dr^J embryos on the right). This apparently stronger expression was found to be a function of age, older wild type embryos being the ones that showed the most intense labelling in this region. A difference in the shape of the hindbrain region between wild type and dr^J mutant embryos was obvious by this stage (Figure 4.3 D, E).

At E11.5, the limb buds and dorsal root ganglia region were also labelled by the *Pou2f1* probe, although the former stained less intensely than at E10.5 (compare Figure 4.3C with D, E). Staining was seen in the otic vesicles as expected, but sections though these structures showed staining compatible with trapping of the riboprobe (not shown). Sections of E11.5 embryos confirmed the pattern of progressive restriction of expression: In the limb buds, only a band of stained cells was seen, beneath the outer ectoderm (Figure 4.4D), possibly corresponding to the dermomyotome. The mesoderm-derived pericardium also showed strong expression of *Pou2f1* although the myocardium was negative (Figure 4.4C). Labelling of neural crest cells on their migration from the neural tube is shown in Figure 4.4B. By E11.5, there is still faint expression in the somites (Figure 4.5C).

In summary, the expression of *Pou2f1* becomes progressively restricted to mesoderm-derived tissues outside the head (dermomyotome, pericardium, somites), and also in cephalic structures surrounding the developing neural tube. In the cranial region, expression is strongest in the mesoderm surrounding

the midbrain-hindbrain boundary. The differences encountered in the intensity and area labelled at the midbrain-hindbrain boundary, between wild type and homozygous mutant embryos, were not consistently found in all cases and could either be a consequence of age differences or the result of morphological abnormalities at the hindbrain level in the mutants. No other differences were found in the temporal or spatial pattern of expression of *Pou2f1* between *dreher* genotypes.

4.3.3. Confirming the sequence of the *astrotactin* clone before preparation of the RNA probe

Sequencing of more than a hundred bases of the *astrotactin* plasmid confirmed the expected cDNA sequence, before starting preparation of the RNA probe (see Figure 4.2).

4.3.4. Analysis of the expression pattern of *astrotactin* in wild type and dr^J/dr^J embryos by wholemount *in situ* hybridisation

No positive signal of expression was obtained with the sense probe in any of the genotypes.

At E9.5, with the antisense probe, no expression of *astrotactin* is seen in any of the genotypes. These embryos were hybridised together with E10.5 and E11.5 embryos of the same genotype, making it unlikely that the lack of staining was due to technical failure.

There were no significant differences in the pattern of expression of *astrotactin* between wild type, heterozygous and dr^J homozygous mutant embryos at E10.5

or E11.5. Figure 4.8 shows the pattern of expression of *astrotactin* in wild type and homozygous mutant *dr*^{J} embryos as revealed by wholemount *in situ* hybridisation.

At E10.5, strong expression was seen in cephalic regions at, and rostrally to, the midbrain-hindbrain isthmus (Figure 4.7). Additionally, expression of *astrotactin* was observed in structures belonging to the peripheral nervous system, namely in cranial ganglia and nerves (Figure 4.8).

Coronal sections through the telencephalic vesicles, midbrain and hindbrain show that the neurepithelium of the first two was diffusely labelled by the *astrotactin* riboprobe, while in the hindbrain only discrete areas of staining were present in the lateral and basal regions of the neurepithelium (Figures 4.9 to 4.11). In the developing peripheral nervous system, staining was seen in the trigeminal ganglion (V cranial nerve), facio- acoustic complex (VII-VIII cranial nerves), glossopharyngeal ganglion (IX cranial nerve) and vagus nerve (X cranial nerve).

At E11.5, the spatial pattern of expression of *astrotactin* appeared to be restricted to in the central nervous system, rostrally to the midbrain-hindbrain boundary (Figures 4.7C, 4.8). Coronal sections through the telencephalic vesicles show that labelling was limited mostly to the inner part of the neurepithelium, except for the dorso-lateral region of that structure, where the strongest expression was seen in the outer part of the cortical plate (Figure 4.11). Mesoderm-derived tissues overlying the telencephalic vesicles were unlabelled.

Figure 4.7

Wholemount *in situ* hybridisation with an *astrotactin* riboprobe on *dr*^{J} embryos at E9.5 (20 somite-stage), E10.5 (35 somite-stage) and E11.5 (45 to 50 somite-stage).

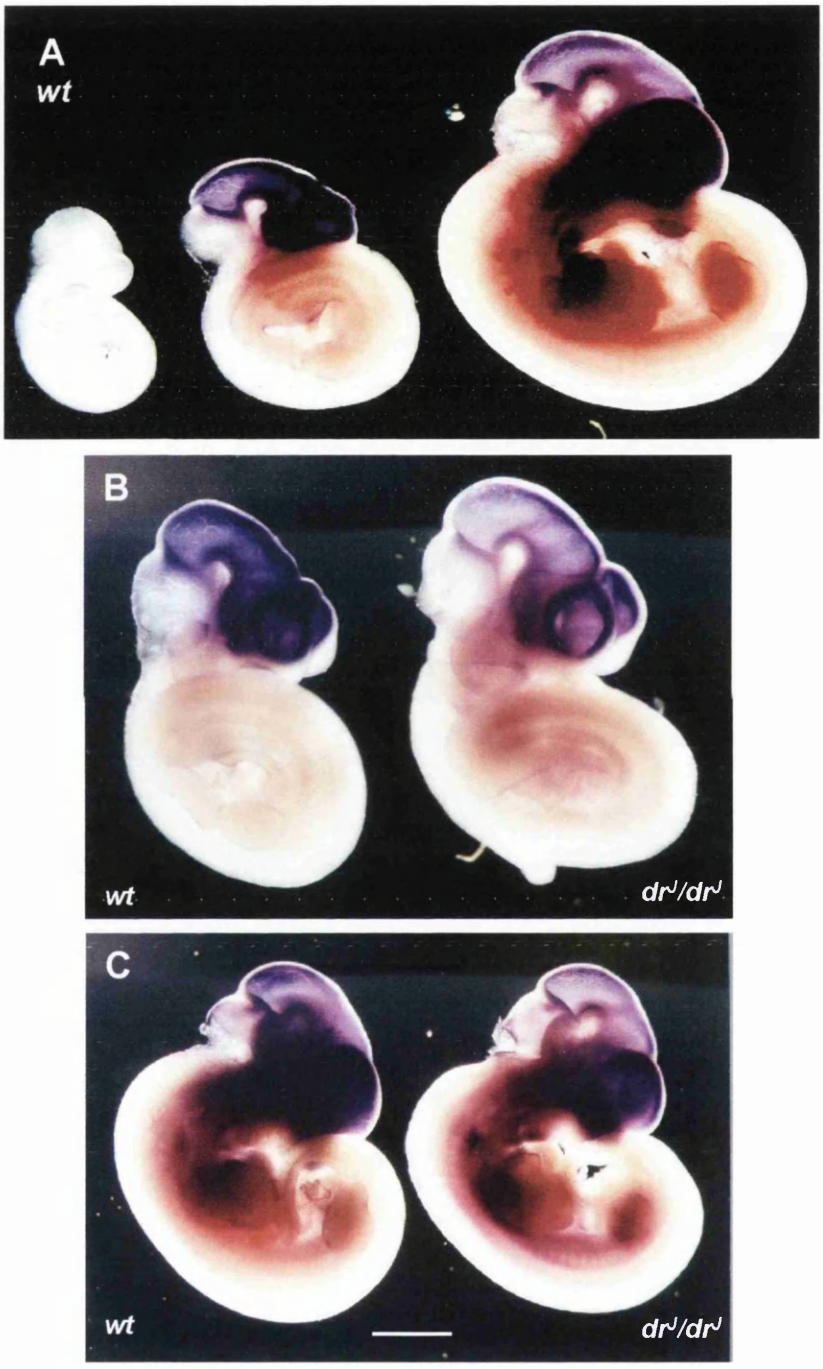

(A) Wild-type embryos: From left to right: E9.5 (no expression), E10.5 and E11.5 (expression is seen in the CNS at, and rostrally to, the midbrain -hindbrain boundary). **(B)** E10.5 embryos and **(C)** E11.5 embryos. Left is wild type, right is homozygous mutant. The pattern of staining is similar in both genotypes. Scale bar represents: (A) 600 μm. (B) 470 μm. (C) 1200 μm.

Figure 4.8

Expression of *astrotactin* in the developing peripheral nervous system as seen by wholemount *in situ* hybridisation on wild type and dr^J/+ embryos at E10.5

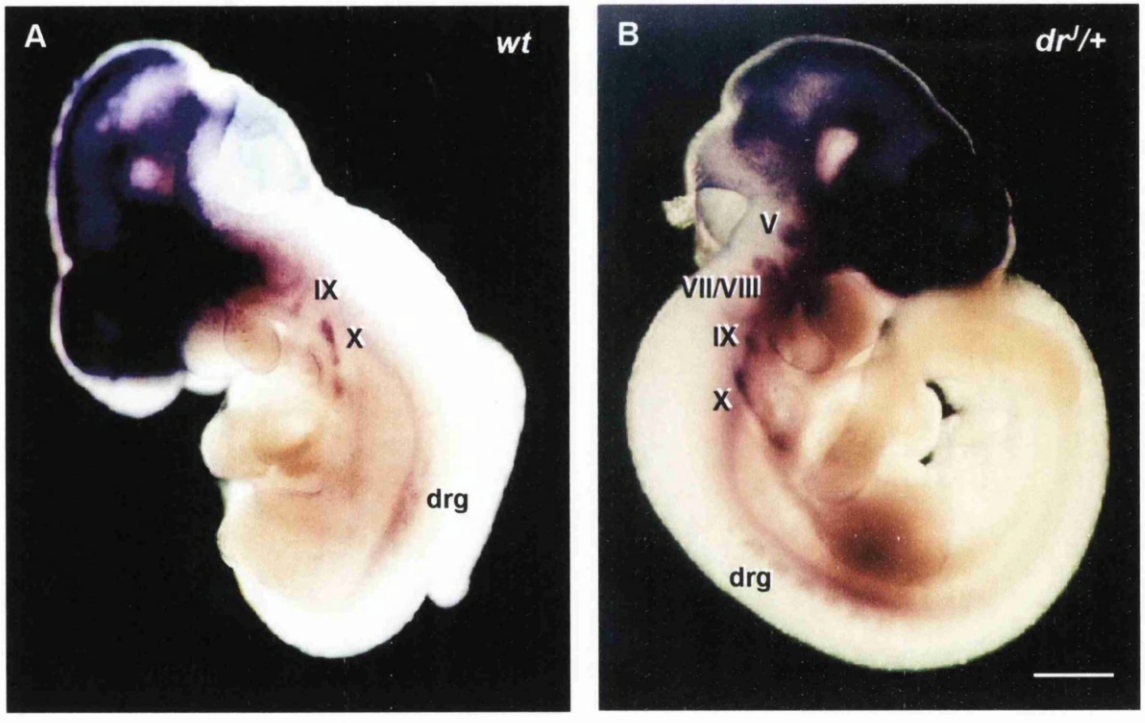

(A) Wild type and **(B)** dr^J/+ embryos at E10.5, to illustrate expression of the riboprobe in the peripheral nervous system. Labelling is seen in the trigeminal ganglion (**V**), facio-acoustic complex (**VII-VIII**), glossopharyngeal ganglion (**IX**), in fibres of the vagus nerve (**X**), as well as in dorsal root ganglia (**drg**) adjacent to the forelimb bud. Scale bar represents: (A): 460 μm (B): 420 μm.

Figure 4.9

Vibratome sections of wild type embryos at E10.5: expression of *astrotactin* in the central and peripheral nervous system

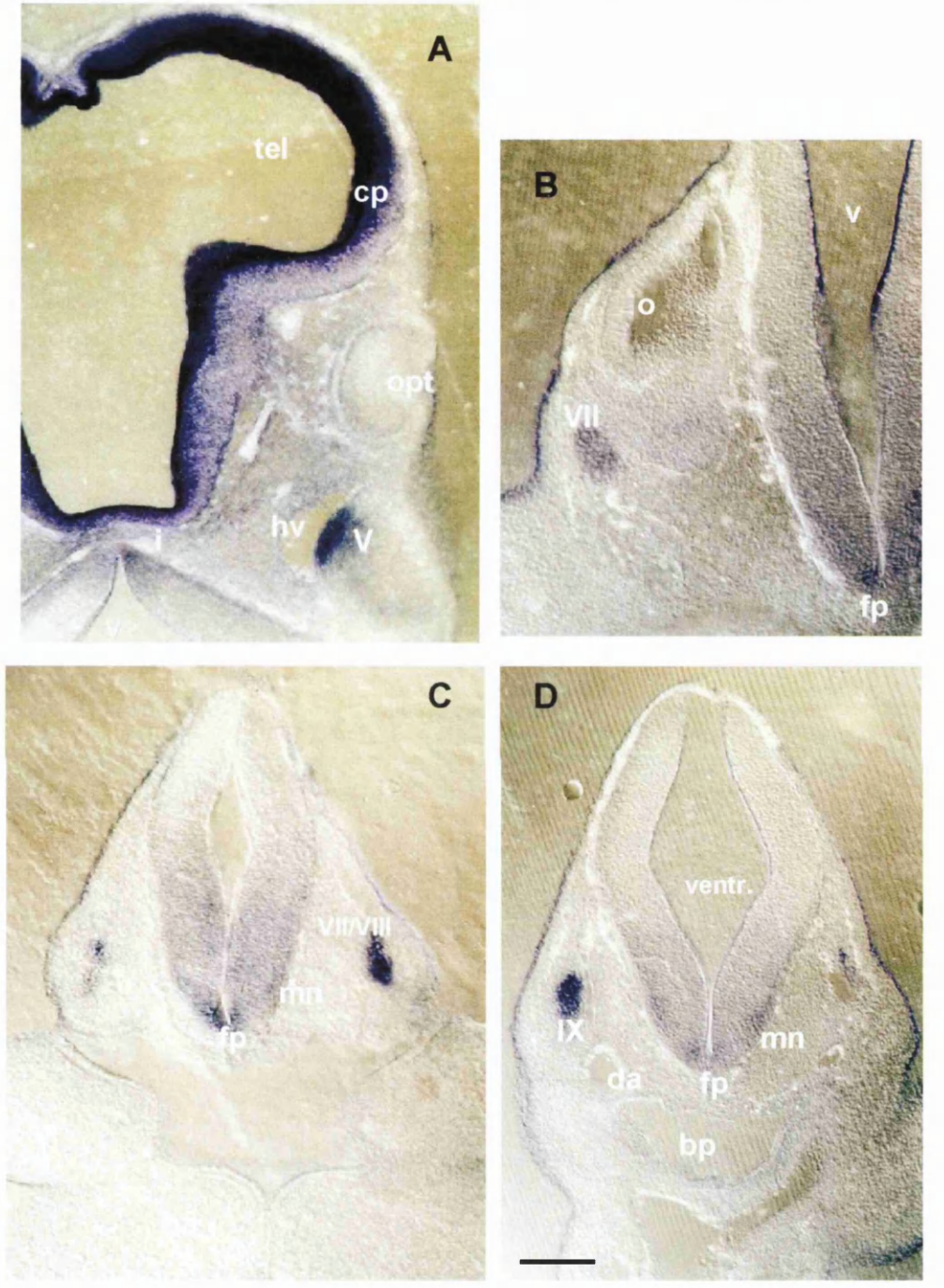

(A) Coronal section through the optic cups and midbrain-hindbrain ithmus. The cortical plate and the trigeminal ganglion express *astrotactin* mRNA. **(B)** Section through the otic vesicles: the nucleus of the facial nerve is labelled. **(C)** Section through the branchial arches, showing facial (VII) neural crest tissue migrating into the 2nd branchial arch. **(D)** Section at the level of the heart. The glossopharyngeal ganglion is labelled by the riboprobe.The floorplate and motor nerve origin area in the developing neural tube also express the *astrotactin* probe, as seen in (A) to (C). **V:** trigeminal ganglion. **VII**: facial neural crest tissue. **VII-VIII**: facio-acoustic complex. **IX**: glossopharyngeal ganglion. **X**: Fibres of the vagus nerve. **da**: dorsal aorta. **bp**: branchial pouch. **cp**: cortical plate. **opt**: optic cup. **o**: otic vesicle. **hv**: primary head vein. tel: telencephalic vesicle. **ventr.:**fourth ventricle. **mn**-motor nerve origin. **fp**: floor plate. Scale bar represents: (A) and (D) 600 μm, (B) 750 μm, (C) 850 μm.

Figure 4.10

Vibratome sections through the hindbrain of wild type embryos at E10.5 after wholemount *in situ* hybridisation with an *astrotactin* riboprobe

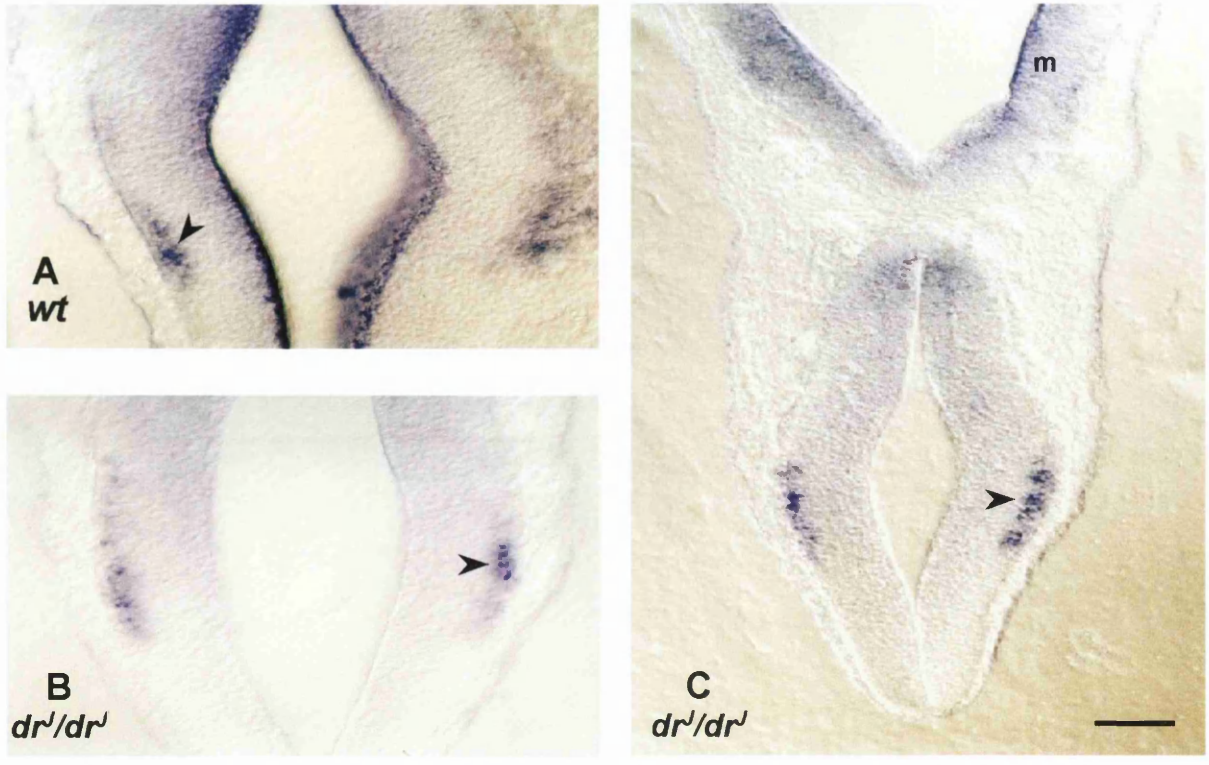

Coronal sections through the midbrain-hindbrain boundary. (A) Wild type . (B) dr^J/dr^J . (C) dr^J/dr^J . Cells expressing the probe bilaterally in the neurepithelium of the hindbrain are probably migrating neurons (arrowheads). The neurepithelium of the midbrain (m) also expresses the *astrotactin* riboprobe. Mesoderm-derived tissues around the neuroepithelium show no expression.
Scale bar represents: (A) 280 μm, (B) 330 μm, (C) 500 μm.

Figure 4.11

Vibratome sections through the telencephalic vesicles of *dr*^{J} embryos at E11.5 after wholemount *in situ* hybridisation with an *astrotactin* riboprobe

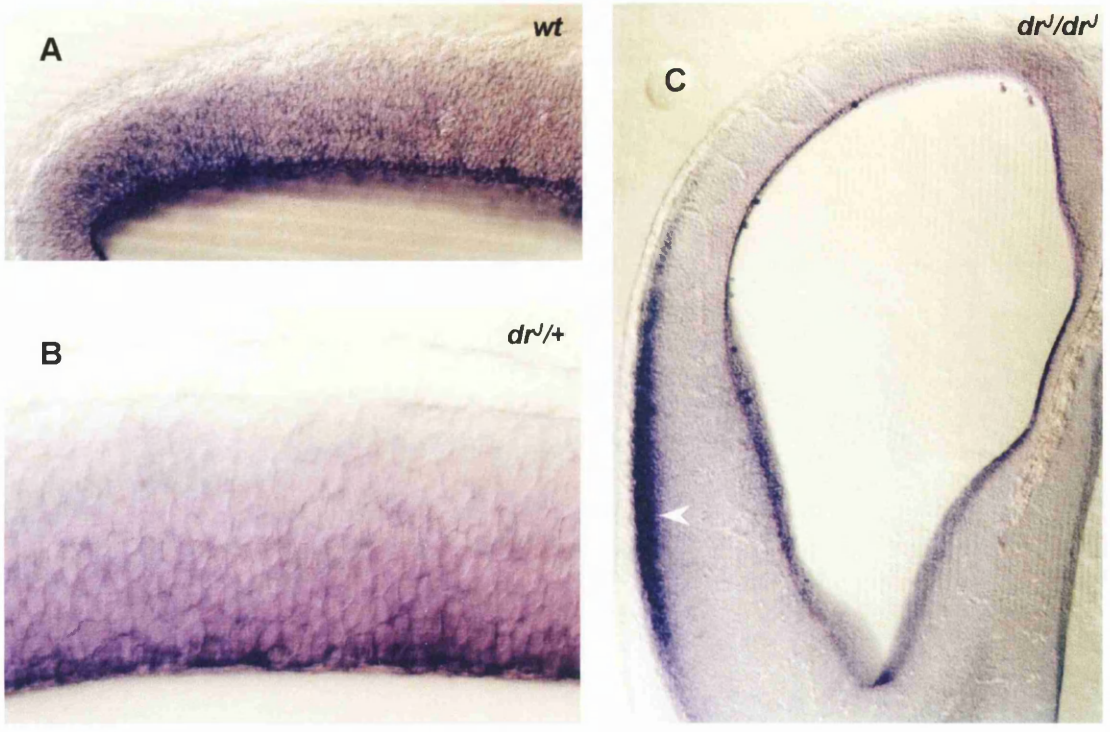

Coronal sections through the telencephalic vesicles. Expression is stronger in the inner part of the neurepithelium (A,B), except for the dorso-lateral region of that structure, where intense labelling is seen in an external, band-like region (C-arrowhead). (A) Wild type. (B) *dr*^{J}/+ . (C) *dr*^{J}/*dr*^{J}. Scale bar represents: (A) 130 μm, (B) 100 μm. (C) 250 μm.

In summary, by wholemount *in situ* hybridisation, the expression of *astrotactin* starts between E9.5 (18-20 somite stage) and E10.5 (35-40 somite stage), and follows the same temporal and spatial pattern in wild type, heterozygous and homozygous mutant embryos. Expression appears to be restricted to structures of the central and peripheral nervous system.

4.4. Discussion

4.4.1. Sequencing of the POU-specific domain of *Pou2f1* fails to disclose mutations in dr^J/dr^J mice.

In accordance with recently published mapping data by other authors, which have excluded *Pou2f1* as a candidate for the *dreher* gene, no differences were found in the present analysis in the sequences of the POU specific domain or in a short fragment of the 3' region of *Pou2f1* between homozygous mutant dr^J and control mice.

4.4.2. The expression of *Pou2f1* is not widespread and its spatial and temporal pattern is similar in all 3 genotypes

By wholemount *in situ* hybridisation, *Pou2f1* displays a quite restricted pattern of expression between E9.5 and E11.5. The present data are in opposition to the notion of a widespread expression throughout the embryo that has been reported by other authors (Suzuki *et al.,* 1993; Sekiguchi *et al.,* 1994; Dominov and Miller, 1996; Zheng *et al.,* 1996). The studies presented here show that expression of *Pou2f1* becomes progressively restricted to mesoderm-derived tissues and to cephalic structures, in keeping with what has been described in Xenopus (Veenstra *et al.,* 1995). Although the pattern of hybridisation of the labelled probe in dr^J embryos was similar to that reported in Xenopus (Veenstra *et al.,* 1995) (in that it was seen in dorsal root ganglia, somites, branchial arches and limb buds), no expression was detected in the neuroepithelium of embryos used for the present study, but rather in the mesoderm-derived tissues that surround it. *In situ* expression studies on rat embryos had previously indicated

that *Pou2f1* is expressed in the neurepithelium (He *et al.,* 1989). The reason for this discrepancy is unclear.

The putative expression of *Pou2f1* in the otic vesicles could not be confirmed, since the labelling obtained could not be distinguished from non-specific trapping of the digoxygenin-labelled probe within the otic vesicle itself.

The stronger band of labelling in the mesoderm-derived tissues around the midbrain-hindbrain boundary, seen in a few wild type embryos, was probably related to their older gestational age. Alternatively, this difference in labelling could be secondary to the malformation of the hindbrain region seen in all dr^J homozygous mutant embryos at E11.5. There were no other consistent differences in the temporal or spatial expression of *Pou2f1* in wild type, dr^J/+ or dr^J/ dr^J embryos at the three time points that were chosen (E9.5, E10.5 and E11.5).

4.4.3. The expression of *astrotactin* is restricted to neural tissues and is similar in all three genotypes

By wholemount *in situ* hybridisation, *astrotactin* is expressed only in neurectoderm-derived structures. No significant differences in the pattern of staining were seen between genotypes. *Astrotactin* expression begins in the CNS between E9.5 and E10.5, shortly before the onset of neuronal migration in the cortical plate. This is in agreement with findings published by other authors on the expression of this gene by neurons undergoing glial-guided migration (Stitt *et al.,* 1991; Zheng *et al.,* 1996). *Astrotactin* was found to be expressed in the cortical plate, where neurons are actively migrating to their respective

cortical layers. The observation of a stronger expression in the outer region of the dorso-lateral cortical plate of E11.5 embryos may be explained by the fact that migration of the early-maturing neurons destined for the marginal zone starts in the more rostral and lateral areas of the cortical plate (Price *et al.*, 1997).

4.4.4. *Astrotactin* is also expressed in the developing peripheral nervous system.

Expression of the *astrotactin* riboprobe was seen in both the epithelium of the neural tube and in structures that give rise to the mature peripheral nervous system such as cranial ganglia and nerves, as well as dorsal root ganglia. No differences were noted among the three genotypes at E10.5 or E11.5.

There have been no previous reports on the expression of *astrotactin* in the peripheral nervous system. The present data suggest that, besides its known role in glial-guided neuronal migration in the central nervous system, *astrotactin* may be an important molecular component of neuronal migration in the peripheral nervous system as well.

Chapter 5

External phenotype and survival of *dr*^{J} mutant mice

5.1. Introduction

Previously published work on *dreher* alleles has focused mainly on external phenotypic features and on the analysis of crosses for the demonstration of allelism and gene mapping. The first description of *dreher* was by Falconer and Sierts-Roth in 1951 . It concerned wild mice (*dr*), selected for their circling behaviour. *dr* was considered to be an autosomal recessive mutation with full penetrance. Since then, the phenotypes of three other alleles (dr^{J}, dr^{sst} and dr^{2J}) have been reported . All four *dreher* mutant alleles share common features, such as circling, head tossing, white abdominal patches of fur and a short or blunt tail (Falconer and Sierts-Roth, 1951; Lyon, 1961; Sweet and Wahlsten, 1983; Wahlsten *et al.,* 1983; Washburn and Eicher, 1986). Table 5.1 summarises available data on their phenotype. In the case of *dr*, detailed descriptions of the ear and cerebellar defects, and of their embryonic development, have also been reported (Bierwolf, 1956; Fischer, 1956; Bierwolf, 1958; Fischer, 1958).

This Chapter includes descriptions of the external phenotype as well as pre- and post-natal survival data of dr^{J} mutant mice in relationship to wild-type littermates. The present findings are compared with those originating from previous reports on this and other *dreher* alleles.

Table 5.1

Origin and phenotypic characteristics of mutant *dreher* alleles

Allele name / symbol	Origin (type of mutation, strain)	Circling, head tossing	Deafness	abnormal righting reflexes	splaying of hind-limbs	hyper-activity	white coat patches	head bleb	short or blunt tail	age at which homozygotes are first recognisable	reproduction and fertility	Ref.[s]
dreher dr	Wild mice	+	+	+	+	+	+ (81.8%)	NR	+ (progeny of cross with T)	From P12-15 (head tilt, abnormal righting reflexes)	Decreased fertility in females	**1**
dreher J dr^{J} (formerly sst^{J})	Spontaneous C3B6-A/A^{w-J}-ank	+	+	+	NR	+	+	+ (70%)	+	From birth: filament at tailtip	Homozygotes do not reproduce	**2**
shaker short-tail dr^{sst}	Spontaneous Balb/cCF	+	NR	+	+	+	+ (26%)	+	+	From birth (reduced tail length-99%, head bleb-74%)	NR	**3**
dreher 2J dr^{2J}	Spontaneous AKR/J	+	+	NR	NR	NR	+ progeny of crosses with C57BL/6J	NR	+	NR	Females are infertile (hypoplasia of Müllerian ducts)	**4**

+ - present. **NR** - Not reported. **Ref.[s]** – references. 1: Falconer and Sierts-Roth, 1951; Lyon, 1961. 2- Sweet and Wahlsten, 1983. 3- Wahlsten *et al.,* 1983. 4- Washburn and Eicher, 1986.

5.2. Methods

5.2.1. Breeding and maintenance of animals, assessment of survival rates

General breeding strategy and animal maintenance conditions are described in Chapter 2. All embryos and post-natal animals used for this part of the study originated from matings between heterozygous male and female dr^J mice.

In order to assess the periods and magnitude of presumed loss of homozygous mutant mice, embryos and post-natal animals were genotyped at different stages. Genotyping was done in each case with the two microsatellite DNA markers flanking the *dreher* locus, *D1Mit452* and *D1Mit15* (see Chapter 3 for details). The number of individuals in each category was estimated at three different time-points: E11.5, P6-12 (i.e. when the phenotype of the mutants first becomes apparent) and P21 (i.e. at weaning age).

5.2.1.1.Survival of embryos

To estimate prenatal loss, the proportions belonging to the various genotypes (as determined by typing with the two flanking markers, *D1Mit452* and *D1Mit15*) were determined among 109 embryos at E11.5 (coming from 12 litters), and compared to the expected frequencies for an autosomal recessive trait. E11.5 embryos used for estimating survival rates were from the same litters as those collected for whole-mount *in situ* hybridisation (see Chapter 4). Prior to genotyping, each embryo was dissected from its extra-embryonic membranes and examined under a stereomicroscope for the presence of external distinguishing features. Those with recombinant genotypes at the flanking

markers were systematically excluded from the analysis, as the *dr*^{J} genotype was not unequivocal in those cases. It was assumed that the probability of genetic recombination between flanking markers is unlikely to vary between the different *dr*^{J} genotypes, and thus would not influence the final proportion of embryos in each of the 3 groups (*dr*^{J}/*dr*^{J}, *dr*^{J}/+ and +/+).

5.2.1.2. Survival of post-natal animals

Studies of post-natal survival were performed on the same animals as those used in the bromodeoxyuridine (BrdU) labelling experiment (see Chapter 7). Progeny were genotyped between P10 and P15 using *D1Mit452* and *D1Mit15* as markers. In order to enhance the survival chances of *dr*^{J} homozygous mutants in large litters, most or all of the heterozygous mice, or those with a normal external phenotype and a recombinant genotype, were culled. At least three pups were always maintained in each litter. Because of this early selection procedure, and since all other animals were sacrificed at P21 (before their genotype could be ascertained by test-breeding with a known heterozygote), it was impossible to distinguish wild-type from heterozygous mice in the case of meiotic recombination between the flanking markers.

For this reason, wild-type and heterozygous mice were considered together as a single group (expected to comprise 75% of each litter on average) for the purpose of estimating survival rates. The number of surviving homozygous mutants was determined by checking all mice daily in a given litter for balance abnormalities (abnormal righting reflexes and circling behaviour). Genotype at the *dreher* locus of phenotypically mutant mice was confirmed in each case by PCR analysis showing a *dr*^{J}/*dr*^{J} pattern for one or both flanking markers. Mice

with balance abnormalities (i.e. presumed dr^J/dr^J), but with a recombinant genotype, were also scored as dr^J/dr^J, on the assumption that balance abnormalities are a fully penetrant trait of homozygous mutants (see Chapter 3 for details).

5.3. Results

5.3.1. External phenotype of *dr^J/dr^J* embryos and mice

5.3.1.1. Distinguishing features of *dr^J/dr^J* embryos

Several *dr^J* litters of different embryonic ages (E9.5, E10.5, E11.5 and E15.5) were collected. Whereas no specific characteristics were noted in E9.5 or E10.5 embryos, a distinctive conformation of the hindbrain region was seen in a subset of E11.5 embryos (15 out of a total of 93 embryos, from 10 litters). These abnormal embryos showed a recess in the hindbrain region, that made the back of the head look quite prominent, (almost cone-shaped, in some cases) and increased the curvature of the dorsum (see Figure 4.3D,E). In all cases where this abnormal configuration was seen, genotyping confirmed a *dr^J/dr^J* genotype for both the flanking microsatellite markers. None of the embryos showing a *dr^J/dr^J* genotype at these two loci had a normal phenotype. Five normal-looking embryos had recombinant genotypes. Of these, a single instance of *dr^J/dr^J* genotype at one of the loci (*D1Mit 452*) was seen, the other marker (*D1Mit15*) showing a heterozygote-type pattern of PCR product. By E15.5, this morphological abnormality of the hindbrain was no longer visible, and *dr^J/dr^J* fetuses were indistinguishable from *dr^J/+* and *+/+* littermates.

5.3.1.2. Phenotype of post-natal *dr^J/dr^J* mice

Genotyping each animal under study provided a solid basis for comparing post-natal *dr^J/dr^J* mice with their normal littermates and confirmed that heterozygous animals could not be distinguished from wild-type mice. The descriptions below refer, therefore, only to homozygous mutant *dr^J* mice.

5.3.1.2.1. Balance abnormalities

Homozygous mutant *dr*^{J} mice could usually be identified reliably from 6 to 12 days of age, because of their abnormal righting reflexes: they experience difficulties in returning to the upright position when they are laid on their backs. Distinguishing them from normal littermates is sometimes possible a few days earlier, if they have sufficiently prominent white fur patches. Older animals tilt and toss their heads, splay their hindlimbs apart when walking (see Figure 5.1 A), display circling behaviour (running in circles to one or the other side), and are hyperactive, running around almost incessantly and jumping occasionally when disturbed. In our colony, the circling behaviour was a fully penetrant trait, as established by phenotype-genotype correlations (see Chapter 3 for details). Homozygous mutant *dr*^{J} mice tend to curl their bodies ventrally and clasp their feet when held by the tail (Figure 5.1 D), whereas wild-type and heterozygous animals raise their heads and extend their bodies in an attempt to return to the upright posture.

Evaluation of the severity of the circling behaviour was hindered by the overall hyperexcitability of the mutants to minor non-auditory stimuli and by the superimposed signs of malnutrition (related to the balance defect and resulting inability to feed properly).

5.3.1.2.2. Deafness

Circling (homozygous mutant) *dr*^{J} mice do not have a hearing startle reaction, suggesting they have impaired auditory ability, as described for other *dreher* alleles. No systematic tests were done on the mutants to confirm this deficiency.

Figure 5.1

External phenotype of *dr*^{J} homozygous mutants

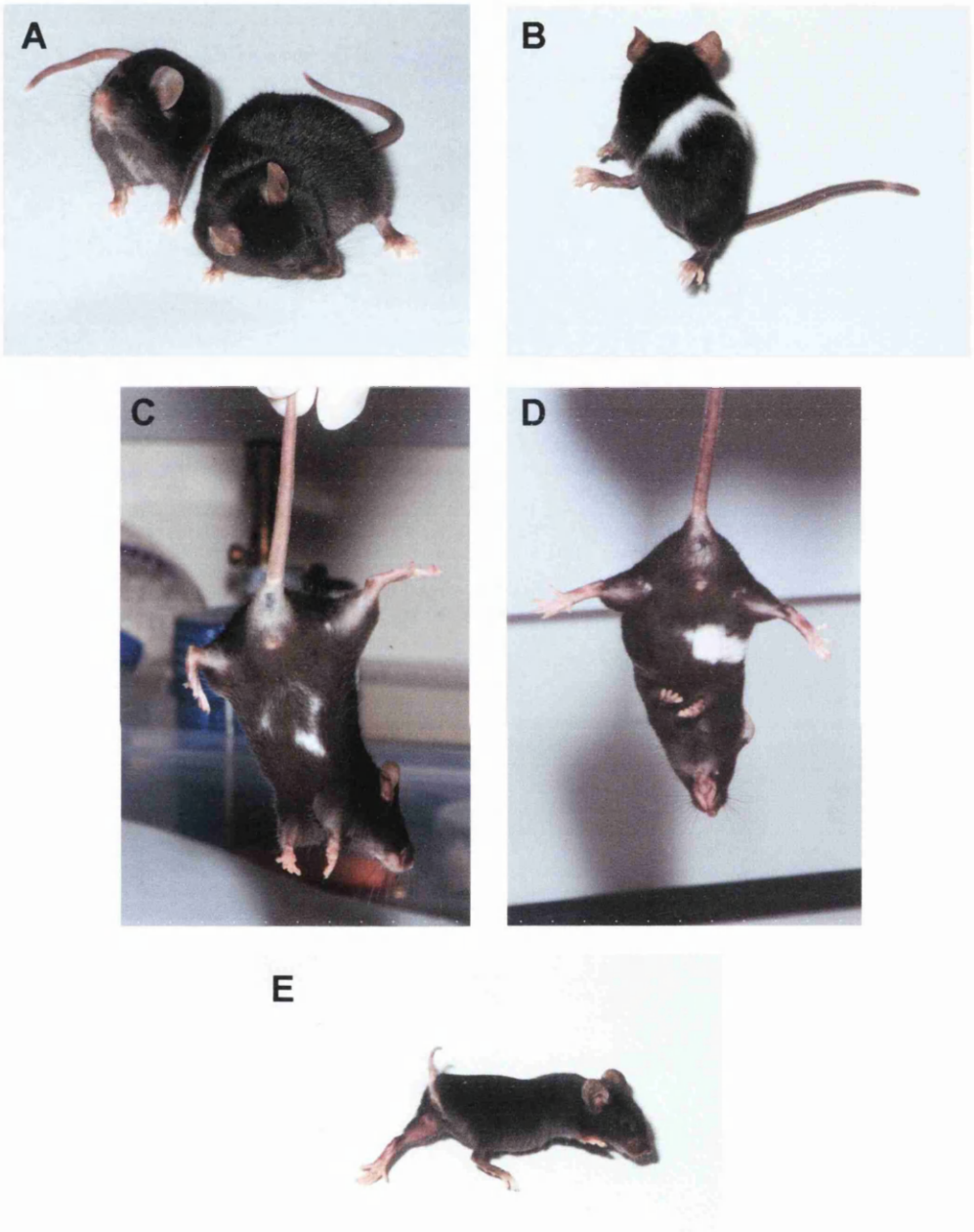

(A) Head tossing and splaying of hindlimbs. **(B)** A mutant trying to turn around and losing balance. Notice the white belt of fur extending dorsally. **(C)** and **(D)** Different types of white belly spots. When held by the tail, mutants usually curl ventrally, clasping their forelimbs, as in (D). The posture in (C) is much more normal, resembling that seen in heterozygotes and wild type mice. **(E)** A mutant with a very short tail. Notice filament at distal tip.

5.3.1.2.3. White coat hair patches

Most, but not all of the homozygous mutants had white hair patches (see Figure 5.1 B/C/D). Of 78 mice identified with a dr^J/dr^J phenotype (including either 10-15 day mice with abnormal righting reflexes, or older mice with clear-cut circling behaviour), 66 (84.6%) also had white belly spots, whereas the remaining 12 (15.4%) displayed no coat colour abnormalities. The white patches were uni- or bilateral, most often abdominal. They were frequently flame-shaped, either single or multiple. They ranged from a few white hairs in the paramedian region of the abdomen to almost complete belts (i.e. they were both abdominal and dorsal). No white belly spots were seen in mice with a $dr^J/+$ or wild-type genotype.

5.3.1.2.4. Tail abnormalities

In our colony, only 5 out of 78 (6.4%) circling dr^J/dr^J mice had a very short tail, i.e. of less than half the normal length. A short tail was associated with a blunt end in all cases except one, where the tail had a filament at its distal tip (depicted in Figure 5.1 E). In one case, the short tail was bent at approximately half-length. Of the short-tailed mice, 3 had no belly spots, one had a faint white abdominal half-belt and the other one had a small abdominal spot. These mice came from the progeny of 4 different females with a common origin (i.e. they belonged to the progeny of a common male, from the second set of backcrosses established to build the dr^J colony). The small number of animals with tail defects makes it difficult to detect any positive or negative correlation between the presence of a short or blunt tail and other features of homozygous mutant dr^J mice. Tail abnormalities were not observed in heterozygous or wild type mice.

5.3.1.2.5. Other features

No spontaneous behavioural seizures were observed among homozygous mutant mice in the *dr*^{J} colony. No epilepsy induction procedures or any other tests were carried out to demonstrate increased susceptibility to seizures or an abnormal brain activity.

5.3.2. General features: growth, viability and fertility

5.3.2.1. Growth and survival rates

Weaning age (P21) homozygous mutants (n= 13) had on average a significantly ($p<0.001$) lower mean body weight (5.60+/- 1.50g) than wild-type mice (n=22) of the same age (9.95 +/-2.70g). The proportion of weaning age animals with phenotypic characteristics of homozygous mutants identified in each litter resulting from crossing heterozygous *dr*^{J} mice was much lower than would be expected for an autosomal recessive mutation (25%). This was true even when selective culling procedures were used to maximise survival of *dr*^{J}/*dr*^{J} mice (see section 5.2.1 and Chapter 3 for details).

5.3.2.1.1. Survival of embryos

Distribution by genotype of 109 embryos at E11.5 is shown in Table 5.2. Six embryos showed recombinant genotypes. It was assumed that these embryos would be distributed between the three genotypes in the same proportions as the remaining non-recombinant 103 embryos, and so the recombinants were omitted from the analysis.

Table 5.2

Genotype distribution among E11.5 *dr*^{J} embryos

Genotype at the *dreher* locus	Observed number (%)	Expected number (%)
+/+	30 (29.1%)	25.75 (25%)
dr^{J}/+	54 (52.4%)	51.5 (50%)
dr^{J}/*dr*^{J}	19 (18.4%)	25.75 (25%)
Total number of embryos included in the analysis	103	

All embryos originated from crosses between *dr*^{J} /+ males and females.
In 6 out of the initial 109 E11.5 embryos, there was a meiotic recombination between one of the flanking microsatellite markers (used for genotyping) and *dr*^{J}.
In these cases, the genotype at the *dr*^{J} locus was impossible to determine, and such embryos were excluded from the analysis. Difference between expected and observed values is not statistically significant, according to a 3x2 contingency test: $\chi^2 = 2.59$ and $0.25<p<0.5$.

Table 5.2 shows that *dr*^{J}/*dr*^{J} embryos appear under-represented among the 103 non-recombinant embryos, whereas +/+ and *dr*^{J}/+ appear more frequent than expected. The observed proportions are, however, not significantly different from the expected 1:2:1 ratio for an autosomal recessive trait, as indicated by a χ^2 test.

5.3.2.1.2. Survival of *dr*^{J} mice post-natally

A total of 156 mice (belonging to 21 litters resulting from crosses between heterozygous animals) were checked daily for balance abnormalities and white belly spots (i.e. for the homozygous phenotype). At the time of identification of abnormal mice (usually between P6 and P12), a total of 128 mice were still alive (corresponding to a loss of 17.9% of animals). Among the live animals, 18 were identified as having a *dr*^{J}/*dr*^{J} phenotype. This corresponds to 11.5% of all animals born in those litters and 14.1% of mice remaining at the time of phenotypical identification. Despite the procedure of culling normal-looking mice with recombinant genotypes and heterozygous animals, four deaths (22.2%) still occurred among phenotypically mutant mice between the time of their first identification and P21. The numbers of phenotypically and genotypically homozygous mutant mice are compared to the total number of normal (*dr*^{J}/+ and +/+) mice in Table 5.3. At the time of identification of mutant mice, 14.1% were *dr*^{J}/*dr*^{J} and 85.9% were either *dr*^{J}/+ or +/+ considered together. These values differ significantly from the expected values of 25% for *dr*^{J}/*dr*^{J} and 75% for *dr*^{J}/+ and +/+ (χ^2= 8.17 and 0.001<*p*<0.01).

In contrast to this observed loss of *dr*^{J}/*dr*^{J} mutants in early postnatal life, homozygous *dr*^{J} mutants that survived the weaning period were found capable

Table 5.3

Numbers of phenotypically normal and mutant *dr*^{J} mice surviving to different post-natal ages

	No. of live animals at birth	No. of animals at P6-P12		No. of live animals at P21
		Observed	Expected	
All genotypes	156	128	-	ND
+/+ and *dr*^{J}/+	ND	110 (85.9%)	96	ND
***dr*^{J}/*dr*^{J}**	ND	18 (14.1%)	32	14

Percentage values are shown in brackets. ND: not determined.

Differences between observed and expected values at P6-P12 are statistically significant: $\chi^2 = 8.17$ and $0.001 < p < 0.01$.

of living for longer than 12 months (n=2), demonstrating that the homozygous genotype is not incompatible with prolonged adult life.

5.3.2.2. Reproduction

Matings between male and female *dr^{J}/dr^{J}* mice (n=2 pairs) yielded no pregnancies. No attempts at intercrossing homozygous mutants with either heterozygous or wild-type mice were made. The genital apparatus of either male or female mice was not examined.

5.4. Discussion

5.4.1. External phenotype of *dreher* embryos

According to Deol (1964), homozygous mutant *dreher* mice can be recognised as early as E9, because of hindbrain conformational anomalies. These are followed on day 10 by the first detectable abnormalities of the otic vesicles, consisting of retarded development of the endolymphatic duct and Anson's folds. Based on these observations, it was suggested that the induction of the otic vesicle by the neural tube is disturbed in *dreher* mutant embryos. However, Deol (1964) provided no confirmation of the genotype of the examined embryos to validate these findings. In the present study, it did not prove possible to discern consistent morphological differences under the stereomicroscope between genotyped dr^J/dr^J embryos and their normal littermates, at E9.5 and E10.5.

In contrast to the findings at E9.5 and E10.5, an abnormal hindbrain shape was found in E11.5 dr^J homozygous mutants. This defect is probably a fully penetrant characteristic, and seems likely to be related to the pathological features reported by Bierwolf (1958), in *dr* embryos. According to this author, as early as E11 there is a thickening of the caudal part of the IV ventricle, which entails a shortening of the future choroid plexus region. This coexists with a delayed opening of the foramen of Magendie, causing hydrocephalus and consequent thinning of the cerebellar anlage, that will ultimately lead to abnormal development of the cerebellum and occasionally to the formation of cysts in the posterior fossa. That the abnormal shape of the hindbrain is not detectable at E15.5 is similar to the description of Deol (1964), and may be

related to bulging of the dilated fourth ventricle, with masking of the hindbrain defect on macroscopic examination of the whole embryo. Although the possibility cannot be excluded that minor abnormalities of the neural tube (undetected on the basis of external examination alone) are a feature of homozygous mutants, the present data do not provide support for the hypothesis of Deol (1964), that there is failed neural induction of otic vesicle development in *dr/dr* embryos. On the other hand, the present findings are in keeping with the observations of Fischer (1958). This author studied *dr* embryos (either by intercrossing *dr/dr* mice or by mating *dr/dr* mice with *dr/+*) of different ages, starting from E9. Because he saw no abnormalities of the otic vesicles before day 11, he concluded that the abnormal ear development was unlikely to be due to failure of induction by the neighbouring hindbrain structures. The issue of how ear abnormalities are generated in *dreher* mice remains to be elucidated, and may be crucial for a full understanding of the pathogenetic mechanisms leading to the *dreher* phenotype. It was considered beyond the scope of the present studies.

5.4.2. External phenotype of post-natal animals

The abnormal external phenotype of mutant *dreher* mice and its alleles has been the subject of many reports (see Table 5.1.). The mutant phenotype includes balance abnormalities, deafness, white coat patches, a short tail and a head bleb (Falconer and Sierts-Roth, 1951; Lyon, 1961; Sweet and Wahlsten, 1983; Wahlsten *et al.,* 1983; Washburn and Eicher, 1986). This phenotype resembles that of shaker-short (*sf*), (Dunn, 1934), which, according to Sweet and Wahlsten (1983), and Wahlsten, et al. (1983), was probably also a mutation

at the *dreher* locus. Unfortunately, the *st* mutation is now extinct and allelism was never proven.

5.4.2.1. Balance abnormalities and deafness

Both balance abnormalities (including delayed onset or absence of righting reflexes, incessant circling, ataxic gait, head tilt and frequent falls) and deafness (as shown by an absent startle reaction to sound) have been reported previously in all of the *dreher* alleles (Falconer and Sierts-Roth, 1951; Lyon, 1961; Sweet and Wahlsten, 1983; Wahlsten *et al.,* 1983; Washburn and Eicher, 1986). A ventral curling reaction when mutants are held by the tail, as described by Bierwolf (1956), is also likely to be due to balance defects. Disturbances of balance can be explained by an abnormal embryonic development of the otic vesicles and cerebellum, both of which have been described in *dr* homozygous mutants (Bierwolf, 1958; Fischer, 1958). The otic vesicles were not examined in this study, but approximately half of dr^J/dr^J brains that were examined had a cerebellum of reduced size (see Chapter 6).

5.4.2.2. White coat patches

White coat patches have been described in various proportions of *dr*, dr^J, dr^{sst} and dr^{2J} mutant mice. They were seen in over 80% of dr^J homozygous mutants in our colony. Although there is no mention of coat colour abnormalities in the original description of *dr* (Falconer and Sierts-Roth, 1951), the occurrence of white belly spots as well as a frequently incomplete belt of white hair was reported in homozygous mutant *dr* mice obtained during a linkage analysis (Lyon, 1961). In a description of dr^J (Sweet and Wahlsten, 1983), only 26% of homozygous mutant mice had white coat patches. In dr^{2J}, arising on an AKR/J

background, white spots were noted only in F2 mice from a linkage cross involving the C57BL/6J inbred strain (Washburn and Eicher, 1986).

Although wild type and heterozygous *dr*^{J} mice used for the present study were indistinguishable in their external phenotype, a proportion of *dr*^{J} */+* animals in another colony of the same allele had white belly spots (Patrylo *et al.,* 1990). The authors attributed the coat defect to an exacerbation of the *dr*^{J} mutation, brought about by some unknown environmental influence. They concluded that *dr*^{J} is a semi-dominant mutation, and by analogy with *weaver*, speculated that it probably results from a loss-of function type of mutation of the involved gene. The variability in the proportion of homozygous mutant animals having white coat patches, even in different colonies of the same allele may be due to different genetic backgrounds and to environmental influences. The cause of the white coat patches is unknown but may be due to diminished numbers of melanocytes in the ventral midline, as observed for instance in *splotch* (*Pax3*) heterozygous mutants (Asher *et al.,* 1996). If this is the case, homozygosity for *dr*^{J} must lead to only a partial loss of melanocytes, so that the majority of the coat is normal, with pigment defects mainly in the ventral midline, where the melanocyte migration pathway is longer.

5.4.2.3. Short tails and head blebs

Short-tailed animals have been reported among homozygous mutants of *dreher* alleles. In the case of *dr*, shorter than normal tails were found among the progeny from crosses between *dr/dr* mice and *Brachyury* (T/+) mutants. No underlying bony defects were found in alizarin-stained preparations of the skeleton of such mice (Lyon, 1961).

Published reports indicate that the proportions of short-tailed *dreher* mice vary not only according to the allele under study, but also between different colonies of the same allele. Animals with a mutant phenotype and a short or blunt-ended tail were seldom seen among the mice used for this study (the dr^{J} allele on a B6C3Fe-a/a background). In contrast with this observation, dr^{J} mutant mice in a different colony (Sweet and Wahlsten, 1983) were easily identified at birth, because of a filament at the tail tip. In another study by Wahlsten, et al. (Wahlsten *et al.,* 1983), the proportion of short-tailed dr^{sst} homozygous mutants was so high (99%), that this feature alone was used as a means of identifying them at birth. Differences in penetrance or genetic background could be the basis for such discrepancies.

The latter argument, or alternatively an environmental defect, can also be used to explain why, despite the reports of a midline head bleb (possibly a meningocele or an encephalocele) among dr^{J} and dr^{sst} homozygous mutant mice (Sweet and Wahlsten, 1983; Wahlsten *et al.,* 1983), no single mouse with this type of abnormality was seen in our dr^{J} colony. Since the presence of a head bleb at birth has been correlated with a poor prognosis (Wahlsten *et al.,* 1983), it is also possible that prenatal death after E11.5 is responsible for the loss of the most severely affected individuals (i.e. those that have a head bleb). On the other hand, embryos at E11.5 did not display any abnormalities of cranial structure indicative if an incipient head bleb. The underlying mechanisms leading to the formation of head blebs are still unclear.

5.4.3. Fertility of homozygous mutants

Our inability to obtain progeny by intercrossing homozygous mutant male and female mice could be caused by reduced fertility in *dreher* females, as originally reported in *dr* (Falconer and Sierts-Roth, 1951) or infertility, as in dr^{2J} (Washburn and Eicher, 1986). Falconer and Sierts-Roth (1951) reported that matings between homozygous mutant females and heterozygous males seldom resulted in pregnancies, whereas they could successfully cross mutant males with heterozygous females. In the dr^{2J} allele, which occurred on an AKR/J background, lack of success in matings between homozygotes was investigated and attributed to underdeveloped uterus and Fallopian tubes, because of a deficient differentiation of the Müllerian ducts (Washburn and Eicher, 1986). Alternatively, the circling behaviour itself could have a major negative impact on mating. This issue awaits further investigation.

5.4.4. Survival

The first description of *dr* (non-inbred background) indicated an autosomal recessive-type of inheritance (Falconer and Sierts-Roth, 1951), with full penetrance, based on the finding of expected Mendelian proportions of the various genotypes, presumably ascertained by test-breeding. There was no apparent increased mortality among *dr*/*dr* mice (Falconer and Sierts-Roth, 1951). The authors weighed mice weekly, from birth until adulthood, and found no statistically significant differences between homozygotes and normal-looking animals at any of the time-points chosen. It is difficult to explain the discrepancy between these results and the significant difference between the mean weight of 3 week-old normal and homozygous mutant mice found in our study, especially since the litters included in our analysis were usually quite small,

owing to selective culling procedures. It should be remembered that the mice included in this study were exposed *in utero* to BrdU, as part of the birthdating study (Chapter 7). However, there is no reason to believe that BrdU is teratogenic at the dose used in the present study (Miller and Nowakowski, 1988). It is conceivable that a disproportionately high number of deaths among the homozygous mutants during the first 10 days after birth may have gone unnoticed, since the presence of balance abnormalities (and hence the number of mutants) could only be ascertained reliably after that period. Moreover the initial description of Falconer and Sierts-Roth (Falconer and Sierts-Roth, 1951) does not indicate that homozygous mutant *dr* mice had a less severe phenotype than dr^J/dr^J mice in our colony. Among the *dreher* alleles on an inbred genetic background, however, viability of homozygous mutants seems to be affected (Sweet and Wahlsten, 1983; Wahlsten *et al.,* 1983; Patrylo *et al.,* 1990). Table 5.4 shows a comparison of the published reports on viability of mutant *dreher* alleles.

The present results suggest a disproportionate loss of dr^J/dr^J animals before the end of the second postnatal week, since only 14.1% of mice alive at P6 to P12 had a dr^J/dr^J genotype. Whether this is due to a disproportionate prenatal loss (after E11.5) could not be determined in our series: homozygous mutants could be identified morphologically only after the first week post-natally. Moreover, no individual marking of mice (e.g. ear-piercing) was done before that age to allow for a retrospective phenotype-genotype correlation to be established. It is uncertain, therefore, whether there is a late pre-natal or early post-natal mortality (or both) among dr^J/dr^J mice, although previous reports seem to indicate that there is a major loss of dreher homozygotes in the first few post-

Table 5.4

Viability of homozygous mutant *dreher* alleles

Allele	Origin/ background	Increased mortality among homozygous mutants	References
dr	Wild mice, **Non-inbred**	No	1
dr	Probably inbred *	High among hydrocephalics on 1st few days and around 4 weeks post-natally.	2
dr^{sst}	Inbred, Balb/cCF	High, especially on P1-2, also at weaning Higher among mice with head blebs	3
dr^{J}	Inbred, C3B6-A/$A^{w\text{-}J}$-ank	High pre-weaning mortality	4
dr^{J}	Inbred, B6C3Fe	Yes: Lower than expected numbers of mutants.	5
dr^{J}	Inbred, B6C3Fe-a/a	Yes, before end of 2nd post-natal week	This study

There is no published information on viability of mutant dr^{2J} mice.
**dr* mice provided to Bierwolf by Falconer and Sierts-Roth (Bierwolf, 1956) were bred. No details of the breeding procedure were reported. References: 1-Falconer and Sierts-Roth, 1951. 2-Bierwolf, 1956. 3-Wahlsten *et al.,* 1983. 4-Sweet and Wahlsten, 1983. 5-Patrylo *et al.,* 1990.

natal days (Wahlsten *et al.,* 1983; Patrylo *et al.,* 1990). In the case of dr^{sst}, among which 99% of homozygotes could be identified at birth by their head blebs and blunt or short tails, there was a high mortality, which peaked in the first two postnatal days and after weaning (Wahlsten *et al.,* 1983). Bierwolf reported similar results in *dr* (Bierwolf, 1956), The cause of death among homozygotes in the immediate post-natal period has not been determined, but may be due to an extreme degree of hydrocephaly and the ensuing effects of increased intracranial pressure. A high mortality around the time of weaning is probably related to starvation: before then, mutants cannot compete poorly with their littermates for the mother's milk; after weaning, their incessant circling behaviour makes it difficult for them to eat solid food dispensed onto the cage tops. In the present study, placing moist pellets on a daily basis inside the cage increased the likelihood of survival through the immediate post-weaning period. A few homozygotes that survived beyond weaning age had a normal life span (i.e. a survival of over 12 months), in agreement with what has been previously reported in the case of *dr* (Bierwolf, 1956).

5.4.5. Final comments

The present observations on the external phenotype of dr^{J} mutant mice are in general agreement with previous reports on this allele (Sweet and Wahlsten, 1983). A distinctive morphological feature relating to hindbrain structure was described in E11.5 dr^{J}/dr^{J} embryos. There was an increased postnatal mortality among homozygous mutants, in keeping with published data on this and other *dreher* alleles on an inbred background (Bierwolf, 1956; Sweet and Wahlsten, 1983; Wahlsten *et al.,* 1983; Patrylo *et al.,* 1990). The lower survival rate of the mutants seems to be at least partially related to starvation secondary to their incessant circling behaviour.

Chapter 6

Brain abnormalities in *dr*^{J} mutant mice

6.1. Introduction

The brain phenotype of *dreher* mutants has been the subject of only a few reports (see Table 6.1). Early publications on the *dr* allele (Bierwolf, 1956; Bierwolf, 1958) did not mention any abnormalities of the cerebral cortex, but provided detailed descriptions of the histopathological features and embryogenesis of cerebellar defects. The latter include a small cerebellum, with poorly formed *folia* and disorganised stratification. These findings were reported in two other alleles (dr^{sst} and dr^{J}) (Sekiguchi *et al.,* 1992; Wahlsten *et al.,* 1983; Sweet and Wahlsten, 1983). Abnormalities of the hippocampus (both of the pyramidal cell layer and the dentate gyrus) are known to occur in both the dr^{J} and the dr^{sst} alleles (Sekiguchi *et al.,* 1992; Wahlsten *et al.,* 1983; Nowakowski and Wahlsten, 1985a; Nowakowski and Wahlsten, 1985b). Additional pathological features include hydrocephalus (Bierwolf, 1956; Bierwolf, 1958), heterotopia of the olfactory bulbs (Sekiguchi *et al.,* 1987), deformed colliculi and a thin *corpus callosum* (Bierwolf, 1956; Bierwolf, 1958). More recently, abnormalities of the cerebral neocortex have been described in dr^{J} homozygous mutants, namely the presence of heterotopic neurons in the layer I and cell-free spaces in the underlying layers (Sekiguchi *et al.,* 1987; Sekiguchi *et al.,* 1994).

This chapter includes descriptions of the brain defects of dr^{J} homozygous mutant mice. Particular attention is given to the analysis of the neocortical defects, namely to the characterisation of misplaced (i.e. heterotopic) cells in layer I and to other, previously unreported, abnormalities of the pial-glial boundary (i.e. the *glia*

Table 6.1

Brain abnormalities in homozygous mutant alleles of *dreher*

	CEREBELLUM			CEREBRAL CORTEX		Other abnormalities	Ref.[s]
	Reduced size	Abnormal foliation	Abnormal lamination	Neocortical abnormalities	Hippocampal abnormalities		
dr	+	+	+	NR	NR	Hydrocephalus Deformed colliculi and deep cerebellar nuclei	1
dr^{sst}	+	+	+	NR	Incomplete or absent dentate gyrus	Deformed colliculi Thin corpus callosum	2
dr^{J}	+	+	+	Heterotopic neurones in layer I Cell-free spaces in layers II-IV	Dispersion/ectopias of pyramidal neurones/granule cells of dentate gyrus Partial or complete absence of dentate gyrus (more severe in infra-pyramidal limb) Reduced cell density and thickness of entorhinal cortex	Heterotopia of olfactory bulbs	3

NR - Not reported; + - present. References (Ref.[s]): 1-Bierwolf, 1956. 2-Wahlsten *et al.*, 1983. 3-Sekiguchi *et al.*, 1992; Patrylo *et al.*, 1990; Wahlsten *et al.*, 1983; Sekiguchi *et al.*, 1987; Nowakowski and Wahlsten, 1985a; Nowakowski and Wahlsten, 1985b; Sekiguchi *et al.*, 1994

limitans) overlying the areas affected by the heterotopias (see General introduction). The findings described in this chapter suggest that disruption of this membrane may be a causative factor in the production of misplaced cells in dr^J brains. Data obtained in this study are compared with that originating from previous reports on this and other *dreher* alleles. Finally, a working hypothesis concerning the pathogenesis of the cerebral cortical defects of dr^J mutant brains is proposed on which to base further analysis.

6.2. Methods

All animals used for this part of the study originated from matings between heterozygous male and female *dr*^{J} mice. Genotyping was done with the two microsatellite DNA markers flanking the *dreher* locus, *D1Mit452* and *D1Mit15,* as described in Chapter 3. Additional methods included perfusion-fixation of post-natal mice, dissection and processing of brains, and histological techniques using both routine and immunocytochemical techniques.

6.2.1. Perfusion-fixation

In order to achieve optimal preservation of the brain for histological examination, post-natal mice were fixed *in vivo* prior to removal of the brain from the skull. Briefly, each animal was terminally anaesthetised, either with an intra-peritoneal injection of a 0.1 ml/g body weight solution of 25% Hypnovel® (Midazolam 5mg/ml) and 25% Hypnorm® (Fentanyl citrate 0,315 mg/ml and Fluanisone 10 mg/ml) in sterile distilled water, or in the case of neonates, by cryoanaesthesia. An adequate level of anaesthesia was confirmed by the absence of reflexes to painful stimuli applied to the limbs. Once the abdominal cavity was opened, the spleen was removed, rinsed in sterile PBS and snap-frozen in dry ice (for future DNA isolation). The diaphragm was opened and the thorax was cut on both sides of the sternum to expose the heart. The right atrium was nicked in order to allow blood and perfusion solution to exit the circulation. Immediately thereafter, a 21- to 25-gauge needle (depending on the size of the animal), connected to a 2-way perfusion system containing PBS and 4% paraformaldehyde (PFA) in PBS (pH 7.3-7.4), was inserted into the left ventricle. A brief (around 30 seconds) flush of PBS was followed by an

intracardial perfusion of 4% PFA in PBS for 5 to 10 minutes, depending on the size of the mouse. An efficient perfusion was associated with increasing liver pallor and progressive rigidity of the whole body. After disconnecting the perfusion system, the head was isolated by a section immediately posterior to the skull.

6.2.2. Dissection, processing, and embedding of brains

The brain was dissected from the skull under a stereomicroscope, weighed and immersed in 4% PFA in PBS solution for 2 hours at room temperature. Prior to processing, it was sectioned coronally into 4 slices as depicted in Figure 6.1, then transferred manually to vials containing 50% IMS (industrial methylated spirit) in distilled water. Littermates of either genotype used for analysis (+/+ and dr^J/dr^J) were processed together. Further processing was carried out in a Shandon automatic tissue processing machine (Shandon Hypercenter 2) as shown in Table 6.2. The processed brain slices were embedded in paraffin wax.

6.2.3. Sectioning of wax-embedded blocks

Blocks were routinely sectioned at a thickness of 10 μm using a rotatory microtome (Microm). Sections were floated onto a warm (40-45°C) distilled water bath and mounted on coated slides. The latter were prepared by immersing slides serially in a 1% aqueous TESPA (3-aminopropyltrietoxysilane, Sigma) solution, twice in acetone and twice in distilled water, then drying them overnight at 37°C. After sectioning, mounted sections were left to dry on a warm (32°C) plate overnight, then stored at room temperature.

Figure 6.1

Schematic dorsal (left) and ventral (right) views of a normal mouse brain to show slices selected prior to processing

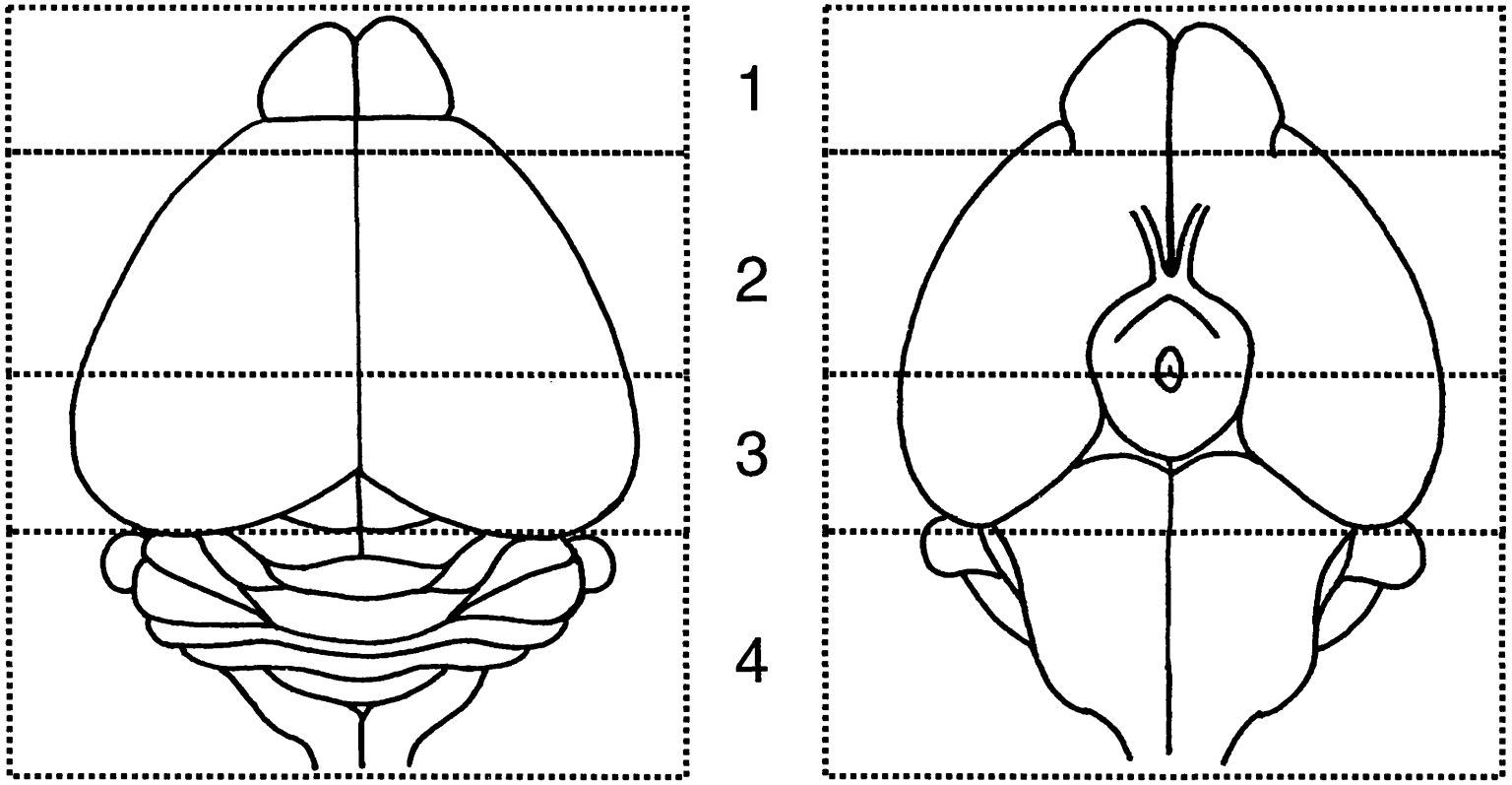

Each brain was sectioned in the coronal plane, in order to obtain four slices (1 to 4).

Table 6.2

Protocol for the automatic processing of brain tissue

Solution	Time	Temperature
70% IMS	8 h	Room temperature
90% IMS	1 h	Room temperature
100% IMS	1 h	Room temperature
100% IMS	1 h	Room temperature
100% IMS	1 h	Room temperature
Chloroform	40 min	Room temperature
Chloroform	40 min	Room temperature
Chloroform	40 min	Room temperature
Wax	1 h	60°C (under vacuum)
Wax	1 h	60°C (under vacuum)

After removal of the brain from the skull, each brain was sectioned in the coronal plane into four slices (1 to 4). These were post-fixed in 4% PFA in PBS, then immersed in 50% IMS (Industrial methylated spirit), before starting automatic processing according to the protocol above.

6.2.4. Brains and cortical regions selected for study

Figure 6.2 shows schematic drawings of the main levels of section that were analysed, as well as the corresponding neocortical areas.

Histological anomalies were sought in the neocortex at 3 different levels (A, B and C) in 8 *dr*^{J}/*dr*^{J} and 8 *+/+* brains at P21 with cresyl violet-stained sections. Additional levels (D, E and F) were studied in two brains per genotype. Table 6.3 summarises the number of cases of P21 mice of each genotype studied according to section levels and stains.

Additionally, four brains from *dr*^{J} neonates (2 *dr*^{J}/*dr*^{J} and 2 *+/+*) and two brains from adult *dr*^{J} mutants were examined. Only wild-type animals (i.e. no heterozygotes) were used as normal controls, since histological abnormalities of the hippocampus have been reported in approximately half of brains from proven *dr*^{J} /+ mice, suggesting there is haplo-insufficiency (Patrylo *et al.,* 1990).

6.2.5. Routine histological stains

Routine histopathological stains were used to demonstrate the overall cytoarchitecture of the brain (H&E and cresyl-violet staining) and as a first step to study the superficial pial-glial boundary (Gordon and Sweet silver impregnation for reticular fibres).

6.2.5.1. Hematoxylin and eosin (H&E) staining

Sections were dewaxed by immersing twice in Histoclear (National Diagnostics) for 10 minutes, re-hydrated by immersion in IMS solutions of decreasing

Figure 6.2

Selected coronal sections through the cerebral hemispheres and corresponding cortical areas

Section level:

A - through the anterior part of the frontal cortex, anterior to the corpus callosum.

B - Through the anterior part of the corpus callosum and the anterior commissure.

C - Through the anterior part of the hippocampus.

D - Through the posterior part of the hippocampus.

E - Through the posterior tip of the hippocampus and the occipital cortex.

F - Posterior to the hippocampus, through the occipital cortex.

Cortical areas (numbered on the external surface of each section):

4, 6, 8, 10 and 11: frontal region.

1, 3, 3a, and 40: parietal region.

17, 18a and 18b: occipital region.

13 and 14: insular region.

22, 36 and 41: temporal region.

24 and 25: anterior medial cortical region.

29a, 29b and 29c: posterior medial cortical region.

27, 35, 49: retro-hippocampal region.

Adapted from Caviness, 1975 .

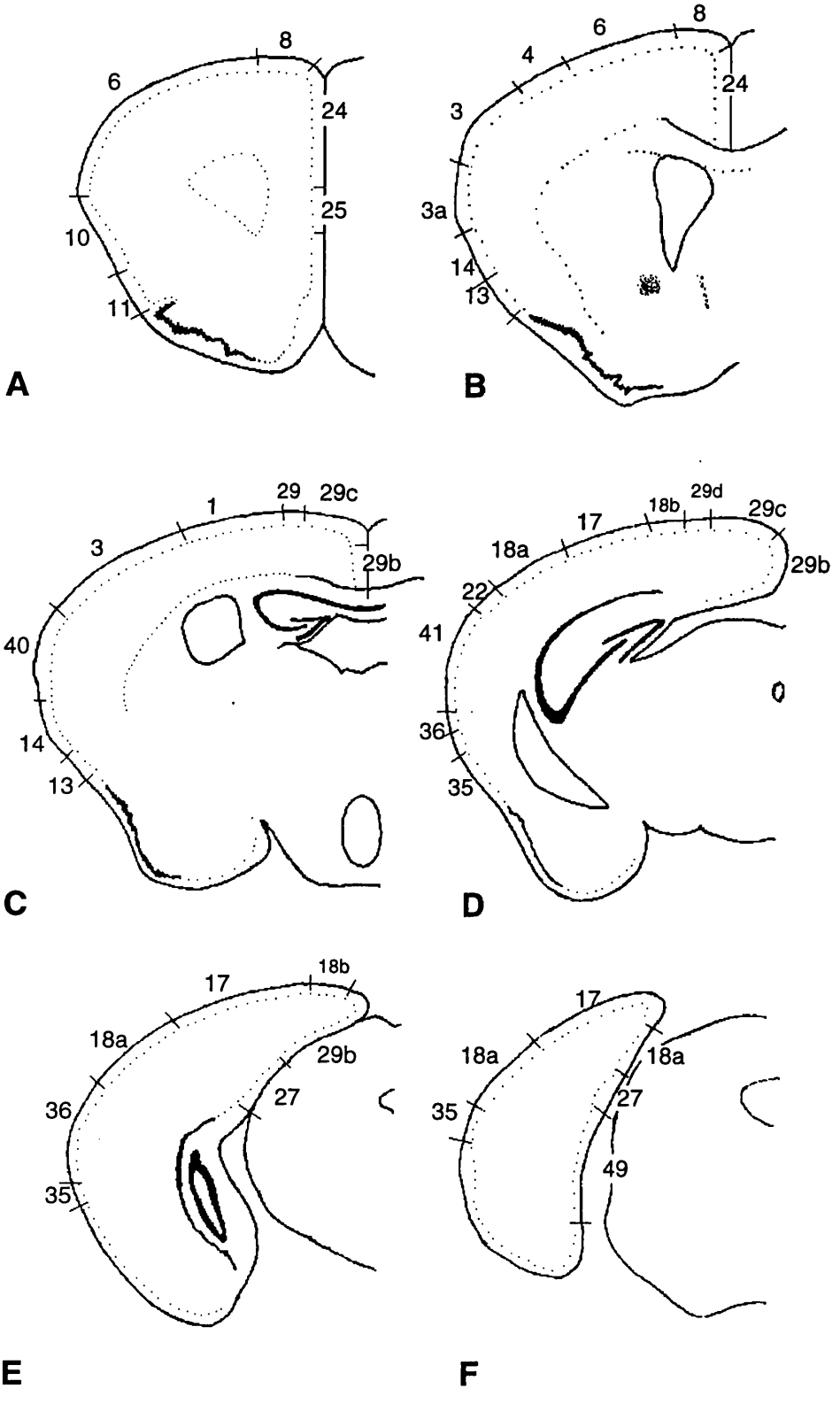
8
6
24
25
10
11
A
8
6
4
24
3
3a
14
13
B
1
29
29c
3
29b
40
14
13
C
17
18b
29d
29c
18a
29b
22
41
36
35
D
18b
17
18a
29b
27
36
35
E
17
18a
18a
27
35
49
F

Table 6.3

Number of cases of each genotype studied for each level of section and stain (P21 mice only)

	A		B		C		D		E		F	
	+/+	dr^J/dr^J	+/+	dr^J/dr^J	+/+	dr^J/dr^J	+/+	dr^J/dr^J	+/+	dr^J/dr^J	+/+	dr^J/dr^J
CV	8	10	8	10	8	10	2	2	2	4	2	2
HE	-	-	2	3	2	3	-	-	-	-	2	2
Reticulin	-	-	1	1	8	8	-	-	-	-	-	-
GFAP	-	-	5	5	1	-	-	-	-	-	-	-
NeuN	-	-	-	-	8	8	-	-	-	-	-	-
F. VIII	-	-	3	3	1	-	-	-	-	-	-	-
Laminin	-	-	-	1	8	8	-	-	-	-	-	-

CV - cresyl violet; **HE** - haematoxylin and eosin; **Reticulin** - Gordon and Sweet silver impregnation for reticular fibres; **GFAP** - anti-glial fibrillary acidic protein immunostaining; **NeuN** - anti-neuronal nuclei immunostaining; **F. VIII** - anti-von Willebrand (factor VIII) immunostaining; **Laminin** – anti-laminin immunostaining. **–** No staining was performed. Levels **A** to **F** are depicted in Figure 6.2.

concentration (100%, 95%, 70%), and rinsed in distilled water, stained in Ehrlich's Hematoxylin solution (Sigma) for 10 minutes, rinsed again in distilled water, then washed under running cold tap water for 5 minutes. Sections were subsequently dipped for a few seconds in a 1% solution of undiluted HCl in 70% IMS to differentiate, washed again in running cold tap water for 5 minutes with frequent agitation, stained with a 1% aqueous Eosin Yellowish solution (Gurr Certistain) for 2 minutes. Finally, they were washed under cold tap water until clear, de-hydrated in 95% and 100% IMS solutions, cleared with Histoclear for ten minutes, mounted with DPX mounting medium (Fischer Scientific) and coverslipped. Under hematoxylin and eosin, the nucleus appears dark blue and the cytoplasm stains in varying shades of pink.

6.2.5.2. Cresyl-violet (Nissl) staining

Sections were dewaxed by immersing twice in Histoclear (National Diagnostics) for ten minutes. They were then dehydrated by immersion in IMS solutions of decreasing concentration (100%, 95%, 70%), rinsed in distilled water, stained in a filtered cresyl violet acetate solution (Sigma) for 5 minutes, rinsed again in distilled water, immersed in 70%, then 95% IMS, quickly differentiated in a 2.5% solution of acetic acid in 95% IMS, then immersed in 100% IMS, cleared with Histoclear for ten minutes, mounted with DPX and coverslipped. Cresyl violet stains characteristic aggregates of rough endoplasmic reticulum in the cytoplasm of neurons, called Nissl bodies. The latter stain purple to dark blue, nuclei stain purple blue.

6.2.5.3. Gordon and Sweet silver impregnation for reticular fibres

This was performed according to the Gordon and Sweet reticular fibre staining method used routinely by the Histopathology Department of Great Ormond Street Hospital for Children. Briefly, sections were dewaxed by immersing twice in xylene for 5 minutes each. After re-hydrating with IMS solutions of decreasing concentration and rinsing in tap water, then in distilled water, sections were treated with 0.25% acidified potassium permanganate for 5 minutes and bleached in oxalic acid until the brown colour disappeared. They were quickly rinsed in distilled water, treated with 5% iron alum for 15 minutes, rinsed again in distilled water, impregnated with freshly filtered ammoniacal silver solution for approximately two minutes, rinsed twice in distilled water, reduced in 10% formalin in tap water for 1 minute, washed with distilled water, immersed in 0.2% gold chloride for 30 seconds, rinsed in distilled water and fixed in 5% sodium thiosulphate for 1 minute. Subsequently, they were rinsed again in distilled water, counterstained with Neutral Red (0.05% Nuclear Fast Red in a 5% aqueous solution of aluminium sulphate), dehydrated in 70%, 95% and 100% IMS solutions, cleared with xylene for 5 minutes, mounted with Canada Balsam (Sigma) and coverslipped. Reticular fibres are collagen-containing connective tissue fibres. They appear grey to black. Nuclei are stained red.

6.2.6. Immunocytochemical methods

6.2.6.1. General overview

Immunocytochemistry was used in order to identify various cellular components with a high degree of selectivity on paraformaldehyde-fixed, paraffin-embedded brain tissue from *dr*^{J} mice. Immunocytochemical techniques were carried out

either with polyclonal (raised in rabbit) or monoclonal (raised in mouse) primary antibodies.

Antibodies directed against glial fibrillary acidic protein allow for labelling of normal and pathological (e.g. reactive) astrocytes. The usefulness of anti-NeuN immunostaining in the identification of neurons in formalin-fixed, paraffin embedded human tissues has recently been reported (Wolf *et al.,* 1996). Endothelial cells are distinctively decorated with anti-Factor VIII antibodies. Anti-laminin antibodies were used to demonstrate basal lamina (e.g. of vessels and epithelia). The various types of antibodies, characteristics and working dilutions are shown in Table 6.4.

After incubating the sections with the primary antibody (either a monoclonal or a polyclonal antibody), a secondary, biotinylated antibody was applied to the sections. Commercially available avidin-biotin-peroxidase systems were used for labelling. Visualisation of peroxidase activity was with 3,3'-diaminobenzidine (DAB) precipitation: A DAB solution (Sigma Fast DAB) containing peroxidase substrate was prepared by dissolving DAB, 0.7 mg/ml, urea hydrogen peroxide 0.7 mg/ml and 0.06M Tris buffer in distilled water. This solution was applied to each section for 5-10 minutes, until a brown precipitate appeared. Blocking of endogenous (cerebral) peroxidase activity was performed, whenever necessary, by incubating sections in a dilute hydrogen peroxide solution prior to exposure to the primary antibody. Unmasking of antigen sites was achieved when needed by boiling the sections in a microwave oven. Control sections were included for all immunocytochemical labelling procedures. Negative controls consisted of sections not having received the primary antibody. Positive

Table 6.4

Antibodies and sera used in the immunohistochemical study

Antigen	Type of primary antibody	Target structure	Manufacturer	Reference	Working dilution	Secondary antibody	Blocking serum
Glial fibrillary acidic protein (GFAP)	Polyclonal (rabbit anti-cow)	Astrocytes	DAKO	Z 0334	1:500	Biotinylated goat anti-rabbit	Normal goat serum
Neuronal nuclei (NeuN)	Monoclonal (mouse anti-mouse)	Postmitotic neurons	Chemicon	MAB377	1:1000	Biotinylated rabbit anti-mouse	Normal rabbit serum
Von Willebrand factor (f. VIII)	Polyclonal (rabbit anti-human)	Blood vessels	DAKO	A 082	1:1000	Biotinylated goat anti-rabbit	Normal goat serum
Laminin	Polyclonal (rabbit anti-mouse)	Basement membranes	Sigma	L-9393	1:50	Biotinylated goat anti-rabbit	Normal goat serum

controls consisted of either a section from a tissue known to label with that antibody (for example a section from a normal cerebellum as a control for the neuronal marker NeuN) or a section from a *dr*^{J} brain that had tested positive in a previous immunolabelling run.

6.2.6.2. Anti-glial fibrillary acidic protein (anti-GFAP) immunolabelling

Sections were dewaxed by immersing twice in Histoclear for ten minutes each. They were then re-hydrated by immersion in IMS solutions of decreasing concentration (100%, 95%, 70%), and rinsed in distilled water (dH_2O), before blocking endogenous peroxidase activity in 3% hydrogen peroxide (in distilled water) for 15 minutes. Sections were again rinsed in dH_2O, then in PBS, and incubated with rabbit anti-cow polyclonal antibody (anti-GFAP, DAKO) 1:500 diluted in blocking serum applied on sections at room temperature in a humid chamber for 1 hour. Blocking serum was obtained by diluting normal goat serum (DAKO) 1:5 in PBS. The primary antibody was then washed off with PBS, and sections were incubated with the secondary antibody (biotinylated goat anti-rabbit antibody, DAKO, 1:200 in blocking serum) for 30 minutes at room temperature in a humid chamber. Sections were again washed with PBS, then incubated for 30 minutes with an avidin-biotin horseradish peroxidase solution (ABComplex/HRP, DAKO) at room temperature in a humid chamber. After rinsing sections once more with PBS, peroxidase was revealed with a diaminobenzidine (DAB) solution as described above. Sections were rinsed in tap water, then in distilled water, counterstained with cresyl violet acetate (Sigma) for 5 minutes, then dehydrated by immersion in IMS solutions of increasing concentration (70%, 95%, 100%), cleared with Histoclear, mounted with DPX and coverslipped.

6.2.6.3. Anti-NeuN (anti-neuronal nuclei) immunolabelling

Staining of neuronal nuclei and perikarya was performed by modification of a protocol of Wolf, et al. (1996). Slides were heated on a 60°C hotplate for a few seconds to melt the wax, then dewaxed by immersing in Histoclear, re-hydrated in a graded series of aqueous IMS solutions (100%, 95%, 70%) and rinsed in distilled water, before blocking endogenous peroxidases as described above. They were rinsed again in distilled water, washed in 0.05 M TBS (pH 7.6) and boiled in a 0.01 M citrate buffer (pH 6.0) in a microwave oven for 10 minutes. The slides were allowed to cool for 15 minutes in this buffer at room temperature, and then for a further 5 minutes under running cold tap water. They were placed in a humid chamber, and incubated with blocking serum (normal rabbit serum, DAKO, 1:8 diluted in TBS pH 7.6) applied on the slide for 30 minutes, then overnight with the primary antibody (monoclonal antibody MAB377 anti-NeuN, Chemicon, 1:1000 dilution in blocking serum). On the following morning, the primary antibody was washed off with TBS, and sections were incubated first with blocking serum, then with the secondary antibody (biotinylated rabbit-anti mouse antibody DAKO 1:200 in blocking serum) for 30 minutes at room temperature in a humid chamber. Sections were again washed with TBS, then incubated for 30 minutes with an avidin-biotin horseradish peroxidase solution (ABComplex/HRP, DAKO), at room temperature in a humid chamber. After rinsing sections once more with PBS, peroxidase was revealed with a diaminobenzidine (DAB) solution as described before. Sections were rinsed in tap water, then in distilled water, lightly counterstained with Mayer's hematoxylin (Sigma) for 2 minutes, then dehydrated in IMS solutions, cleared with Histoclear, mounted with DPX and coverslipped.

6.2.6.4. Anti-factor VIII immunolabelling

Sections were dewaxed by immersing in Histoclear, re-hydrated in IMS and rinsed in distilled water, before blocking endogenous peroxidases as described above. They were washed with distilled water, then with PBS, and digested for 10 minutes with protease (Protease type XXIV, Sigma, 0.02% in PBS) at 37°C. After rinsing in PBS once more, they were incubated with blocking serum (normal goat serum in PBS 1:5) for 15 minutes, then with rabbit anti-human von Willebrand factor antibody (DAKO) 1:1000 diluted in blocking serum, applied on sections at room temperature in a humid chamber for 1 hour. The primary antibody was washed off with PBS, and sections were incubated with the secondary antibody (biotinylated goat anti-rabbit antibody, DAKO 1:200 in blocking serum) for 30 minutes at room temperature in a humid chamber. Sections were again washed with PBS, then incubated for 30 minutes with an avidin-biotin horseradish peroxidase solution (ABComplex/HRP, DAKO) at room temperature in a humid chamber. After rinsing sections once more with PBS, peroxidase was revealed with a diaminobenzidine (DAB) solution as described before. Sections were rinsed in tap water, then in distilled water, lightly counterstained with Mayer's hematoxylin (Sigma) for 2 minutes, then dehydrated in IMS solutions, cleared with Histoclear, mounted with DPX and coverslipped, as described before.

6.2.6.5. Anti-laminin immunolabelling

Sections were de-waxed by immersing in xylene for 5 minutes. They were then re-hydrated by immersion twice in 100% ethanol, before blocking endogenous peroxidase activity with 3% hydrogen peroxide for 15 minutes. They were rinsed

in tap water and boiled in a 0.01 M citrate buffer (pH 6.0) in a microwave oven for 10 minutes. The slides were allowed to cool in tap water for 5 minutes. They were washed in TBS (pH 7.4-7.6) and pre-incubated with blocking serum (normal goat serum, DAKO, 1:5 in TBS) for 10 minutes in a humid chamber. The primary anti-laminin antibody (Sigma, 1:50 in blocking serum) was applied on the sections for 1 hour in a humid chamber. Following two 5 minute washes with TBS, sections were incubated with the secondary antibody (biotinylated goat anti-rabbit antibody DAKO 1:250 in TBS) for 30 minutes at room temperature in a humid chamber. Sections were again washed twice for five minutes each with TBS, then incubated for 30 minutes with an avidin-biotin horseradish peroxidase solution (ABComplex/HRP, DAKO), at room temperature in a humid chamber. After rinsing sections once more with PBS, peroxidase was revealed with a diaminobenzidine (DAB) solution as described before. Sections were rinsed in tap water, then in distilled water, lightly counterstained with Mayer's hematoxylin (Sigma) for 3 minutes, then dehydrated in 70% and 100% ethanol, cleared with xylene, mounted with Entellan (Merck Diagnostica) and coverslipped.

6.2.7. Photography

Whole brains were photographed with a Zeiss SV11 Stereomicroscope. Sections were photographed with a Zeiss Axiophot transmitted light microscope.

6.3. Results

6.3.1. Macroscopic abnormalities of the brain in homozygous *dr^J* mutant mice

Macroscopic abnormalities included an overall small brain (including both the cerebral hemispheres and the cerebellum), occasionally associated with a malformed midbrain. Hydrocephalus was seldom seen in *dr^J* mutants.

6.3.1.1. Reduced brain size in *dr^J* homozygous mutant mice

Brains of *dr^J/dr^J* mice at P21 were usually of smaller size than age-matched wild-type animals. (see Figure 6.3). Total brain weight, as measured after removal from the skull, was on average 0.37+/-0.06 g for *dr^J/dr^J* (n=13) and 0.50 +/- 0.06 g for wild-type mice (n=22), with a statistically significant difference ($p<0.001$) between the two genotypes (Table 6.5). Body weight was also statistically smaller in *dr^J/dr^J* mice than in wild type littermates (Table 6.5), although there was no close relationship between brain and body weight: the correlation coefficient between body and brain weight values was 0.60 for wild-type mice (n=22) and 0.78 for *dr^J/dr^J* (n=13). A small cerebellum was seen in 18 out of 32 *dr^J/dr^J* cases in which the brain was examined (age range: 3 weeks to 10 months, average 10.6 weeks). In some cases, both the midline cerebellar structures (vermis) and cerebellar hemispheres seemed to be mildly affected (9 cases). In others, there was a disproportionate reduction in size of the vermis, in relationship to the relatively normal-looking cerebellar hemispheres (9 cases). In the most severe cases, there was almost no identifiable cerebellar parenchyma, and the almost complete

Table 6.5

Brain and body weight in wild-type and homozygous mutant *dr*^{J} mice at P21

	+/+ (n=22)	*dr*^{J}/*dr*^{J} (n=13)	*p* value
Mean brain weight	0.50 ±0.06	0.37 ±0.06	<0.001
Mean body weight	9.95 ±2.70	5.58 ±1.50	<0.001
Correlation coefficient (brain-body weight)	0.60	0.78	

Mice were weighed at P21, before being anaesthetised and perfusion-fixed.

Whole brains were weighed immediately after removal from the skull.

Figure 6.3

Dorsal view of the fixed brains of *dr*^{J} mice

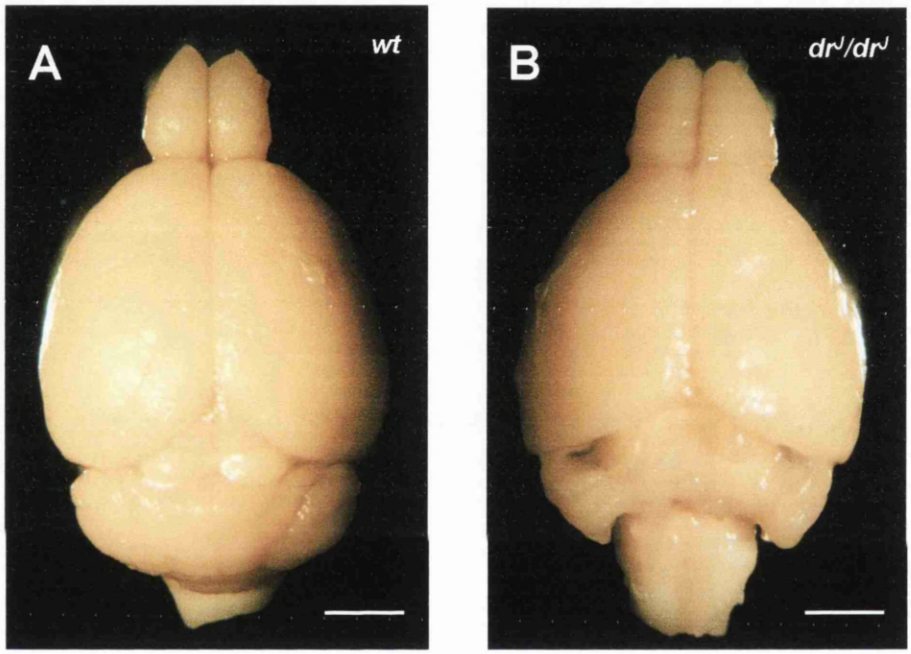

Notice the overall smaller brain and the severely reduced size of the cerebellum (affecting both the vermis and the cerebellar hemispheres) in the adult homozygous *dr*^{J} mutant **(B)**, when compared to the brain of an age-matched, wild-type *dr*^{J} mouse **(A).** Scale bar represents 2.5 mm.

absence of midline structures allowed the floor of the IV ventricle to become visible on a dorsal view of the brain (Figure 6.3). A very small cerebellum was associated in three cases with deformation of the midbrain colliculi (data not shown).

6.3.1.2. Hydrocephalus was a rare event in *dr^J* mutants

Dilatation of the lateral ventricles was seen in only one out of the 16 *dr^J/dr^J* cases aged P1 to 24 weeks (average=9.6 weeks) and in none of the 12 wild-type brains (aged between P1 and 3 weeks, average 2 weeks) that were examined. Although brains were not systematically examined for an enlarged IV ventricle, this defect was nevertheless obvious at the time of removal of the brain from the skull in 8/16 cases, because it coexisted with a cerebellar midline (vermian) defect.

6.3.2. Microscopic abnormalities in the neocortex of *dr^J/dr^J* mice

6.3.2.1. Nature and spatial distribution of the neocortical defects

In the neocortex of *dr^J* mutants at P21, abnormalities were found mainly in the frontal and parietal lobes, but were seen bilaterally in the occipital lobes in one case. They were most conspicuous in areas 4, 6 and 8 of the frontal cortex and in areas 1 and 3 of the parietal cortex. They consisted of ruffling of the upper border of layer II, areas of low cellularity (mainly in layer II as well), heterotopic cells in layer I and abnormalities of the *glia limitans*, associated with a network of intra-cortical vessels within layer I. These abnormal histological features were not seen in any of the wild type control brains.

6.3.2.2. Inter- and intra-individual variability in the severity of the neocortical abnormalities

The severity of the cortical defect was highly variable from animal to animal, namely in the extent of affected neocortex and the apparent number of heterotopic cells in layer I (not quantified). It also varied in severity from one hemisphere to the contralateral one in a given mouse. The most severely affected side varied from frontal to parietal level in some cases and was not necessarily ipsilateral to that of the most affected hippocampus (see below).

6.3.2.3. Heterotopic layer I cells are neuronal

The presence of excessive numbers of cells in neocortical layer I was assessed on sections stained with hematoxylin and eosin and/or cresyl violet staining in all brains studied (Figures 6.4 and 6.5). The neuronal nature of the heterotopic cells was confirmed in selected cases (8 *dr*^{J}/*dr*^{J} and 8 *+/+* mice at three weeks of age) by immunolabelling with a nerve cell-specific antibody (anti-NeuN). The latter decorates neuronal nuclei and perikaryal cytoplasm with minor labelling of cytoplasmic processes, in such a way that each cell stands out of the background neuropil (Figure 6.6).

Most of these heterotopic cells did not have the same morphology as the normal bipolar, horizontal Cajal-Retzius cells of layer I. In contrast, heterotopic cells most closely resembled layer II neurons, with oval to pyramidal-shaped cell bodies and large nuclei (see Figure 6.5E). They were frequently misoriented (Figure 6.5E). Heterotopic cells were either distributed diffusely throughout large areas of layer I or, more commonly, occurred in small clusters (Figure 6.5 A). When abundant, the

Figure 6.4

Appearance of the cerebral cortex in *dr*^{J} mice: hematoxylin and eosin staining

Coronal sections through the cerebral hemispheres. (A) and (C) Wild-type. (B) and (D) Homozygous *dr*^{J} mutant.

(A) and (B) Low-magnification view of the whole parietal cortex. The normal stratification of the cerebral cortex is seen in (A). Notice the low cellularity of the molecular layer (layer I). Layers II to VI are the most densely cellular. (B) Cortical layering is not significantly disturbed in the mutant, except for layer I, which is more cellular in *dr*^{J}/*dr*^{J} than in wild type controls. (C) and (D): The appearance of cerebral neocortex at the level of the inter-hemispheric fissure. The wild type exhibits a well delineated pial-glial boundary (C), in contrast to the mutant brain (D), which shows an irregular external brain surface with increased numbers of vessels and excessive numbers of cells in the outer part of layer I. Scale bar represents: (A) and (B) 175 μm (C) and (D) 100 μm.

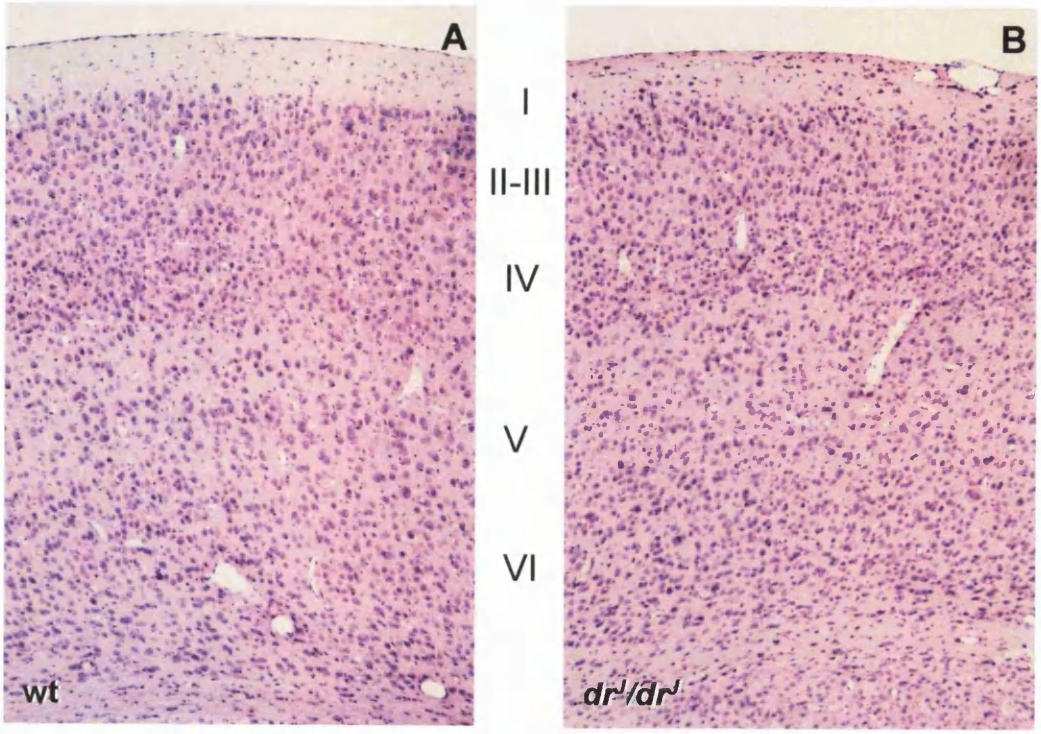
A
B
I
II-III
IV
V
VI
wt
dr^J/dr^J

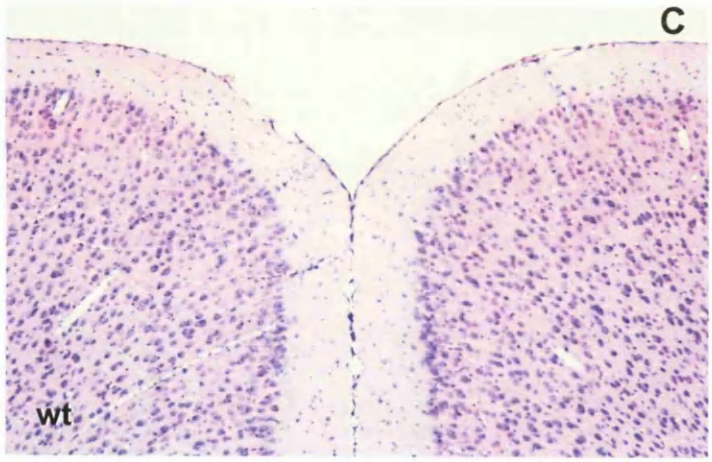
C
wt

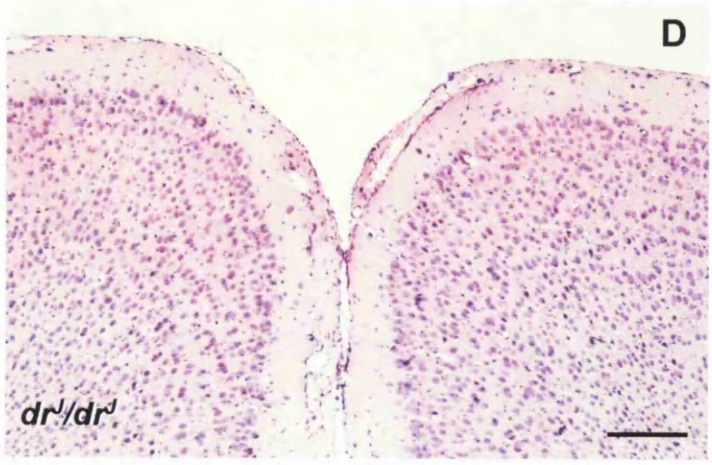
D
dr^J/dr^J

Figure 6.5

Histological features of heterotopic cells in layer I of the neocortex of *dr*^{J} mutant mice: Cresyl violet staining

Cresyl violet-stained coronal sections through the cerebral hemispheres of *dr*^{J} mice at P21:

(A) Homozygous mutant. Section through the frontal and parietal areas of the cortex in a homozygous mutant, to show different collections of heterotopic cells. From left to right: diffuse deposits (arrow), nodular collections (open arrowhead) and apparent protrusions of layer II into layer I (black arrows).
(B) Homozygous mutant. Notice scattered disoriented cells with neuronal morphology in layer I. There is blurring of the transition between layers I and II.
(C) Another mutant brain. This section shows linear structures running beneath the pial-glial barrier in a parallel to oblique direction (arrowhead). Scattered heterotopic cells are seen within layer I, both internal and external to these structures.
(D) Homozygous mutant. Heterotopic cells are seen in layer I and occupy the leptomeningeal space as well (star).
(E) High power view of a mutant brain, showing cells with neuronal morphology (e.g. that pointed by the arrowhead).
(F) Inter-hemispheric fissure in a wild type mouse: notice the smooth upper limit of layer II and the poorly-cellular layer I.
(G) Corresponding area in the brain of a homozygous mutant littermate. Notice "digitations" (arrowheads) of heterotopic cells apparently originating from layer II. Scale bar represents: (A) 400μm, (B) 50μm (C) 100μm, (D) 200μm. (E) 100μm, (F) and (G) 200 μm.

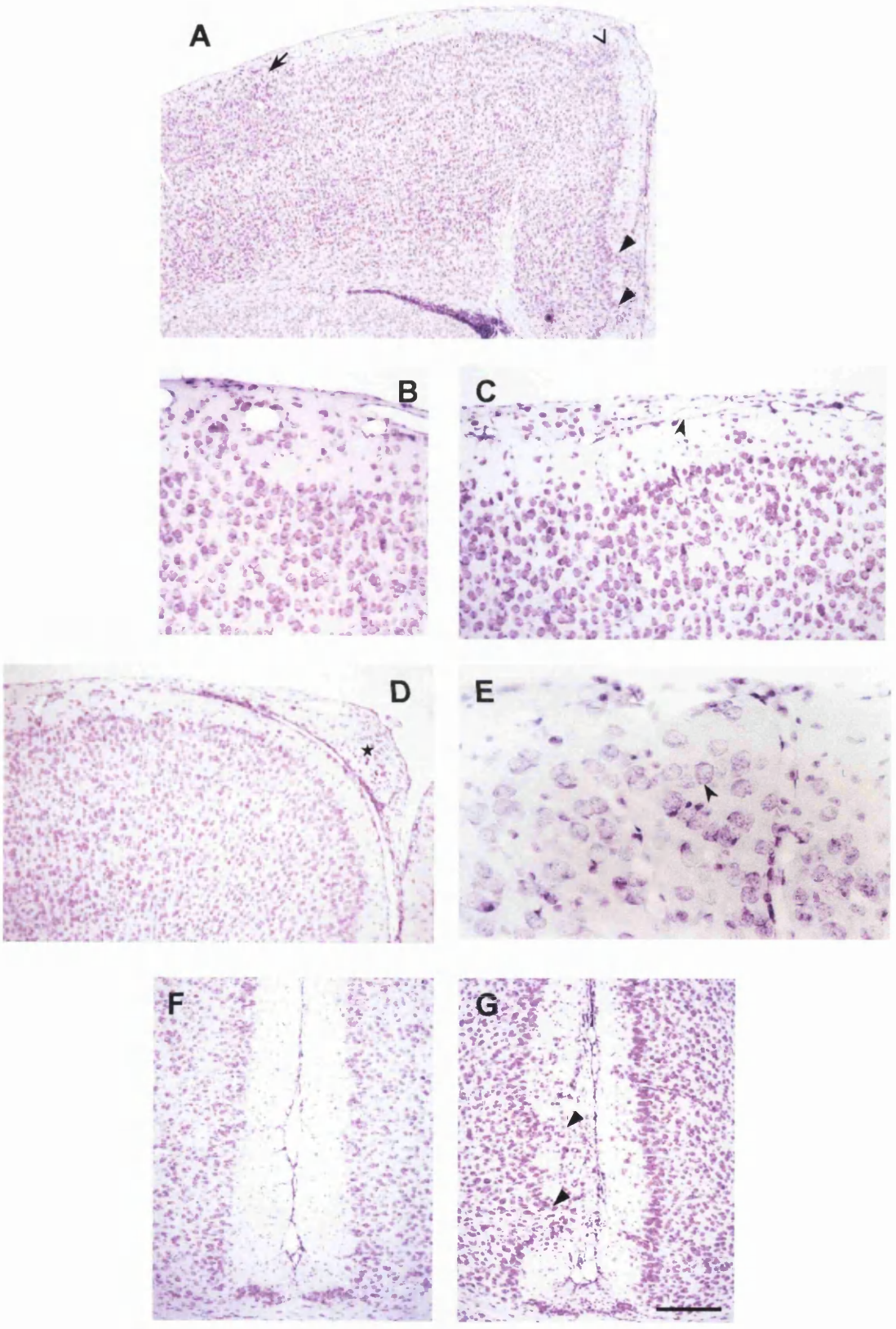
A
B
C
D
E
F
G

Figure 6.6

Immunocytochemical characterisation of heterotopic cells in the neocortex of *dr*^{J} mice

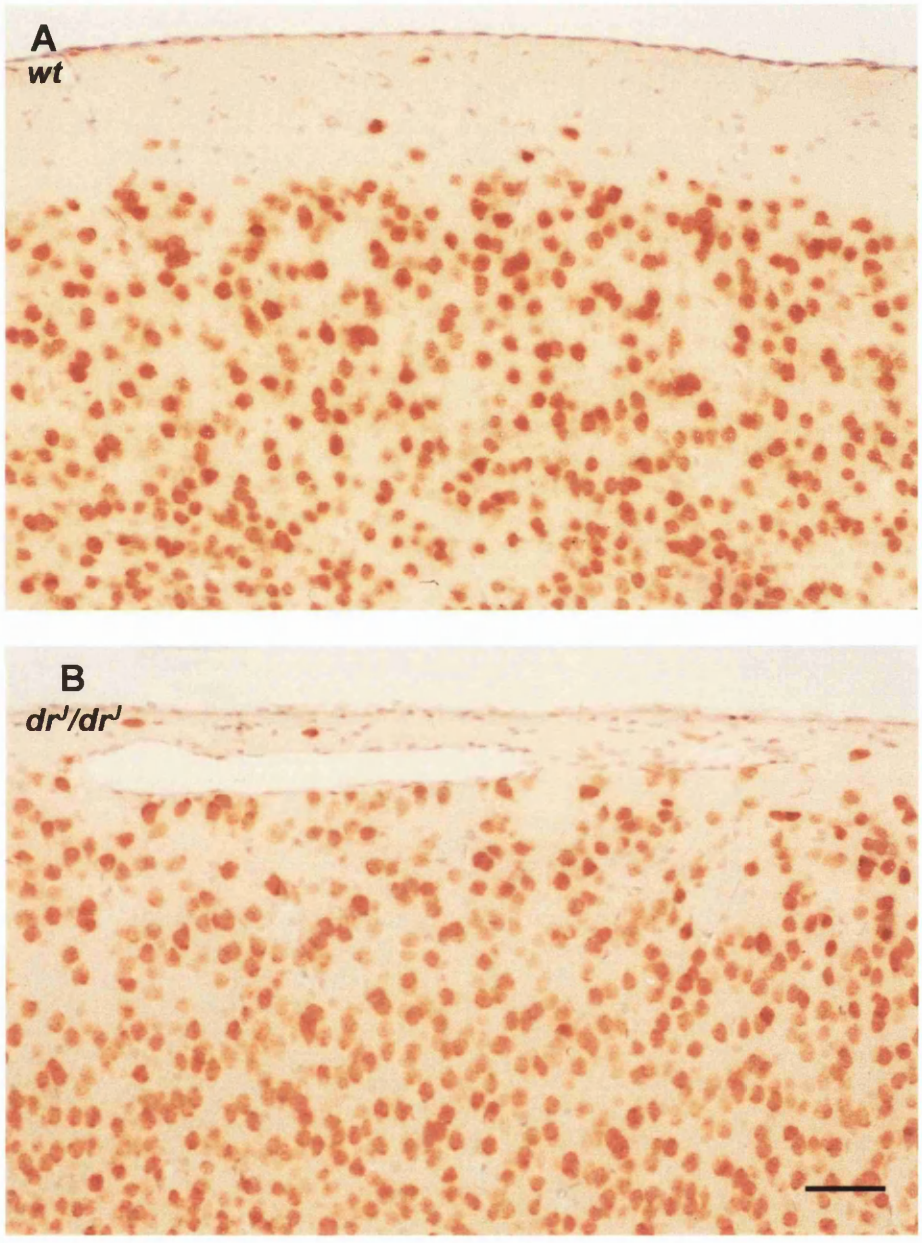

Coronal sections through the parietal cortex (level C) were immunolabelled with an anti-neuronal nuclei (anti-NeuN) antibody. **(A)** Wild type mouse. Notice well demarcated layer I, where few labelled cell are seen. **(B)** Homozygous mutant littermate. Numerous heterotopic cells are seen in layer I. Their nuclei are strongly NeuN-positive. Scale bar represents 60 μm in both images.

heterotopic cells contributed to a blurring of the transition between layers I and II (Figure 6.5A). In some cases, the appearance was that of finger-like expansions from layer II into layer I, abutting onto the surface of the brain (Figure 6.5A, B and G). Collections of heterotopic cells were sometimes seen invading the leptomeningeal space (Figure 6.5D).

Heterotopic layer I neurons were found bilaterally in both frontal and parietal areas of the cortex in all *dr*^{J}/*dr*^{J} brains, but in none of the wild-type controls. The more extensive diffuse deposits were found in area 3 of the parietal cortex, but prominent heterotopic clusters were also seen in parietal area 1 and in areas 4, 6 and 8 of the frontal cortex. Areas situated near the midline, and the lateralmost regions of both cortices, tended to show little or no pathological changes. In most cases, heterotopias did not extend laterally into areas 10 or 40 (relatively or completely spared in 6/8 cases), nor medially: areas 24, 29 and 3a were devoid of heterotopic clusters or diffusely distributed heterotopic cells in 5/8, 5/8 and 3/8 cases respectively. In a single case, the occipital cortex (areas 17, 18, 22 and 29) was also affected bilaterally.

6.3.2.4. Heterotopic layer I neurons of *dr*^{J}/*dr*^{J} mutants are associated with abnormalities of the glia limitans and with abnormal layer I vessel organisation

Two particular histological abnormalities of layer I were found in the brains of weaning age homozygous mutants: an abnormal vascular network and an abnormal glia limitans. These defects were intimately related with each other and had the same spatial distribution as heterotopic layer I neurons. The defects were seen by hematoxylin and eosin staining and were also

demonstrated by silver impregnation and immunocytochemical techniques in all *dr*^{J}/*dr*^{J} brains studied, whereas they were never seen in wild-type brains. The morphology and distribution of astrocytes in the vicinity of these abnormal structures were also examined.

6.3.2.4.1. Abnormal vascular network

Normal layer I vessels are usually perforating vascular channels that originate in the leptomeninges, and penetrate the brain approximately at right angles to the pial surface (Figures 6.7 and 6.8). Coronal sections of the parietal lobe of 3 *dr*^{J}/*dr*^{J} and 3 wild-type controls (all P21), were used for immunolabelling with anti-von Willebrand factor (factor VIII) antibodies.

In normal brains, anti-von Willebrand factor immunolabelling results in the staining of small vessel walls as well as the continuous *glia limitans* (see Figure 6.8). This confirmed the vascular nature of the intra-cortical channels. A similar pattern was demonstrated with anti-laminin antibody immunolabelling, which highlights basement membranes (Figure 6.7).

In the brains of homozygous mutants, vascular profiles appeared more numerous (not quantified) and their disposition was preferentially parallel, rather than perpendicular to the pial surface (i.e. to the external glial limiting membrane). These features were seen exclusively in areas with an abnormal *glia limitans* and coexisted with heterotopic layer I neurons. No such vascular network was seen in the brains of normal mice or in areas of normal-looking cortex in homozygous mutants (e.g. temporal neocortex). Vessels appeared quite prominent in all brains

Figure 6.7

Anti-laminin immunostaining in the parietal cortex of *dr^{J}* mice

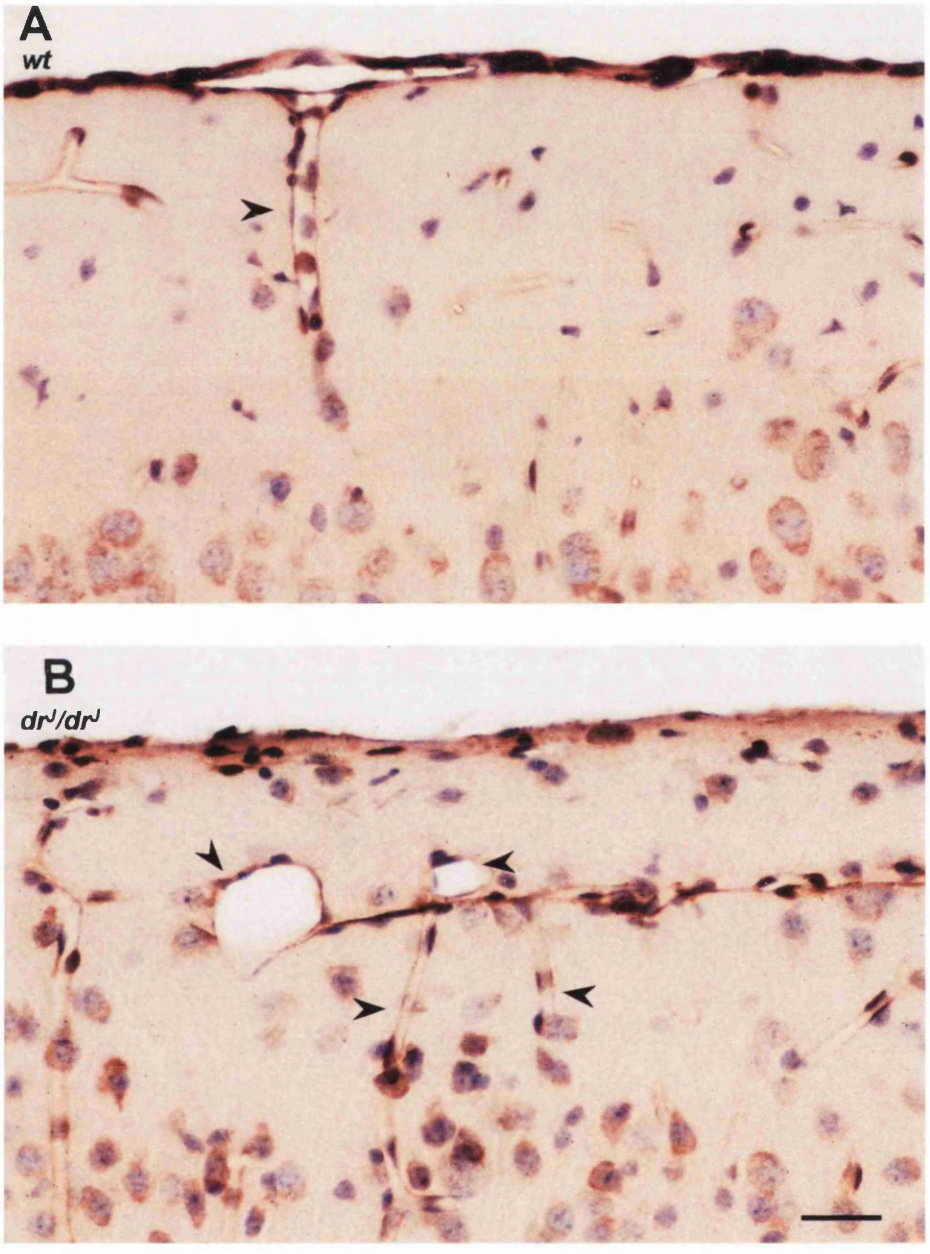

Basement membranes such as those of the *glia limitans* and blood vessels are labelled by anti-laminin antibodies.

(A) Notice normal perforating vessels originating from the pial surface in a wild type brain (arrowhead). Staining of the pial-glial interface is strong and continuous. **(B)** In the brain of homozygous mutants, vessels originate from the putative accessory or misplaced glial limiting membrane (arrowheads). Staining at the pial-glial interface is uneven and fainter than that seen in wild type brains. Scale bar represents 25 μm in both images.

Figure 6.8

Immunohistochemical characterisation of blood vessels in the neocortex of *dr*^{J} mice

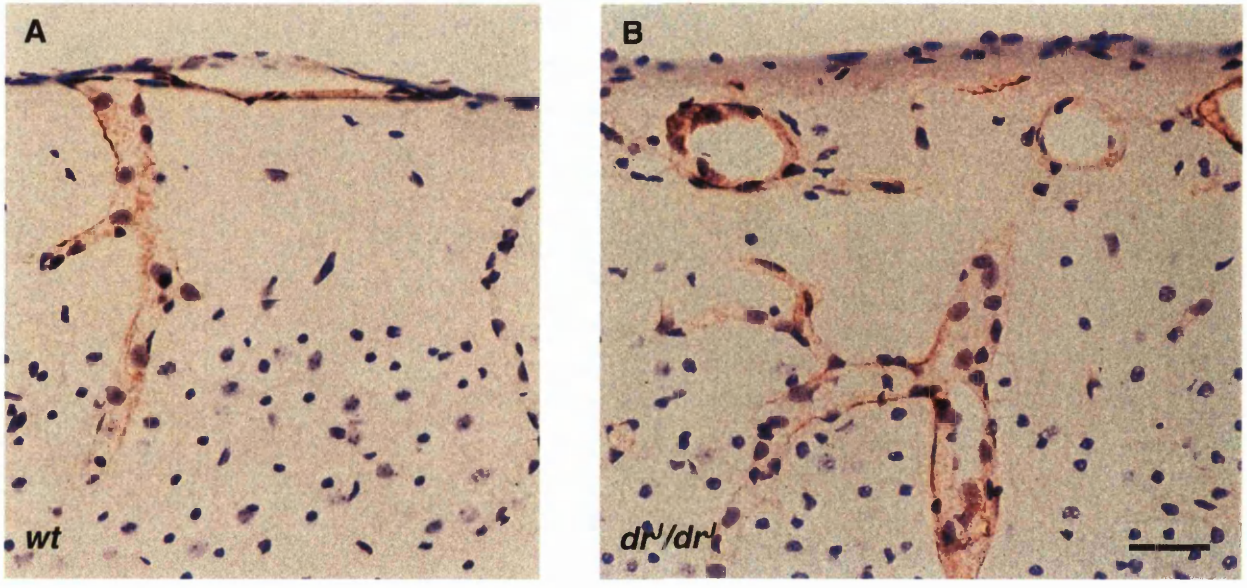

Anti-factor VIII (von Willebrand factor) immunostaining. Scale bar represents 30 μm.
(A) Perforating vessel penetrating the brain at an approximately right angle to the pial surface in the wild type mouse (P21). **(B)** View of a similar region in the brain of an age-matched homozygous mutant mouse. Vessels are situated within layer I, bearing no apparent relationship to the brain surface.

studied, because the perfusion technique used for fixation causes artifactual blood vessel dilatation.

6.3.2.4.2. Abnormal *glia limitans*

Linear structures, appearing as broken lines, usually arranged in a parallel fashion to the brain surface in the outer two thirds of layer I, were first seen on cresyl violet- or HE-stained sections from 11 dr^J/dr^J, but in none of 8 +/+ age-matched wild-type brains at P21. They were either isolated or continuous with vessel walls or with the external surface of the brain (i.e. with the normal localisation of the pial-glial interface), in which case they assumed a more oblique direction. These structures were unlabelled with anti-factor VIII antibodies, but they were highlighted with a reticular fibre impregnation technique (Figure 6.9) and with anti-laminin antibodies (Figure 6.7). They probably represent a broken, abnormally positioned glial limiting membrane. Reticular fibre staining also demonstrated a focally discontinuous pial-glial membrane at the surface of the brain (see Figure 6.9) in the affected cortical regions of dr^J/dr^J mice.

6.3.2.4.3. Relationship between discontinuities of the *glia limitans* and the position of heterotopic neurons

Although there was a close spatial relationship between the presence of abnormalities of the glia limitans and that of heterotopic layer I neurons, no direct correlation could be found between the position of breaks in the *glia limitans* and that of heterotopic neurons. Misplaced neurons could be seen both internal and external to the putative fragments of the *glia limitans* (e.g. Figure 6.7B), and heterotopic cells did not show a preference to concentrate in places

Figure 6.9

Reticular fibre staining of the neocortex in *dr*^{J} mice

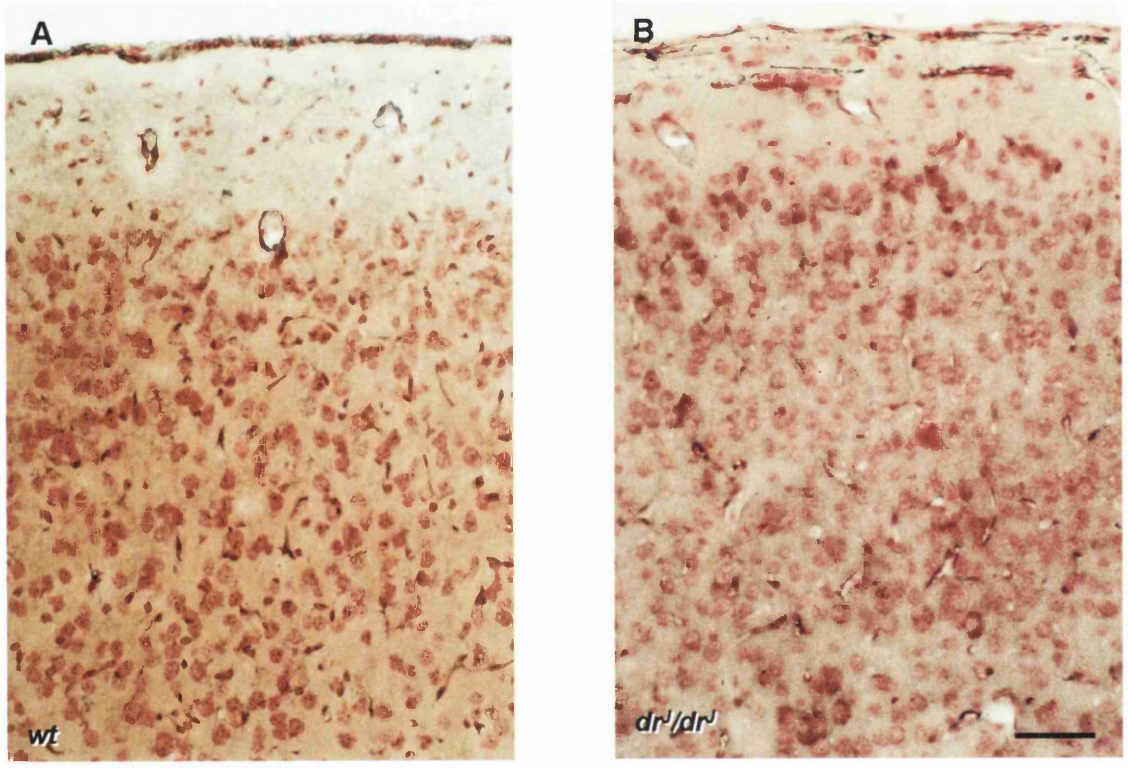

Gordon and Sweet silver impregnation for reticular fibres. Reticular fibres stain grey to black. Notice continuous, even staining of the pial-glial junction in the wild-type (A) and focally disrupted, discontinuous staining in the homozygous mutant (B). Scale bar represents 100 μm.

of apparent disruption of the pial-glial interface. Moreover, collections of heterotopic neurons were sometimes seen just beneath the pial surface of the brain, external to fragments of the remaining *glia limitans*, which itself overlaid a relatively well preserved molecular layer and coexisted with no major disruption of the underlying cortical architecture (Figure 6.5C). Regions of higher concentration of heterotopic cells nevertheless coincided with areas of more disturbed vascular organisation within layer I. The area occupied by heterotopic cells was always larger than the area containing abnormal vessels.

6.3.2.5. Astrocyte morphology and distribution in areas of abnormal *glia limitans*

The spatial distribution of astrocytes in the normal (*+/+*) and abnormal (dr^J/dr^J) layer I was studied with an immunohistochemical technique using anti-GFAP antibodies (Table 6.4). Coronal sections through frontal and parietal areas of the cerebral cortex (level B) were studied in the brains of 5 dr^J/dr^J and 5 +/+ mice of weaning age (i.e. P21). In sections from wild-type brains, astrocytes were in small numbers and usually associated with vessels or the pial surface at the *glia limitans* (Figure 6.10A). In regions containing heterotopias from the brains of dr^J mutants, GFAP-positive astrocytes seemed to be present in increased numbers (this was not specifically quantified) and delineated both the aberrant vascularisation of layer I and the abnormal, disrupted *glia limitans*, to which some of them were connected (Figure 6.10B and C). Astrocytes not overtly in contact with these structures showed either a fusiform or a stellate appearance with prominent processes. In normal-looking regions from dr^J/dr^J brains, astrocytes were indistinguishable in morphology and distribution from those of wild-type controls.

Figure 6.10

Immunohistochemical characterisation of glial cells in the neocortex of *dr*^{J} mice

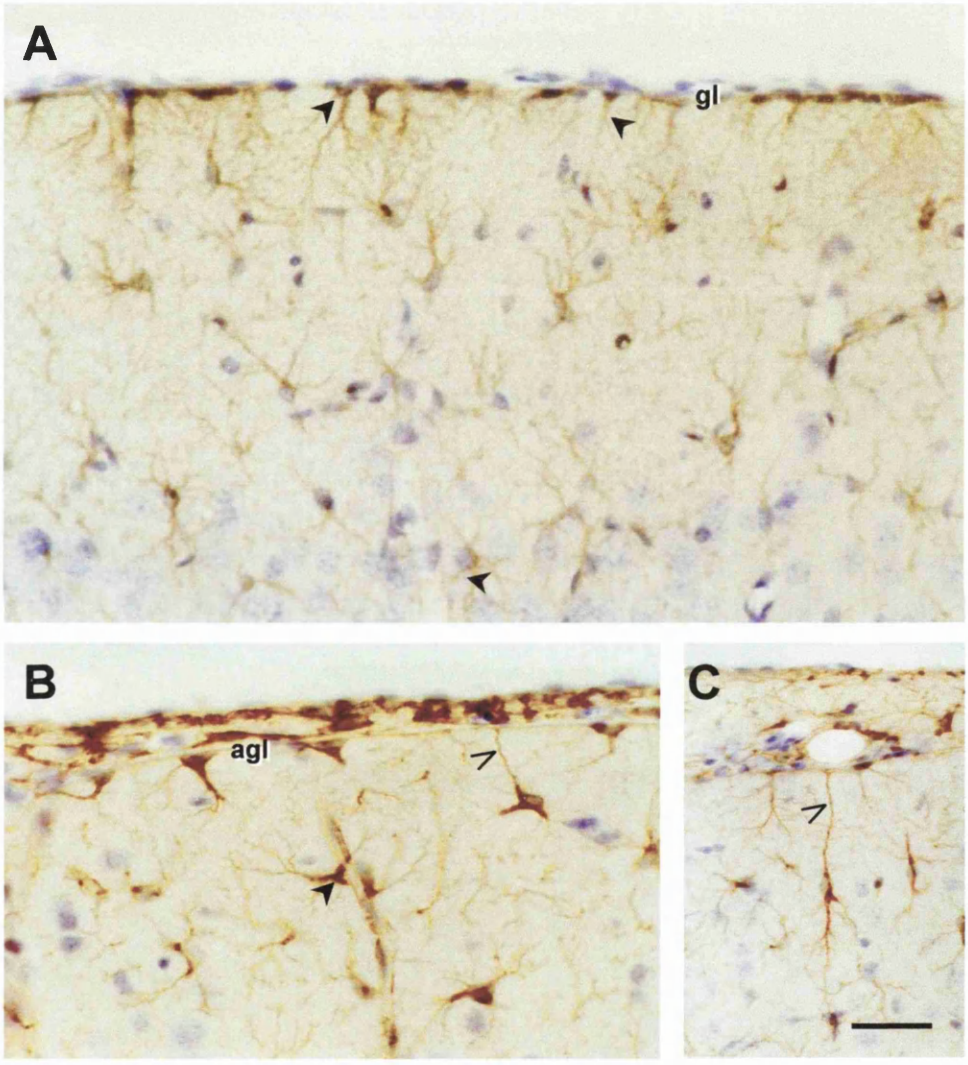

Anti-GFAP immunostaining Astrocytes are GFAP-positive.

(A) Wild-type mouse at P21. Astrocytes can be seen adhering to the inner surface of the glia limitans (gl) and to the walls of small blood vessels (arrowheads).
(B) and (C) In the homozygous *dr*^{J} mutant (also at P21), GFAP-positive cells maintain a similar relationship to the abnormal glia limitans (open arrows) and vessel walls (arrowhead).
Scale bar represents: (A): 60 μm. (B): 35 μm. (C): 25 μm.

6.3.2.6. Blurring of boundaries between cortical layers and intracortical free spaces

Blurring of boundaries between adjacent layers was obvious for layers I and II, but only in the areas containing heterotopias. The boundaries between adjacent layers IV to VI were usually easy to delineate, although they were not always as sharp as those of wild-type brains (Figure 6.4).

Neuron-free spaces in layer II, sometimes extending down to layer III were seen in 7 out of 8 dr^J/dr^J brains at P21. A deeper area devoid of cells, co-existing with splitting of upper layer II was seen in one case of a homozygous mutant neonate (see Fig. 6.11 C).

6.3.2.7. Other neocortical abnormalities seen in neonatal brains

The appearance of the external surface of the neocortex of neonatal drdr mice was sometimes that of thick leptomeninges (Figure 6.11B). Two other types of anomaly were seen in two from neonatal mutant brains, when these were compared with age-matched wild-type mice. These consisted of areas of increased density of upper layer II and loss of the radial alignment of neurons that is still noticeable at this age in wild type animals (compare Figure 6.11A with 6.11B).

6.3.3. Microscopic abnormalities in the hippocampus and cerebellum of dr^J/dr^J mice

The main purpose of the microscopic brain analysis was to investigate cerebral neocortical abnormalities in homozygous mutant dr^J mice. Brief descriptions of the hippocampal abnormalities and of the cerebellar defects are included below.

Figure 6.11

Appearance of the cerebral neocortex in neonatal *dr*^{J} mice

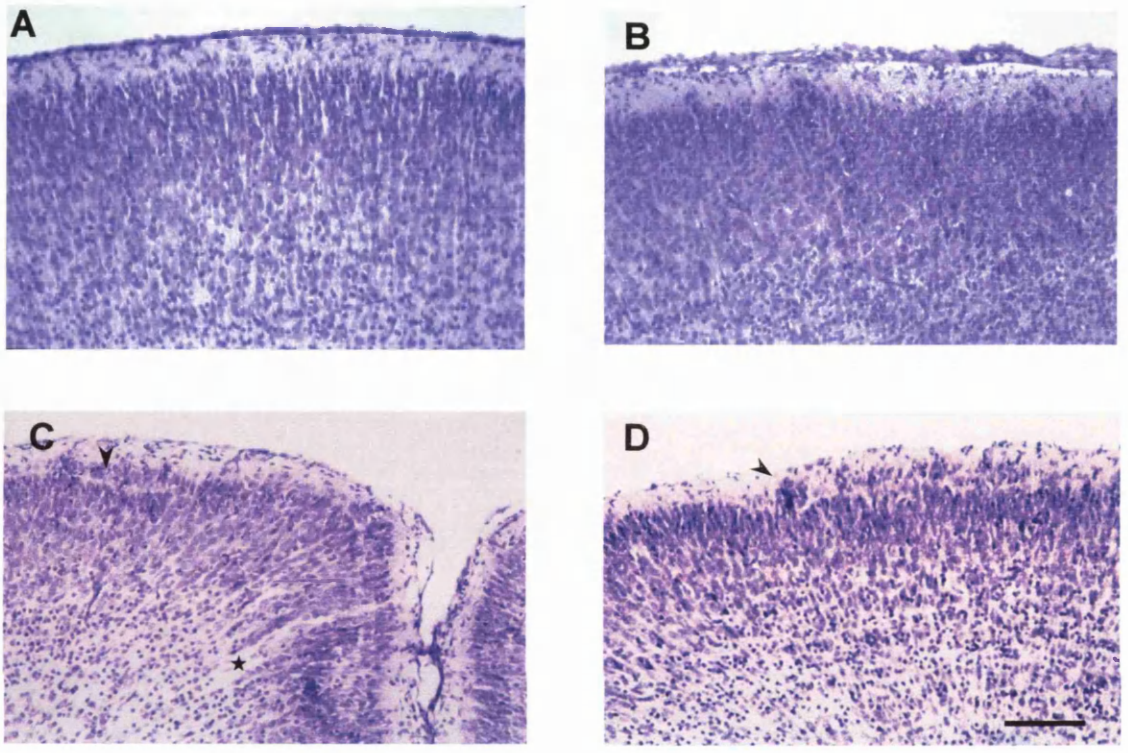

Coronal sections through the neocortex of newborn *dr*^{J} mice. (A) and (B): Hematoxylin and eosin staining. (C) and (D): Cresyl violet staining.

(A) Wild-type mouse. Notice smooth upper border of layer II, low cellularity of layer I, thin leptomeninges

(B) Homozygous mutant. There is thickening of the leptomeninges, as well as clusters of heterotopic cells in layer I, waviness of the upper border of layer II, and blurring of the normal radial alignment of cells in underlying layers.

(C) Higher magnification of another homozygous mutant *dr*^{J} brain. There is splitting of upper layer II (arrowhead) and neuron-free spaces in the layers underneath (star).

(D) A similar mutant brain, with a cluster of heterotopic cells in layer I (arrowhead).

Scale bar represents: (A) and (B): 90 μm. (C) and (D): 50 μm.

6.3.3.1. Hippocampal abnormalities in the brains of *dr*^{J}/*dr*^{J} mice

The hippocampus was examined on coronal sections taken at several (2 to 5) levels from 9 homozygous mutant and 8 wild type *dr*^{J} mice at P21. Abnormalities of the hippocampus were present in all of the mutant brains, in both the pyramidal layer and the dentate gyrus and comprised partial absence and/or dispersion of granule cells of the dentate gyrus, as well as dispersion of nerve cells of the pyramidal layer (Table 6.6 and Figure 6.12).

All mutant cases showed either unilateral (n=1) or bilateral (n=8) dispersion of neurons in the CA3 field of the hippocampus, with actual unilateral (n=5) or bilateral (n=3) splitting of that layer. In 4 cases, these abnormalities extended to fields CA2 and CA1. In 2 cases, lesions were bilateral but asymmetric (the most severely affected side being the right in one case and the left in two others). In some cases, there was more or less obvious undulation of the pyramidal stratum.

The main abnormalities found in the dentate gyrus of *dr*^{J}/*dr*^{J} mice at P21were mild granular cell dispersion in 2/9 cases, and a small, cap-like gyrus in 5/9 cases. In 9/9 cases, a disproportionately short infra-pyramidal limb was seen, which fused with the thalamus (2/9 cases) (Figure 6.12). In a single case, there was undulation of the dentate gyrus. No correlation was found between the severity of hippocampal abnormalities and the neocortical pathology in the same brain.

The hippocampus was also examined in coronal sections of brains from two *dr*^{J}/*dr*^{J} and four wild type neonates. Abnormalities of the dentate gyrus are quite

Table 6.6

Histological abnormalities found in the hippocampus of 9 homozygous mutant (*dr^J/dr^J*) mice at P21, compared to 8 age-matched wild-type controls

(A) Pyramidal cell layer

Histological abnormality	*dr^J/dr^J*	*+/+*
Dispersion of pyramidal neurons	9/9(L) 7/9(R)	0/8
Splitting of pyramidal cell layer (usually CA3/CA2)	5/9(L) 5/9(R)	0/8

(B) Dentate gyrus

Histological abnormality	*dr^J/dr^J*	*+/+*
Small, compact	7/9(L) 7/9(R)	0/8
Short infra-pyramidal limb	8/9(L) 7/9(R)	0/8

Hippocampal features were studied in cresyl violet-stained coronal sections through at least two antero-posterior levels (C and D) of the hippocampus. (L)-left hemisphere. (R)-right hemisphere.

Figure 6.12

Histological appearance of the hippocampus in wild-type and homozygous mutant *dr*^{J} mice

Upper row: cresyl violet-stained coronal sections through the hippocampus of a wild-type **(A)** and a homozygous mutant **(C)** mouse at P21. Notice the rudimentary dentate gyrus in the mutant (dg) and the normally formed supra- (spb) and infra-pyramidal blades (spb) of the dentate gyrus in the wild-type control. In some cases, there was lateral dispersion and splitting of the pyramidal cell layer (pcl), as well as fusion of the infrapyramidal blade with the thalamus **(B).**
CA1,2 and 3- pyramidal cell layer fields.

Lower row: anti-NeuN immunolabelling shows an overall smaller hippocampus in the mutant **(E)** when compared with the wild-type **(D)**. Note that the magnification is the same in both photographs. The dentate gyrus in the mutant is also compact and small. Scale bar represents: (A), (C), (D) and (E) 180 μm; (B) 90 μm.

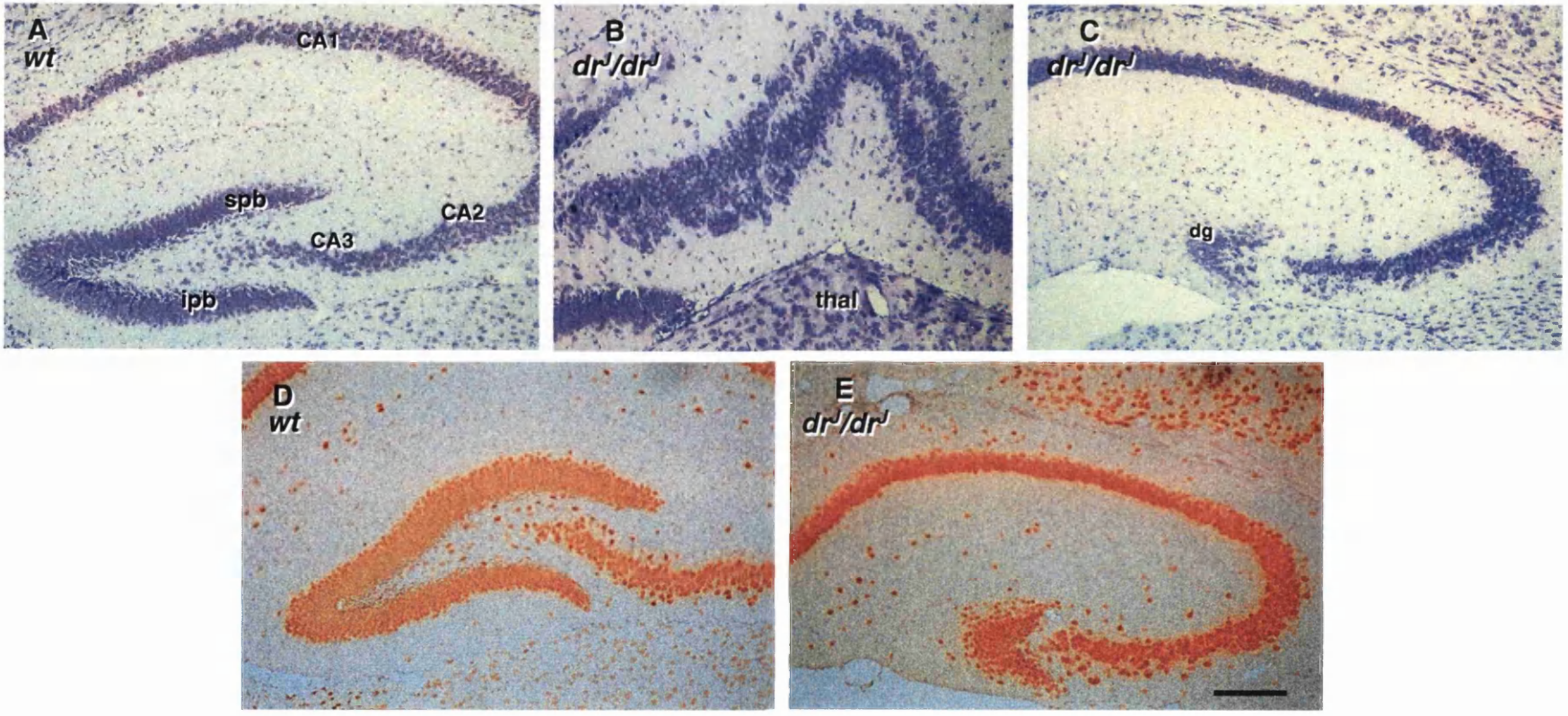
A
wt
CA1
spb
CA2
CA3
ipb
B
dr^J/dr^J
thal
C
dr^J/dr^J
dg
D
wt
E
dr^J/dr^J

difficult to assess at this age, since formation of this structure is still ongoing at birth. In the pyramidal layer, however, the same abnormalities that have been described for the weaning-age mice (P21) were also seen bilaterally in both cases that were examined. They were absent in the eight wild-type brains used as controls.

6.3.3.2. Cerebellar defects

Only a small number of cases were assessed for cerebellar abnormalities: Four neonatal mice (2 +/+ and 2 dr^J/dr^J) and one 6-week-old homozygous mutant were studied. Approximately half of dr^J/dr^J brains that were examined had a cerebellum of reduced size. Except for a smaller size, no significant differences were seen between neonatal wild-type and mutant brains. In contrast, the six week-old mutant cerebellum showed significant histological defects (Figure 6.13). Gross examination disclosed a small and poorly foliated cerebellum. Microscopically, the cerebellar hemispheres were normally stratified, but the vermis was very abnormal. It contained a region of heterotopia consisting of an admixture of all the different neuronal cell types (Figure 6.13).

There was no correlation, in individual mutant mice, between the severity of the cerebellar hypoplasia (as assessed macroscopically), the neuronal migration defect in the cerebral cortex and the presence or absence, or extent, of white hair coat patches.

Figure 6.13

Microscopic appearance of the cerebellum in a homozygous mutant *dr*^{J} mouse

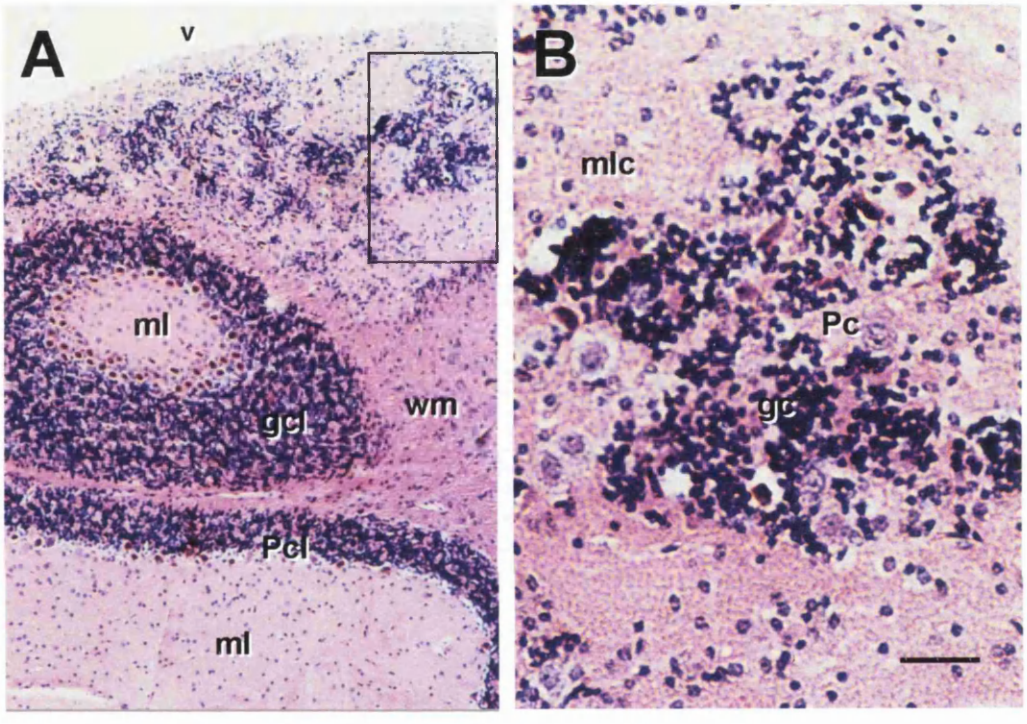

Coronal section through the vermis of a 6 week-old circling, white belly spotted male. Macroscopically, there was a small cerebellum.

(A) The molecular layer (ml), Purkinje cell layer (Pcl) and granule cell layer (gcl) are readily identifiable in the lower part of the figure, whereas in the upper area next to the fourth ventricle (v), the normal pattern of stratification is lost. wm-white matter.

(B) Detail of the insert in (A): the heterotopia contains cells belonging to the three cortical layers. Pc-Purkinje cells. gc-granule cells. mlc-molecular layer cells.

Scale bar represents: (A) 120 μm. (B) 30 μm.

6.4. Discussion

The results described in this Chapter confirm previous observations on brain abnormalities of *dr*^{J} mutants, while providing new evidence that may help to elucidate the pathogenesis of heterotopic layer I cells.

6.4.1. Macroscopic abnormalities of the brain

A small brain was a constant finding among *dr*^{J} mutants included in this study. Differences in brain weight between wild type and *dr*^{J}/*dr*^{J} littermates may be related to generally retarded growth or to the intrinsic abnormalities of the brain of homozygous mutants. A cerebellum of reduced size was obvious on gross inspection in half of the cases examined and probably accounts, in part, for the reduced brain weight in mutant homozygotes. Minor foliation defects were not systematically searched for and could have been present in an even higher proportion of abnormal cerebella among *dr*^{J}/*dr*^{J} brains. These observations are in general agreement with previous descriptions of variable cerebellar abnormalities in *dr* (Bierwolf, 1956), *dr*^{J} (Sekiguchi *et al.,* 1992), and *dr*^{sst} (Wahlsten *et al.,* 1983) homozygous mutants.

In the present series, distorted superior and inferior colliculi in the midbrain were seen in a few cases in which the cerebellum was severely affected macroscopically. Malformation of the quadrigeminal plate in the midbrain has been previously reported in *dr* (Bierwolf, 1956) and *dr*^{sst} (Wahlsten *et al.,* 1983) and may be a consequence of hydrocephalus. A midline parietal bleb has also been described in *dr*^{sst} and *dr*^{J} (Wahlsten *et al.,* 1983; Sweet and Wahlsten, 1983), but this defect was not observed in homozygous mutant *dr*^{J} mice in the

present study. Although the nature of such midline blebs is unclear from previous studies, their position and association with dilatation of the ventricular system suggest that they could represent cephaloceles (i.e. protrusions of brain tissue through a skull opening). The absence of head blebs and the lack of severe hydrocephaly among the *dr*^{J} mutant mice analysed in the present study could indicate that the *dr*^{J} mice in our colony exhibit a milder cerebral phenotype than that reported in previous published accounts.

6.4.2. Hydrocephalus and the pathogenesis of cerebellar abnormalities

Dilatation of the IV ventricle was reported in 4% (Falconer and Sierts-Roth, 1951) and 11% (Bierwolf, 1956) of mice in *dr* colonies, but its presence is not mentioned in published reports of other alleles. Examination of the IV ventricle was not performed systematically in the present study, although obvious enlargement of the IV ventricle was seen in half of the cases where a severely affected vermis was noted. In our series, only 1 of these cases had a marked dilatation of the whole ventricular system.

Bierwolf (1958; 1956) proposed that dilatation of the IV ventricle was likely to play a major role in the origin of the cerebellar abnormalities. The midline cerebellar structures (i.e. the vermis) form earlier than the lateral ones (cerebellar hemispheres) and, hence, development of the former is expected to be most severely disturbed (Bierwolf, 1958) because it coincides with the period when the first pathological features of hindbrain development are seen (this study (Bierwolf, 1956)). This may explain why in Bierwolf's series (1956) (and in the present study) the vermis was often severely affected (even absent)

whereas the cerebellar hemispheres were relatively well preserved. According to the same author (Bierwolf, 1956), hydrocephalic animals were often identified at birth by the shape of the skull, which remained abnormal into adulthood. Although it is possible that minor differences in the shape of the skull in newborn animals might have gone unnoticed in the mutants used for the present study, major skull defects were never noted in any of the many newborn litters that were examined. Moreover, older animals had no obvious head anomalies. This difference in prevalence of hydrocephaly may be explained on the basis of the different alleles used (Bierwolf studied *dr*, in contrast to the present study on dr^J) and/or differences in genetic background (non-inbred *dr* versus inbred dr^J mice). Alternatively, this discrepancy may result from pre-natal or early post-natal loss of the most severely affected (i.e. severely hydrocephalic) mice, before their external identification was possible. In this regard, it is interesting to note that there were significant prenatal and pre-weaning mortality among dr^J/dr^J mice in the present study (Chapter 5).

6.4.3. Comparison of the dr^J mutant phenotype with previous reports on *dreher* alleles and other animal models

6.4.3.1. Comparison with previous reports on *dreher* alleles

Excessive numbers of cells in layer I of the neocortex have been reported previously in dr^J, although no immunocytochemical techniques have been used to confirm their presumed neuronal nature. Anti-NeuN labelling clearly demonstrated the heterotopic cells to be neuronal. Although it remains possible that glial cells (e.g. astrocytic) comprise a minor proportion of the cells contributing to the increased cellularity of layer I, this non-neuronal population must be a small minority of the heterotopic cells.

Small intra-cortical areas devoid of any cellular elements were found in almost all of the dr^J/dr^J brains studied. Their localisation was restricted to layers II and/or III of the frontal or parietal cortex. Their presence was not necessarily topographically related to heterotopic clusters of neurons in the overlying molecular layer and did not coexist with a significant disorganisation of the underlying layers, in contrast to the report of Sekiguchi, et al (1994) for the same allele. Regions of low cellularity and cell-free areas may result from abnormalities of neuronal migration or to excessive localised apoptosis. These hypotheses were, however, not tested.

The present observation of an abnormal glial limiting membrane associated with a network of abnormally arranged vessels in layer I of the neocortex has not been described before in dr^J or any other *dreher* mutant allele. That these abnormalities are not artifactual but rather a consequence of the mutation itself is supported by the fact that they were seen in all the dr^J/dr^J brains examined but in none of the wild-type ones. Moreover, layer I heterotopias were only present in areas with an abnormal *glia limitans*.

6.4.3.2. Comparison with other animal models - heterotopias and the role of the *glia limitans*

Heterotopic collections of cells in neocortical layer I have been reported in many genetic and non-genetic animal models (see Tables 6.7.and 6.8). In some

Table 6.7

Non-genetic (toxic and traumatic) animal models primarily associated with heterotopias in layer I of the cerebral cortex

Type of experiment/ animal	Increased cell density in layer I or MZ	Abnormal GL	Lamination defect	Abnormally oriented neurons	Lepto-meningeal heterotopias	Abnormal RGF	Other cortical defects	Ref.
Puncture wounds of cortical surface (newborn rats/mice)	+	+	+	+	+	+	Cell-free areas, abnormal layering below heterotopias	1
Cryogenic lesions of brain (newborn rats)	+	+	+	+	+	+	Polymicrogyria, neuronal loss (layers IV-VI), increased no. pial vessels	2
Ablation of meninges with 6-OHDA (newborn mice)	+	+	+	NR	NR	NR	Loss of Cajal-Retzius cells	3
Intra-ventricular administration of NT-4 (rat embryos)	+	-	NR	NR	-	NR	NR	4
Low-dose ibotenate (newborn hamsters)	+	NR	+	+	NR	-	Intracortical heterotopias	5
In utero exposure to cocaine (mice)	+	NR	+	+	NR	+	Loss of radial alignment of neurons. Dispersion of E14-born neurons through layers I-VI	6

References (Ref.): 1- Rosen, *et al.*,1992. 2 – Humphreys, *et al.*, 1991; Suzuki and Choi, 1991. 3- Supèr, *et al.*, 1997. 4- Brunstrom, *et al.*, 1997. 5- Marret, *et al.*, 1996; Gressens, *et al.*, 1996. 6-Gressens, *et al.*, 1992

GL: glia limitans. **RGF**: radial glial fibres. **MZ**: marginal zone. **NR**: not reported. **+**: present. **-**:absent. **6-OHDA**: 6-Hydroxydopamine. **NT-4**: neurotrophin-4

Table 6.8

Genetic mouse models associated with heterotopias in layer I of the cerebral cortex

Mutant / K.O.	Increased cell density in MZ or layer I	Abnormal GL	Lamination defect	Abnormally oriented neurons	Leptomeningeal heterotopias	Abnormal RGF	Other neocortical defects	Ref.
cdk5-deficient (K.O.)	+	NR	+	+	NR	NR	NR	1
CPP32-deficient (K.O.)	+	NR	+	NR	NR	NR	Low no. of pyknotic cell clusters in the fetal brain	2
sey (small eye)	+	+	+	+	+	NR	Low no. cells in CP and IZ. Intracortical heterotopias	3
MARCKS-deficient (K.O.)	+	+	NR	NR	+	-	NR	4
rl (reeler)	+	NR	+	+	NR	NR	Intracortical fibre bundles	5
scm (scrambler), yot (yotari)	+	NR	+	NR	NR	NR	Intracortical fibre bundles	6
Immune-deficient strains (NZB, BXSB, Snell dwarf)	+ (focal)	+	+ (focal)	+	+	+	Neuron-free areas , rippling of layers II-VI	7
dr^{J} (dreher^{J})	+	+	Absent or minor	+ This study	+	NR	Cell-free areas in layers II-VI. Rippling of layer II	8

References (Ref.): 1- Ohshima, *et al.*, 1996; Gilmore, *et al.*, 1998. 2- Kuida, *et al.*, 1996. 3- Schmahl, 1993. 4- Blackshear, *et al.*, 1997. 5- Caviness, 1982; Goffinet, 1979. 6- Sheldon, *et al.*, 1997; Howell, *et al.*, 1997. 7- Sherman, *et al.*, 1985, 1990, 1992. 8-This study; Sekiguchi, *et al.*, 1994

GL: glia limitans. **RGF**: radial glial fibres. **MZ**: marginal zone. **K.O.**: knock-out. **NR**: not reported. **+**: present. **-**:absent

cases, the presence of misplaced layer I neurons coexists and seem to be causally related with abnormalities of the pial-glial interface. Such is the case with cold lesions, puncture wounds and chemical injuries to the surface of the brain, which produce destruction of the leptomeninges and disappearance of the *glia limitans*. In these cases, pathological findings are often restricted to the cortex underlying the area of leptomeningeal injury.

6.4.3.2.1. Non-genetic animal models

The importance of an intact external glial limiting membrane or *glia limitans* for the normal development of the brain has been shown previously. For instance, heterotopic collections of neurons can be seen in the brain of newborn mice that have been subject to minute puncture wounds (Rosen *et al.,* 1992) or chemical lesions (Supèr *et al.,* 1997a) of the leptomeninges that disrupt the *glia limitans* before the end of the period of neuronal migration. Meningeal cells have also been shown to play a critical role in neurogenesis and cytoarchitectural organisation of the normally stratified cerebellum (Hartmann *et al.,* 1992). Selective destruction of meningeal cells over the medial surface of the cerebral hemispheres of newborn hamsters with 6-hydroxydopamine (6-OHDA) prevents the normal formation of the infra-pyramidal blade of the dentate gyrus (Hartmann *et al.,* 1992). The ensuing meningeal cell loss is associated with thinning and rupturing of the underlying basement membrane, hence with the disappearance of the *glia limitans*, over the medial cerebral hemispheres and the thalamus. A rudimentary form of the infra-pyramidal blade is seen only in those areas where both a new meningeal layer and a new glial limiting membrane, have reappeared after the lesion occurred. In the areas where the destruction was irreversible, a fusion between the anlage of the dentate gyrus

and the adjacent diencephalon could be seen and the infra-pyramidal blade was missing (Hartmann *et al.,* 1992). These changes can only be produced at a time when the anlage of the supra-pyramidal blade already existed, but the anlage of the infra-pyramidal blade had not formed yet.

The features described above closely resemble some of the abnormalities seen in dr^J mutants, namely the rudimentary dentate gyrus and the fusion of its infra-pyramidal blade with the adjacent thalamus (Figure 6.12). The data presented here also suggest that both the abnormalities of the neocortex and those of the hippocampus seen in dr^J/dr^J mice could both result from an abnormality of the glial limiting membrane. Along with other studies on the importance of the leptomeninges for the normal neurogenesis and stratification of the cerebellum (Sievers *et al.,* 1994; Pehlemann *et al.,* 1985), the present findings further support the role of mesenchymal- epithelial interactions (i.e. between meningeal cells and the underlying brain parenchyma) for the normal development of the brain.

Further insight into the possible mechanisms of disordered cortical development following lesions of the cortical surface has been brought about by Supèr and colleagues, who studied degeneration and regeneration of Cajal-Retzius (CR) cells (1997a; 1997b). 6-OHDA was applied to the neocortical surface of newborn mice, resulting in the loss of not only meningeal cells, but also CR cells of layer I, leaving other cortical neurons unaffected (Supèr *et al.,* 1997a). This resulted in subtle abnormalities of neocortical layering, namely in the blurring of boundaries between layers II-III and IV of the parietal cortex, as well as

an increased cell density in layers V and VI. Because both the loss of meningeal cells and that of Cajal-Retzius cells could be blocked by normetanephrine, the authors suggest that the latter may be dependent upon the trophic influence of meningeal cells for their survival, and that their loss may contribute to the abnormal architecture of the cerebral neocortex of 6-OHDA-lesioned mice (Supèr *et al.,* 1997a).

It remains to be elucidated whether the *glia limitans* of mutant *dr*^{J} mice fails to develop properly or forms normally and is damaged during the late period of neurogenesis. Neither is it known whether proteolysis is a key factor in the genesis of an abnormal *glia limitans* in these mutants. No special immunolabelling techniques were used to highlight CR cells, therefore no counts were made that would allow us to detect possible CR cell loss in *dr*^{J} mutants when compared to wild type controls. Such counts might also be hindered by the fact that, at the age the brains were studied (P21), compensatory changes resulting from CR cell loss might have occurred. A second study by Supèr and colleagues (1997b) showed that following a freezing injury of the cerebral cortex of newborn mice, CR cells are capable of repopulating layer I. They may be seen at P12 in layer I of the lesioned brains, but not in age-matched controls. It may be possible that these cells migrate from intact areas surrounding the lesioned area (Supèr *et al.,* 1997b).

6.4.3.2.2. Genetic models

There are also several genetic animal models in which heterotopic layer I cells are a prominent feature and coexist with disruption of the *glia limitans*. Such heterotopias have been described in the brains of immune-deficient strains of

mice, such as the New Zealand Black (NZB), BXSB, and Snell dwarf mice (Sherman *et al.,* 1990a), and they closely resemble those seen in dyslexic humans (Sherman *et al.,* 1985). They are usually associated with neuron-free spaces in the layers below the heterotopia, and, unlike dr^J, may be associated with a focally disrupted cortical architecture. Discrete defects of the *glia limitans* coexist with misplaced neurons in NZB mice (Sherman *et al.,* 1992), but no abnormal arrangement of vessels was described in this or other strains of auto-immune mice. Moreover, disruptions of the *glia limitans* in NZB mice show a preference for the left somato-sensory cortex and the heterotopias are usually single large collections of neurons that protrude into the leptomeningeal space. In contrast, the heterotopias seen in dr^J mutants consist of bilateral, multiple small clusters or diffusely distributed neurons. While no studies of the immune system have been conducted in *dreher* alleles, their phenotype does not suggest the presence of immune dysfunction.

The MARCKS-deficient mouse is another genetic mouse model in which disruption of the *glia limitans* is thought to be responsible for abnormal neuronal migration. MARCKS is a substrate for protein kinase C. Pathological findings in the brain of MARCKS-deficient mice include a severe phenotype of exencephaly, agenesis of brain commissures and defective cortical lamination. Widespread heterotopia in the leptomeninges, protruding through defects in the *glia limitans* have been described in homozygous mutant embryos. Clusters of migratory neuroblasts appear to exit the brain parenchyma through breaks in the basal lamina (Blackshear *et al.,* 1997). The authors postulate that this gene mutation acts through decreased expression or increased proteolysis of basal lamina proteins and chondroitin sulphate proteoglycans in the marginal zone. It

is difficult to establish a comparison between MARCKS-deficient mice and *dr*^{J} mutants, because the former die *in utero* and have a very severe phenotype, whereas the latter have a milder phenotype that is compatible with a normal postnatal lifespan. Moreover, the pre-natal development of *dr*^{J} brains has not been studied. Agenesis of the brain commissures has not been reported in any of the *dreher* alleles, although a thin *corpus callosum* was described in homozygous mutant *dr*^{sst} mice (Wahlsten *et al.,* 1983).

6.4.4. Comparison with some human pathological conditions

As an isolated or main neuropathological finding, heterotopic collections of neurons in the molecular layer have been described in the frontal cortex of patients with primary generalised epilepsy (Meencke and Janz, 1984; Meencke, 1998), and are a constant finding in the cerebral cortex of individuals with developmental dyslexia (Humphreys *et al.,* 1990; Galaburda *et al.,* 1985; Galaburda, 1993) (see Table 6.9). They can also be found as a feature of a much more severe condition with multisystem involvement such as certain syndromes associated with muscular dystrophy (Williams *et al.,* 1984; Miller *et al.,* 1991; Nagato *et al.,* 1996; Takada *et al.,* 1987).

In primary generalised epilepsy, an increased neuronal density in layer I of the frontal cortex may be associated with abnormally oriented neurons, increased numbers of nerve cells in the white matter and the persistence of a columnar arrangement of cortical neurons (Meencke and Janz, 1984). The absence of overt seizures in *dr*^{J}/*dr*^{J}, their cerebellar and ear developmental abnormalities

Table 6.9

Human pathological conditions primarily associated with heterotopias in layer I of the cerebral cortex

Pathological condition	Increased cell density in layer I	Abnormal *glia limitans*	Lamination defect	Abnormally oriented neurons	Lepto-meningeal heterotopias	Abnormal radial glia	Other neocortical defects	Ref.[s]
Primary generalised epilepsy	+	NR	-	+	NR	NR	Persistence of columnar arrangement of neurones. Increased numbers of neurones in white matter	1
Developmental dyslexia	+ (mostly left inferior frontal)	+ (focally)	+	+/-	NR	NR	Blurring of boundary between adjacent layers. Intra-cortical scars in females	2

References (Ref.): 1 - Meencke and Janz, 1983, 1984; Meencke and Veith, 1992;. Meencke, 1998. **2** - Galaburda, et al., 1985; Galaburda, 1993; Humphreys, et al., 1990

NR: not reported. **+**: present. **-**:absent.

and the fact that neuropathological changes in the neocortex of epileptic patients have not been associated with an abnormal *glia limitans,* all make it unlikely that pathological changes secondary to epilepsy play a major role in the formation of layer I heterotopias in *dr*^{J} mice.

In developmental dyslexia, a condition which is more common in males, numerous clusters of neurons are seen in layer I, mostly in the inferior frontal and superior temporal gyri, and these are usually more prominent in the left cerebral hemisphere (Galaburda *et al.,* 1985). A varying degree of abnormal cortical architecture may be seen, ranging from blurring of the boundaries between adjacent layers to focal microgyria (Galaburda *et al.,* 1985; Galaburda, 1993). Defects of the *glia limitans* are often found at the edges of the microgyric cortex, and these are associated with displacement of layer II neurons into the molecular layer (Galaburda, 1993). Macroscopically, symmetrical *planum temporale* (i.e. a region of the neocortex, situated at the posterior end of the superior temporal gyrus on each of the cerebral hemispheres, functionally related to language)(Galaburda *et al.,* 1993; Galaburda, 1999) are seen in every case (Galaburda *et al.,* 1999). In females, the presence of intracortical, myelinated or non-myelinated, scars predominates over the heterotopic clusters (Humphreys *et al.,* 1990). This discrepancy between findings in male and female dyslexics has been attributed to the faster maturation of the female cortex.

Fukuyama congenital muscular dystrophy (FCMD), Walker-Warburg syndrome and muscle-eye brain disease are human disorders associating muscular dystrophy with ocular dysgenesis and lissencephaly, a severe neuronal

migration defect of the CNS. Microscopically, one of the features is glio-neuronal heterotopia in the leptomeninges (Williams *et al.,* 1984; Miller *et al.,* 1991; Nagato *et al.,* 1996; Takada *et al.,* 1987). Breaches in the *glia limitans*, which could be a primary or secondary event, have been considered a central event in the pathogenesis of leptomeningeal heterotopia in FCMD (Saito *et al.,* 1999; Nakano *et al.,* 1996; Takada *et al.,* 1987), allowing for migration of neurons and glial cells and inducing glio-mesenchymal proliferation (increased numbers of reactive astrocytes and vessels). Although much more severe than the changes seen in *dr*^{J} mutants, the pathological features seen in these muscular dystrophies (breaches in the *glia limitans*, prominent astrocytes and increased numbers of vessels) are qualitatively similar to those described in the present study. Cerebellar hypoplasia, such as seen in *dr*^{J} is also a common feature of FCMD and the Walker-Warburg syndrome (Leyten *et al.,* 1991). Diagnostic criteria for both these conditions require the presence of muscular dystrophy, of which there have been no reports in any of the *dreher* mutants.

The expression in the skeletal muscle of several genes coding for adhesion molecules has been found to be defective in patients with congenital muscular dystrophies, namely of laminin β2 in the Walker-Warburg syndrome and of laminin α2 in FCMD (Cohn *et al.,* 1997; Wewer *et al.,* 1995). Laminins are a family of glycoproteins found in basement membranes, including that of the external glial limiting membrane (Cohn *et al.,* 1997; Choi, 1994). They are also one of the components of the extracellular matrix that interacts with other glycoproteins at the muscle cell surface. These, in turn, are connected to the intracellular cytoskeleton (Brown, 1996). Although the muscles and eyes have not been examined histologically in homozygous mutant *dr*^{J} mice, no apparent

anomalies of muscle function or visual function were detected. Moreover, no anomalies of balance or hearing have been described in either FCMD or Walker-Warburg syndrome that would suggest a disturbed embryological development of the otic vesicles in either of these two conditions. The histopathological similarities between the brain phenotype of *dr*^{J} mouse mutants and that of FCMD and Walker-Warburg syndrome patients suggest that the genetic pathway involved in the production of cerebral abnormalities in *dr*^{J} mutant mice may involve genes coding for basement membrane or extra-cellular matrix molecules playing a role in cell adhesion.

The cerebellar abnormalities seen in *dreher* mutants have been considered by Bierwolf (1956) and Sekiguchi (1996) to closely resemble the human malformation Dandy-Walker syndrome (Benda, 1954), which includes a cystic enlargement of the fourth ventricle and the posterior fossa, associated with an agenesis or hypoplasia of the vermis. Atresia of the cerebellar foramina may or may not be present. Symptomatic hydrocephalus is a feature of the syndrome, as well as ataxia, nystagmus and apneic spells. A meningocele may be present, but is usually occipital (Bindal *et al.,* 1991). Parietal cephaloceles (i.e. with the same location as the head bleb seen in *dreher* mutants) have been described in association with Dandy-Walker syndrome, but are an extremely rare finding (Curnes and Oakes, 1988). Granule cell aggregates may be seen in the cerebellar white matter, and the normal cortical lamination may be disrupted (Taggart and Walker, 1942), as is the case with several *dreher* alleles. Nevertheless, the other central pathological features of *dreher* brains (neocortical heterotopias and inner ear defects) have so far not been reported in cases of Dandy-Walker syndrome. This syndrome may be associated with other

malformations of the CNS and may also be caused by teratogenic drugs such as warfarin (Kaplan, 1985). No single gene causing Dandy-Walker syndrome has so far been identified.

6.4.5. Conclusion

Taken together, the newly described abnormality of the glia limiting membrane suggest that this may be a crucial event in the cascade of events leading to the accumulation of heterotopic neurons in layer I of *dr^{J}/dr^{J}* brains (see proposed model in Figure 6.14), and that changes in extracellular matrix- or basement membrane-associated molecules could be implicated directly or indirectly in the genesis of this defect. In the presence of a focally disrupted *glia limitans*, a subset of migrating neurons could be displaced into layer I and the leptomeningeal space.

There are, however, other possible mechanisms of production of layer I heterotopias: excessive production of early generated neurons destined to reside in layer I or alternatively a failure of the normal programmed cell death that occurs in late gestation and early post-natal period which dramatically reduces the number of these early generated cells. In the *CPP-32* knock-out mouse, for example, there is a defect in apoptosis, which causes excessive numbers of neurons to escape physiological death during development (Kuida *et al.,* 1996). An increased number of neurons thus persist in layer I of the cerebral cortex of *CPP-32* mutant mice. The timing of production of the heterotopic cells in *dr^{J}/dr^{J}* brains could provide clues as to their origin. Are they generated throughout the whole period of neurogenesis? Are they mostly or exclusively born in the earliest stages of neocortical histogenesis, i.e. are they destined for the marginal zone? The fact that many of the misplaced cells have a similar morphology to the pyramidal neurons of layers II and III, and that deeper neocortical layers seem to be at least relatively unaffected, could

Figure 6.14

Proposed model for the formation of heterotopias in the neocortex of *dr*^{J} mutant mice

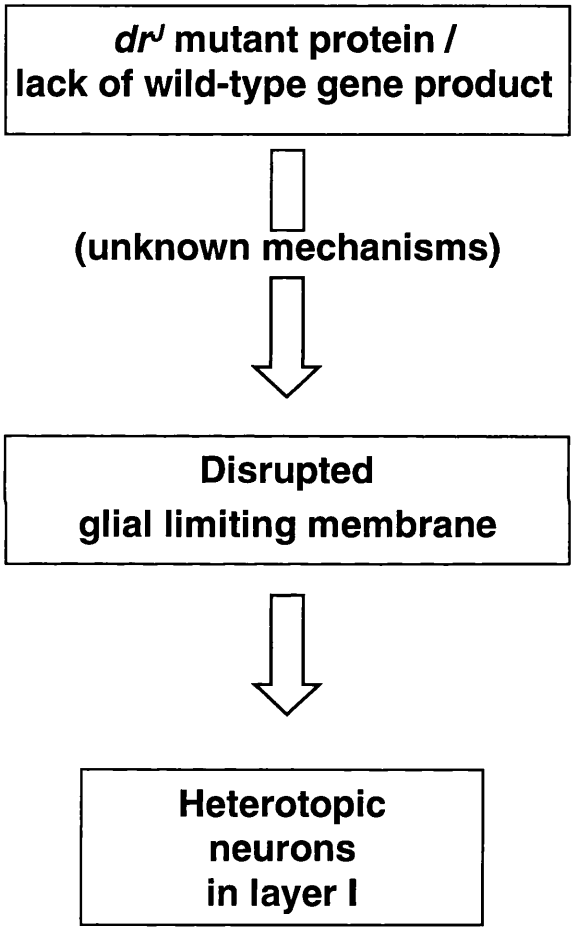

A model for the production of heterotopias in the neocortex of *dr*^{J} mutants: It is proposed that the *dr*^{J} gene defect causes a primary or secondary defect of the *glia limitans,* resulting in the excessive migration of neurons into the cell-poor layer I.

indicate that the mutation influences exclusively or solely the later stages of migration. Pyramidal cells of the CA3 field of the hippocampus are the latest in that stratum to finish their migration (Angevine, 1965) and they are also the most severely and frequently affected in *dr*^{J} mutants. The dentate gyrus was also affected in all *dr*^{J}/*dr*^{J} brains studied. The onset of neurogenesis in this structure coincides with that of CA 3 pyramidal cells and is not concluded until after birth (Stanfield and Cowan, 1979; Angevine, 1965). However, if present from the stage of early corticogenesis, a defective *glia limitans* could disturb the whole period of neuronal migration.

In order to test these ideas concerning the timing of generation of heterotopic neurons directly, BrdU-labelling studies have been performed, as described in the next chapter. These experiments aim at birthdating the heterotopic cells (i.e. determining the date of their last post-mitotic cycle) which may help to elucidate the pathogenesis of heterotopias in *dr*^{J}/*dr*^{J} brains.

Chapter 7

Developmental studies of neocortical abnormalities in *dr*^{J} mutant mice

7.1. Introduction

7.1.1. General background

Heterotopic neurons in layer I of the cerebral neocortex have been described previously in *dr*^{J} mutants (Sekiguchi *et al.,* 1987; Sekiguchi *et al.,* 1994), and they are a consistent feature of the brains of *dr*^{J}/*dr*^{J} mice that were used for the present study. However, no experimental studies of the mechanisms underlying their genesis have been reported to date. The purpose of this Chapter is to address the issue of how heterotopic neurons are produced in *dr*^{J} mutant brains.

7.1.2. Hypotheses to explain layer I heterotopias in *dr*^{J} mutant brains

Excessive numbers of neurons in layer I of the cerebral cortex may be the result of defects in neuronal migration or reflect an imbalance between cell proliferation and cell death during corticogenesis. These two general mechanisms are not mutually exclusive, and could be acting together to produce the final abnormality.

7.1.2.1. Defects of neuronal migration

A primary defect of radial glial cells could be responsible for the overmigration of those neurons destined to settle in deeper *strata* of the cerebral cortex, so that they ultimately settle in the normally cell-poor molecular layer. Sekiguchi and colleagues (1987) suggested that the *dr*^{J} mutation was responsible for small focal disruptions of neuronal

migration and proposed that these could be related to focal disruption of radial glial fibres (Sekiguchi *et al.,* 1994). Their hypothesis was based on the similarity between the microscopical appearance of heterotopic neurons in newborn rats and mice subjected to puncture wounds of the brain surface (Rosen *et al.,* 1992) and those of *dr*^{J} mutants (Sekiguchi *et al.,* 1994). However, no further investigations were conducted in order to demonstrate the nature of this putative radial glia abnormality.

Abnormalities of the glia limiting membrane appear to play a causative role in the severe neuronal migration defect of the MARCKS mutant mouse (Blackshear *et al.,* 1997) (see also Chapter 6-Discussion). A defective *glia limitans* (such as that seen in *dr*^{J} mutants) could result from a primary defect of the cells that are responsible for its formation (i.e. meningeal and glial cells), or from a secondary insult from an extrinsic origin (e.g. increased proteolysis of the basement membrane). Meningeal cells contribute to the formation of both the interstitial matrix and basement membrane at the pial-glial boundary, and they have the ability to induce the formation of radial glial endfeet of the *glia limitans* (Sievers *et al.,* 1994b). Loss of this trophic influence could result in disruption of the *glia limitans*. In vitro studies using co-cultures of glial and meningeal cells have also stressed not only the growth-promoting effects of meningeal cells on glia, but also the growth-inhibiting effects of glial cells on meningeal cells (Struckhoff, 1995). An abnormal increase of this inhibition secondary to a defect intrinsic to radial glial cells could also prevent the normal formation of the *glia limitans*.

Heterotopic layer I neurons could result from neuron-intrinsic defects. These may, for example, interfere secondarily with the binding of neurons to radial glial cells. Astrotactin, a cell-surface molecule expressed by neurons undergoing glial-guided neuronal migration is one of the molecules involved in this binding. It has been shown that cerebellar granule neuron binding to glial cells and their migration along radial glial fibres may be severely disturbed by anti-*astrotactin* antibodies in an *in vitro* system (Stitt and Hatten, 1990).

Genetically determined abnormalities of the extracellular matrix may disturb neuronal migration (see Chapter 1). For instance, increased adhesivity of migrating neurons caused by mutations in *reelin*, a gene coding for a secreted protein produced by Cajal-Retzius (CR) cells, has been suggested as the mechanism by which neocortical histogenesis in the *reeler* mutant mouse becomes severely distorted (Hoffarth *et al.,* 1995).

Other secreted molecules may be involved in the process of normal migration: Cajal-Retzius cells are known to be able to alter the phenotype of glial cells (Soriano *et al.,* 1997). *In vitro* experiments using explants of embryonic CR cells co-cultured with adult cerebellar tissue induce the transformation of Bergmann glia cells into cells with radial glial phenotype. The effect is produced by a diffusible factor, distinct from Reelin, since Cajal-Retzius cells isolated from the cortex of *reeler* mutants show similar effects when co-cultured with adult cerebellar tissue. Embryonic CR cells are also capable of changing the direction of granule cell migration in the same culture system. Other as yet unidentified

molecules such as these may also affect neuronal migration and generate misplaced neurons.

7.1.2.2. Disturbed balance between proliferation and cell death

Heterotopic cells in dr^J/dr^J mice could be early migrating neurons (pre-plate neurons) destined to become layer I cells that fail to undergo programmed cell death. The majority of the earliest born neurons that settle in the marginal zone are fated to die (Wood *et al.,* 1992; Price *et al.,* 1997) during the late fetal stages or the early post-natal period. If they fail to do so, they may contribute to an excessive cell density of the molecular layer (i.e. layer I) in the adult brain. Alternatively, if excessive numbers of neurons destined to the marginal zone are produced, this may also result in their accumulation in layer I of the adult animal. Overproduction of neurons is the mechanism that has been put forward to explain the collections of neurons in the marginal zone of the cerebral cortex of rat embryos, after the injection of neurotrophin-4 into their lateral ventricles (Sheppard and Pearlman, 1997).

During cerebral development of the rat, a subset of the cells originating from the lateral ganglionic eminence first migrate to the surface of the telencephalic vesicle and subsequently move tangentially into the preplate of the neocortex, to settle as Cajal-Retzius cells (De Carlos *et al.,* 1996). This population of neurons does not use radial glia as a scaffold for migration (hence the name "glia-independent neuronal migration"). Excessive production or decreased cell death of these

tangentially-migrating cells could be responsible for the heterotopias of *dr*^{J} mutants.

7.1.3. BrdU-labelling as a method for the study of corticogenesis

The mechanisms of normal corticogenesis in mammals have been elucidated through the use of DNA-labelling (birthdating) techniques (Angevine and Sidman, 1961; Caviness and Sidman, 1973; Caviness, 1982; Takahashi *et al.,* 1992). These involve the administration to a pregnant female, during the period of embryonic neurogenesis, of a marker that is incorporated into DNA during S-phase of the cell cycle, and can be easily detected at a later stage of development. Commonly used markers include tritiated thymidine, which can be detected by autoradiography, e.g. (Caviness, 1982), and bromodeoxyuridine (BrdU), a non-radioactive thymidine analogue, which can be revealed by immunocytochemical methods (Miller and Nowakowski, 1988). Proliferating cells in the ventricular zone incorporate the S-phase marker during the labelling period, while the marker becomes progressively diluted in those cells that re-enter the cell cycle following labelling (e.g. those cells which have not yet been committed to a neuronal fate). Therefore, only cells labelled during most of their final S-phase are persistently and strongly marked by this technique.

There is an essential assumption behind these birthdating studies: neuronal migration in the mammalian cerebral neocortex occurs in a sequential and orderly manner. Cohorts of cells destined to become the

neurons of a given deep layer (e.g. layer VI) become post-mitotic, migrate and settle in their final positions much earlier than those cells destined to become occupy neurons of more superficial cortical layers (Sidman and Rakic, 1973) (See General Introduction). Depending on the position of strongly labelled nuclei in the adult animal, for example, it is possible to infer the approximate date of birth of those cells, i.e. the day when they have become post-mitotic.

7.1.4. Aim of the present experiments

As an initial step to distinguish between the two main pathogenetic hypotheses mentioned above, experiments were designed which involve the *in vivo* labelling of embryonic brain DNA with BrdU. By determining the period of production of neuronal heterotopias in the neocortex of dr^{J} mutants, useful information may be obtained concerning the most likely mechanism for their genesis. If, for instance, the great majority of heterotopic cells is labelled after injections in the early stages of migration, i.e., when most cells destined for layer I are usually born, an imbalance between proliferation and cell death or excessive tangential migration could be possible mechanisms. If, on the other hand, heterotopic cells were labelled mainly in the later stages of corticogenesis, or throughout the period in which postmitotic neurons are born, then a primary defect of neuronal migration would be a more likely explanation. According to the results obtained in the present BrdU-labelling studies, it will be possible to design new experiments to further elucidate the origin of heterotopic neurons.

7.2. Methods

7.2.1. Generation of experimental litters and BrdU injection protocol

Heterozygous *dr*^{J} animals were mated overnight. Pregnancy was ascertained by the presence of a vaginal plug on the following morning between 9:00 and 9:30 a.m. Twelve o'clock noon on plug day was considered to be day 0.5 post-conception (E0.5). Pregnant females were given a single intra-peritoneal injection of 70 μg of BrdU per gram of body weight between 12:00 and 12:30 on day 11.5, 13.5, 15.5 or 17.5 of gestation. Females were allowed to deliver and their progeny were ear-marked and genotyped (usually between days 6 and 10 of postnatal life) using *D1Mit452* and *D1Mit15* as flanking microsatellite DNA markers (see Chapter 3). In large litters, some or all of the heterozygous mice and those with a normal external phenotype and recombinant genotypes were subsequently culled, in order to enhance the survival chances of the circling animals. See Chapter 3 for details of the genotyping and culling procedures. All circling animals had a *dr*^{J}/*dr*^{J} pattern for one or both flanking microsatellite markers. The inclusion in the study of circling mice with recombinant genotypes was based on previous evidence of a full penetrance of the circling phenotype (see Chapter 3).

Surviving animals of both genotypes (*+/+* and *dr*^{J}/*dr*^{J}) were examined on the 21st day of post-natal life (P21), the day of birth being

Figure 7.1

BrdU labelling: Experimental protocol

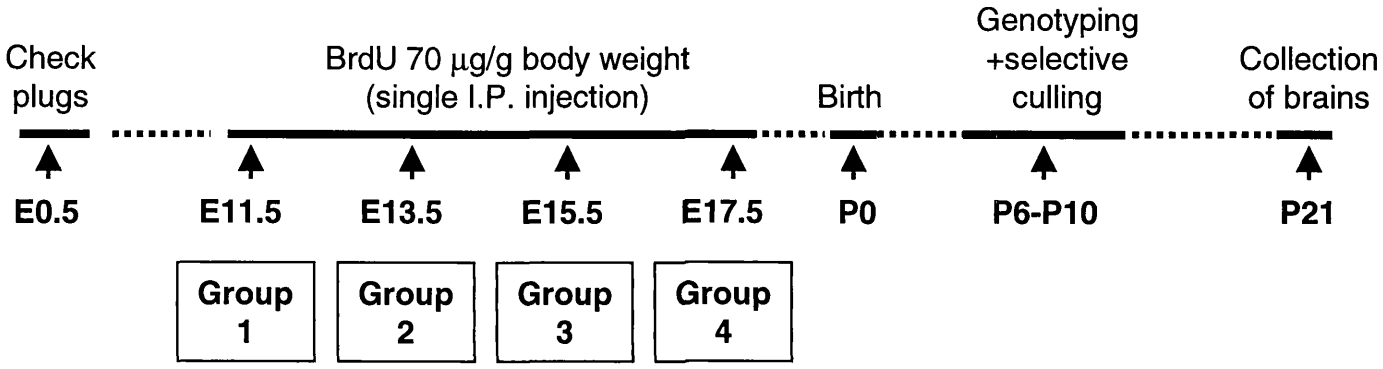

Each pregnant female was given a single intraperitoneal injection of 70 µg BrdU per gram of body weight on either gestation day 11.5, 13.5, 15.5 or 17.5. Their progeny was genotyped between days 6 and 10 of post-natal life. Most or all animals with heterozygous and recombinant genotypes, but a normal phenotype were selectively culled. At P21, surviving wild-type and homozygous mutant mice were perfusion-fixed and their brains were collected.

considered P0. Figure 7.1 shows the BrdU-labelling protocol. For each stage of BrdU injection (E11.5, E13.5, E15.5 and E17.5), two mutants and two wild-type animals were studied. Whenever possible, mutants were compared to wild-type littermates.

7.2.2. Perfusion-fixation, tissue processing and sectioning

On day 21 of postnatal life (P21), animals were weighed, anaesthetised and perfusion-fixed as described previously (see section 6.2.1). Each brain was removed from the skull, processed, then embedded in paraffin wax and prepared as 10 μm-thick sections as described before (sections 6.2.2 and 6.2.3).

7.2.3. Routine staining and immunolabelling

Selected sections from each level were stained with Cresyl violet (see Section 6.2.5.2 for details of the staining procedure). Adjacent sections (serial whenever possible) were subsequently immuno-labelled with anti-BrdU antibodies, according to the immunohistochemistry protocol below.

7.2.3.1. Immunolabelling with anti-bromodeoxyuridine antibodies

This protocol was slightly modified from that of Katie Gillies and David Price (personal communication). Sections were de-waxed by immersing twice in Histoclear for 10 minutes. They were then dehydrated by immersion in ethanol solutions of decreasing concentration (100%, 95%, 70%), rinsed in distilled water and digested by immersion in a 0.1% trypsin (Sigma) solution in 0.1%

calcium chloride at 37°C for 20-30 minutes. They were rinsed in Tris buffered saline (made by diluting a 10 x TBS stock solution [15.18g Tris base pH 7.6 to 1l in dH_2O] in normal saline solution to obtain the 1x TBS working solution) for 10 minutes. Sections were exposed to a 1N HCl solution at 60°C for 8 minutes to denature DNA and expose the BrdU epitopes. They were subsequently rinsed in running tap water for 5 minutes, pre-blocked with blocking serum [a 1:5 solution of normal rabbit serum (DAKO) in TBS] for 15 minutes, then incubated for 2 hours with the primary anti-BrdU antibody (monoclonal antibody, DAKO M0744 prepared by diluting the antibody 1:20 in blocking serum). The primary antibody was then washed off by pouring TBS over the slides, then by immersion (twice, for 5 minutes each, in TBS). After incubating sections again with blocking serum for 15 minutes, then with the secondary antibody (biotinylated rabbit anti-mouse immunoglobulin, DAKO) for 30 minutes, they were rinsed by pouring TBS over slides, then immersing them twice in TBS for 5 minutes. An avidin-biotinylated horseradish peroxidase solution (ABComplex/HRP, DAKO) was applied to the sections for 30 minutes. After rinsing with PBS, peroxidase staining was revealed with a diaminobenzidine (DAB) solution (Sigma Fast DAB peroxidase substrate, prepared by dissolving DAB, 0.7 mg/ml, urea hydrogen peroxide 0.7 mg/ml and 0.06M Tris buffer in distilled water). DAB solution was applied to each section for 5-10 minutes, until a brown precipitate appeared. Sections were thoroughly rinsed in tap water, briefly immersed in distilled water and counterstained with a freshly-filtered, aqueous cresyl violet solution (1% Cresyl violet acetate, Sigma) for 4 to 5 minutes, then re-hydrated by immersion in ethanol solutions of increasing strength (70%, 95%). After quick differentiation by immersing in acid alcohol

(2.5% glacial acetic acid in 95% ethanol), sections were immersed in 100% ethanol, cleared with Histoclear, and mounted with DPX.

7.2.4. Morphometric analysis

7.2.4.1. Assessing the general process of migration

In order to compare neuronal migration in the cerebral cortex of wild-type and mutant *dr*^{J}/ *dr*^{J} mice, all BrdU-positive cells in a 0.76 mm-wide area of the parietal cortex region at level C were drawn with a *camera lucida* adapted to a transmitted light microscope, using a x 20 objective (Figure 7.2 A and B). A x40 objective was used only when doubts remained about the positivity of a given nucleus. Only those nuclei with dense staining of more than half of the nucleus were counted as BrdU-positive at all times. These nuclei have taken up BrdU on the day of their last mitosis, for most of the duration of their last S-phase. Cells that did not show this pattern are likely to have divided after taking up BrdU or to have been labelled for only a short period during S-phase. These cells have not been enumerated since their date of birth could not be estimated with precision (Del Rio and Soriano, 1989; Gillies and Price, 1993; Price *et al.,* 1997). In order to avoid counting the same cell twice, all labelled cells co-localising in two adjacent sections were excluded from the analysis. Endothelial cell nuclei were also not counted; they were identified on the basis of their elongated, fusiform shape and localisation in vessel walls. BrdU-positive cell counts in each cortical layer or set of layers (in the case of layers I,II and III) were used to build graphs of their distribution in relationship to date of labelling (E11.5, E13.5, E15.5, E17.5).

Significant differences in brain size were found between mutants and wild-type animals (see Chapter 6), that could result in an overestimation of the density of BrdU-positive cells in the mutants whenever counting an area of similar size in both genotypes.

To overcome this problem a conversion factor was sought that would enable extrapolation of the area of counting from other parameters (such as a correlation between brain weight and cortical thickness). No parameter was found from which to extrapolate the area of counting in the mutants. For this reason, the number of BrdU-positive cells was expressed as a percentage of the total number of cells in the area of counting (see Discussion).

In a separate analytical protocol, all BrdU-positive cells in the neocortical ribbon of *dr*^{J} mice of both genotypes were counted using a computer image analysis programme (Voron, Biocom, conceived by Charles Duyckaerts, Paris; see also Duyckaerts *et al.,* 1992) . This method could not be used for layer distribution analysis because the quality of the image was poorer than that obtained with the more straightforward *camera lucida* technique. With the latter method, however, it was possible to quickly draw large areas of the neocortex, thus obtaining charts of BrdU-positive cells for each genotype and for each embryonic age of labelling.

Figure 7.2

Areas of counting of BrdU-positive cells

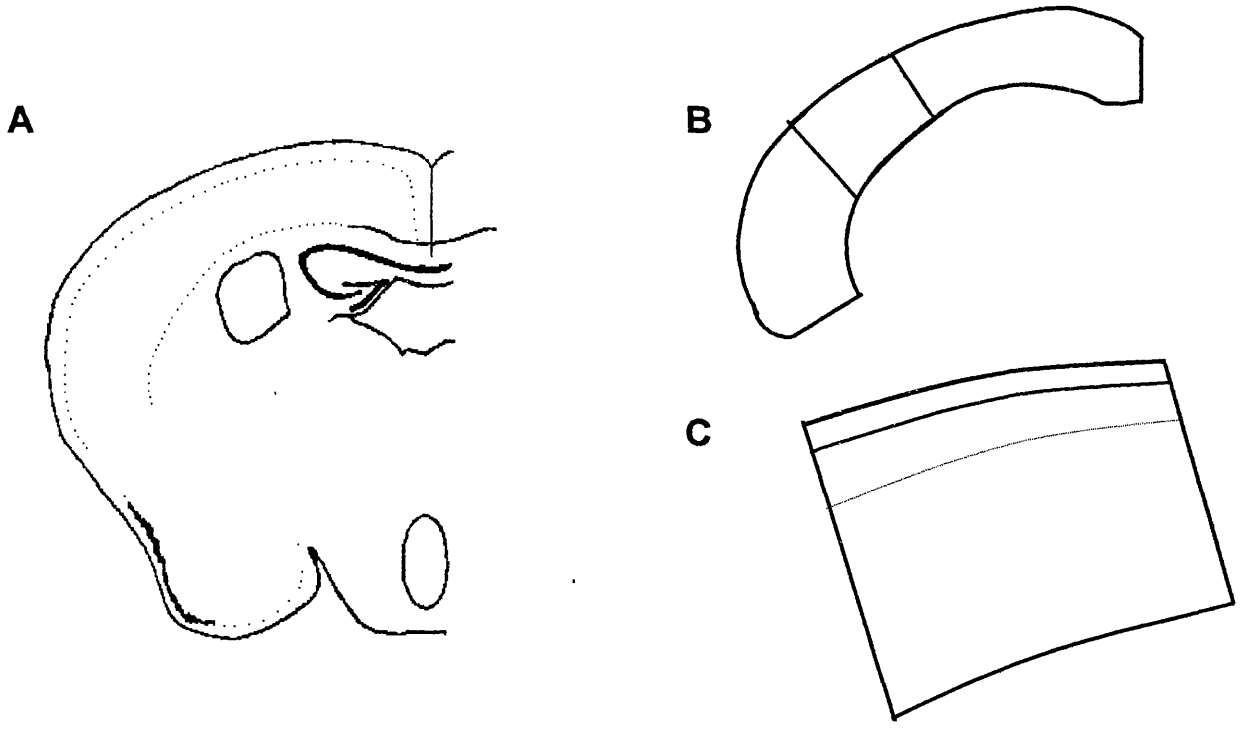

(A) Cell counts were carried out at the posterior parietal level (level C).
(B) All BrdU-positive cells were counted in large areas of the neocortex (in blue). A 0.76 mm-wide area through the full thickness of the parietal cortex (in black) was selected for the purpose of studying the layer distribution of BrdU-positive cells.
Cell counts in each layer were expressed as a percentage of the total number of positive cells in all layers.
(C) The mean date of birth of layer I heterotopic cells was calculated by estimating the labelling index (no. BrdU-positive cells / total no. cells) for each date of injection. Cells were counted in a narrow strip of the cortex underneath the abnormal *glia limitans* (in red). The dashed line shows the expected thickness of layer I in a wild type brain. See section 7.2.4. for details.

7.2.4.1.1. Distribution of BrdU-positive cells: pooling of cell counts of layers I, II and III

In the process of cell counting, it was difficult to distinguish between adjacent layers I-II in the mutants and between layers II and III in both genotypes. In fact, there is no obvious border between layers II and III of the normal parietal cortex of the mouse (Caviness, 1975) (see also Figure 6.4). Moreover, although the border between layers I and II is easily seen in sections of wild-type brains, molecular layer heterotopias make it difficult to differentiate between layers I and II in the mutants. Initially, it was thought that if a direct relationship existed between the thickness of layer I and that of the cortical ribbon in wild-type animals, it would be possible to infer the expected thickness of layer I in mutant brains. Unfortunately, however, a more detailed study failed to reveal a consistent ratio of layer I thickness to total cortical thickness in wild-type brains. Subsequently, another attempt was made to determine the boundaries of layer I in the neocortex of mutants, based on the fact that the outer and inner boundaries of layer I are often clearly visible at the inter-hemispheric fissure level in the brains of *dr*^{J} mutants. However, no close relationship was found at this level between the thickness of layer I and that of the cortical ribbon at the same level. Since the upper border of layer IV was found to be readily delineated in all sections of the parietal neocortex, from both wild-type and *dr*^{J}/ *dr*^{J} cortex, it was decided to pool counts of positive cells of layers I, II and III for analysis in brains of both genotypes. Cells in layers IV, V and VI were clearly distinguishable in both wild-type and mutant brains, and these were counted and analysed separately.

7.2.4.2. Determining the mean date of birth of heterotopic layer I cells

In order to assess the mean date of birth of heterotopic layer I cells in mutant brains, the labelling index of BrdU-positive cells in outer layer I (i.e. the number of BrdU-positive cells / the total number of cells in the area of counting) underneath the abnormal glial limiting membrane was estimated in two mutant brains at each date of labelling (E11.5, E13.5, E15.5, E17.5). To avoid including layer II cells because of blurring of the layer I/II boundary, cell counts were restricted to a thin ribbon underneath the pial-glial membrane (thickness of one x40 field) (see Figure 7.2C). The value obtained was plotted against the mean date of birth of BrdU-positive cells in layers I+II+III, IV, V and VI of both wild type and mutant animals (see below-Statistical analysis).

7.2.4.3. Statistical analysis

Statistical analysis and graphical plotting were carried out using Microsoft Excel software. As stated previously, for the purpose of studying the distribution of BrdU-positive cell counts in the parietal cortex, the latter were expressed as a percentage of the total number of positive cells in the area of counting, for each gestational age of BrdU injection:

$$\frac{\text{Number of BrdU-positive cells in layer } \alpha \text{ x100}}{\text{Number of BrdU-positive cells in all layers}}$$

Mean values were obtained for each pair of mice (two cases for each age of labelling per genotype), and plotted with their standard errors of the mean (SEM), calculated as follows:

$$\text{SEM} = \frac{\text{standard deviation (SD) for each pair of values}}{\sqrt{2}}$$

For estimating the mean date of birth of BrdU-positive cells in layers I+II+III, IV, V or VI in the area of counting of the parietal cortex, the following formula was used:

Mean date of birth of layer α cells =

$$\sum \left(\frac{\text{No. of BrdU - positive cells in layer } \alpha \text{ at E}\beta \times \beta}{\sum \text{No of BrdU - positive cells in layer } \alpha \text{ (at all ages of injection)}} \right)$$

where Eβ is the gestational age (E11.5, E13.5, E15.5 or E15.5) of fetuses at the time that pregnant females received BrdU injections, and α is the cortical layer. The mean value of each pair of cases from each genotype was then plotted along with their respective standard errors.

For instance, for the purpose of determining the mean date of birth of layer VI neurons in one of the wild type brains, the number of labelled cells at each date of injection were tabulated as seen below:

	Number of BrdU-positive cells in layer VI	
	Case #1	Case#2
E11.5	4	6
E13.5	53	60
E15.5	0	1
E17.5	3	1
Total	60	68

The value for the mean birthdate of BrdU-positive cells counted in layer VI in each of the wild type brains was calculated as follows:

Mean date of birth (case #1) =

$$= \frac{4 \times 11.5}{60} + \frac{53 \times 13.5}{60} + \frac{0 \times 15.5}{60} + \frac{3 \times 17.5}{60} = 0.77 + 11.9 + 0 + 0.88 = 13.57$$

Mean date of birth (case #2) =

$$= \frac{6 \times 11.5}{68} + \frac{60 \times 13.5}{68} + \frac{1 \times 15.5}{68} + \frac{1 \times 17.5}{68} = 1.01 + 11.91 + 0.23 + 0.26 = 13.41$$

The mean value and standard error of the mean (SEM) for cases #1 and #2 were 13.49 ± 0.08. Therefore, the mean date of birth of layer VI cells was E13.49.

The mean date of birth of heterotopic layer I cells was extrapolated from the labelling index (L.I.):

$$\text{Labelling index (\%)} = \frac{\text{number of BrdU - positive cells} \times 100}{\text{total number of cells}} \quad \text{in the area of counting in layer I}$$

This as determined in two mutant brains at each date of labelling (E11.5, E13.5, E15.5, E17.5), as below:

$$\text{Mean date of birth of heterotopic layer I cells} =$$

$$= \text{Mean (case1:case 2)} \left[\Sigma \frac{(\text{L.I. of BrdU-positive cells at E}\beta \times \beta)}{\Sigma \text{ L.I. at all ages of injection}}\right],$$

where Eβ is the gestational age (E11.5, E13.5, E15.5 or E15.5) of fetuses at the time that pregnant females received BrdU injections, and L.I. is the labelling index. Standard error of the mean was calculated as described above. Two cases were studied per day of injection. An example of how the mean date of birth of heterotopic neurons has been determined is given below.

	BrdU labelling index in outer layer I (%)	
	Case #1	Case#2
E11.5	0	0
E13.5	15	10
E15.5	30	25
E17.5	55	65
Total	100	100

For case #1, the mean date of birth of heterotopic cells would be:

Mean date of birth (case #1)=

$$= \frac{0 \times 11.5}{100} + \frac{15 \times 13.5}{100} + \frac{30 \times 15.5}{100} + \frac{55 \times 17.5}{100} = \frac{0}{100} + \frac{202.5}{100} + \frac{465}{100} + \frac{962.5}{100} = 16.30$$

Mean date of birth (case #2) =

$$= \frac{0 \times 11.5}{100} + \frac{10 \times 13.5}{100} + \frac{25 \times 15.5}{100} + \frac{65 \times 17.5}{100} = \frac{0}{100} + \frac{135}{100} + \frac{387.5}{100} + \frac{1137.5}{100} = 16.60$$

The mean value of the two cases (i.e. the mean date of birth of heterotopic cells) is 16.45.

7.3. Results

7.3.1. Survival of progeny from BrdU-injected females

All females injected with BrdU carried their pregnancies to term. No evidence of external malformation was seen among the 26 litters that were born.

From all of the mice born in this experiment (n=180, from 26 litters), only 10% had a mutant circling phenotype (n=18). Despite the culling procedures used to improve their chances of survival, only 14 of these mutants survived to P21. From these, the quality of the perfusion was poor in 3 mice and 3 further brains were damaged during a tissue processor breakdown. Thus, 8 brains from *dr^{J}/dr^{J}* were analysed in these experiments, and compared to 8 brains from wild type controls (see Table 7.1). Three pairs of unrelated mice were used (all mice labelled on E13.5 and one pair of mice labelled on E17.5). Each of the remaining five pairs of mice used for comparison consisted of wild type and *dr^{J}/dr^{J}* littermates.

7.3.2. Distribution of BrdU-positive cells in the parietal cortex of wild-type and homozygous mutant *dr^{J}* mice

Figure 7.3 shows the total number of BrdU-positive cells in the area of counting (posterior parietal level) for each date of BrdU injection. Apparently higher numbers of cells are BrdU-positive with injections at E13.5 and E15.5 in the wild type brains, when compared with the

Table 7.1

Number of animals at different stages of the birthdating experiment with BrdU

	No. of litters injected	No. of pups born	*dr*^{J}/*dr*^{J} mice				wild type mice	
			No. identified after birth	No. remaining at P21	No. perfused	No. brains analysed	No. perfused	No. brains analysed
E 11.5	3	28	2	2	2	2	8	2
E 13.5	6	39	4	4	4	2	6	2
E 15.5	11	78	6	5	5	2	10	2
E 17.5	6	35	6	3	3	2	7	2
Total	26	180	18	14	14	8	31	8

E 11.5 to E 17.5: gestational age of fetuses at the time that pregnant females received BrdU injections.

Figure 7.3

Total number of BrdU-positive cells in the parietal cortex of *dr*^{J} mice as a function of the age of labelling

The total number of BrdU-positive cells in a 0.76 μm-wide area of the parietal cortex was counted in each case. Each bar represents the mean value of two cases, plotted with its standard error. Two-way analysis of variance showed that there are no significant differences between the two genotypes in the total number of labelled cells in area of counting ($p=0.316$). Significant differences ($p=0.0132$) were found in the number of BrdU-positive cells between gestational days of injection.

mutants, although these differences are not statistically significant. At E11.5 and E17.5, the total number of labelled cells is small and not significantly different between genotypes.

The relative distribution of BrdU-positive nuclei among the different cortical layers (expressed as a percentage of the total number of BrdU-positive nuclei) was similar in both wild-type and mutant neocortex, as can be seen in Figure 7.4 . Few cells were BrdU-positive that had been labelled with E11.5 injections (Figure 7.3) and, for both genotypes, they were mostly confined to layer VI, presumably corresponding to remaining neurons originating from the embryonic subplate. Strongly labelled cells were seen (on the same sections) in other brain areas such as the thalamus, ruling out a possible failure of the immunocytochemical technique. The inside–out gradient of corticogenesis of layers II to VI seen in wild type brains was preserved in the mutant: neurons destined for deeper layers (e.g. layer VI) are produced earlier than those migrating to more superficial ones (e.g. layers II and III). Moreover, there were no significant differences in the relative proportion of BrdU-positive cell counts in layers IV, V or VI, between wild-type and mutant cortices (see Figure 7.4)

These findings were confirmed by analysis of computer-generated images of the distribution of BrdU positive cells in the neocortex of wild type and homozygous mutant mice labelled *in utero* at E11.5, E13.5, E15.5 and E17.5. The pattern (Figure 7.5) again illustrates the similarities in the distribution of labelled neurons in the brains of mice

Figure 7.4

Distribution of BrdU positive cells by age of injection and cortical layer

Counts were carried out in the parietal cortex (level C). The number of BrdU-positive cells in each layer or set of layers is expressed as a percentage of the total number of positive cells in the area of counting.

Statistical analysis was carried out using two-way analysis of variance. It showed that there were no significant differences in the percentage of labelled cells in any of the layers between genotypes. p values were 0.475 for layers I+II+III, 0.439 for layer IV, 0.701 for layer V, 0.849 for layer VI.

Comparison between gestational days of injection (E11.5, E13.5 E15.5 and E17.5) yielded significant differences for each layer. p values were as follows: 0.0000245 for layers I+II+III, 0.00113 for layer IV, 0.00603 for layer V and 0.0000494 for layer VI.

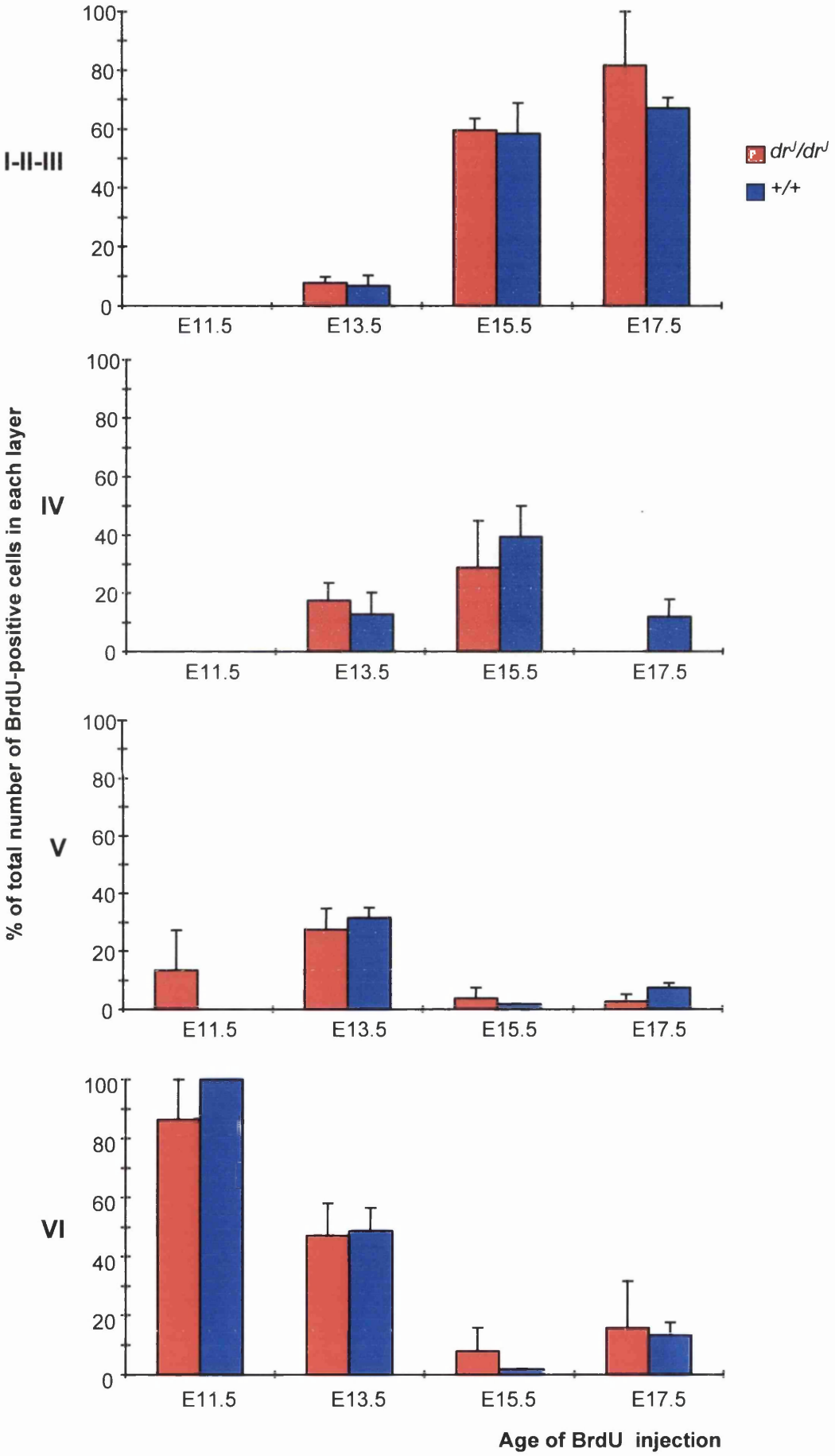
I-II-III
IV
V
VI
% of total number of BrdU-positive cells in each layer
100
80
60
40
20
0
E11.5
E13.5
E15.5
E17.5
dr^J/dr^J
+/+
Age of BrdU injection

Figure 7.5

Computer-assisted drawings of the whole of the neocortex of wild-type and mutant *dr*^{J} mice (level C)

(A) Wild-type mice: most BrdU-positive cells labelled with E11.5 injections are found in deep layer VI, and are probably subplate-derived. Injections at later dates during corticogenesis label neurons that settle into progressively more superficial layers.

(B) *dr*^{J}/*dr*^{J} mice: the overall process of neuronal migration in the neocortex seems to be preserved in the mutants. Most BrdU-positive cells labelled with E11.5 injections are found in deep layer VI. Injections at later dates during corticogenesis will label cohorts of neurons that settle into progressively more superficial layers. Note increased numbers of layer I cells labelled at E15.5 and E17.5, corresponding to heterotopic neurons.

A

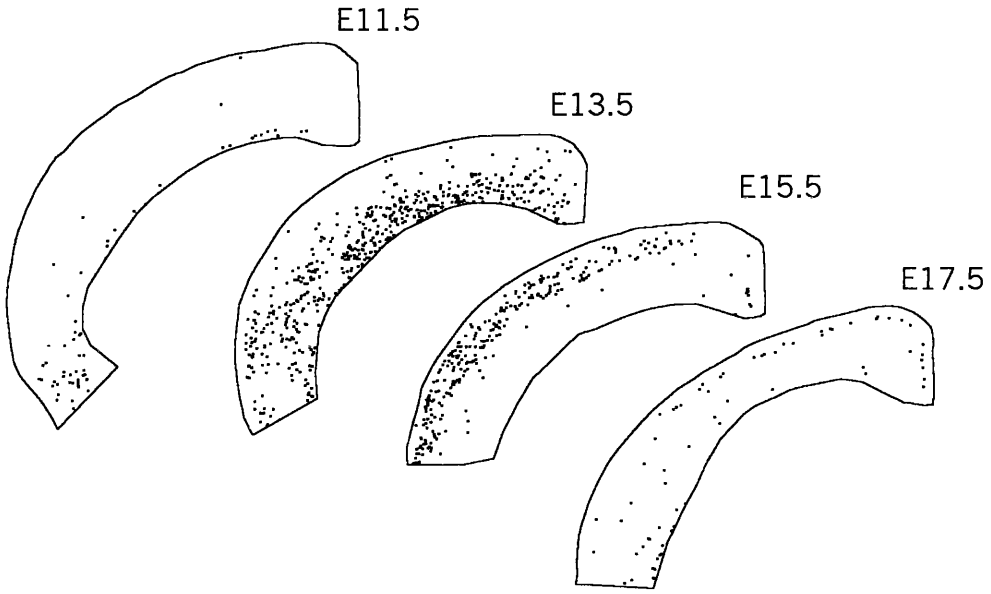

B

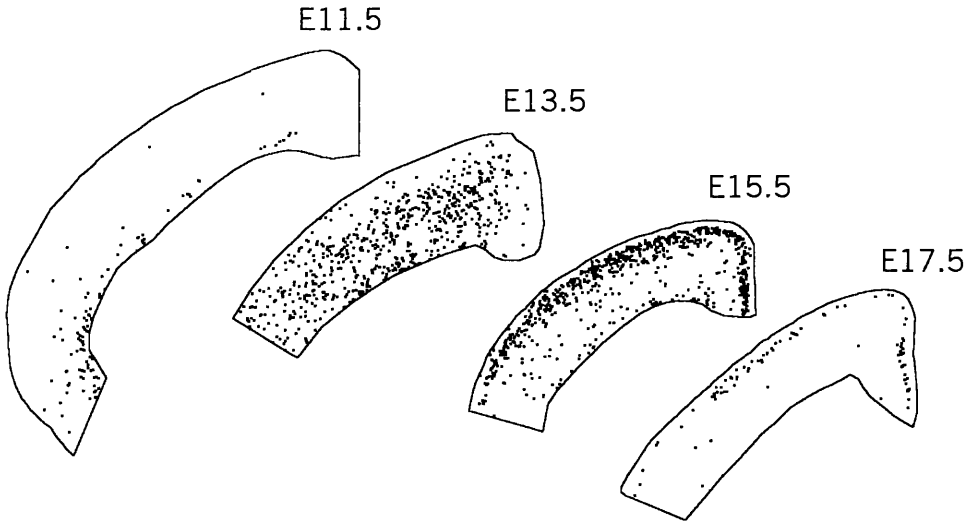

belonging to both genotypes. A few neurons, predominantly destined for deep layer VI, are strongly labelled with E11.5 injections. Waves of migrating neurons generated later than this occupy progressively more superficial positions. There seems to be an excessive number of BrdU-positive cells, labelled exclusively at E15.5 and E17.5, underneath the cortical surface in mutant brains.

7.3.3. Birthdating of heterotopic layer I cells in *dr^{J}/dr^{J}* brains

The mean birthdate of heterotopic cells in outer layer I (see Methods section) of mutant brains was found to be E15.2. This mean date of birth resembles that of layers I+II+III, and not those of layers IV, V or VI (Figure 7.6). In the normal neocortex of the mouse, cells destined for layer I are among the first to be generated during corticogenesis (Caviness, 1982). One would expect injections at E11.5 to label these early-generated cells. No BrdU-positive cells were seen in layers I+II+III with injections at E11.5 in the present studies, which suggests that cells of layers II and III (i.e. late generated cells) are the only ones to account for the mean value (E15.2), obtained for the heterotopic neurons in *dr^{J}/dr^{J}* brains.

Figure 7.6

Mean age of birth of heterotopic layer I cells compared to that of BrdU-positive cells of layers I-VI

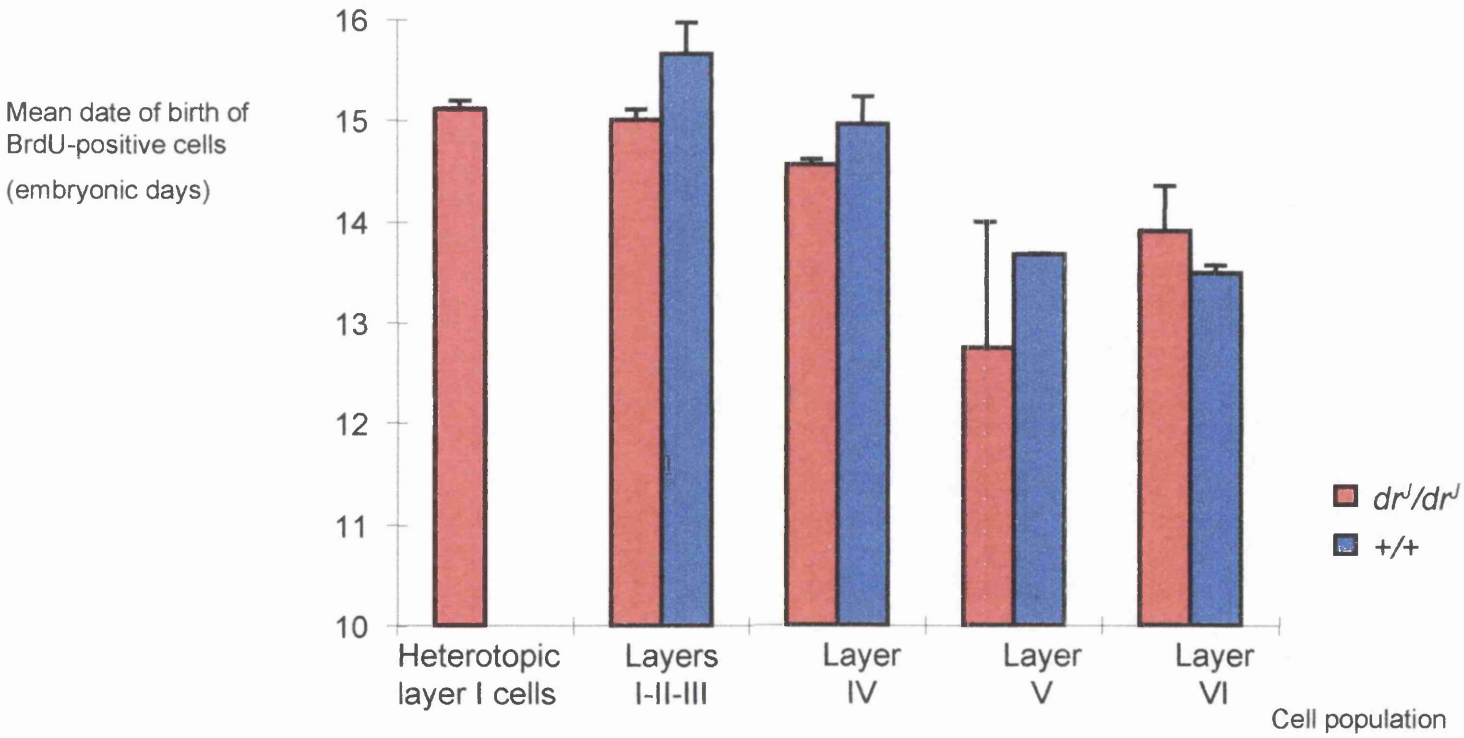

Two brains of each genotype were studied at the posterior parietal level. Each bar represents the mean value of two cases, plotted with its standard error. The mean date of birth of heterotopic layer I neurons indicates that they are generated during the late stages of corticogenesis (at the same time as layers II and III). See section 7.3.4.

7.4. Discussion

7.4.1. The main steps of organisation of the cerebral neocortex are preserved in *dr*^{J} mutant fetuses.

Neither the total numbers, nor the percentage values of BrdU-positive cells in each layer of the parietal cortex for each day of injection vary significantly between wild type and homozygous mutant *dr*^{J} mice (see Figures 7.3 and 7.4). This indicates that there are no major differences between the two genotypes in the pace and date of birth of neurons destined for the different layers: the normal inside-out pattern of genesis of layers II-VI (Caviness, 1982) is preserved in mutant brains. These results also make it unlikely that increased proliferation is the pathogenetic mechanism by which layer I heterotopias are produced in *dr*^{J} mutant mice.

7.4.2. Heterotopic cells of *dr*^{J} mutant brains are produced during late neurogenesis.

Heterotopic layer I cells are produced at approximately the same time as those destined for layers II and III, as estimated by the BrdU labelling behaviour of cells in the outermost part of layer I of the parietal cortex of *dr*^{J} mutant mice. Mean embryonic age of birth of the heterotopic cells is 15.2 days, compared with 15.0 days for the pooled layers I+II+III. The number of early produced BrdU-positive cells (i.e. destined for layer I) included in this sample is quite small, making it unlikely that these cells play a role in determining the time of birth. The fact that no significant

differences were found between the numbers of labelled cells in *dr^{J}/dr^{J}* and wild-type parietal cortex for cells labelled with day E11.5 injections (see Figure 7.4) suggests that lack of programmed cell death is unlikely to play a major role in the production of the heterotopias. The generation of heterotopic cells at a later period of neurogenesis is in keeping with the morphological data obtained with the routine histological stains, which showed that many of these ectopic cells resemble those of normal layers II and III.

7.4.3. Are heterotopias confined to layer I ?

In the present study, cytoarchitectural abnormalities of layers II-VI were found to be small and were not present in all cases (see also Chapter 6). They were most easily seen on cresyl violet-stained sections of neonatal brains. This is in agreement with another published series on *dr^{J}* brains, in which neuron-free spaces in layers II –VI were seen in 7 out of ten cases. Moreover, a previous report on sections of *dr^{J}/dr^{J}* brains impregnated by the Golgi method (Sekiguchi *et al.,* 1987) has described the presence of abnormally oriented dendritic trees in layers II to VI of the neocortex. The origin of these minor abnormalities is unclear. In the present study, the distinction between layers III-IV, IV-V and V-VI was readily achieved in both normal and *dr^{J}/dr^{J}* brains, indicating that if an abnormality of neuronal migration exists in these deeper layers of *dr^{J}/dr^{J}* brains, it is likely to be a very subtle one. It remains nevertheless possible that minor abnormalities of layering exist but are obscured by the higher cellularity of deeper layers, whereas

these more easily observed against the background neuropil in the relatively cell-poor molecular layer.

7.4.4. Evidence for a disturbance of late neuronal migration in the brains of *dr*^{J} mutant mice

The findings concerning the timing of generation of neocortical defects in *dr*^{J}/*dr*^{J} mice are consistent with previously published work on other regions of the brain in *dreher* mutants, and with earlier findings in this thesis (Chapter 6). Previous reports on the microscopical appearance of the hippocampus in *dr*^{J} (Nowakowski and Wahlsten, 1985b; Sekiguchi *et al.,* 1992) suggested that pathological changes in the pyramidal layer are usually more severe in or restricted to CA3, the hippocampal field containing the last cells in the pyramidal layer to be generated (Angevine, 1965). Furthermore, previous DNA-labelling studies using tritiated thymidine have addressed the issue of how abnormalities found in the hippocampus and dentate gyrus (but not the neocortex) of *dr*^{J} mutant mice are generated (Nowakowski,1985a). The authors have suggested that the histological abnormalities result from both decreased late cell proliferation and disrupted late neuronal migration. Evidence for diminished late cell proliferation came from the finding of failure of formation of the inferior limb of the dentate gyrus. Evidence for disrupted neuronal migration was based on a comparison of the most affected side to the least severely affected, where the former lacked late generated cells, i.e., those in the most superficial layers (Nowakowski and Wahlsten, 1985b). These findings are in

agreement with a disruption of the late stage of neuronal migration in *dreher* mutant brains.

The abnormalities of the external limiting membrane described earlier (Chapter 6) may contribute to the preferential disruption of late neuronal migration in dr^J/dr^J mice . This may be due to the fact that late migrating neurons (i.e. those of layers II and III) have to travel the farthest along radial glial fibres before settling in their final location and so may be the most perturbable in their migration. An additional mechanism could involve the destruction of the already formed glial limiting membrane specifically during late corticogenesis, allowing for neurons destined for deeper layers to settle normally, but disturbing the guidance of later migrating neurons to their final positions.

The present findings do not exclude the hypothesis that heterotopic cells in layer I might be tangentially migrating neurons arising from the lateral ganglionic eminence. If this were the main pathogenetic mechanism, however, one would expect that the heterotopias would extend beyond the neocortex, along the path for tangential migration, and this was not observed. Moreover, an additional mechanism would have to be sought to explain the disruption of the glial limiting membrane and its close spatial association with the areas of heterotopic neurons.

Taken together, these results argue against decreased cell death or excessive proliferation as the cause of heterotopias in dr^J/dr^J brains.

They favour neuronal migration abnormalities as the underlying mechanism, but do not allow a distinction to be made between the different possible explanations for such a migration abnormality, the nature of which will have to be elucidated through future experimental approaches (See Chapter 8-Final Discussion).

Chapter 8

Final discussion

8.1. The *dr*^{J} mutant mouse is a model for neuronal migration defects

During development of the cerebral neocortex in *dr*^{J} homozygous mutant mice, a small fraction of neurons become misplaced in the normally cell-poor layer I. The data presented in this thesis indicate that these heterotopic neurons derive predominantly, or exclusively, from late-migrating neuroblasts. Moreover, it appears that these neuronal heterotopias are likely to result from disruption of the external glial limiting membrane, rather than from an imbalance between cell proliferation and apoptosis. The *dr*^{J} mutant mouse is, therefore, an interesting model for the study of CNS neuronal migration defects, because it brings into focus the importance of tissue interactions at the brain surface for the development of the normal stratified neocortex.

8.2. Unanswered questions

8.2.1. What is the nature of the gene mutated in *dreher*?

Although the *dreher* gene has not yet been identified, clues to the nature of the protein it encodes may be discerned from the phenotype of the *dreher* mutant alleles. Published reports indicate that the *dreher* gene is involved in neuronal migration, both in the CNS (cerebral neocortex, cerebellum, hippocampus, olfactory bulbs) and probably also in the PNS. This latter point is less clear, but a neural crest related defect seems likely in view of the white belly spots, which form a consistent feature of the phenotype. The defect of the *glia limitans* described in the present work is a novel finding, and resembles in

quality (although not in severity) those seen in the developing brains of MARCKS-mutant mice and in the cerebral cortex of patients with Fukuyama congenital muscular dystrophy (FCMD). It is therefore tempting to speculate that *dreher* may code for a molecule involved in cell adhesion or that somehow affects basement membrane integrity (e.g. by proteolytic destruction or by the lack, or reduced expression, of one of its constituents).

8.2.2. Why do *dr^J* homozygous mutants not have seizures?

Neuronal migration defects are often associated with epilepsy, both in humans (Sarnat, 1992; Meencke and Janz, 1984), and in mouse models (Chae *et al.,* 1997; Hirotsune *et al.,* 1998). Nevertheless, there are various animal models of neuronal migration defects in which spontaneous seizures are not observed (Flint and Kriegstein, 1997), even though they might be expected based on the brain pathology. For instance, the microdysgenesis-like abnormalities seen in rats subjected to freezing injuries of the cortical surface in the neonatal period (Humphreys *et al.,* 1991) do not cause spontaneous seizures, although there is an increased sensitivity to epileptogenic stimuli in this and other animal models exhibiting neuronal migration defects (Flint and Kriegstein, 1997).

Spontaneous seizures were not observed among *dr^J/dr^J* mutants in the present study. Moreover, there have been no other reports of seizures in any *dreher* allele. It remains possible, however, that a low threshold for epileptiform activity exists in these mutants.

8.2.3. Do *dr*^{J}/*dr*^{J} mice have learning disabilities similar to those reported in New Zealand Black mice?

From what has been published on the relationship between layer I heterotopias and learning disabilities in both dyslexic patients and New Zealand Black mice (Sherman *et al.,* 1985; Sherman *et al.,* 1990a), one would expect that *dr*^{J} homozygous mutant mice would have low scores in tasks designed to assess this specific dysfunction. Given the incessant circling behaviour of the mutants, however, testing this hypothesis seems virtually impossible.

8.2.4. Is there a condition in humans which resembles the *dreher* phenotype?

A comparison of the *dreher* phenotype with known human syndromes has been presented in Chapter 6. However, a few issues have not been raised in the previous discussion.

It is possible that a similar constellation of findings exists in humans, but that the relatively mild brain abnormalities are overshadowed by the more overt aspects of the phenotype, such as impaired hearing and disturbed balance. Interestingly, a locus for autosomal dominant non-syndromic deafness has been localised to 1q21-q23, close to the human POU2F1 gene (Fagerheim *et al.,* 1996), in the human genomic region syntenic to that in which *dreher* is situated. This condition presents itself as progressive hearing loss unassociated with other clinical manifestations. However, possible brain abnormalities in these patients are likely to have been overlooked in the absence of epilepsy. Moreover, subtle balance problems could have gone undetected. In fact, a

delay in the age of walking and other minor signs of impaired balance are common findings in children with hearing impairment (Petit, 1996).

It is important to stress that the phenotypes of human and mouse mutations in homologous genes are often not identical (Wynshaw-Boris, 1996). Among other reasons, this may be due to differences in the type of mutation (e.g. duplication of a part of a gene in one species versus deletion in the other), differences between species in biochemical pathways (e.g., a toxic product may accumulate in one species, but not in the other) or variation in developmental programmes (e.g. the smooth, agyric brain of mouse is unlikely to serve as a suitable model for the formation of the convoluted human cerebral cortex). Indeed, it should be remembered that even intraspecific differences (different genetic backgrounds, as those of unrelated inbred strains), may influence the phenotypes resulting from a particular given mutation (Searle *et al.,* 1994; Wynshaw-Boris, 1996), so it is not surprising that a similar genetic aetiology may produce quite different phenotypes in mouse and human.

8.3. Possible areas for future research

The present thesis has not been able to explore in detail all of the areas of developmental biology underlying the origin of neuronal migration defects in *dreher* mice. Below are some ideas for further analysis of this system.

8.3.1. Assessment of prenatal brain development in *dr^J/dr^J* mice

Abnormalities of neocortical architecture, and thick leptomeninges, are readily seen in the brains of neonatal *dr^J* mutant mice (see Chapter 6), but it remains to be determined at what time during prenatal development the first brain abnormalities occur. According to the hypothesis put forward in Chapter 6, abnormalities of the *glia limitans* play a causative role in the production of neuronal heterotopias. The former are therefore expected to precede, developmentally, the misplacement of neurons in layer I. Testing this hypothesis would involve the comparison of mutant with wild type brains at serial days of prenatal development. The integrity of both the *glia limitans* and the radial glial cells could be assessed with antibody markers directed against basement membrane components (e.g. anti-laminins), and against radial glial cells [e.g. anti-RC2 antibodies (Misson *et al.,* 1988)], respectively. Any defects that are identified could be correlated with abnormalities of the marginal zone (e.g. clusters of heterotopic cells) to determine which defect appears first in corticogenesis. Further studies could also include examining the expression of ECM molecules (such as fibronectin and chondroitin sulphate proteoglycans) and of ECM-like molecules (such as Reelin) during corticogenesis in wild type and *dr^J* homozygous mutant mice.

An analysis of the *in situ* expression of genes involved in patterning of the midbrain-hindbrain boundary [e.g. *Wnt-1* and *Otx-2* (Millet *et al.,* 1996)]may provide valuable insight into the origin of the cerebellar abnormalities seen in *dr^J/dr^J* mutants. This study would complement the *in situ* hybridisation work with *Pou2f1* described in the present thesis,

which suggested an early abnormality at the midbrain-hindbrain boundary in dr^J/dr^J embryos. Although previous morphologic studies on the abnormal development of the otic vesicle in *dr* have suggested that failure of induction of this structure by the neighbouring hindbrain is unlikely, this possibility has not been excluded. In this regard, it would be useful to analyse the *in situ* expression of genes known to play a role in induction and development of the otic vesicles (such as *Fgf-3*, *Nkx-5.1* and *Hoxa-1* (Steel and Brown, 1994; Hadrys *et al.,* 1998)).

Creating and analysing chimaeric mice (Mullen and Herrup, 1979), containing various proportions of wild type and dr^J/dr^J cells may help to understand whether the *dreher* mutation causes a defect intrinsic to cortical neurons or a defect which is not primarily neuronal (for instance owing to an extracellular matrix abnormality). If the cells in which the mutation has its primary effect are neuronal, heterotopias will be seen to contain only mutant neurons. In contrast, if wild type cells are found in heterotopias, this will argue in favour of a non-cell autonomous origin of layer I defects in dr^J/dr^J mutants.

8.3.2. Complementary studies on the morphological aspects of the neocortical defect

In the present study, heterotopic cells were identified as neuronal by use of a marker for postmitotic neurons (NeuN). However, they have not been further characterised. This could be achieved through the use of appropriate immunohistochemical techniques. Cajal-Retzius cells could be identified by anti-calretinin antibodies, whereas neurons belonging to layers II and III of the cerebral cortex stain positive with

VIP (vasoactive intestinal peptide). This neuropeptide has been used to label the heterotopic molecular layer neurons of New Zealand Black mice (Sherman *et al.,* 1990b). According to the hypothesis proposed in Chapter 7, heterotopic layer I neurons belong to the cohorts of late-generated cells destined for layers II and III. They would, therefore, be expected to be anti-calretinin negative and most likely anti-VIP positive. This is a specific prediction that could be readily tested.

8.3.3. Extension of morphological studies to other areas of the brain

The cerebellum and hippocampus, like the neocortex, are brain regions where glial-guided neuronal migration takes place. Since all three regions are affected by the *dreher* mutation, it would be interesting to study the development of these brain structures in the light of the findings presented in this work. In particular, it will be interesting to test the hypothesis that developmental defects of both cerebellum and hippocampus may occur as a consequence of destruction of meningeal cells (and therefore of the *glia limitans*) (Pehlemann *et al.,* 1985; Hartmann *et al.,* 1992).

8.3.4. Identification of the *dreher* gene: another step in understanding normal brain development

The recent, refined mapping of the *dreher* region has allowed several genes to be ruled out as candidates for the *dreher* mutation and has paved the way for positional cloning of *dreher*. Identification of the gene mutated in *dreher* will

open up new possibilities in terms of elucidating the functions of this gene in both brain and ear formation.

Unravelling the mysteries of the *dreher* mouse mutant will add yet another step towards a fuller understanding of normal and pathological brain development in mammals.

Adachi, T., Aoki, J., Manya, H., Asou, H., Arai, H. and Inoue, K. (1997). PAF analogues capable of inhibiting PAF acetylhydrolase activity suppress migration of isolated rat cerebellar granule cells. *Neurosci. Lett.* **235**, 133-136.

Allendoerfer, K.L. and Shatz, C.J. (1994). The subplate, a transient neocortical structure: Its role in the development of connections between thalamus and cortex. *Ann. Rev. Neurosci.* **17**, 155-218.

Angevine, J.B. (1965). Time of neuron origin in the hippocampal region: An autoradiographic study in the mouse. *Exp. Neurol.* 1-70.

Angevine, J.B. and Sidman, R.L. (1961). Autoradiographic study of cell migration during histogenesis of cerebral cortex in the mouse. *Nature* **192**, 766-768.

Anton, E.S., Marchionni, M.A., Lee, K.F. and Rakic, P. (1997). Role of GGF/neuregulin signaling in interactions between migrating neurons and radial glia in the developing cerebral cortex. *Development* **124**, 3501-3510.

Arrigo, G. (1997). Assignment of the tenascin-R gene (Tnr) to mouse chromosome 4 band E2 by fluorescence in situ hybridization; refinement of the human TNR location to chromosome 1q24. *Cytogenet Cell Genet.* **78**, 145-1446.

Asher, J.H.J., Harrison, R.W., Morell, R., Carey, M.L. and Friedman, T.B. (1996). Effects of Pax3 modifier genes on craniofacial morphology, pigmentation, and viability: a murine model of Waardenburg syndrome variation. *Genomics* **34**, 285-298.

Bayer, S.A. and Altman, J. (1990). Development of layer I and the subplate in the rat neocortex. *Exp. Neurol.* **107**, 48-62.

Benda, C.E. (1954). The Dandy-Walker syndrome or the so-called atresia of the foramen Magendie. *J. Neuropathol. Exp. Neurol.* **13**, 14-29.

Bergstrom, D.E., Gagnon, L.H. and Eicher, E.M. (1999). Genetic and physical mapping of the *dreher* locus on mouse Chromosome 1. *Genomics* **59**, 291-299.

Bierwolf, D. (1956). Kleinhirnmissbildungen durch hereditaeren Hydrocephalus bei der Hausmaus. *Wiss. Z. Univ. Halle* **6**, 1237-1282.

Bierwolf, D. (1958). Die Embryogenese des Hydrocephalus und der Kleinhirnmissbildungen beim Dreherstamm der Hausmaus. *Morphol. Jahr.* **99**, 542-612.

Bindal, A.K., Storrs, B.B. and McLone, D.G. (1991). Occipital meningoceles in patients with the Dandy-Walker syndrome. *Neurosurgery* **28**, 844-847.

Blackshear, P.J., Silver, J., Nairn, A.C., Sulik, K.K., Squier, M.V., Stumpo, D.J. and Tuttle, J.S. (1997). Widespread neuronal ectopia associated with secondary defects in cerebrocortical chondroitin sulphate proteoglycans and basal lamina in MARCKS-deficient mice. *Exp. Neurol.* **145**, 46-61.

Blanchard, A.D., Sinanan, A., Parmentier, E., Zwart, R., Broos, L., Meijer, D., Meier, C., Jessen, K.R. and Mirsky, R. (1996). Oct-6 (SCIP/Tst-1) is expressed in Schwann cell precursors, embryonic Schwann cells, and post-natal myelinating Scwann cells: Comparison with Oct-1, Krox-20, and Pax-3. *J. Neurosci. Res.* **46**, 630-640.

Blaschke, A.J., Staley, K. and Chun, J. (1999). Widespread programmed cell death in proliferative and postmitotic regions of the fetal cerebral cortex. *Development* **122**, 1165-1174.

Blaschuk, K.L. and ffrench-Constant, C. (1998). Notch is tops in the developing brain. *Curr. Biol.* **8**, 334-337.

Brown, R.H. (1996). Dystrophin-associated proteins and the muscular dystrophies: a glossary. *Brain Pathology* **6**, 19-24.

Cameron, R., Klein, L., Shyjan, A.W., Rakic, P. and Levenson, R. (1994). Neurons and astroglia express distinct subsets of Na,K-ATPase alpha and beta subunits. *Brain Res Mol Brain Res* **21**, 333-343.

Carnemolla, B., Leprini, A., Borsi, L., Querzé, G., Urbini, S. and Zardi, L. (1996). Human Tenascin-R: Complete primary structure, pre-mRNA alternative splicing and gene localization on chromosome 1q23-q24. *J. Biol. Chem.* **271**, 8157-8160.

Carraway, K.L.3. and Burden, S.J. (1995). Neuregulins and their receptors. *Curr. Opin. Neurobiol.* **5**, 606-612.

Caviness, V.S. (1975). Architectonic map of neocortex of the normal mouse. *J. Comp. Neurol.* **164**, 247-263.

Caviness, V.S. (1982). Neocortical histogenesis in normal and reeler mice: a developmental study based upon tritiated thymidine autoradiography. *Dev. Brain Res.* **4**, 293-302.

Caviness, V.S.J. (1989). Normal development of cerebral neocortex. In: Evrard, P. and Minkowski, A. (Eds.) *Developmental neurobiology.* pp. 1-10. New York: Raven Press]

Caviness, V.S. and Sidman, R.L. (1973). Time of origin of corresponding cell classes in the cerebral cortex of normal and reeler mutant mice: an autoradiographic analysis. *J. Comp. Neurol.* **148**, 141-152.

Caviness, V.S., Takahashi, T. and Nowakowski, R.S. (1995). Numbers, time and neocortical neurogenesis: a general developmental and evolutionary model. *Trends Neurosci.* **18**, 379-383.

Chae, T., Kwon, Y.T., Bronson, R., Dikkes, P., Li, E. and Tsai, L.-H. (1997). Mice lacking p35, a neuronal specific activator of Cdk5, dysplay cortical lamination defects, seizures, and adult lethality. *Neuron* **18**, 29-42.

Chenn, A. and McConnell, S.K. (1995). Cleavage orientation and the asymmetric inheritance of Notch1 immunoreactivity in mammalian neurogenesis. *Cell* **82**, 631-641.

Choi, B.H. (1994). Role of the basement membrane in neurogenesis and repair of injury in the central nervous system. *Microsc. Res. Tech.* **28**, 193-203.

Chong, S.S., Pack, S.D., Roschke, A.V., Tanigami, A., Carrozzo, R., Smith, A.C., Dobyns, W.B. and Ledbetter, D.H. (1997). A revision of the lissencephaly and Miller-Dieker syndrome critical regions in chromosome 17p13.3. *Hum. Mol. Genet.* **6**, 147-155.

Cohn, R.D., Herrmann, R., Wewer, U.M. and Voit, T. (1997). Changes of laminin beta 2 expression in congenital muscular dystrophy. *Neuromusc. Disord.* **7**, 373-378.

Copeland, N.G., Jenkins, N.A., Gilbert, D.J., Eppig, J.T., Maltais, L.J., Miller, J.C., Dietrich, W.F., Weaver, A., Lincoln, S.E., Steen, R.G., Stein, L.D., Nadeau, J.H. and Lander, E.S. (1993). A genetic linkage map of the mouse: Current applications and future prospects. *Science* **262**, 57-66.

Cornall, R.J., Aitman, T.J., Hearne, C.M. and Todd, J.A. (1991). The generation of a library of PCR-analyzed microsatellite variants for genetic mapping of the mouse genome. *Genomics* **10**, 874-881.

Curnes, J.T. and Oakes, W.J. (1988). Parietal cephaloceles: radiographic and magnetic resonance imaging evaluation. *Pediatr Neurosci* **14**, 71-76.

D'Arcangelo, G., Miao, G.G., Chen, S.-C., Soares, H.D., Morgan, J.I. and Curran, T. (1995). A protein related to extracellular matrix proteins deleted in the mouse mutant reeler. *Nature* **374**, 719-723.

Das, G.D. (1979). Gliogenesis and ependymogenesis during embryonic development in the rat. An autoradiographic study. *J. Neurol. Sci.* **43**, 193-204.

De Carlos, J.A., López-Mascaraque, L. and Valverde, F. (1996). Dynamics of cell migration from the lateral ganglionic eminence in the rat. *J. Neurosci.* **16**, 6146-6156.

Del Rio, J.A. and Soriano, E. (1989). Immunocytochemical detection of 5'-bromodeoxyuridine incorporation in the central nervous system of the mouse. *Dev. Brain Res.* **49**, 311-317.

Deol, M.S. (1964). The origin of the abnormalities of the inner ear in dreher mice. *J. Embryol. exp. Morphol.* **12**, 727-733.

Des Portes, V., Pinard, J.M., Billuart, P., Vinet, M.C., Koulakoff, A., Carrié, A., Gelot, A., Dupuis, E., Motte, J., Berwald-Netter, Y., Catala, M., Kahn, A., Beldjord, C. and Chelly, J. (1998). A novel CNS gene required for neuronal migration and involved in X-linked subcortical laminar heterotopia and lissencephaly syndrome. *Cell* **92**, 51-61.

Dietrich, W., Katz, H., Lincoln, S.E., Shin, H.S., Friedman, J., Dracopoli, N.C. and Lander, E.S. (1992). A genetic map of the mouse suitable for typing intraspecific crosses. *Genetics* **131**, 423-447.

Dietrich, W.F., Miller, J.C., Steen, R.G., Merchant, M., Damron, D., Nahf, R., Gross, A., Joyce, D.C., Wessel, M., Dredge, R.D., Marquis, A., Stein, L.D., Goodman, N., Page, D.C. and Lander, E.S. (1994). A genetic map of the mouse with 4,006 simple sequence length polymorphisms. *Nat. Genetics* **7**, 220-227.

Dobyns, W.B., Andermann, E., Andermann, F., Czapansky-Beilman, D.K., Dubeau, F., Dulac, O., Guerrini, R., Hirsch, B., Ledbetter, D.H., Lee, N.S., Motte, J., Pinard, J.M., Radtke, R.A., Ross, M.E., Tampieri, D., Walsh, C.A. and Truwit, C.L. (1996). X-linked malformations of neuronal migration. *Neurology* **47**, 331-339.

Dobyns, W.B., Guerrini, R., Czapansky-Beilman, D.K., Pierpont, M.E., Breningstall, G., Yock, D.H., Bonnani, P. and Truwit, C.L. (1997). Bilateral periventricular nodular heterotopia with mental retardation and syndactyly in boys: a new X-linked mental retardation syndrome. *Neurology* **49**, 1042-1047.

Dobyns, W.B., Truwit, C.L., Ross, M.E., Matsumoto, N., Pilz, D.T., Ledbetter, D.H., Gleeson, J.G., Walsh, C.A. and Barkovich, A.J. (1999). Differences in the gyral pattern distinguish chromosome 17-linked and X-linked lissencephaly. *Neurology* **53**, 270-277.

Dominov, J.A. and Miller, J.B. (1996). POU homeodomain genes and myogenesis. *Dev. Genet.* **19**, 108-118.

Douville, P. and Carbonetto, S. (1992). Genetic linkage analysis in recombinant inbred mice of P40, a putative clone for the high-affinity laminin receptor. *Mamm. Genome* **3**, 438-446.

Dunn, L.C. (1934). A new gene affecting behavior and skeleton in the house mouse. *Proc. Nat. Acad. Sci.* **20**, 230-232.

Duyckaerts, C., Delaère, P., Costa, C. and Hauw, J.-J. (1992). Factors influencing neuronal density on sections: quantitative data obtained by computer simulation. In: Conn, P.M. (Ed.) *Computers and computations in the neurosciences.* pp. 526-548. San Diego: Academic Press]

Edmondson, J.C., Liem, R.K., Kuster, J.E. and Hatten, M.E. (1988). Astrotactin: A novel neuronal cell surface antigen that mediates neuron-astroglial interactions in cerebellar microcultures. *J. Cell Biol.* **106**, 505-517.

Edwards, M.A., Yamamoto, M. and Caviness, V.S.J. (1990). Organization of radial glia and related cells in the developing murine CNS. An analysis based upon a new monoclonal antibody marker. *Neuroscience* **36**, 121-144.

Fagerheim, T., Nilssen, O., Raeymaekers, P., Brox, V., Moum, T., Elverland, H.H., Teig, E., Omland, H.H., Fostad, G.K. and Tranebjaerg, L. (1996). Identification of a new locus for autosomal dominant non-syndromic hearing impairment (DFNA7) in a large Norwegian family. *Hum. Mol. Genet.* **5**, 1187-1191.

Falconer, D.S. and Sierts-Roth, U. (1951). Dreher, ein neues Gen der Tanzmausgruppe bei der Hausmaus. *Z. indukt. Abstamm. Vererbungsl.* **84**, 71-73.

Feng, L. and Heintz, N. (1995). Differentiating neurons activate transcription of the brain lipid-binding protein gene in radial glia through a novel regulatory element. *Development* **121**, 1719-1730.

Fink, J.M., Hirsch, B.A., Zheng, C., Dietz, G., Hatten, M.E. and Ross, M.E. (1997). Astrotactin (ASTN), a gene for glial-guided neuronal migration, maps to human Chromosome 1q25.2. *Genomics* **40**, 202-205.

Fischer, H. (1956). Morphologische und mikroskopisch-anatomische Untersuchungen am Innenohr eines Stammes spontanmutierter Hausmause (Dreher). *Z. mikr. -anat. Forsch.* **62**, 348-406.

Fischer, H. (1958). Die Embryogenese der Innenohrmissbildungen bei dem Spontanmutierten Dreherstamm der Hausmaus. *Z. mikr. -anat. Forsch.* **64**, 476-497.

Fishell, G. and Hatten, M.E. (1991). Astrotactin provides a receptor system for CNS neuronal migration. *Development* **113**, 755-765.

Fishell, G., Mason, C.A. and Hatten, M.E. (1993). Dispersion of neural progenitors within the germinal zones of the forebrain. *Nature* **362**, 636-638.

Flint, A.C. and Kriegstein, A.R. (1997). Mechanisms underlying neuronal migration disorders and epilepsy. *Curr. Opin. Neurol.* **10**, 92-97.

Friede, R.L. (1989a). Gross and microscopic development of the central nervous system. In: Friede, L.R. (Ed.) *Developmental neuropathology.* 2nd edn. pp. 2-20. Berlin: Springer-Verlag]

Friede, R.L. (1989b). Dysplasias of cerebral cortex. In: Friede, L.R. (Ed.) *Developmental neuropathology.* 2nd edn. pp. 331-346. Berlin: Springer-Verlag]

Galaburda, A.M. (1993). Neuroanatomic basis of developmental dyslexia. *Neurologic Clinics* **11**, 161-173.

Galaburda, A.M., Corsiglia, J., Rosen, G.D. and Sherman, G.F. (1999). Planum temporale asymmetry, reappraisal since Geschwind and Levitsky. *Neuropsychologia* **25**, 853-868.

Galaburda, A.M., Sherman, G.F., Rosen, G.D., Aboitiz, F. and Geschwind, N. (1985). Developmental dyslexia: four consecutive patients with cortical anomalies. *Ann Neurol* **18**, 222-233.

Gillies, K. and Price, D.J. (1993). The fates of cells in the developing cerebral cortex of normal and methylazoxymenthanol acetate-lesioned mice. *Eur. J. Neurosci.* **5**, 73-84.

Gilmore, E.C., Ohshima, T., Goffinet, A.M., Kulkarni, A.B. and Herrup, K. (1998). Cyclin-dependent kinase 5-deficient mice demonstrate novel developmental arrest in cerebral cortex. *J Neurosci* **18**, 6370-6377.

Glaser, T., Jepeal, L., Edwards, J.G., Young, S.R., Favor, J. and Maas, R.L. (1994). *PAX6* gene dosage effect in a family with congenital cataracts, aniridia, anophthalmia and central nervous system defects. *Nat. Genetics* **7**, 463-470.

Gleeson, J.G., Allen, K.M., Fox, J.W., Lamperti, E.D., Berkovic, S., Scheffer, I., Cooper, E.C., Dobyns, W.B., Minnerath, S.R., Ross, M.E. and Walsh, C.A. (1998). *doublecortin,* a brain-specific gene mutated in human X-linked lissencephaly and double cortex syndrome, encodes a putative signaling protein. *Cell* **92**, 63-72.

Gleeson, J.G., Minnerath, S.R., Fox, J.W., Allen, K.M., Luo, R.F., Hong, S.E., Berg, M.J., Kuzniecky, R., Reitnauer, P.J., Borgatti, R., Mira, A.P., Guerrini, R., Holmes, G.L., Rooney, C.M., Berkovic, S., Scheffer, I., Cooper, E.C., Ricci, S., Cusmai, R., Crawford, T.O., Leroy, R., Andermann, E., Wheless, J.W., Dobyns, W.B., Ross, M.E. and Walsh, C.A. (1999). Characterization of mutations in the gene *doublecortin* in patients with double cortex syndrome. *Ann. Neurol.* **45**, 146-153.

Goffinet, A.M. (1979). An early developmental defect in the cerebral cortex of the reeler mouse. A morphological study leading to a hypothesis concerning the action of the mutant gene. *Anat. Embryol.* **157**, 205-216.

Greenwald, I. (1994). Structure/function studies of lin-12/Notch proteins. *Curr. Opin. Genet. Dev.* **4**, 556-562.

Hadrys, T., Braun, T., Rinkwitz-Brandt, S., Arnold, H.-H. and Bober, E. (1998). Nkx5-1 controls semicircular canal formation in the mouse inner ear. *Development* **125**, 33-39.

Hartmann, D., Sievers, J., Pehlemann, F.W. and Berry, M. (1992). Destruction of meningeal cells over the medial crebral hemisphere of newborn hamsters prevents the formation of the infrapyramidal blade of the dentate gyrus. *J. Comp. Neurol.* **320**, 33-61.

Hattori, M., Adachi, H., Tsujimoto, M., Arai, H. and Inoue, K. (1994). Miller-Dieker lissencephaly gene encodes a subunit of brain platelet-activating factor. *Nature* **370**, 216-218.

He, X., Treacy, M.N., Simmons, D.M., Ingraham, H.A., Swanson, L.W. and Rosenfeld, M.G. (1989). Expression of a large family of POU-domain regulatory genes in mammalian brain development. *Nature* **340**, 35-42.

Hearne, C.M., McAleer, M.A., Love, J.M., Aitman, T.J., Cornall, R.J., Ghosh, S., Knight, A.M., Prins, J.-B. and Todd, J.A. (1991). Additional microsatellite markers for mouse genome mapping. *Mamm. Genome* **1**, 273-282.

Herrmann, B., Bucan, M., Mains, P.E., Frischauf, A.M., Silver, L.M. and Lehrach, H. (1986). Genetic analysis of the proximal portion of the mouse t complex: evidence for a second inversion within t haplotypes. *Cell* **44**, 469-476.

Hirotsune, S., Fleck, M.W., Gambello, M.J., Bix, G.J., Chen, A., Clark, G.D., Ledbetter, D.H., McBain, C.J. and Wynshaw-Boris, A. (1998). Graded reduction of *Pafah1b1* (*Lis1*) activity results in neuronal migration defects and early embryonic lethality. *Nature Genet.* **19**, 333-339.

Hoffarth, R.M., Johnston, J.G., Krushel, L.A. and Van der Koy, D. (1995). The mouse mutation reeler causes increased adhesion within a subpopulation of early postmitotic cortical neurons. *J. Neurosci.* **15**, 4838-4850.

Hoopes, C.W., Taketo, M., Ozato, K., Liu, Q., Howard, T.A., Linney, E. and Seldin, M.F. (1992). Mapping of the mouse Rxr loci encoding nuclear retinoid X receptors RXR alpha , RXR beta and RXR gamma. *Genomics* **14**, 611-617.

Hsieh, C.-L., Sturm, R., Herr, W. and Francke, U. (1990). The gene for the ubiquitous octamer-binding protein Oct-1 is on human cromosome 1, region cen-q32 and near Ly-22 and Ltw-4 on mouse chromosome 1. *Genomics* **6**, 666-672.

Humphreys, P., Kaufmann, W.E. and Galaburda, A.M. (1990). Developmental dyslexia in women: neuropathological findings in three patients. *Ann Neurol* **28**, 727-738.

Humphreys, P., Rosen, G.D., Press, D.M., Sherman, G.F. and Galaburda, A.M. (1991). Freezing lesions of the developing rat brain: a model for cerebrocortical microgyria. *J Neuropathol Exp Neurol* **50**, 145-160.

Hunter, K.W., Watson, M.L., Rochelle, J., Ontiveros, S., Munroe, D., Seldin, M.F. and Housman, D.E. (1993). Single-strand conformation polymorphism (SSCP) mapping of the mouse genome: Integration of the SSCP, microsatellite, and gene maps of mouse Chromosome 1. *Genomics* **18**, 510-519.

Jaffe, J., Hochberg, M., Riss, J., Hasin, T., Reich, L. and Laskov, R. (1995). Cloning, sequencing and expression of two isoforms of the murine Oct-1 transcription factor. *Biochim. Biophys. Acta* **1261**, 201-209.

Jordan, T., Hanson, I., Zaletayev, D., Hodgson, S., Prosson, J., Seawright, A., Hastie, N. and Van Heyningen, V. (1992). The human PAX6 gene is mutated in two patients with aniridia. *Nat. Genet.* **1**, 328-332.

Kaplan, L.C. (1985). Congenital Dandy-Walker malformation associated with first trimester warfarin: a case report and literature review. *Teratology* **32**, 333-337.

Kobayashi, K., Nakahori, Y., Myiake, M., Matsumura, K., Kondo-Iida, E., Nomura, Y., Segawa, M., Yoshioka, M., Saito, K., Osawa, M., Hamano, K., Sakakihara, Y., Nonaka, I., Nakagome, Y., Kanazawa, I., Nakamura, Y., Tokunaga, K. and Toda, T. (1998). An ancient retrotransposal insertion causes Fukuyama-type congenital muscular dystrophy. *Nature* **394**, 388-394.

Koyasu, S., Hussey, R.E., Clayton, L.K., Lerner, A., Pedersen, R., Delany-Heiken, P., Chau, F. and Reinherz, E.L. (1994). Targeted disruption within the CD3zeta/eta/theta/Oct-1 locus in mouse. *EMBO J.* **13**, 784-797.

Kuida, K., Zheng, T.S., Na, S., Kuan, C., Yang, D., Karasuyama, H., Rakic, P. and Flavell, R.A. (1996). Decreased apoptosis and premature lethality in CPP32-deficient mice. *Nature* **384**, 368-372.

Leyten, Q.H., Renkawek, K., Renier, W.O., Gabreels, F.J., Mooy, C.M., Laak, H.J. and Mullaart, R.A. (1991). Neuropathological findings in muscle-eye-brain disease. Neuropathological delineation of MEB-D from congenital muscular dystrophy of the Fukuyama type. *Acta Neuropathol* **83**, 55-60.

Love, J.M., Knight, A.M., McAleer, M.A. and Todd, J.A. (1990). Towards construction of a high resolution map of the mouse genome using PCR-analysed microsatellites. *Nucleic Acids Res.* **18**, 4123-4130.

Lyon, M.F. (1961). Linkage relations and some pleiotropic effects of the dreher mutant of the house mouse. *Genet. Res. Camb.* **2**, 92-95.

Marin-Padilla, M. (1978). Dual origin of the mammalian neocortex and evolution of the cortical plate. *Anat. Embryol.* **152**, 109-126.

Marin-Padilla, M. (1995). Prenatal development of fibrous (white matter), protoplasmic (gray matter), and layer I astrocytes in the human cerebral cortex: a Golgi study. *J. Comp. Neurol.* **357**, 554-572.

McConnell, S.K. (1995). Constructing the cerebral cortex: Neurogenesis and fate determination. *Neuron* **15**, 761-768.

McConnell, S.K. and Kaznowski, C.E. (1991). Cell cycle dependance of laminar determination in developing cerebral cortex. *Science* **254**, 282-285.

Meencke, H.-J. (1998). Neuron density in the molecular layer of the frontal cortex in primary generalized epilepsy. *Epilepsia* **26**, 450-454.

Meencke, H.-J. and Janz, D. (1984). Neuropathological findings in primary generalized epilepsy: A study of eight cases. *Epilepsia* **25**, 8-21.

Miller, G., Ladda, R.L. and Towfighi, J. (1991). Cerebro-ocular dysplasia - muscular dystrophy (Walker-Warburg) syndrome. *Acta Neuropathol.* **82**, 234-238.

Miller, M.W. and Nowakowski, R.S. (1988). Use of bromodeoxyuridine-immunohistochemistry to examine the proliferation, migration and time of origin of cells in the central nervous system. *Brain Res.* **457**, 44-52.

Millet, S., Bloch-Gallego, E., Simeone, A. and Alvarado-Mallart, R.-M. (1996). The caudal limit of Otx2 gene expression as a marker of the midbrain-hindbrain boundary: a study using in situ hybridisation and chick/quail homotypic grafts. *Development* **122**, 3785-3797.

Misson, J.P., Edwards, M.A., Yamamoto, M. and Caviness, V.S. (1988). Identification of radial glial cells within the developing murine central nervous system: studies based upon a new immunohistochemical marker. *Dev. Brain Res.* **44**, 95-108.

Misson, J.P., Takahashi, T. and Caviness, V.S.J. (1991). Ontogeny of radial and other astroglial cells in murine cerebral cortex. *Glia* **4**, 138-148.

Mullen, R.J. and Herrup, K. (1979). Chimeric analysis of mouse cerebellar mutants. In: Breakfield, X.O. (Ed.) *Neurogenetics: genetic approaches to the nervous system.* pp. 173-196. New York: Elsevier]

Muskavitch, M.A. (1994). Delta-notch signaling and Drosophila cell fate choice. *Dev. Biol.* **166**, 415-430.

Nagato, Y., Funahashi, M., Takada, K. and Toda, T. (1996). Are breaches in the glia limitans the primary cause of the polymicrogyria in the Fukuyama-type congenital muscular dystrophy (FCMD)?- Pathological study of the cerebral cortex of an FCMD fetus. *Acta Neuropathol.* **91**, 313-321.

Nakano, I., Funahashi, M., Takada, K. and Toda, T. (1996). Are breaches in the glia limitans the primary cause of the micropolygyria in Fukuyama-type congenital muscular dystrophy (FCMD)? - Pathological study of the cerebral cortex of an FCMD fetus. *Acta Neuropathol.* **91**, 313-321.

Northcutt, R.G. and Kas, J.H. (1995). The emergence and evolution of mammalian neocortex. *Trends Neurosci.* **18**, 373-379.

Nowakowski, R.S. and Wahlsten, D. (1985a). Asymmetric development of the hippocampal region in the shaker short-tail (sst) mutant mouse. *Soc. Neurosci. Abstr.* **11**, 989

Nowakowski, R.S. and Wahlsten, D. (1985b). Anatomy and development of the hippocampus and dentate gyrus in the shaker short-tail (sst) mutant mouse. *Anat. Rec.* **211**, 140A

Ogawa, M., Miyata, T., Nakajima, K., Yagyu, K., Seike, M., Ikenaka, K., Yamamoto, H. and Mikoshiba, K. (1995). The reeler gene-associated antigen on Cajal-Retzius neurons is a crucial molecule for laminar organization of cortical neurons. *Neuron* **14**, 899-912.

Ohno, H., Goto, S., Taki, S., Nakano, H., Miyatake, S., Amoe, T., Ishida, Y., Maeda, H., Shirai, T., Rajewsky, K. and Saito, T. (1994). Targeted disruption of the CD3eta locus causes high lethality in mice: modulation of Oct-1 transcription on the opposite strand. *EMBO J.* **13**, 1157-1165.

Ohshima, T., Ward, J.M., Huh, C.G., Longenecker, G., Veeranna, Pant, H.C., Brady, R.O., Martin, L.J. and Kulkarni, A.B. (1996). Targeted disruption of the cyclin-dependent kinase 5 gene results in abnormal corticogenesis, neuronal pathology and perinatal death. *Proc Natl Acad Sci U S A* **93**, 11173-11178.

O'Rourke, N.A., Chenn, A. and McConnell, S.K. (1997). Postmitotic neurons migrate tangentially in the cortical ventricular zone. *Development* **124**, 997-1005.

Patrylo, P.R., Sekiguchi, M. and Nowakowski, R.S. (1990). Heterozygote effects in *dreher* mice. *J. Neurogenetics* **6**, 173-181.

Pehlemann, F.W., Sievers, J. and Berry, M. (1985). Meningeal cells are involved in foliation, lamination, and neurogenesis of the cerebellum: evidence from 6-hydroxydopamine-induced destruction of meningeal cells. *Dev Biol* **110**, 136-146.

Peng, L., Martin-Vasallo, P. and Sweadner, K.J. (1997). Isoforms of Na,K-ATPase alpha and beta subunits in the rat cerebellum and in granule cell cultures. *J Neurosci.* **17**, 3488-3502.

Pesheva, P., Gloor, S., Schachner, M. and Probstmeier, R. (1997). Tenascin-R is an intrinsic autocrine factor for oligodendrocyte differentiation and promotes cell adhesion by a sulfatide-mediated mechanism. *J Neurosci.* **17**, 4642-4651.

Pesheva, P., Spiess, E. and Schachner, M. (1989). J1-160 and J1-180 are oligodendrocyte-secreted nonpermissive substrates for cell adhesion. *J Cell Biol.* **109**, 1765-1778.

Petit, C. (1996). Genes responsible for human hereditary deafness: symphony of a thousand. *Nature Genet.* **14**, 385-391.

Pogulis, R.J., Geddes, T.J. and Freytag, S.O. (1995). Murine collagen intron-binding factor I (CIBF-I) is the same protein as transcription factor Oct-1. *Gene* **158**, 231-235.

Pompa, J.L., Wakeham, A., Correia, K.M., Samper, E., Brown, S., Aguilera, R.J., Nakano, T., Honjo, T., Mak, T.W., Rossant, J. and Conlon, R.A. (1997). Conservation of the Notch signaling pathway in mammalian neurogenesis. *Development* **124**, 1139-1148.

Price, D.J., Aslam, S.A., Tasker, L. and Gillies, K. (1997). Fates of the earliest generated cells in the developing murine neocortex. *J. Comp. Neurol.* **377**, 414-422.

Rakic, P. (1988). Specification of cortical areas. *Science* **241**, 170-176.

Rakic, P. (1990). Principles of neural cell migration. *Experientia* **46**, 882-891.

Rakic, P. (1995). Radial versus tangential migration of neuronal clones in the developing cerebral cortex. *Proc. Natl. Acad. Sci. USA* **92**, 11323-11327.

Reichardt, L.F. and Tomaselli, K.J. (1991). Extracellular matrix molecules and their receptors: functions in neural development. *Ann. Rev. Neurosci.* **14**, 531-570.

Reid, C.B., Liang, I. and Walsh, C. (1995). Systematic widespread clonal organization in cerebral cortex. *Neuron* **15**, 299-310.

Rice, F.L. and Van der Loos, H. (1977). Development of the barrels and barrel field in the somatosensory cortex of the mouse. *J. Comp. Neurol.* **171**, 545-560.

Roessler, E., Belloni, E., Gaudenz, K., Jay, P., Berta, P., Scherer, S.W., Tsui, L.C. and Muenke, M. (1996). Mutations in the human *Sonic Hedgehog* gene cause holoprosencephaly. *Nature Genet.* **14**, 357-360.

Rosen, G.D., Sherman, G.F., Richman, J.M., Stone, L.V. and Galaburda, A.M. (1992). Induction of molecular layer ectopias by puncture wounds in newborn rats and mice. *Dev. Brain Res.* **67**, 285-291.

Ross, M.E., Allen, K.M., Srivastava, A.K., Featherstone, T., Gleeson, J.G., Hirsch, B., Harding, B.N., Andermann, E., Abdullah, R., Berg, M., Czapansky-Beilman, D.K., Flanders, D.J., Guerrini, R., Motte, J., Mira, A.P., Scheffer, I., Berkovic, S., Scaravilli, F., King, R.A., Ledbetter, D.H., Schlessinger, D., Dobyns, W.B. and Walsh, C.A. (1997). Linkage and physical mapping of X-linked lissencephaly/SBH (*XLIS*): a gene causing neuronal migration defects in the human brain. *Human Mol. Genet.* **6**, 555-562.

Rubenstein, J.L. and Beachy, P.A. (1998). Patterning of the embryonic forebrain. *Curr. Opin. Neurobiol.* **8**, 18-26.

Ryan, A.F., Crenshaw III, E.B. and Simmons, D.M. (1991). Gene expression in normal and abnormal inner ears. *Ann. N. Y. Acad. Sci.* **630**, 129-132.

Saito, Y., Murayama, S., Kawai, M. and Nakano, I. (1999). Breached glia limitans-basal lamina complex in Fukuyama-type congenital muscular dystrophy. *Acta Neuropathol.* **98**, 330-336.

Sarnat, H.B. (1992). Disorders of neuroblast migration. In: Sarnat, H.B. (Ed.) *Cerebral dysgenesis: embryology and clinical expression.* pp. 245-274. New York: Oxford University Press]

Schmahl, W., Knoedlseder, M., Favor, J. and Davidson, D. (1993). Defects of neuronal migration and the pathogenesis of cortical malformations are associated with Small eye (Sey) in the mouse, a point mutation at the Pax-6-locus. *Acta Neuropathol* **86**, 126-135.

Schmechel, D.E. and Rakic, P. (1979). A Golgi study of radial glial cells in developing monkey telencephalon: morphogenesis and transformation into astrocytes. *Anat. Embryol.* **156**, 115-152.

Schoeler, H.R. (1991). Octamania: The POU factors in murine development. *Trends Genet.* **7**, 323-329.

Schoeler, H.R., Hatzopoulos, K., Balling, R., Suzuki, N. and Gruss, P. (1989). A family of octamer-specific proteins present during mouse embryogenesis: evidence for a germline-specific expression of an Oct factor. *EMBO J.* **8**, 2543-2550.

Searle, A.G., Edwards, J.H. and Hall, J.G. (1994). Mouse homologues of human hereditary disease. *J. Med. Genet.* **31**, 1-19.

Sekiguchi, M., Abe, H., Shimai, K., Huang, G., Inoue, T. and Nowakowski, R.S. (1994). Disruption of neuronal migration in the neocortex of the dreher mutant mouse. *Dev. Brain Res.* **77**, 37-43.

Sekiguchi, M., Abe, H., Nagato, Y., Tanaka, O., Guo, H. and Nowakowski, R.S. (1996). The abnormal distribution of mossy fiber bundles and morphological abnormalities in hippocampal formation of dreher J (drJ/drJ) mouse. *Dev. Brain Res.* **92**, 31-38.

Sekiguchi, M., Nowakowski, R.S. and Wahlsten, D. (1987). Distribution of cytoarchitectonic abnormalities in the central nervous system of the dreher mutant mouse. *Anat. Rec* **218**, 123A

Sekiguchi, M., Shimai, K., Guo, H. and Nowakowski, R.S. (1992). Cytoarchitectonic abnormalities in hippocampal formation and cerebellum of dreher mutant mice. *Dev. Brain Res.* **67**, 105-112.

Seldin, M.F. (1994). Mouse Chromosome 1. *Mammalian Genome* **5**, S1-S21.

Seldin, M.F. (1997). Mouse Chromosome 1. *Mamm. Genome* **7**, S3-S27.

Sheldon, M., Rice, S.R., D'Arcangelo, G., Yoneshima, H., Nakajima, K., Mikoshiba, K., Howell, B.W., Cooper, J.A., Goldowitz, D. and Curran, T. (1997). Scrambler and yotari disrupt the disabled gene and produce a reeler-like phenotype in mice. *Nature* **389**, 730-737.

Sheppard, A.M., Hamilton, S.K. and Pearlman, A.L. (1991). Changes in the distribution of extracellular matrix components accompany early morphogenetic events of mammalian cortical development. *J. Neurosci.* **11**, 3928-3942.

Sheppard, A.M. and Pearlman, A.L. (1997). Abnormal reorganization of preplate neurons and their associated extracellular matrix: an early manifestation of altered neocortical development in the reeler mutant mouse. *J. Comp. Neurol.* **378**, 173-179.

Sherman, G.F., Galaburda, A.M. and Geschwind, N. (1985). Cortical abnormalities in brains of New Zealand mice: a neuropathologic model of dyslexia? *Proc. Nat. Acad. Sci.* **82**, 8072-8074.

Sherman, G.F., Morrison, L., Rosen, G.D., Behan, P.O. and Galaburda, A.M. (1990a). Brain abnormalities in immune defective mice. *Brain Res.* **532**, 25-33.

Sherman, G.F., Stone, J.S., Rosen, G.D. and Galaburda, A.M. (1990b). Neocortical VIP neurons are increased in the hemisphere containing focal cerebrocortical microdysgenesis in New Zealand Black mice. *Brain Res.* **532**, 232-236.

Sherman, G.F., Rosen, G.D., Stone, L.V., Press, D.M. and Galaburda, A.M. (1992). The organization of radial glial fibers in spontaneous neocortical ectopias of newborn New Zealand Black mice. *Dev. Brain Res.* **67**, 279-283.

Shin, H.S., Flaherty, L., Artzt, K., Bennet, D. and Ravetch, J. (1983). Inversion in the H-2 complex ot t-haplotypes in mice. *Nature* **306**, 380-383.

Sidman, R.L. and Rakic, P. (1973). Neuronal migration, with special reference to developing human brain: A review. *Brain Res* **62**, 1-35.

Sievers, J., Pehlemann, F.W., Gude, S. and Berry, M. (1994a). A time course study of the alterations in the development of the hamster cerebellar cortex after destruction of the overlying meningeal cells with 6-hydroxydopamine on the day of birth. *J Neurocytol* **23**, 117-134.

Sievers, J., Pehlemann, F.W., Gude, S. and Berry, M. (1994b). Meningeal cells organize the superficial glia limitans of the cerebellum and produce components of both the interstitial matrix and the basement membrane. *J. Neurocytol.* **23**, 135-149.

Soriano, E., Dumesnil, N., Auladell, C., Cohen-Tannoudji, M. and Sotelo, C. (1995). Molecular heterogeneity of progenitors and radial migration in the developing cerebral cortex revealed by transgene expression. *Proc. Natl. Acad. Sci. USA* **92**, 11323-11327.

Soriano, E., Alvarado-Mallart, R.M., Dumesnil, N., Del Rio, J.A. and Sotelo, C. (1997). Cajal-Retzius cells regulate the radial glia phenotype in the adult and developing cerebellum and alter granule cell migration. *Neuron* **18**, 563-677.

Stanfield, B.B. and Cowan, W.M. (1979). The development of the hippocampus and dentate gyrus in normal and reeler mice. *J. Comp. Neurol.* **185**, 423-460.

Steel, K.P. and Brown, S.D. (1994). Genes and deafness. *Trends Genet.* **10**, 428-435.

Stitt, T.N. and Hatten, M.E. (1990). Antibodies that recognize astrotactin block granule neuron binding to astroglia. *Neuron* **5**, 639-649.

Stitt, T.N., Gasser, U.E. and Hatten, M.E. (1991). Molecular mechanisms of glial-guided neuronal migration. *Ann N Y Acad Sci.* **633**, 113-121.

Stoykova, A., Fritsch, R., Walther, C. and Gruss, P. (1996). Forebrain patterning defects in *Small eye* mutant mice. *Development* **122**, 3453-3465.

StrucKhoff, G. (1995). Cocultures of meningeal and astrocytic cells - a model for the formation of the glial-limiting membrane. *Int. J. Devl Neuroscience* **13**, 595-606.

Sturm, R.A., Das, G. and Herr, W. (1988). The ubiquitous octamer-binding protein Oct-1 contains a POU domain with a homeobox subdomain. *Genes Dev.* **2**, 1582-1599.

Supèr, H., Martínez, A. and Soriano, E. (1997a). Degeneration of Cajal-Retzius cells in the developing cerebral cortex of the mouse after ablation of meningeal cells by 6-hydroxydopamine. *Dev. Brain Res.* **98**, 15-20.

Supèr, H., Sust, P.P. and Soriano, E. (1997b). Survival of Cajal-Retzius cells after cortical lesions in newborn mice: a possible role for Cajal-Retzius cells in brain repair. *Dev. Brain Res.* **98**, 9-14.

Supèr, H., Soriano, E. and Uylings, H.B. (1998). The functions of the preplate in development and evolution of the neocortex and hippocampus. *Brain Res. Rev.* **27**, 40-64.

Suzuki, N., Peter, W., Ciesiolka, T., Gruss, P. and Schoeler, H.R. (1993). Mouse Oct-1 contains a composite homeodomain of human Oct-1 and Oct-2. *Nucleic Acids Res.* **21**, 245-252.

Sweet, H.O. and Wahlsten, D. (1983). Shaker short-tail (sst). *Mouse News Lett* **69**, 26.

Sweet, H.O., Bronson, R.T., Johnson, K.R., Cook, S.A. and Davisson, M.T. (1996). Scrambler, a new neurological mutation of the mouse with abnormalities of neuronal migration. *Mamm. Genome* **7**, 798-802.

Takada, K., Nakamura, H., Suzumori, K., Ishikawa, T. and Sugyiama, N. (1987). Cortical dysplasia in a 23-week fetus with Fukuyama muscular dystrophy (FCMD). *Acta Neuropathol.* **74**, 300-306.

Takahashi, T., Nowakowski, R.S. and Caviness, V.S. (1992). BUdR as an S-phase marker for quantitative studies of cytokinetic behaviour in the murine cerebral ventricular zone. *J. Neurocytol.* **21**, 185-197.

Tan, S.S. and Breen, S. (1993). Radial mosaicism and tangential cell dispersion both contribute to mouse neocortical development. *Nature* **362**, 638-640.

Tan, S.S., Faulkner-Jones, B., Breen, S.J., Walsh, M., Bertram, J.F. and Reese, B.E. (1995). Cell dispersion patterns in different cortical regions studied with an X-inactivated transgenic marker. *Development* **121**, 1029-1039.

Temple, S. and Qian, X. (1995). bFGF, neurotrophins, and the control of cortical neurogenesis. *Neuron* **15**, 249-252.

The Boulder Committee (1970). Embryonic Vertebrate central nervous system: revised terminology. *Anat. Rec.* **166**, 257-262.

Veenstra, G.J., Beumer, T.L., Peterson-Maduro, J., Stegeman, B.I., Karg, H.A., van der Vliet, P.C. and Destrée, O.H. (1995). Dynamic and differential Oct-1 expression during early early Xenopus embryogenesis: persistence of Oct-1 protein following down-regulation of the RNA. *Mech. Dev.* **50**, 103-117.

Verrijzer, C.P. and van der Vliet, P.C. (1993). POU domain transcription factors. *Biochim. Biophys. Acta* **1173**, 1-21.

Verrijzer, C.P., Kal, A.J. and van der Vliet, P.C. (1990). The DNA binding domain (POU domain) of transcription factor oct-1 suffices for stimulation of DNA replication. *EMBO J.* **9**, 1883-1888.

Wahlsten, D., Lyons, J.P. and Zagaja, W. (1983). Shaker short-tail, a spontaneous neurological mutant in the mouse. *J. Heredity* **74**, 421-425.

Washburn, L. and Eicher, E.M. (1986). A mutation at the dreher locus, (dr2J). *Mouse News Lett* **75**, 28-29.

Wewer, U.M., Durkin, M.E., Zhang, X., Laursen, H., Nielsen, N.H., Towfighi, J., Engvall, E. and Albrechtsen, R. (1995). Laminin beta 2 chain and adhalin deficiency in the skeletal muscle of Walker-Warburg syndrome (cerebro-ocular dysplasia-muscular dystrophy). *Neurology* **45**, 2099-2101.

Wichterle, H., García-Verdugo, J.M. and Alvarez-Buylla, A. (1997). Direct evidence for homotypic, glia-independent neuronal migration. *Neuron* **18**, 779-791.

Wilkinson, D.G. (1992). The theory and practice of in situ hybridization. In: Wilkinson, D.G. (Ed.) *In situ hybridization: A practical approach.* pp. 1-13. Oxford: IRL Press]

Wilkinson, D.G. (1993). In situ hybridization. In: Stern, C.D. and Holland, P.W. (Eds.) *Essential developmental biology: A practical approach.* pp. 257-274. Oxford: IRL Press]

Williams, R.S., Swisher, C.N., Jennings, M., Ambler, M. and Caviness, V.S. (1984). Cerebro-ocular dysgenesis (Walker-Warburg syndrome): Neuropathologic and etiologic analysis. *Neurology* **34**, 1531-1541.

Wintergerst, E.S., Fuss, B. and Bartsch, U. (1993). Localization of Janusin mRNA in the central nervous system of the developing and adult mouse. *Eur J Neurosci.* **5**, 299-310.

Wolf, H.K., Buslei, R., Schmidt-Kastner, R., Schmidt-Kastner, P.K., Pietsch, T., Wiestler, O.D. and Bluemcke, I. (1996). NeuN: A useful neuronal marker for diagnostic histopathology. *J. Histochem. Cytochem.* **44**, 1167-1171.

Wood, J.G., Sascha, M. and Price, D.J. (1992). Evidence that the earliest generated cells of the murine cerebral cortex form a transient population in the subplate and marginal zone. *Dev. Brain Res.* **66**, 137-140.

Wynshaw-Boris, A. (1996). Model mice and human disease. *Nature Genet.* **13**, 259-260.

Xuan, S., Baptista, C.A., Balas, G., Tao, W., Soares, V.C. and Lai, E. (1995). Winged helix transcription factor BF-1 is essential for the development of the cerebral hemispheres. *Neuron* **14**, 1141-1152.

Yang, G., Douville, P., Gee, S. and Carbonetto, S. (1998). Nonintegrin laminin receptors in the nervous system: Evidence for lack of relationship to P40. *J. Neurobiol.* **23**, 491-506.

Zheng, C., Heintz, N. and Hatten, M.E. (1996). CNS gene encoding astrotactin, which supports neuronal migration along glial fibers. *Science* **272**, 417-419.